DETECTION AND ANALYSIS OF COHERENT STRUCTURES WITHIN AND ABOVE TALL-VEGETATED CANOPIES

A dissertation submitted to the

FACULTY OF BIOLOGY, CHEMISTRY AND GEOSCIENCES

OF THE UNIVERSITY OF BAYREUTH, GERMANY

to attain the academic degree of

DR. RER. NAT.

presented by

CHRISTOPH THOMAS

Diplom Geoökologe

born November 24, 1974
in Detmold/ Lippe, Westfalen

Bayreuth, April 2005

DETECTION AND ANALYSIS OF COHERENT STRUCTURES
WITHIN AND ABOVE TALL-VEGETATED CANOPIES

Supervisor Prof. Dr. Thomas Foken

Die vorliegende Arbeit wurde in der Zeit von Januar 2002 bis April 2005 an der Universität Bayreuth am Lehrstuhl für Hydrologie, Abteilung Mikrometeorologie, unter Betreuung von Prof. Dr. Thomas Foken angefertigt.

Vollständiger Abdruck der von der Fakultät für Biologie, Chemie und Geowissenschaften der Universität Bayreuth genehmigten Dissertation zur Erlangung des akademischen Grades eines Doktors der Naturwissenschaften (Dr. rer. nat.).

Promotionsgesuch eingereicht am: 05.04.2005

Wissenschaftliches Kolloquium am: 16.06.2005

Prüfungsausschuss:

Prof. Dr. Th. Foken (Erstgutachter)
Prof. Dr. C. Zetzsch (Zweitgutachter)
Prof. Dr. E. Matzner (Vorsitzender)
Prof. Dr. B. Huwe
PD Dr. G. Aas

Dekan: Prof. Dr. O. Meyer

Contents

List of manuscripts

The dissertation is presented in cumulative form. It consists of six individual manuscripts. One manuscript was reviewed and accepted for publication and is currently in press, a pre-print version is online available. All other manuscripts have been submitted and are still in the review process.

Manuscripts in print (preprint version available online)

Thomas, C. and Foken, T., 2005. Detection of long-term coherent exchange over spruce forest using wavelet analysis. Theor. Appl. Climatol.: DOI: 10.1007/s00704-004-0093-0. (Appendix B)

Submitted manuscripts

Thomas, C., Mayer, J.-C., Meixner, F.X. and Foken, T., 2005. Analysis of low-frequency turbulence above tall vegetation using a Doppler sodar. Boundary-Layer Meteorol.: submitted. (Appendix C)

Thomas, C. and Foken, T., 2005. Coherent structures in a tall spruce canopy: temporal scales, structure spacing and terrain effects. Boundary-Layer Meteorol.: submitted. (Appendix D)

Thomas, C. and Foken, T., 2005. Flux contribution of coherent structures and its implications for the exchange of energy and matter in a tall spruce canopy. Boundary-Layer Meteorol.: submitted. (Appendix E)

Ruppert, J., Thomas, C. and Foken, T., 2005. Scalar similarity for Relaxed Eddy Accumulation methods. Boundary-Layer Meteorol.: submitted. (Appendix F)

Zhang, G., Thomas, C., Leclerc, M. Y., Karipot, A., Gholz, H. L. and Foken, T., 2005. On the effect of clearcuts on forest canopy fluxes. Theor. Appl. Climatol.: submitted. (Appendix G)

Acknowledgements

I wish to express my gratitude to all persons who contributed to this thesis in some way. Particularly, I wish to thank

Summary

Coherent structures are an inherent phenomenon of the atmospheric turbulent flow in the proximity to tall-vegetated canopies. Although coherent structures have called increasing attention of the turbulence community during the past decades, the basic mechanisms of their emergence, their contributions to exchange processes and their importance for conventional flux determination methods remain poorly understood or even unknown. In particular, no studies have been published yet dealing with long-term observations rather than exemplary case studies using short-term data. This dissertation aims at the enhanced understanding of the driving mechanisms and statistical properties of coherent structures within and above tall-vegetated canopies through an extensive analysis using long-term observations. Thereby, it places a specific emphasis on the implications of coherent structures for exchange processes and assesses their impact on conventional flux determination methods such as the eddy covariance and relaxed eddy accumulation techniques. Data were mainly obtained using tower-based single-point turbulence measurements and acoustic remote sensing technique (Sodar-Rass) during extensive field campaigns conducted in summer 2003.

The developed wavelet software tool for detection and analysis of coherent structures is verified to extract coherent structures objectively under varying environmental conditions and thus allows determining their statistics in long-term datasets. In the proximity to the plant canopy, the temporal scales of coherent structures typically range between 20 s and 35 s. The temporal scales of coherent structures in the horizontal wind velocity, the sonic temperature and the concentration of carbon dioxide and water vapour exceed those of the vertical wind velocity. Within the canopy, the temporal scales of all vector and scalar variables collapse at approx. 24 s to 28 s resulting in an enhanced symmetry. Besides this, coherent structures with temporal scales up to 220 s are evidenced well above the canopy with the aid of acoustic remote sensing. The application of the canopy mixing-layer analogy to the data partially yields departures of the ratio m between the streamwise structures spacing of coherent structures and the canopy shear scale from the prediction m = 7...10. The departures are due to the influence of the terrain affecting the shape of the canopy wind profile and therefore the vertical wind shear. An agreement is found for flows which are forced to reorganise downstream of flow obstacles. The vertical wind shear is identified as the main driving force from which coherent structures emerge close to the canopy. In the layer well above the canopy diabatic processes facilitate the generation of coherent structures of large temporal scales. Clearcuts in a fairly homogeneous canopy cause additional structures in the turbulent flow with large temporal scales. Coherent structures contribute about 16 % to total the momentum transfer and about 26 % to the total fluxes of buoyancy, carbon dioxide and latent heat. A scheme for the qualitative classification of exchange regimes between the atmosphere and the canopy is developed analysing the ejection and sweep phases of coherent structures along the vertical profile in the canopy. The presence of coherent structures causes flux errors in the eddy covariance method below 4 %. The effect of this flux error for long-term observations is negligible as individual flux errors average out. Coherent structures of large temporal scales significantly influence the scalar similarity required for the relaxed eddy accumulation technique. These flow structures are responsible for the diurnal changes of the scalar similarity observed in the traces of acoustic temperature and concentration of carbon dioxide and water vapour.

Zusammenfassung

Kohärente Strukturen sind ein inhärenter Bestandteil der atmosphärischen Turbulenz über hoher Vegetation. Obwohl die Turbulenzforschung innerhalb der letzten Jahrzehnte kohärente Strukturen zunehmend in den Mittelpunkt ihres Interesses gerückt hat, blieben die grundlegenden Mechanismen ihrer Entstehung, ihr Beitrag zu Austauschprozessen und ihre Bedeutung für konventionelle Austauschbestimmungsverfahren weitgehend unverstanden. Vor allem die Untersuchung umfangreicher Datensätze anstelle von Einzelstudien fehlte bislang. Das Ziel der vorliegenden Dissertation ist ein erweitertes Verständnis der Entstehungsmechanismen und der statistischen Eigenschaften kohärenter Strukturen in und über hoher Vegetation durch die Untersuchung umfangreicher Zeitreihen. Besondere Bedeutung kommt dabei den Auswirkungen kohärenter Strukturen auf den Gesamtaustauschprozess und Austauschbestimmungsverfahren wie die Eddy-Kovarianz-Methode und die Relaxed-Eddy-Akkumulations-Technik zu. Die Datengrundlage wurde hauptsächlich im Rahmen umfangreicher Feldexperimente im Sommer 2003 erhoben. Dabei kamen Verfahren zur Turbulenzmessung auf Türmen und akustische Fernerkundung zur Anwendung.

Das selbstentwickelte Softwareprogramm, das die Wavelet-Transformation für die Erkennung und Untersuchung verwendet, gewährleistet eine objektive Bestimmung kohärenter Strukturen in Zeitreihen unter wechselnden meteorologischen Umweltbedingungen. Es schafft damit die Voraussetzung für eine Langzeitstudie über kohärente Strukturen. Kohärente Strukturen über hoher Vegetation haben charakteristische Zeitskalen zwischen 20 s und 35 s. Die Zeitskalen im Horizontalwind und in den Skalaren der akustischen Temperatur und der Konzentration von Kohlendioxid und Wasserdampf sind dabei größer als im Vertikalwind. Innerhalb hoher Vegetation gleichen sich die Zeitskalen der vektoriellen und skalaren Größen, die zwischen 24 s und 28 s liegen. Die Vegetation führt damit zu einer Erhöhung der Symmetrie kohärenter Strukturen. In größerer Entfernung zur Oberfläche konnten ebenfalls kohärente Strukturen mit deutlich längeren Zeitskalen von bis zu 220 s mithilfe der akustischen Fernerkundung nachgewiesen werden. Die Anwendung der Verwirbelungsschicht-Analogie auf die Datensätze ergab teilweise erhebliche Abweichungen des berechneten Verhältnisses m von der Vorhersage m = 7...10. Das Verhältnis m ist definiert als mittlerer Abstand kohärenter Strukturen entlang der Strömung zur Scherungslängenskala im Bestand. Die Abweichungen können auf die Oberflächengestalt zurückgeführt werden, die Einfluss auf das Windprofil im Bestand und damit auf die Windscherung nehmen. Eine Übereinstimmung wird für Strömungen erzielt, die sich im Nachlauf von Strömungshindernissen neu formieren müssen. Die große Windscherung an der Oberkante hoher Vegetation ist im hohen Maße verantwortlich für die Entstehung kohärenter Strukturen nahe der Vegetation. In größerer Entfernung zur Oberfläche können zunehmend diabatische Prozesse Einfluss nehmen. Kahlschläge in sonst homogener Vegetation erzeugen zusätzliche turbulente Flussstrukturen, die große zeitliche Skalen aufweisen. Kohärente Strukturen haben einen mittleren Flussbeitrag von 16 % am Impulsaustauscb und von 26 % am Auftriebsstrom, dem Kohlendioxidfluss und dem Austausch latenter Wärme. Zur Klassifikation typischer Austauschzustände zwischen der Atmosphäre und hoher Vegetation wurde ein Schema entwickelt, das eine qualitative Bewertung erlaubt. Es basiert auf dem physikalischen Prozess des Energietransportes, der durch die Phasen der Auf- und Abwärtsbewegung kohärenter Strukturen hervorgerufen wird. Kohärente Strukturen

verursachen bei Anwendung der konventionellen Eddy-Kovarianz-Methode über hoher Vegetation einen Flussbestimmungsfehler von unter 4 %. Dieser Fehler mittelt sich für längere Zeitabschnitte heraus und wird damit vernachlässigbar. Kohärente Strukturen mit großen Zeitskalen üben einen deutlichen Einfluss auf die skalare Ähnlichkeit aus, die Voraussetzung für die Anwendung der Eddy-Akkumulations-Technik ist. Sie sind verantwortlich dafür, dass sich die skalare Ähnlichkeit zwischen akustischer Temperatur und der Konzentration von Kohlendioxid und Wasserdampf im Tagesverlauf verändert.

1 Introduction

Coherent structures in the proximity to plant canopies have been receiving close attention by the turbulence community over the past decades. The spatially large and well-organised coherent structures are an inherent phenomenon of atmospheric turbulence above rough surfaces and significantly contribute to the exchange of momentum, heat, and matter between the canopy and the atmosphere (e.g. Bergström and Högström, 1989; Raupach, 1981). Coherent structures represent the rather deterministic part of atmospheric turbulence in contrast to the well-known high-frequency turbulence which underlies stochastic laws.

1.1 Definition of coherent structures

The variety of definitions of coherent structures reported in literature depends on the spatial and temporal context of the observations. In the proximity to the plant canopy, coherent structures are defined as low-frequent flow patterns which differ significantly from the well-known high-frequency turbulence. In general, this flow pattern can be described as large-amplitude excursions from the mean with a distinct shape. In time series of vector variables coherent structures show up as fairly symmetric, triangle-shaped like pattern, whereas in time series of scalars they have a more asymmetric ramp-like shape. The underlying physical process causing the shape of an individual coherent structure consists of an inertial upward motion (ejection, burst) followed by a rapid downward motion (sweep, gust). The duration of coherent structures typically spans several seconds up to a few minutes. In addition to the descriptive definition of coherent structures, a more physical definition was given by Blackwelder (1987). He described a coherent structure as a vortex of fluid occupying a confined spatial volume characterized by a distinct phase relationship between flow variables (vectors) and its flow constituents (scalars) as its evolves in space and time.

1.2 Emergence of coherent structures

Coherent structures within and above tall vegetated canopies have been observed by many authors focusing on different aspects (e.g. Bergström and Högström, 1989; Brunet and Irvine, 2000; Gao et al., 1989; Lu and Fitzjarrald, 1994; Paw U et al., 1992; Raupach et al., 1989; Raupach et al., 1996). However, the driving mechanisms which control the generation of coherent structures have not been identified unambiguously. Based on the similarity between structural dynamical properties of coherent structures in changing diabatic conditions, Gao et al. (1989) identified the vertical wind shear as the main mechanism driving the generation of coherent structures. The results of Paw U et al. (1992) supported this finding as they reported a functional relationship between the occurrence frequency of coherent structures and a specific canopy shear scale which depends on the horizontal wind speed at canopy top $\overline{U_{h_c}}$ and the canopy height h_c. Simultaneously to these findings, Raupach et al. (1989; 1996) proposed a theory for near neutral stratification which is called the canopy mixing-layer analogy. According to this theory, the turbulent flow close to the plant canopy can be described analogously to the flow in a plane mixing-layer evolving between two coflowing streams of different velocities under laboratory conditions. The theory is valid only in the roughness sublayer (RSL) close to the canopy, i.e. the layer in which the flow is dominated by the presence of the canopy roughness elements. The canopy mixing-layer analogy predicts

coherent structures to emerge from the Kelvin-Helmholtz instabilities caused by the inflected mean horizontal velocity profile. The streamwise spacing of coherent structures Λ_x in the time series of a variable x is a unique, linear function of the canopy shear length scale L_s. The canopy shear scale L_s depends on the magnitude of the horizontal wind speed and the vertical gradient of the horizontal wind speed both at canopy top. Brunet and Irvine (2000) demonstrated that the canopy mixing-layer is valid not only for near neutral flows, but also under stable and unstable conditions.

The atmospheric stability or any diabatic process in the atmosphere were identified to have a quantitative rather than a qualitative effect on the emergence of coherent structures in the turbulent flow close to plant canopies (Finnigan, 2000). However, evidence has been provided that diabatic processes may have a modifying influence on the flow properties of coherent structures (e.g. Brunet and Irvine, 2000).

1.3 Detection of coherent structures

The critical step in the analysis of coherent structures is to find an objective method to identify and to extract them from the turbulent signal. The turbulent signal of an arbitrary vector or scalar variable in the atmospheric boundary layer consists of the superimposed signals of the stochastic random-like high-frequent turbulence, the well-organised coherent structures and any additional processes such as advection and convection.

Many detection methods have been developed to study the coherent structures in particular. Classical approaches which were used by researchers are the Variable Interval Time-Averaging (VITA) technique (e.g. Blackwelder and Kaplan, 1976) or the Windowed Averaged Gradient (WAG) technique (Bisset et al., 1990). They are based on the comparison of statistical moments between the entire time series and a short period thereof and are sensitive to the sharp jumps of the signal produced by the sudden sweep motion of coherent structures. These methods depend on the adjustment of threshold values which limits their application for an objective detection (Bogard and Tiederman, 1986). The quadrant analysis (Lu and Willmarth, 1973; Wallace et al., 1972) has been widely used by researchers to study coherent structures. This technique was mainly applied to determine the flux contribution of coherent structures. It sorts an instantaneous value of a turbulent time series into one of the quadrants of a 2-D plane which is spanned by the fluctuation of the two variables corresponding to the flux. However, the traditional quadrant analysis has some shortcomings as it depends on the definition of threshold values to exclude flux contributions emerging from other processes than coherent structures. The use of fixed threshold criteria may encourage the subliminal involvement of other processes than coherent structures in the analysis, as dynamic properties of coherent structures may change during the day. Further, the quadrant analysis leads to a systematic underestimation of flux contributions from the ejection motions of coherent structures (Gao et al., 1989). The latter is a consequence of the naturally occurring asymmetry between the sweep and ejection motion of coherent structures, as the sweep motion consists of fewer strong events in contrast to the ejection motion which is characterised by more frequent moderate events. In conclusion, the quadrant analysis has been found useful for the determination of the flux contribution of coherent structures to momentum and scalar fluxes (e.g. Katul et al., 1997; Shaw, 1985), but provide only poor information about their spatial or temporal characteristics. The introduction of the mathematical wavelet transform (Grossmann et al., 1989; Grossmann and Morlet, 1984;

Kronland-Martinet et al., 1987) into the field of turbulence research investigating coherent structures provided the opportunity to develop objective detection methods which do not require the definition of threshold values. As the wavelet transform is a time-scale analysis, it reveals information about both the scale (frequency) and the moment of occurrence (time) of coherent structures. Therefore it is possible to identify processes at their specific scales in the time domain, i.e. to derive detailed spatial and temporal statistics of coherent structures. The choice of the proper wavelet function is the most important step in the setup of a detection method based on the wavelet transform. The use of a certain wavelet function has a dominant influence on the analysis, as its result depends on the localisation in frequency and time of the wavelet function. Wavelet functions which are well localised in the frequency domain are necessary when characteristic temporal scales of coherent structures are determined. In contrast, wavelet functions well localised in time ought to be preferred for the detection of individual coherent structures in the time series. Collineau and Brunet (1993a, b) demonstrated the merits of the wavelet transform for the objective analysis of coherent structures in the turbulent time series obtained in the RSL above a pine forest. Since then, many studies have been performed with detection and extraction algorithms for coherent structures based on wavelet transform in time series obtained in the atmospheric boundary layer (e.g. Brunet and Irvine, 2000; Chen et al., 2004; Gamage and Hagelberg, 1993; Handorf and Foken, 1997a; Turner and Leclerc, 1994). However, most detection algorithms are either suited for the analysis of short-term periods of measurements or were designed to process specific vector and scalar time series only. A method of analysis offering both an objective and automated detection algorithm for multiple vector and scalar variables and the opportunity to process long-term observations was desirable to derive robust statistics of coherent structures and was developed in this thesis.

1.4 Importance of coherent structures for exchange processes

Coherent structures have been identified as important process for the exchange of momentum and heat between the canopy and the atmosphere (e.g. Bergström and Högström, 1989; Gao et al., 1989; Katul et al., 1997; Shaw et al., 1983). Many studies which have been published during the past decades focused on the specific importance of the ejection and sweep phases of coherent structures to the total atmospheric fluxes (e.g. Bergström and Högström, 1989; Shaw et al., 1983; Wallace et al., 1972). In conclusion they provided evidence that the flux contribution of the strong sweep phase increases with increasing proximity to the plant canopy and exceeds the flux contribution of ejections by far. However, besides these aspects addressing issues of flow dynamics in the proximity to rough surfaces only poor information is available about the impact of coherent structures to the exchange processes in general. In particular, the question of how deep and under which conditions coherent structures may penetrate from above into the canopy remained open so far. These problems become important when studying budgets of energy and matter in natural ecosystems and identifying the individual processes contributing to these budgets. Wichura et al. (2004) proposed a classification of the carbon dioxide exchange regimes in a spruce forest. Based on the comparison between the analysis of dynamic properties of coherent structures and the measurement of atmospheric fluxes of the stable carbon isotope at an observation level above the canopy, they distinguished between coupled and decoupled states between the canopy and the atmosphere. A reliable identification of the physical processes which underlie such

coupling and decoupling processes is crucial for a deeper insight into the mechanisms enabling or constricting the transfer of momentum, heat, and mass between the canopy and the atmosphere.

1.5 Importance of coherent structures for flux determination methods

The dominating influence of coherent structures on the exchange of energy and matter poses the question if coherent structures have an effect on conventional micrometeorological flux determination methods. These methods include direct flux determination approaches such as the eddy covariance (EC) method commonly deployed in long-term measurement programs such as the FLUXNET network as well as indirect flux determination methods such as the relaxed eddy accumulation (REA) technique (Businger and Oncley, 1990). This question is of great importance for practical applications and bases on the following ideas. First, the presence of intermittent coherent structures may violate the assumption of steady-state conditions required for the EC as they represent non-stationarities in terms of the flow dynamics. This violation may directly lead to a systematic over- or underestimation of the derived net balances. Second, the coherent structures may exert an influence on quality control flags derived from quality assessment / quality control protocols commonly applied in long-term measurement programs (Foken et al., 2004). In particular, this may result in discarding intervals with intense intermittent coherent structures from further analysis as they violate the essential requirement of steady-state conditions for the EC method. Third, the REA technique relies on the definition of proxy variables in order to determine the flux of the variable of interest. Assuming that coherent structures significantly contribute to atmospheric fluxes and that they are more efficient in transporting one constituent than others due to different source distributions, the reasonable use of proxy scalars may be limited. Therefore the use of improper proxy scalars may result in systematic errors when applying indirect flux determination methods. In contrast to the great need to get reasonable answers to the upcoming questions, no information has been published yet concerning the influence of coherent structures for micrometeorological flux determination methods.

1.6 Objectives of the thesis

The principal objective of this dissertation was the extensive analysis of coherent structures in multiple vector and scalar variables based on long-term observations within and above tall vegetated canopies. The first objective was the development and verification of an objective detection tool based on the wavelet transform which is applicable under varying environmental conditions and therefore suited for the analysis of long-term observations. The second objective was the identification of the driving mechanisms for the generation of coherent structures through the analysis of dynamic characteristics of coherent structures. The third objective was the determination of the implications of coherent structures for the exchange of energy and matter between the canopy and the atmosphere. The fourth objective was the assessment of the impact of coherent structures on conventional micrometeorological flux determination methods such as the eddy covariance method and the relaxed eddy accumulation technique. These objectives were addressed by the six individual publications presented in Appendices B to G of this thesis.

Thomas and Foken (2005b, Appendix B) address the first objective, i.e. to develop, to establish and to verify an objective and mathematically robust detection algorithm applicable for the time series analysis of vector and scalar traces collected under varying environmental conditions. The latter condition intended to ensure its applicability to future field measurements beyond the data collected and analysed in this thesis. The developed method of analysis was intended to process arbitrary high-frequency single-point measurements of turbulent variables. The presented method ought to skillfully make use of the specific properties of different wavelet functions for the purposes of filtering the time series, determining the characteristic temporal scales of coherent structures and detecting all individual coherent structures contained in a time series. The objective of this paper was to provide a software tool which can be applied either quasi-online or subsequent to field measurements. The quasi-online application provides the opportunity to manage micrometeorological flux measurements depending on the current state of atmospheric turbulence directly in the field.

The papers presented in Appendices C and D address the second objective, i.e. they aim at the identification of the driving mechanisms from which coherent structures emerge or which influence the dynamic characteristics of coherent structures in the proximity to and within plant canopies. Therefore, both papers use data obtained by different measurement techniques. Thomas et al. (2005, Appendix C) use data obtained by acoustic remote sensing (Sodar-Rass) in the layer well above the canopy. For this purpose, acoustic remote sensing was applied for the first time. Thus, an objective of the paper was to demonstrate the general applicability of this method for the observation of coherent structures above plant canopies. The main objective of the paper was to derive information about the presence and characteristics of coherent structures in the layer well above the canopy as conventional tower-based single-point measurements do not reach up to these heights. In addition, Thomas et al. (2005, Appendix C) aimed at the adaptation and extension of the method of analysis presented in Thomas and Foken (2005b, Appendix B) to measurements obtained by acoustic remote sensing. Thomas and Foken (2005a, Appendix D) use long-term high-frequency single-point measurements collected at numerous observation levels above the canopy, at the canopy top and in the canopy. A main objective of this paper was to identify the generating and modifying processes for coherent structures with a special emphasis placed on the effect of the canopy structure and the surrounding terrain on the turbulent canopy flow. Further, it aimed at applying the canopy mixing-layer analogy to the data to verify this theoretical concept for the observed vector and scalar variables. Both objectives contribute to the principal goal to identify the driving mechanisms of coherent structures in the proximity to plant canopies.

Thomas and Foken (2005c, Appendix E) address the third and fourth objective of the thesis aiming at the contribution of coherent structures to the total exchange of energy and matter and its impact on the eddy covariance method. They use the results of Thomas and Foken (2005a, Appendix D) concerning the detection of individual coherent structures and apply the method of conditional sampling to derive the scale-dependent fluxes of coherent structures. Further objectives of this paper were to identify the implications of the flux contributions of coherent structures to the overall exchange and to derive a classification scheme describing typical exchange regimes in a tall plant canopy. Furthermore, the influence of coherent structures to measurements obtained by the eddy covariance method is discussed using a self-developed approach.

The papers presented in Appendices F and G also address the fourth objective of the thesis, i.e. to assess the impact of coherent structures on conventional flux determination methods. Ruppert et al. (2005, Appendix F) investigate the scalar similarity required for the relaxed eddy accumulation as an indirect flux determination method. One main objective of this paper is to determine the influence of coherent structures and larger flow structures on the similarity between different scalar variables during the diurnal course using the method of analysis presented in Appendix B. The study uses data from field experiments conducted over different surfaces such as grassland, an irrigated cotton-plantation and a tall-vegetated forest. Zhang et al. (2005, Appendix G) aim at the influence of changes in the management (clearcut) of a pine forest on the turbulent fluxes which are collected distantly downwind to these changes. In particular, the main objective of this paper was to find changes in the structure of the turbulent flow coming from the clearcuts and the partly undisturbed parts of the forest through the application of the wavelet analysis method presented in Appendix B.

2   Experiments and data

The individual papers presented in Appendices B to G use large datasets collected in numerous field campaigns. The predominant part of the data was collected either as a part of field measurement activities conducted by the Department of Micrometeorology / University of Bayreuth which were supervised by T. Foken or in close cooperation with project partners embedded in the German Atmospheric Research program AFO-2000. The data presented in the publications listed in the Appendices B, C, D, and E were collected during the extensive field campaigns WALDATEM-2003 and ECHO-2003 both conducted in summer 2003. The paper presented in Appendix F uses data obtained during different measurement campaigns, namely the WALDATEM-2003, GRASATEM-2003 and EBEX-2000 experiments. The contained WALDATEM-2003 data were collected in cooperation with my colleague J. Ruppert as we were both members of the researcher's team of the Department of Micrometeorology. The GRASATEM-2003 data were collected by my colleague J. Ruppert within the framework of the LITFASS-2003 experiment in summer 2003. The EBEX-2000 data presented in the manuscript were collected under the supervision of T. Foken by my colleagues C. Liebethal and M. Mauder in summer 2000. The paper presented in Appendix G uses data from a measurement campaign supervised by M. Y. Leclerc and conducted by A. Karipot and H. L. Gholz in autumn / winter 2000.

2.1 WALDATEM-2003

The principal goal of the WALDATEM-2003 (WAveLet Detection and Atmospheric Turbulent Exchange Measurements) field experiment (Thomas et al., 2004) was the intensive investigation of coherent structures and carbon fluxes within and above a tall spruce forest through extensive tower-based measurements in combination with ground-based acoustic remote sensing. The measurements were carried out as a part of the field research activities of the Department of Micrometeorology / University of Bayreuth within the framework of the BITÖK (Bayreuth Institute for Terrestrial Ecosystem Research) funded by the Federal Ministry of Education and Research of Germany (BMBF). The experiment was conducted at the FLUXNET site Weidenbrunnen Waldstein (50°08'N, 11°52'E, 775 m a.s.l.) in the Fichtelgebirge mountains in the North-easterly part of Bavaria, Germany, during the period from May to July 2003. The coniferous canopy mainly consists of Norway spruce trees (*Picea abies* L.) with a mean canopy height of 19 m. The plant area index (PAI) is 5.2, with the main leaf mass concentrated in a height of the 9 m to 17 m above ground (Thomas and Foken, 2005a, Appendix D). The under-storey in the surrounding of the site is fairly sparse and is mainly composed of small shrubs and graminae with a mean height of approximately 0.4 m. A detailed description of the site as well as of the larger-scale topography was given by Gerstberger et al. (2004).

   The WALDATEM-2003 data presented in this thesis were obtained by both single-point measurements at towers and acoustic remote sensing. For the tower-based data, high-frequency turbulence measurements of the 3-D wind velocity vector and sonic temperature using sonic anemometers, and carbon dioxide and water vapour concentration measurements using gas analysers were performed on several observation levels above, at the top, and within the canopy. The acoustic remote sensing device (Sodar-Rass) was deployed to obtain high-resolution time series of the wind velocity vector and sonic temperature in the layer well

above the canopy. In addition to the high-frequency measurements, the means of air temperature, air humidity and horizontal wind velocity were obtained along a vertical profile covering a height range from above the canopy down to the bottom of the subcanopy space. Radiation measurements were carried out above the canopy using up- and downward facing shortwave and longwave radiation sensors. A detailed description of the entire experimental setup and the applied measurement devices can be found in Thomas et al. (2004).

2.2 ECHO-2003

The ECHO-2003 (Emission and CHemical transformation of biogenic volatile Organic compounds) experiment (Koppmann, 2003) aimed at a better understanding of forest stands as a complex source of reactive trace gases into the troposphere. The data of this experiment included in the manuscript of Appendix C were collected during the field campaign in July / August 2003 in close cooperation with the members of the research team of the Biogeochemistry Department of the Max-Planck-Institute for Chemistry in Mainz supervised by F. X. Meixner and J. Kesselmeier within the framework of the ECHO project as a part of the German Atmospheric Research program AFO2000. The experiment was conducted at the Research Center Jülich (50°54'N, 06°24'E, 91 m a.s.l.) near Cologne. The canopy of the site consists of coniferous and deciduous trees with a mean canopy height of 30 m. A detailed description of the sampling site can be found in Aubrun et al. (2005). During this experiment, the data presented in Thomas et al. (2005, Appendix C) were obtained by the acoustic remote sensing system which was operated in a large clearing of approx. 500 x 500 m size. The measurements yielded time series of the wind velocity vector and the acoustic reflectivity in the layer well above the canopy.

2.3 Other experimental data

The GRASATEM-2003 (GRASsland Atmospheric Turbulent Exchange Measurements) experiment aimed at the investigation of atmospheric turbulent fluxes of the stable carbon dioxide isotope ^{13}C over a homogeneous surface. The experiment was carried out within the framework of the LITFASS-2003 experiment (Beyrich, 2004) as a part of the German climate research programme DEKLIM. Measurements were performed over short cut grassland with a mean canopy height of 0.12 m at the Falkenberg experimental site of the German Meteorological Service (52°10'N, 14°07'E, 73 m a.s.l.) in May 2003. A sonic anemometer in combination with a gas analyser was used to obtain high-frequency time series of the 3-D wind vector, the sonic temperature, and the concentration of carbon dioxide and water vapour.

The main objectives of the EBEX-2000 (Energy Balance EXperiment) field campaign (Oncley et al., 2002) were the exact determination of all terms of the energy balance close to the surface and the intercomparison of turbulent measurement devices and data processing methods. Members from European and American science teams of numerous research affiliations participated in the experiment. The group from the University of Bayreuth was led by T. Foken. The experiment was conducted in an irrigated cotton plantation (36°06'N, 119°56'W, 67 m a.s.l.) with a mean canopy height of 1 m during July / August 2000 in southern California, USA. The high-frequency data presented in the manuscript of Appendix F were collected using eddy covariance measurement complexes consisting of sonic anemometers and gas analysers.

The manuscript presented in Appendix G uses data collected during an experiment conducted by the Laboratory for Environmental Physics of the University of Georgia supported by the National Science Foundation, USA. The site near Gainesville, Florida (29º45´N, 82º10´W, 50 m a.s.l.) is an 11-years old slash pine (*Pinus elliottii* Engelm.) managed forest on the premises of the Florida AmeriFlux site with a mean canopy height of 10 m and an average leaf area index of 2.8. A detailed description of the site can be found in Gholz and Clark (2002). The presented data were obtained by a 3-D sonic anemometer yielding high-frequency measurements of the wind velocity vector and the sonic temperature.

3 Results

3.1 Method of detection

The method of detection for coherent structures in the high-resolution turbulence measurements uses the wavelet transform (Grossmann et al., 1989; Grossmann and Morlet, 1984; Kronland-Martinet et al., 1987) as the central mathematical-statistical tool. Its development to the current version as presented in Thomas and Foken (2005b, Appendix B) was based on studies dealing with the general use of the wavelet transform to extract coherent structures from turbulent time traces (Collineau and Brunet, 1993a, b) and using results of some preliminary studies (Handorf and Foken, 1997b; Heinz et al., 1999). However, the software tool which was developed as a principal objective of this thesis enhances and expands the named studies in many aspects, such as (i) its applicability to arbitrary turbulence observations under varying environmental conditions, (ii) its skilful use of different wavelet functions dependent on their specific mathematical properties, (iii) the application of a wavelet low-pass filter to separate high-frequency stochastic turbulence from low-frequency coherent structures, (iv) the opportunity for an automated analysis in a quasi-online mode during field measurements, (v) its scale-specific detection of individual coherent structures in time series depending on the flux direction, and (vi) the determination of scale-specific flux contributions of coherent structures and their corresponding ejection and sweep phases using the conditional sampling technique. In addition, the software tool was developed and written in a new program environment from scratch.

The method of detection (Thomas and Foken, 2005b, Appendix B) starts with the preparation of the time series. In includes an algorithm to remove spikes equivalent to the algorithm reported by Vickers and Mahrt (1997) using adapted criteria, a rotation of the wind vector according to the streamlines of the mean flow at the site using the Planar-fit rotation algorithm (Wilczak et al., 2001), temporal shifting of scalar time series to account for delays in data recording and spatial sensor separation, block averaging of the data to reduce computation time, and a normalization procedure. In addition, the time series are extended by zero-padding in order to prevent border effects and to enlarge the range of event duration scales for the spectral analysis, and are then filtered to remove the fluctuations emerging from stochastic turbulence by a low-pass wavelet filter using a biorthogonal set of wavelet functions. This filter requires the definition of a threshold value for the critical filter frequency separating the high-frequency stochastic turbulence from the low-frequent coherent structures. This threshold value was chosen in agreement with similar studies (Brunet and Collineau, 1994; Chen and Hu, 2003; Lykossov and Wamser, 1995). The spectral analysis of the time series is the next step. The continuous wavelet transform is calculated for event durations within a range from several seconds (6 s) to some minutes (240 s) using the complex Morlet wavelet function as it is best located in the frequency domain. The wavelet variance spectrum is subsequently determined yielding the spectral density as a function of the event duration (frequency). The location of the first maximum in this spectrum is then determined indicating the characteristic temporal scale (event duration) for coherent structures in the time series. The detection of all individual coherent structures in the time series is then performed as the following step. For this purpose, another wavelet transform is calculated but at the prior determined characteristic temporal scale of coherent structures only using the Mexican hat wavelet function as its resulting wavelet coefficients exhibit a zero-crossing at

the detection moment of an individual coherent structure. The introduction of specific criteria for the direction of the change in sign at the zero-crossing for each time series (Thomas and Foken, 2005b, Appendix B, Tab. 2) enables the method to process arbitrary time series under varying environmental conditions. The number of detected zero-crossings corresponds to the number of coherent structures. In the last step, the flux contribution of coherent structures is determined deploying the conditional sampling technique (Antonia, 1981) with a detailed description given in Thomas and Foken (2005c, Appendix E). For this purpose, subsamples each with the length of the characteristic temporal scale of coherent structures are taken at all the detection moments of coherent structures in a time series. The mean coherent structure is determined by superimposing the individual subsamples. A triple decomposition of the turbulent variables (Antonia et al., 1987; Bergström and Högström, 1989) into a mean value, a low-frequency and a high-frequency fluctuating part is then applied. The contribution of the coherent structures to the specific vertical turbulent flux is then given as the cross-product of the mean coherent structure in the vertical wind velocity and the mean coherent structures in the specific variable.
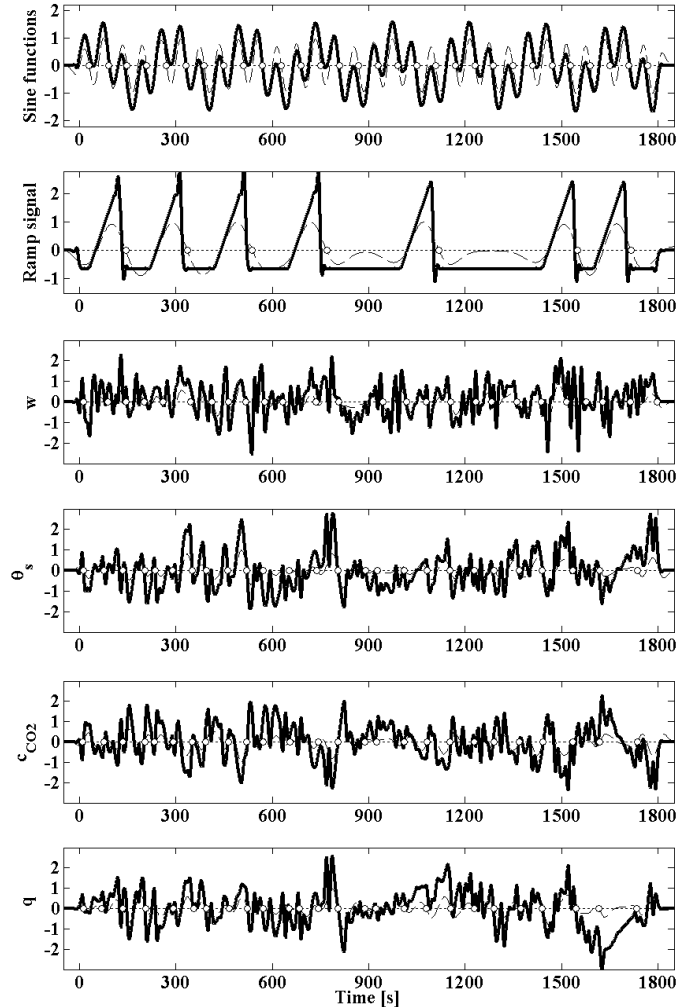
Fig. 1: Detected coherent structures (open circles) in the normalized and low-pass filtered time series of artificial signals (sine function, ramp signals) and real turbulent time series of the vertical wind velocity w, the sonic temperature θ_s, the carbon dioxide concentration c_{CO2} and the water vapour concentration q collected during WALDATEM-2003 on June 24, 2003, 13:00 – 13:30 CET (Figure taken from Thomas and Foken, 2005b, Appendix B, Fig. 4)

An example for the application of this method to real turbulent time series obtained during WALDATEM-2003 and to some artificial signals is given in Fig. 1. The method of detection is sensitive to the sharp localised gradients of the signal occurring at the transition of the ejection to the sweep phase of coherent structures. The detected coherent structures in the scalar variables of sonic temperature, carbon dioxide and water vapour occur almost simultaneously, whereas the moments of detected coherent structures in the vertical velocity slightly precede those of the scalar variables. Fig. 2 presents an example for the conditionally sampled and averaged superimposed coherent structures for the flux determination. It becomes evident that the triangle-like shape of the coherent structures in the horizontal and vertical wind velocity is in contrast to the ramp-like shape of the coherent structures in the scalar traces. The flux contribution of the ejection phase (negative times in the subfigures e-h) exceeds that of the sweep phase (positive times in the subfigures e-h). In summary, the method of detection was found to extract the coherent structures in all vector and scalar time series reliably at their characteristic temporal scale taking into account the changing direction of the vertical scalar fluxes during the diurnal course.
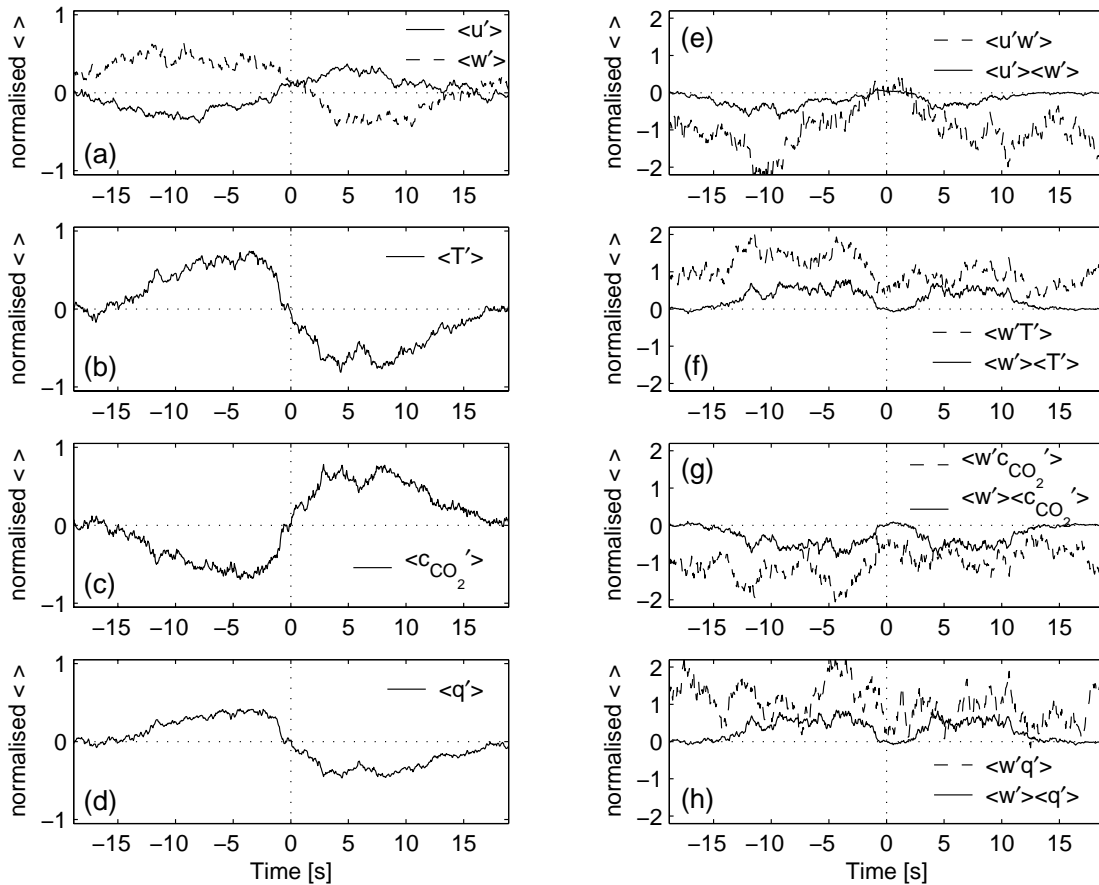
Fig. 2: Normalised superimposed conditional averages < > of (a) - (d) horizontal wind velocity u, vertical wind velocity w, sonic temperature T, carbon dioxide concentration c_{CO2} and water vapour concentration q and (e) - (h) corresponding cross-products for the flux determination of real turbulent time series during WALDATEM-2003 on June 25, 2003, 13:00 - 13:30 CET. The total number of detected coherent structures is 46 and the characteristic temporal scale is 19 s (Figure taken from Thomas and Foken, 2005c, Appendix E, Fig. 2).

3.2 Dynamical characteristics

Thomas and Foken (2005a, Appendix D) reported about the results on the mean temporal scales of coherent structures during the WALDATEM-2003 experiment (Fig. 3). For the vertical wind velocity, a consistent pattern in variation with height becomes apparent for all wind directions. The coherent structures above the forest are generally shorter in time than those within the forest. The characteristic temporal scales of coherent structures in the vertical wind velocity above the canopy ranges between 20 s and 22 s. The extension of the temporal scales at the lowest level within the canopy compared to the uppermost level above the canopy is approximately 18 %. The absolute values of temporal scales of coherent structures in the vertical wind velocity were found to show an insignificant variation with the wind direction. In contrast, the temporal scales of coherent structures in the horizontal wind velocity show a pattern which is opposite to that in the vertical wind velocity. For this variable, the coherent structures are much shorter within the canopy than above. The magnitude of the reduction for the temporal scales depends on the wind direction (W sector 23 %, N sector 30 %, and SE sector 14 %). The absolute values of the temporal scales of coherent structures in the horizontal wind were found to dependent on the wind direction. Coherent structures are shorter for flows coming from the SE sector (approximately 30 s) than from the W and N sector (both approximately 35 s). As the temporal scales of coherent structures within the canopy enlarge in the vertical wind velocity and diminish in the horizontal wind velocity, the canopy enhances the symmetry of coherent structures.
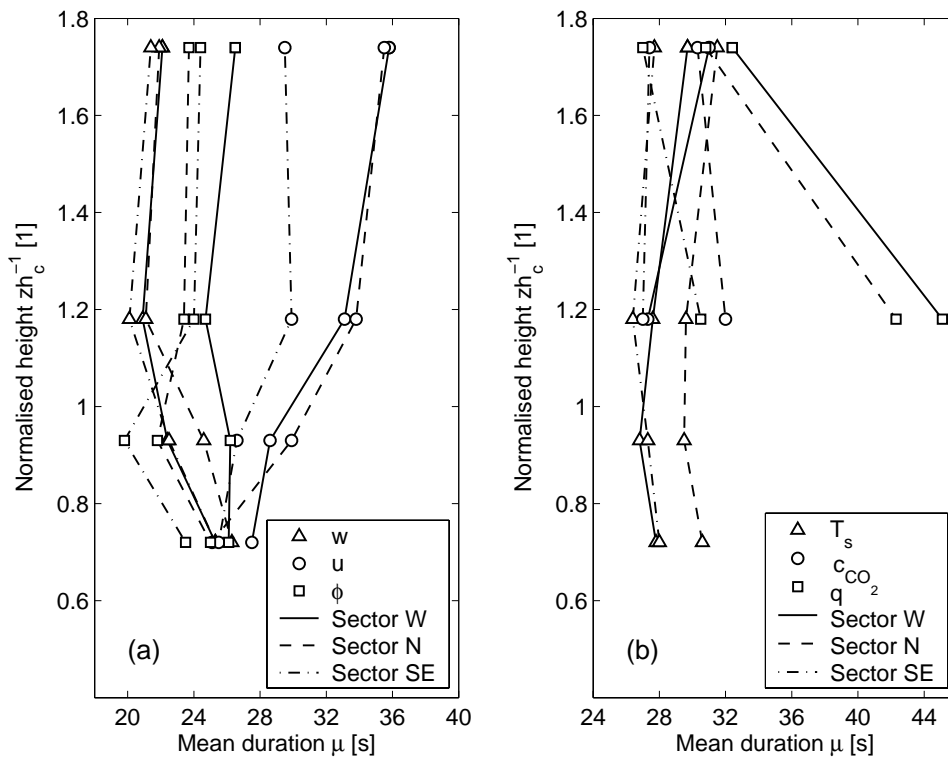
Fig. 3: Mean characteristic temporal scales of coherent structures as a function of normalized height zh_c^{-1} (z: geometrical height above ground, h_c: mean canopy height) and wind direction for (a) vertical wind velocity w, horizontal wind velocity u, wind direction ϕ and (b) sonic temperature T_s, carbon dioxide con-centration c_{CO2} and water vapour concentration q for the entire WALDATEM-2003 dataset. The wind directions were combined in wind direction sectors: Sector W (190° to 310°), Sector N (310° to 60°) and Sector SE (60° to 190°) (Figure taken from Thomas and Foken, 2005a, Appendix D, Fig. 2).

This observation results from the flow resistance exerted on the flow by the roughness elements such as the foliage, the branches and the trunks of the trees. This resistance is greater in the horizontal direction than in the vertical direction. The temporal scales of coherent structures in the wind direction do not show a discernable variation with height or wind direction. The results in the N and SE sector close to the canopy top are assumed to be influenced by waving branches close to the sonic anemometer at higher wind speeds. The mean temporal scales of coherent structures in the scalar variables show almost no variation with height, but with wind direction. For the sonic temperature, the carbon dioxide and the water vapour, the shortest coherent structures were consistently found for flows coming from the SE and W sector. It must be noted that the concentration measurements of carbon dioxide and water vapour at the level closer to the canopy were performed using a closed-path gas analyser. At this observation level, the temporal scales for the water vapour largely departure from those of the other variables and observation heights. Therefore, one must conclude that the use of the closed-path gas analyser leads to a smearing of individual coherent structures in the water vapour traces and thus cannot be recommended for studies focusing on the temporal scales of coherent structures. The smearing of smaller flow structures towards larger ones and the attenuation of the turbulent fluctuations were also observed by previous studies (e.g. Lenschow and Raupach, 1991; Massman, 1991).

The results on the temporal scales of vector and scalar variables above and within tall vegetated canopies available in literature are poor. Most of the studies either limit their variables to sonic temperature and vertical wind velocity only or present instantaneous pictures of the statistics due to small datasets. Collineau and Brunet (1993b) and Gao et al. (1989) reported about temporal scales of coherent structures in tall vegetated canopies using some 30-min intervals. With decreasing height, the authors also observed a decrease of the temporal scales of coherent structures in the horizontal wind velocity, and an increase for those in the vertical wind velocity. No variation was found for those in the scalar variables. However, the symmetry in the horizontal and vertical temporal scales of coherent structures they observed differs from the statistically robust results of the WALDATEM-2003 data.

The most likely explanation for these deviations are the different surface conditions of the topography and the canopy structure both affecting the turbulent flow in the proximity to the rough plant canopy. The topography at the site of the WALDATEM-2003 experiment is different for the three prevailing wind direction sectors West (190˚ to 310˚), North (310˚ to 60˚) and Southeast (60˚ to 190˚). The N sector is characterised by flows approaching from down a valley coming up the mountain ridge, on which the experimental site is located. As the site is located beyond the uppermost part of the ridge, the flow is tilted downward in the direct proximity to the site. The average slope of the terrain where the flow is directed upward is +5.1˚ within this sector. The flow within the SE sector is channelled between two shallow mountains. The elevation of the terrain within this sector increases homogeneously towards the site at an average slope of +2.4˚. In the W sector the winds come from a valley up the mountain ridge at an average slope of +5.0˚. Upstream close to the site, the slope of the terrain reduces to approximately +1.3˚. Thomas and Foken (2005a, Appendix D) demonstrated the influence of the varying terrain on the flow by plotting characteristic indicators of the mean wind profile such as the aerodynamic canopy height (Fig. 4) and the canopy shear length scale L_s (Fig. 5) as a function of the wind direction. The aerodynamic canopy height is defined as the height of the inflection point above ground in the vertical profile of the mean horizontal

wind velocity. The height of the inflection point is a central parameter for the vertical wind shear as it depicts the height in which the flow instabilities emerge (Raupach et al., 1996). The canopy shear length scale L_s is defined as the ratio of the mean horizontal wind velocity to its vertical gradient both measured at the canopy top (Raupach et al., 1989; 1996). Hence, it also embodies a central parameter of the shear flow close to the vegetation. The aerodynamic canopy height was found to show a large dependence on the wind direction. The individual values of the aerodynamic canopy height were observed to scatter approximately 20 % around the visually determined canopy height. The scatter around the mean aerodynamic canopy height can be addressed mainly to natural heterogeneity of the wind profile due to canopy heterogeneity and the modifying effect of the atmospheric stability on the wind profile. The latter was found to be dominant in case of winds coming from the SE and N sector, whereas no discernable effect was observed for the W sector. The canopy shear length scale L_s also depends on the wind direction (Fig. 5). Within the N sector, it varies in correspondence to turning winds. The SE sector is characterized by fairly constant values. The canopy shear length scale exhibits its maximum in the W sector and shows a discernable pattern dependent on the wind direction. In summary, these findings give strong support to the dominant influence of the surface conditions of the terrain predominantly controlling the properties of the canopy flow.
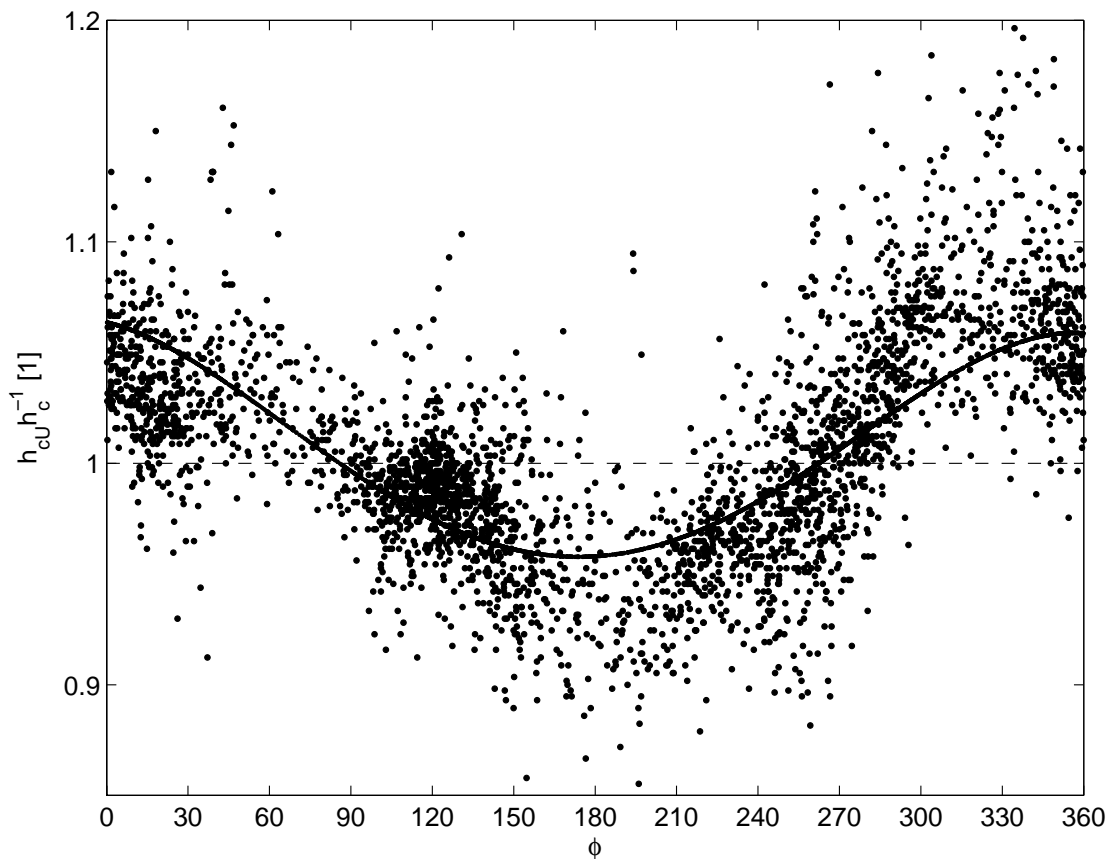
Fig. 4: Aerodynamic canopy height h_{cU} normalised by the visually estimated canopy height $h_c = 19$ m as a function of wind direction ϕ for the entire WALDATEM-2003 dataset; the thick line represents the fitted mean aerodynamic canopy height (Figure taken from Thomas and Foken, 2005a, Appendix D, Fig. 4).
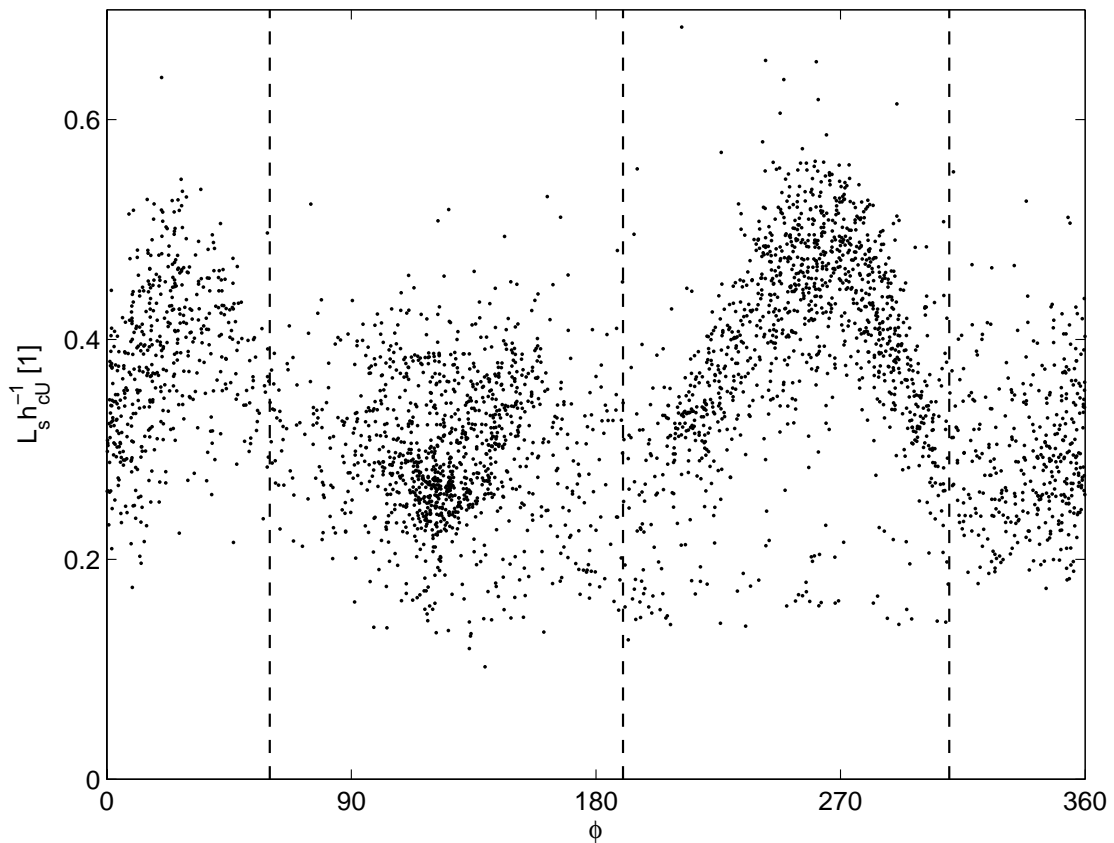
Fig. 5: Canopy shear length scale L_s according to the canopy mixing-layer analogy (Raupach et al., 1989; 1996) normalized by the aerodynamic canopy height h_{cU} as function of the wind direction ϕ for the WALDATEM-2003 data. The borders of the three wind direction sectors (Sector W: 190° to 310°, Sector N: 310° to 60°, Sector SE: 60° to 190°) are marked with dashed lines (Figure taken from Thomas and Foken, 2005a, Appendix D, Fig. 5b).

The effects of the larger-scale topography on the wind profile in the lower atmospheric boundary layer were investigated by Mayer (2005) during the WALDATEM-2003 experiment. The findings of this diploma thesis which was partly supervised in the course of this dissertation also evidence a large influence of the terrain on the flow up to a height of approximately 600 m above ground for the three prevailing wind direction sectors. In summary, it gives strong support to the significant influence of the terrain which was observed for the flow close the canopy.

Zhang et al. (2005, Appendix G) investigated the effect of horizontal heterogeneity of the canopy on the turbulent flow in an area where a large clearcut was made. This clearcut was made in a forest which was previously homogeneous on larger spatial scales of several kilometers. The spectral analysis of the time series collected in approximately 500 m horizontal distance to the clearcut was performed using the wavelet software tool. For flows coming from the clearcut, the superimposed spectra of the vertical wind velocity consistently show an additional significant peak at around 226 s event duration (Fig. 6a). This peak was not observed for winds coming from the homogeneous part of the forest (Fig. 6b). The large-scale heterogeneity of the clearcut thus induced additional turbulent flow structures which have large characteristic temporal scales. Typically, these temporal scales exceed those of the coherent structures observed in the direct proximity to the canopy (Fig. 3).
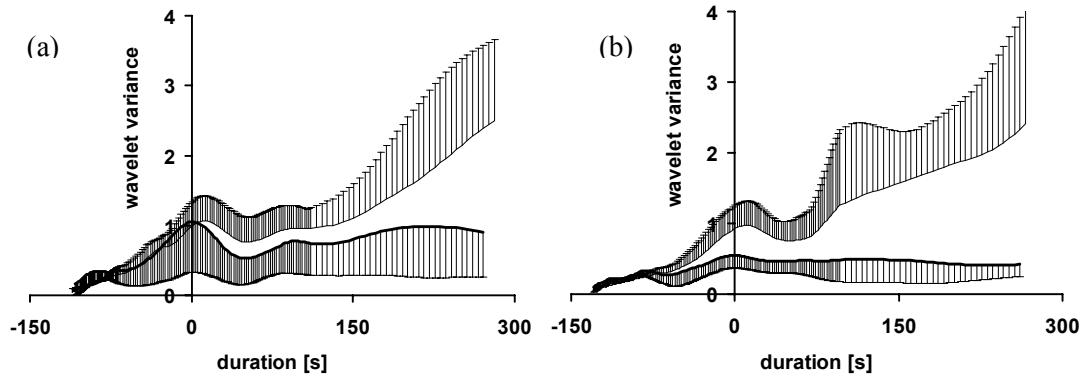
Fig. 6: Superimposed wavelet variance spectra ($10^9[m^2s^{-2}]$, $10^9[K^2]$) of the sonic temperature (upper graph) and of the vertical wind velocity (lower graph) for (a) winds coming from a large horizontal heterogeneity of the canopy (clearcut) and (b) from the fairly homogeneous forest during the experiment in Gainesville, Florida in 2000. Single spectra were centered at the origin of the x-axis in (a) at 128 s ± 32 s for the vertical wind velocity and at 140 s ± 28 s for the sonic temperature and in (b) at 144 s ± 15 s for the vertical wind velocity and at 153 s ± 22 s for the sonic temperature (Figure taken from Zhang et al., 2005, Appendix G, Fig. 2b, a).

Thomas and Foken (2005a, Appendix D) further analysed the dynamic characteristics of coherent structures by applying the canopy mixing-layer analogy (Raupach et al., 1989; 1996) to the WALDATEM-2003 data. This theoretical concept predicts the streamwise spatial spacing between adjacent coherent structures Λ_x as a linear function of the canopy shear scale L_s at the slope m ($\Lambda_x = m \cdot L_s$) and predicts m to be in the range of 7 to 10. Fig. 7 presents the derived mean ratios m for the WALDATEM-2003 dataset. The vertical profiles show a consistent pattern for the observed vector and scalar variables dependent on the wind direction. In the SE sector, the mean ratio m decreases with decreasing height. The absolute values were found to range within 12 to 35 and are much larger than in the other sectors. In the W sector, the ratios m are constant in height and range within 10 to 15 depending on the observed variable. In the N sector, the ratios m are constant above the canopy (8 to 12) and exceed those within the canopy (3 to 8). The results are in agreement with the prediction of Raupach et al. (1996) for coherent structures in the active turbulence represented by the vertical wind velocity for the N and W sector above the canopy and in the sonic temperature for the N sector. The other variables were found to exhibit large departures from the prediction. These departures could be addressed to the influence of the topography and the structure of the canopy on the flow by altering the wind profile (Thomas and Foken, 2005a, Appendix D). The SE sector shows the largest departures from the theory where the vertical wind shear was found to be larger than in the N and W sector. The most likely explanation for the large vertical wind shear in the SE sector is the compression of the streamlines due to the shallow mountains. These flow obstacles are close to the site and the flow has not fully adapted to the new surface conditions when it reaches the site. The ratios m which are constant in height for the W sector point to the fact that the streamwise spacing of coherent structures is not altered by the drag of the canopy in this sector. Here, the vertical wind shear was found to be smaller in comparison to the other sectors. In the N sector, where the ratios m were observed to be in general agreement for most of the observed variables, the flow is assumed to be affected by the shallow elevated part of the ridge which is located upstream to the site.
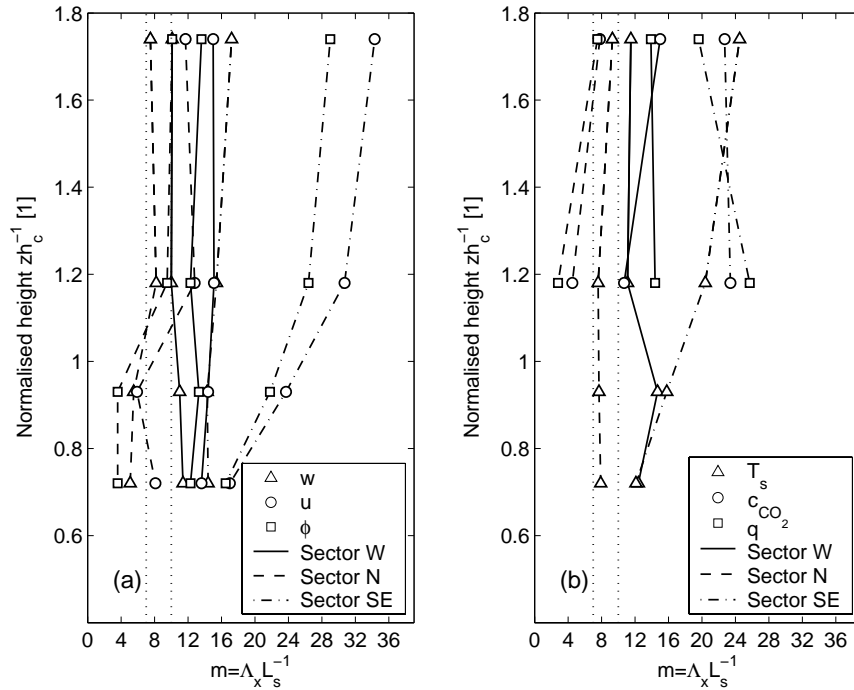
Fig. 7: Vertical profile of the ratio $m = \Lambda_x L_s^{-1}$ (where Λ_x is the spatial spacing between adjacent coherent structures and L_s the canopy shear length scale at the canopy top) according to the canopy mixing-layer analogy as a function of wind direction sector for (a) vertical wind velocity w, horizontal wind velocity u, wind direction f and (b) sonic temperature T_s, carbon dioxide concentration c_{CO2} and water vapour concentration q. The prediction of m = 7...10 by Raupach et al. (1996) is marked with dotted lines (Figure taken from Thomas and Foken, 2005a, Appendix D, Fig. 7).

Overflowing this elevated part, the flow is forced to reorganise with respect to the local properties of the surface resulting in a good agreement to the prediction by Raupach et al. (1996). Departures from the prediction of $m = 7\ldots10$ were reported also by Novak et al. (2000). In wind tunnel studies, the authors identified the tree density to have a modifying effect on the streamwise structures spacing leading to ratios m which also differ from the predicted range.

The properties of coherent structures in the layer well above the canopy were derived from the observation using the acoustic remote sensing system (Thomas et al., 2005, Appendix C). The derived temporal scales of coherent structures in the traces of the vertical wind velocity and the acoustic reflectivity support the results on those derived from the tower-based single-point measurements above the canopy but also give evidence to turbulent flow structures with larger temporal scales up to several minutes (220 s). Through a correlation analysis of the low-frequency part of the wavelet variance spectra corresponding to these larger turbulent flow structures, a diurnal course of their occurrence could be extracted. In Fig. 8, the variation of the correlation coefficient for the spectra of the vertical wind is plotted as a function of height and time for selected days during WALDATEM-2003. The increase of the correlation during the day could be addressed to changes in the correlation coefficients of the low-frequency part of the spectra representing temporal scales from 60 s to 240 s. The correlation of the high-frequency part of the spectra which represents temporal scales from 10 s to 60 s was observed to be high throughout the selected days showing no distinct variation with time.
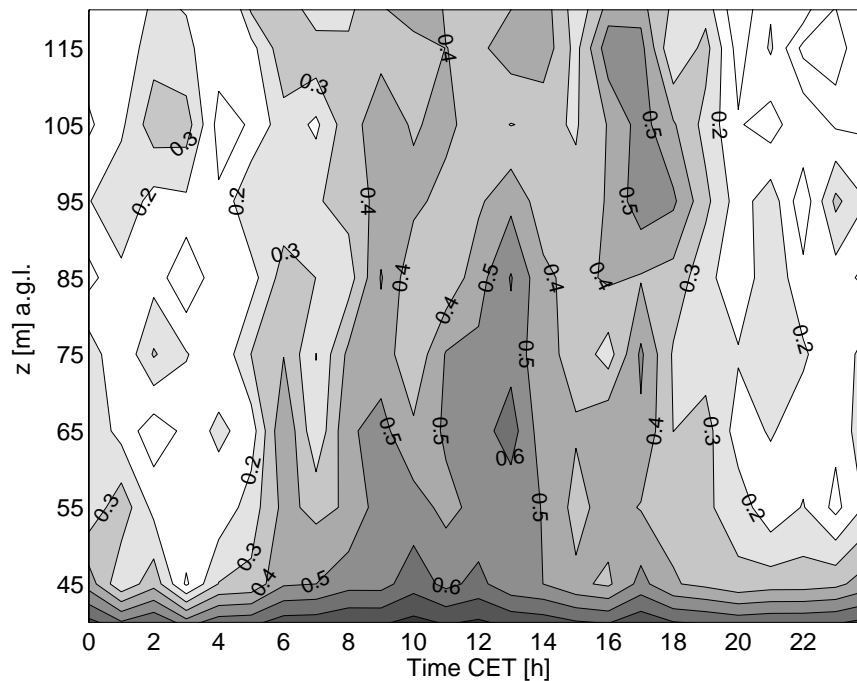
Fig. 8: Time-height cross-section of the ensemble averages of the correlation coefficient between the entire wavelet variance spectra (event durations from 10 s to 240 s) at the reference level (35 m above ground) to higher levels calculated for the vertical wind velocity for 15 selected days during WALDATEM-2003 (Figure taken from Thomas et al., 2005, Appendix C, Fig. 5a).

The different patterns of the occurrence of small and large-scale coherent structures are assumed to indicate different driving mechanisms from which the turbulent flow structures emerge. In summary, the dynamic processes and primarily the large vertical wind shear were found to be responsible for the generation of coherent structures in the proximity to the tall plant canopy.

3.3 Flux contribution of coherent structures to the overall exchange

The mean flux contribution of coherent structures to the total exchange of energy and matter between the forest and the atmosphere was investigated in Thomas and Foken (2005c, Appendix E) using the WALDATEM-2003 dataset (Fig. 9). For the momentum transfer, the mean relative flux contribution was observed to show no significant dependence on the wind direction. Above the canopy, the mean contribution of coherent structures to the total flux is approximately 16 % and slightly increases towards the canopy. Within the canopy, the mean flux contribution diminishes to approximately 13 % at the lower border of the canopy. In contrast to the momentum flux, the mean flux contributions of the scalar fluxes were found to depend on the wind direction for the observation levels above the canopy. For winds from the SE sector, the flux contribution reaches its maximum and yields about 30 % of the total flux. It is worth noting that in this sector the streamwise spacing of coherent structures was found to departure largely from the canopy mixing-layer analogy. This departure could be addressed to the large vertical wind shear present in the SE sector (Thomas and Foken, 2005a, Appendix D). For the N and W sector, the relative flux contribution to the total scalar fluxes ranges between 21 % and 27 % whereas no specific pattern in variation with height could be observed. Within the canopy, the relative flux contribution to the scalar fluxes collapses at

around 26 %. An exception was found for the N sector which is characterized by slightly higher flux contributions (approximately 29 %) near the lower border of the canopy. The intercomparison of the relative contribution of the scalar fluxes yields that coherent structures seem to contribute less to the exchange of latent heat than to those of buoyancy and carbon dioxide. However, one may question the significance of the findings for the different scalar fluxes as the individual flux contributions within a 30-min period may vary from the mean values presented in Fig. 9. These deviations result in a broadening of the derived probability density function for the entire experiment and thus increase its standard deviation (Thomas and Foken, 2005c, Appendix E, Tab. I). Therefore one must take into account that the relative flux contribution shown in Fig. 9 represents the mean for the entire WALDATEM-2003 experiment over a period of about 2.5 months. The large period introduces some scatter due to the diurnal variation and the stochastic nature of the turbulence. However, the relative contribution of coherent structures of about 16 % to the momentum flux and of about 26 % to the scalar transfer gives reliable numbers for the importance of coherent structures to the overall exchange. The assessment of quantitative flux contributions for short-term periods must be done using the corresponding individual 30-min intervals (Thomas and Foken, 2005c, Appendix E).

The results on the flux contribution of coherent structures presented in this thesis only partly agree with those reported in literature. Gao et al. (1989) reported about relative flux contributions of coherent structures to the momentum and the sensible heat exchange in the order of 60 % to 70 %. Their findings exceed those presented in Fig. 9 by a factor of approximately three. One may suspect their detection method to be responsible for the disagreement as they visually selected the most apparent ramps in smoothed time series. This procedure introduces subjectivity in the detection process to some extent. A priori, the comparison with the WALDATEM-2003 dataset is difficult as Gao et al. (1989) analysed a single 30-min interval only. Bergström and Högström (1989) reported about relative flux contributions of coherent structures to the transfers of momentum, sensible heat and latent heat of approximately 90 %. These results exceed those obtained for the WALDATEM-2003 data by a factor of four. Again, the comparison is complicated by their method of analysis as they systematically excluded periods without coherent structures. This procedure results in a systematical overestimation of the flux contribution of coherent structures. Antonia et al. (1987) and Collineau and Brunet (1993b) investigated the turbulent flow under laboratory conditions and above a pine forest. They derived relative flux contributions of coherent structures of about 30 % to the momentum transfer and of about 40 % to the sensible heat flux. Their results are thus similar to those derived in this thesis. One must note that the researchers also used the triple decomposition of the turbulent variables and the conditional sampling technique as applied in this thesis. The choice of a uniform method of detection and analysis may thus facilitate the comparability of relative flux contributions of coherent structures. Further, the results of Antonia et al. (1987) and Collineau and Brunet (1993b) also point to a greater efficiency of coherent structures in transporting scalars than momentum. In contrast to these studies, the contribution of coherent structures to the momentum transfer was found to decrease in the canopy for the WALDATEM-2003 data. However, one must note that the moderate dense spruce canopy at the WALDATEM-2003 site is a very efficient sink for momentum. It absorbs approximately 80 % of the momentum transported down into the canopy within the upper part of the trees where the main foliage is concentrated. The observed difference may thus be addressed to differences in the structure of the canopy.
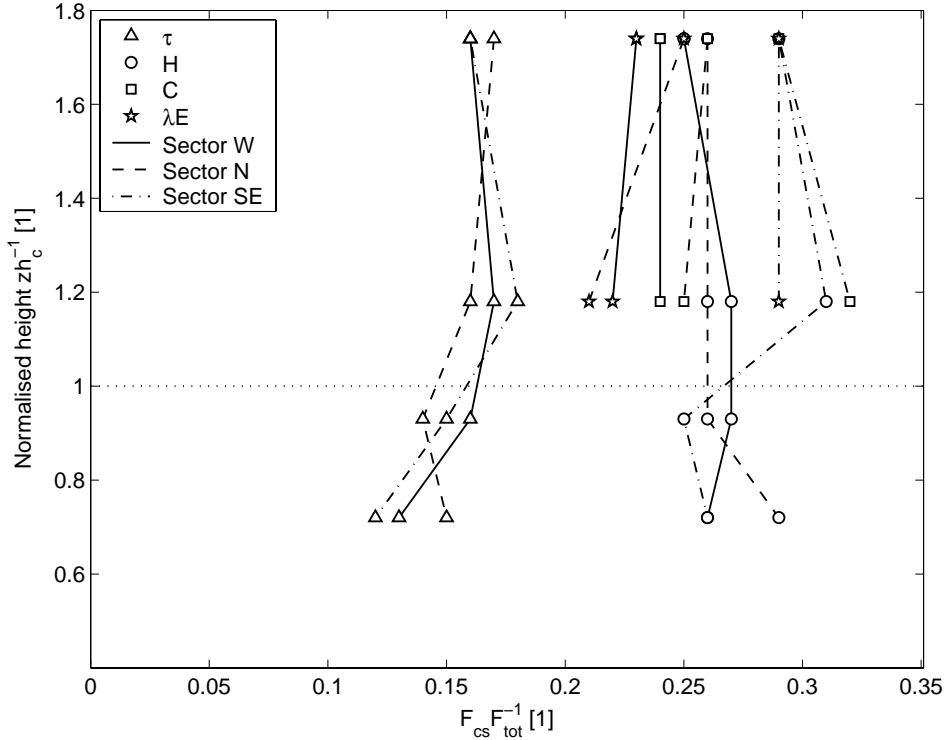
Fig. 9: Mean relative flux contribution of coherent structures to the total flux $F_{cs}F_{tot}^{-1}$ as a function of normalized height zh_c^{-1} (z: geometrical height above ground, h_c: mean canopy height) and wind direction (Sector W: 190° to 310°, Sector N: 310° to 60°, Sector SE: 60° to 190°) for momentum τ, buoyancy H, carbon dioxide C and latent heat λE (Figure taken from Thomas and Foken, 2005c, Appendix E, Fig. 3).

3.4 Implications for the exchange of energy and matter in tall canopies

The implications of coherent structures for the total exchange of energy and matter is derived from the physical picture one gets from the specific analysis of the ejection and sweep phases of coherent structures along the vertical profile in tall-vegetated canopies (Thomas and Foken, 2005c, Appendix E). This physical picture shows an increasing importance of the sweep phases to the exchange with decreasing distance to the canopy during daytime. It follows that the importance of the ejection phases increases with increasing distance to the canopy. These findings compare well to the results reported by other authors (e.g. Raupach, 1981; Shaw et al., 1983; Wallace et al., 1972). During nighttime, only the strong sweep phases significantly contribute to the exchange of energy and matter between the atmosphere and the canopy, while the contribution of the ejection phases are negligible. Based on this physical picture and on the information about how deep coherent structures penetrate into the canopy, the extension of the spatial volume which is controlled by the exchange through coherent structures can be estimated under differing dynamic and diabatic conditions. Hence, the analysis of coherent structures reveals qualitative information about the situation of the total exchange in a canopy. A classification scheme of typical exchange regimes was derived from the analysis of the sweep and ejection phases of coherent structures along the vertical profile, which covered the subcanopy, the canopy and the layer above the canopy,. The subcanopy is defined as the layer below the height where the mean foliage of the canopy is concentrated. In the following, a description outlining the principal characteristics of the five individual exchange regimes is presented according to Thomas and Foken (2005c, Appendix E).

Wave motion (Wa): The flow above the canopy is dominated by internal gravity waves. Internal gravity waves were detected by comparing the characteristic temporal scale of coherent structures derived from the spectral analysis to the Brunt-Vaisala frequency (Thomas and Foken, 2005a, Appendix D). During the presence of interval gravity waves the atmosphere is decoupled from the canopy and no significant exchange takes place.

Decoupled canopy (Dc): The atmosphere is decoupled from the canopy and subcanopy. Even strong sweeps of coherent structures do not penetrate into the canopy and thus do not force an exchange of energy and matter.

Decoupled subcanopy (Ds): The atmosphere is coupled with the canopy to some extent, but not coupled with the subcanopy. Sweeps of coherent structures penetrate from the atmosphere down into the canopy but do not reach the lower levels of it.

Coupled subcanopy by sweeps (Cs): The strong sweep phases of coherent structures force a coupling of the atmosphere with the canopy and the subcanopy. The importance of the ejection phases is negligible. This exchange state is typically assigned in transitions from Ds to C or vice versa.

Fully coupled canopy (C): The atmosphere, the canopy, and the subcanopy are fully coupled. This state is indicated by significant flux contributions of both the sweep and the ejection phases of coherent structures.

An example for the application of the classification scheme to micrometeorological observations during 4 days of the WALDATEM-2003 experiment is presented in Fig. 10. During the night, persistent internal gravity waves were detected. Their emergence was facilitated by the strong radiative cooling indicated by the large negative buoyancy fluxes and the winds coming from the SE sector. In this sector, a shallow mountain facilitates the generation of internal gravity waves downstream of it (Thomas and Foken, 2005a, Appendix D). The classification of the exchange regime (Fig. 10d) indicates a persistent decoupling of the canopy from the atmosphere assigning either Wa or Dc. During the presence of the wave motion, the relative flux contribution of coherent structures seem to increase up to 100 %, but the flux contribution represents 'pseudo' fluxes only. These 'pseudo' fluxes are mathematical artifacts resulting from the dominating wave motion affecting the shape of the signals in the vertical wind velocity and the sonic temperature. The magnitude of the 'pseudo' fluxes depends on the phase shift in the signals of the vertical wind velocity and the sonic temperature emerging from the wave motion. This phase shift of internal gravity waves in vector and scalar variables is a feature of stable boundary layers reported in literature (e.g. Stull, 1988). During daytime, the diabatic stratification was fairly unstable leading to the development of convective clouds during June 1 and June 4 in the afternoon. The first half of the days in the displayed period is characterized either by a decoupled subcanopy (Ds) or by a subcanopy which is in exchange with the atmosphere due to strong sweeps only (Cs). The fully coupled state was generally reached in the second half of the day with the exception of June 3. On this day, the exchange with the subcanopy space is limited to single 30-min intervals only. The verification of the developed classification scheme using results from other micrometeorological measurements such as isotope fluxes or fluxes of reactive scalars (e.g. nitrogen oxide, ozone and volatile organic compounds) is highly desirable and remains to be done in future investigations beyond this thesis.
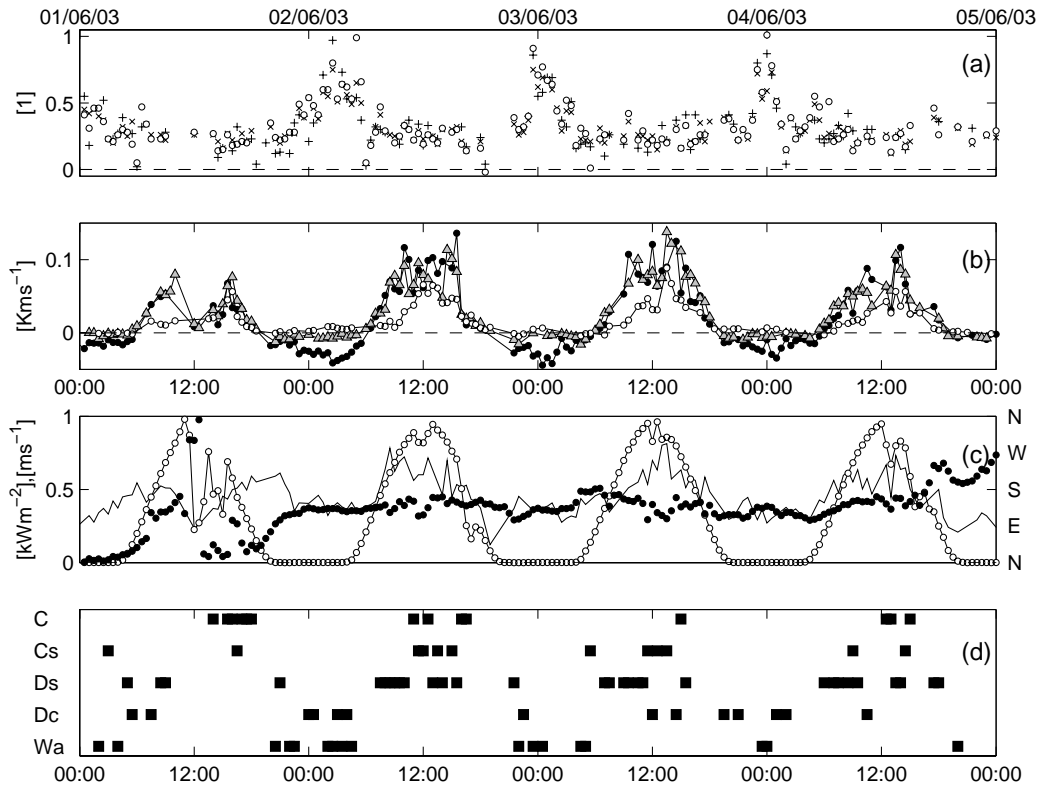
Fig. 10: Measurements and characterisation of the turbulent exchange for the period June 1 to June 4, 2003 during WALDATEM-2003: (a) relative contribution of coherent structures for the carbon dioxide flux (open circles), the buoyancy flux (crosses) and the latent heat flux (pluses) above the canopy; (b) kinematic buoyancy flux above the canopy (filled circles), at the canopy top (grey triangles) and in the subcanopy space (open circles); (c) friction velocity (solid line), incoming shortwave radiation (open circles) and wind direction (filled circles) above the canopy; (d) classification of the exchange regimes according to the scheme derived in this thesis (Figure taken from Thomas and Foken, 2005c, Appendix E, Fig. 9).

3.5 Implications for conventional flux determination methods

The impact of coherent structures on the direct flux determination method of the eddy covariance technique was investigated in Thomas and Foken (2005c, Appendix E) using a self-developed mathematical approach. The general idea behind this approach is that coherent structures may affect the fluxes derived from the eddy covariance method by altering the mean part of a turbulent signal. The mean part of a turbulent signal during the presence of coherent structures is thus assumed to be different from the mean part of a turbulent signal in the absence of coherent structures. Hence, the fluctuation which is derived by subtracting the mean part from the instantaneous signal is also assumed to be altered during the presence of coherent structures. From this follows, that the eddy covariance method may introduce some flux error if coherent structures occur. A detailed description of the approach can be found in Thomas and Foken (2005c, Appendix E).

The flux errors of the eddy covariance method were calculated using the approach described above (Fig. 11). The relative flux error for all considered fluxes generally does not exceed 4 %. The largest values are found for fluxes around zero, where absolute fluxes are negligible which results in unrealistic flux errors. The derived flux errors tend to decrease with increasing magnitude of the flux.
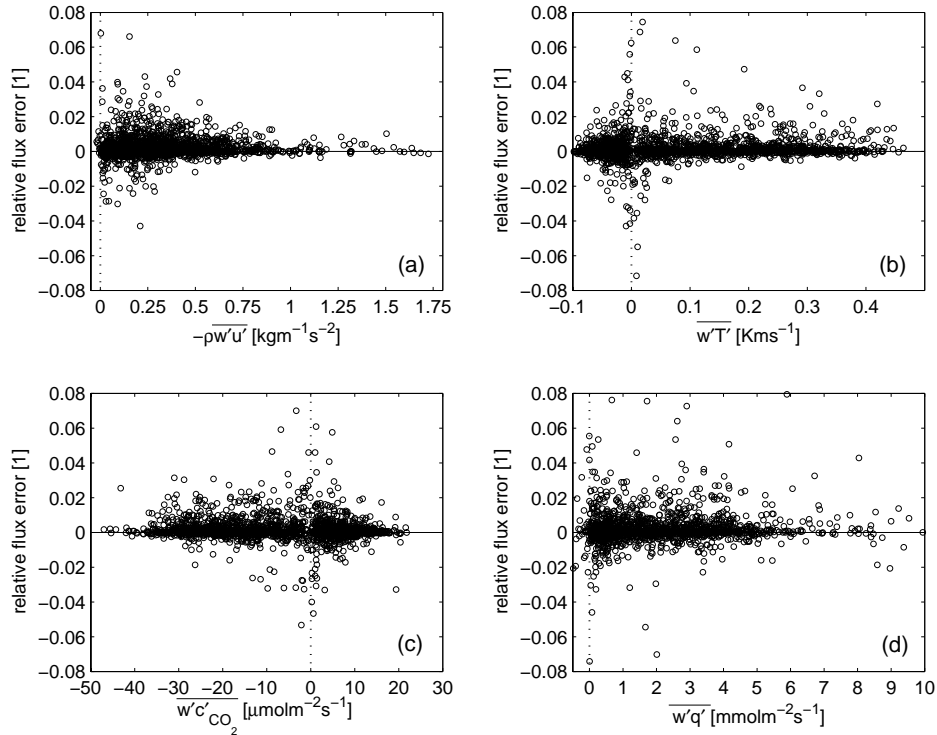
Fig. 11: Relative flux error of the conventional eddy covariance method through the occurrence of coherent structures as a function of the absolute fluxes of (a) momentum, (b) kinematic buoyancy, (c) carbon dioxide and (d) latent heat for the WALDATEM-2003 dataset. Negative (positive) values indicate an under-estimation (overestimation) of the flux using the conventional eddy covariance method (Figure taken from Thomas and Foken, 2005c, Appendix E, Fig. 4).

The displayed flux errors are independent on the relative flux contribution of coherent structures. In summary, no systematic over- or underestimation of the exchange of momentum, buoyancy, carbon dioxide and latent heat could be observed as the mean over all determined flux errors is close to zero.

The impact of coherent structures on an indirect flux determination method was investigated in Ruppert et al. (2005, Appendix G) for the relaxed eddy accumulation (REA) technique. In this study, the authors concentrated on the scalar similarity which is required for the definition of proxy scalars when using REA. The wavelet software tool was applied to the time series collected over three different surface types, and the wavelet variance spectra of the sonic temperature and the concentration of carbon dioxide and water vapour were derived. The spectra were sub-sequently split into ranges representing either small-scale flow structures such as typical coherent structures corresponding to temporal scales from 6 s to 60 s or large-scale flow structures corresponding to temporal scales beyond 60 s up to 240 s. In a last step, the correlation coefficient for the two spectral ranges between the three scalars was calculated. The spectral correlation coefficients for the small-scale flow structures were observed to be generally close to unity (Fig. 12). In contrast, the spectral correlation coefficients for the large-scale flow structures largely departure from unity and exhibit significant scatter. The spectral dissimilarity between different scalars could thus be addressed to differences in the large-scale flow structures. The large-scale flow structures do not primarily represent coherent structures emerging from the dynamic processes close to the canopy, but from other processes generating coherent structures with larger temporal scales such as those observed by the acoustic remote sensing (Thomas et al., 2005, Appendix C).
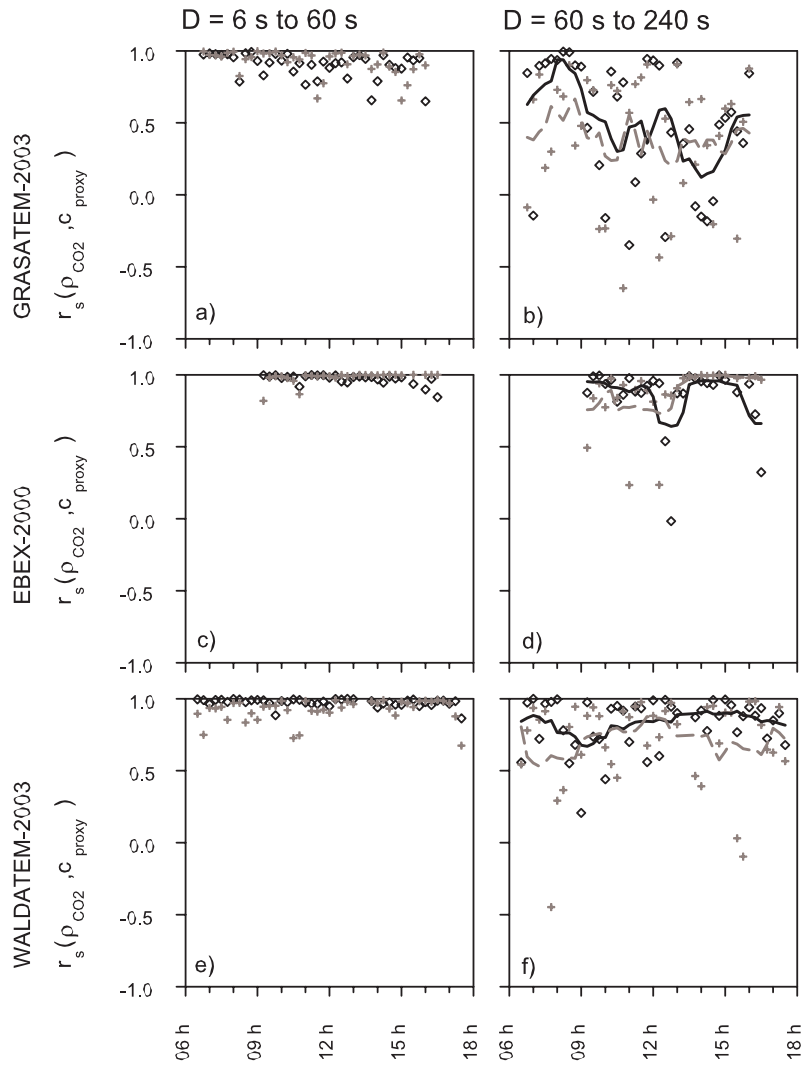
Fig. 12: Time series of the correlation coefficients for the wavelet variance spectra of carbon dioxide and acoustic temperature (diamonds, solid line) and carbon dioxide and water vapour (crosses, dashed line) for a), c), e) small-scale flow structures and b), d), e) large-scale flow structures for three different experiments. The lines depict the running mean over the individual values (Figure taken from Ruppert et al., 2005, Appendix G, Fig. 3).

The spectral similarity in the large-scale range shows a diurnal pattern (Fig. 12b, d, f). In the morning hours, the spectral correlation between carbon dioxide and sonic temperature consistently exceeds that between carbon dioxide and water vapour. For the midday period, no systematic difference can be found as the correlation is consistently high between the observed scalars. In case of the GRASATEM-2003 and EBEX-2000 data, the spectral similarity between carbon dioxide and water vapour is greater than between carbon dioxide and sonic temperature in the afternoon hours. In contrast, the spectral similarity during WALDATEM-2003 is higher between carbon dioxide and sonic temperature than that between carbon dioxide and water vapour also in the afternoon hours. Based on the exemplary analysis of the presented days, it remains unclear whether the observed pattern of the changing similarities during the day is either a systematic effect of the sink / source distribution and strengths or a more random effect of varying meteorological conditions such as changing cloud cover. However, one must expect differences and changes in scalar

similarity above both homogeneous and tall-vegetated heterogeneous surfaces as similar patterns were observed also for other days during the experiments. Summarising, the developed wavelet tool was successful in identifying processes which influence the scalar similarity and reveal useful information about reasonable proxy scalars for indirect flux determination methods such as the REA.

4 Conclusions

The detection and analysis algorithms implemented in the wavelet analysis tool proved to be applicable successfully for the assessment of long-term observations of coherent structures. In particular, the spectral analysis performed using the Morlet wavelet function yields reliable and reasonable results for the temporal scale of the flow patterns of interest, which are contained in the time series, and therefore allows a scale-specific analysis. The integration of routines which adapt the detection process for coherent structures in the time series dependent on the environmental conditions enables this software to process arbitrary turbulent time series under varying environmental conditions. This feature makes it a powerful tool for researchers who are interested in the identification of physical processes in ecosystems.

From the analysis of the dynamic properties of coherent structures above and within tall vegetated canopies, one arrives at the conclusion that coherent structures basically emerge from the dynamic instabilities caused by the large vertical wind shear of the inflected wind profile at canopy top. Hence, the occurrence of coherent structures is mainly attributed to dynamic processes in the proximity of tall-vegetated canopies. However, the observations of coherent structures well above the canopy with the aid of acoustic remote sensing provide evidence that also diabatic processes have an influence on the generation and the dynamic properties of coherent structures. This influence increases with the transition of the turbulent state of the atmosphere towards convection. The results also indicate that the presence of coherent structures in the atmospheric boundary layer is vertically limited to the layer adjacent to the plant canopy with its upper border typically not exceeding five times the canopy height.

The terrain exerts a dominating influence on the dynamic properties of coherent structures through a modification of the wind profile. Thus, dynamic properties of coherent structures such as temporal scales, streamwise structure spacing and flux contribution must be discussed individually in the context of the larger-scale topography and the canopy structure at the specific site. These conditions may change with the wind direction at a specific site. The generation of internal gravity waves downwind of flow obstacles strengthens the necessity to take the terrain into account when studying atmospheric turbulence in heterogeneous terrain such as tall-vegetated canopies. The canopy mixing-layer analogy was found to hold for the active part of turbulence only which is represented best by the vertical wind velocity. In general, large departures from this theoretical concept were observed for non-active turbulence represented by the horizontal wind velocity and scalars such as sonic temperature, and concentration of carbon dioxide and water vapour. The use of the canopy mixing-layer analogy for the identification and interpretation of physical processes in canopies is therefore restricted to coherent structures in the vertical wind only. The horizontal heterogeneity of the terrain facilitates the generation of large turbulent flow structures which may have an effect on turbulent fluxes. The temporal scales of these larger flow structures exceed the temporal scales of typical coherent structures by far.

Coherent structures significantly contribute to the overall turbulent exchange between the canopy and the atmosphere and therefore need to be taken into consideration by researchers studying turbulent fluxes in vegetated ecosystems. For the turbulent exchange above tall-vegetated canopies, coherent structures gain in importance with increasing vertical wind shear and decreasing duration of coherent structures. As these conditions largely depend on the terrain and the canopy structure as mentioned above, exchange processes must be considered

in the spatial context of the site. In general, coherent structures are more efficient in transporting scalar quantities than momentum. The analysis of the flux contributions of the sweep and ejection phases of coherent structures along a vertical profile allows for inferring the volume of the canopy which communicates with the overlying atmosphere. The derived classification scheme of characteristic exchanges regimes between the canopy and the atmosphere was proven to reproduce the diurnal course of exchange conditions in a reasonable manner. It thus allows a reliable qualitative characterisation of the exchange regime in tall-vegetated canopies. Its future application therefore promises to reveal characteristic spatial and temporal patterns in the turbulent exchange and will help to select long-term observations for specific situations of interest.

The eddy covariance method encompasses the entire turbulent fluxes contributed by the high-frequency stochastic turbulence and by the low-frequency organized coherent structures. Hence, the eddy covariance method is also applicable above heterogeneous surfaces such as tall-vegetated canopies. This conclusion approves the eddy covariance method for the derivation of long-term budgets of turbulent fluxes such as evapotranspiration, sensible heat and carbon dioxide above forested ecosystems. However, the influence of coherent structures on short-term budgets calculated using the eddy covariance method may introduce some flux error which needs to be accounted for. The developed detection and analysis software tool is able to identify such flux errors and is therefore recommended as an additional quality control tool for eddy covariance measurements. Based on the results on scalar similarity for the eddy accumulation method, one expects the coherent structures and larger-scale flow structures to have a significant impact on the variability of the spectral similarity between different scalars. As the spectral similarity may change with time or dependent on the underlying physical processes, the assumption of scalar similarity must be rechecked in the presence of coherent structures and larger-scale flow structures. This conclusion necessitates reconsidering e.g. the use of generalized temperature spectra for spectral corrections of other scalar turbulent fluxes in case of the eddy covariance method and the use of proxy scalars for the relaxed eddy accumulation technique.

References

Antonia, R.A., 1981. Conditional sampling in turbulence measurements. Ann. Rev. Fluid Mech., 13: 131-156.

Antonia, R.A., Browne, L.W.B., Bisset, D.K. and Fulachier, L., 1987. A description of the organized motion in the turbulent far wake of a cylinder at low Reynolds numbers. J. Fluid. Mech., 184: 423-444.

Aubrun, S., Koppmann, R., Leitl, B., Moellmann-Coers, M. and Schaub, A., 2005. Physical modelling of an inhomogeneous finite forest area in a wind tunnel - Comparison with field data and Lagrangian dispersion calculations. Agric. For. Meteorol.: in press.

Bergström, H. and Högström, U., 1989. Turbulent exchange above a pine forest. II. Organized structures. Boundary-Layer Meteorol., 49: 231-263.

Beyrich, F. (Ed.), 2004. Verdunstung über einer heterogenen Landoberfläche: Das LITFASS-2003 Experiment - ein Bericht. Deutscher Wetterdienst, Geschäftsbereich Forschung und Entwicklung, Arbeitsergebnisse, No. 79: 100 pp.

Bisset, D.K., Antonia, R.A. and Browne, L.W.B., 1990. Spatial organisation of large structures in the turbulent far wake of a cylinder. J. Fluid. Mech., 162: 389-413.

Blackwelder, R.F., 1987. Coherent structures associated with turbulent transport. In: M. Hirata and N. Kasagi (Eds.), Transport Phenomena in Turbulent Flows: Theory, Experiment and Numerical Simulation. Hemisphere Publishing Corporation, Washington, pp. 69-88.

Blackwelder, R.F. and Kaplan, R.E., 1976. On the wall structure of the turbulent boundary layer. J. Fluid. Mech., 76: 89-112.

Bogard, D.G. and Tiederman, W.G., 1986. Burst detection with single-point velocity measurements. J. Fluid. Mech., 162: 389-413.

Brunet, Y. and Collineau, S., 1994. Wavelet analysis of diurnal and nocturnal turbulence above a maize canopy. In: E. Foufoula-Georgiou and P. Kumar (Eds.), Wavelets in Geophysics. Wavelet Analysis and its Applications. Academic Press, San Diego, pp. 129-150.

Brunet, Y. and Irvine, M.R., 2000. The control of coherent eddies in vegetation canopies: streamwise structure spacing, canopy shear scale and atmospheric stability. Boundary-Layer Meteorol., 94: 139-163.

Businger, J.A. and Oncley, S.P., 1990. Flux measurement with conditional sampling. J. Atmos. Ocean. Technol., 7: 349-352.

Chen, H., Chen, J., Hu, F. and Zeng, Q., 2004. The coherent structure of water vapour transfer in the unstable atmospheric surface layer. Boundary-Layer Meteorol., 111: 543-552.

Chen, J. and Hu, F., 2003. Coherent structures detected in atmospheric boundary-layer turbulence using wavelet transforms at Huaihe River Basin, China. Boundary-Layer Meteorol., 107: 429-444.

Collineau, S. and Brunet, Y., 1993a. Detection of turbulent coherent motions in a forest canopy. Part I: Wavelet analysis. Boundary-Layer Meteorol., 65: 357-379.

Collineau, S. and Brunet, Y., 1993b. Detection of turbulent coherent motions in a forest canopy. Part II: Time-scales and conditional averages. Boundary-Layer Meteorol., 66: 49-73.

Finnigan, J., 2000. Turbulence in plant canopies. Ann. Rev. Fluid Mech., 32: 519-571.

Foken, T., Göckede, M., Mauder, M., Mahrt, L., Amiro, B.D. and Munger, J.W., 2004. Post-field data quality control. In: X. Lee, W.J. Massman and B. Law (Eds.), Handbook of Micrometeorology: A Guide for Surface Flux Measurements. Kluwer, Dordrecht, pp. 181-208.

Gamage, N. and Hagelberg, C., 1993. Detection and analysis of microfronts and associated coherent events using localized transforms. J. Atmos. Sci., 50: 750-756.

Gao, W., Shaw, R.H. and Paw U, K.T., 1989. Observation of organized structures in turbulent flow within and above a forest canopy. Boundary-Layer Meteorol., 47: 349-377.

Gerstberger, P., Foken, T. and Kalbitz, K., 2004. The Lehstenbach and Steinkreuz catchments in NE Bavaria, Germany. In: E. Matzner (Ed.), Biogeochemistry of Forested Catchments in a Changing Environment. Ecological Studies, No. 172. Springer, Heidelberg, pp. 15-41.

Gholz, H.L. and Clark, K.L., 2002. Energy exchange across a chronosequence of slash pine forests in Florida. Agric. For. Meteorol., 112: 87-102.

Grossmann, A., Kronland-Martinet, R. and Morlet, J., 1989. Reading and understanding continuous wavelet transforms. In: J.M. Combes, A. Grossmann and P. Tchamitchian (Eds.), Wavelets: Time-Frequency Methods and Phase Space. Springer-Verlag, New York, pp. 2-20.

Grossmann, A. and Morlet, J., 1984. Decomposition of hardy functions into square integrable wavelets of constant shape. J. Math. Anal., 15: 723-736.

Handorf, D. and Foken, T., 1997a. Analysis of turbulent structure over an Antarctic ice shelf by means of wavelet transformation, 12th Symposium on Boundary Layers and Turbulence. Am. Meteorol. Soc., Vancouver BC, Canada, pp. 245-246.

Handorf, D. and Foken, T., 1997b. Strukturanalyse der atmosphärischen Turbulenz mittels Wavelet-Verfahren zur Bestimmung der Austauschprozesse über dem antarktischem Schelfeis. Deutscher Wetterdienst, Geschäftsbereich Forschung und Entwicklung, Arbeitsergebnisse, No. 47: 49 pp.

Heinz, G., Handorf, D. and Foken, D., 1999. Strukturanalyse der atmosphärischen Turbulenz mittels Wavelet-Verfahren zur Bestimmung von Austauschprozessen über dem antarktischen Schelfeis. Arbeitsergebnisse, Universität Bayreuth, Abt. Mikrometeorologie. Print ISSN 1614-8916. No. 7: 65 pp.

Katul, G., Kuhn, G., Schieldge, J. and Hsieh, C.-I., 1997. The ejection-sweep character of scalar fluxes in the unstable surface layer. Boundary-Layer Meteorol., 83: 1-26.

Koppmann, R., 2003. Emission and chemical transformation of biogenic volatile organic compounds (ECHO), AFO-2000 Newsletter, pp. 7-10.

Kronland-Martinet, R., Morlet, J. and Grossmann, A., 1987. Analysis of sound patterns through wavelet transforms. Int. J. Pattern Recogn., 1: 273-302.

Lenschow, D.H. and Raupach, M.R., 1991. The attenuation of fluctuations in scalar concentrations through sampling tubes. J. Geophys. Res., 96: 15,259-15,268.

Lu, C.H. and Fitzjarrald, D.R., 1994. Seasonal and diurnal variations of coherent structures over a deciduous forest. Boundary-Layer Meteorol., 69: 43-69.

Lu, S.S. and Willmarth, W.W., 1973. Measurements of the structure of Reynolds stress in a turbulent boundary layer. J. Fluid. Mech., 60: 481-512.

Lykossov, V.N. and Wamser, C., 1995. Turbulence intermittency in the atmospheric surface layer over snow-covered sites. Boundary-Layer Meteorol., 72: 393-409.

Massman, W.J., 1991. The attenuation of concentration fluctuations in turbulent flow through a tube. J. Geophys. Res., 96: 15,269-15,273.

Mayer, J.-C., 2005. Characterisation of the atmospheric boundary layer in a complex terrain using Sodar-Rass. Diploma Thesis, University of Bayreuth, Bayreuth, 85 pp.

Novak, M.D., Warland, J.S., Orchansky, A.L., Kettler, R. and Green, S., 2000. Wind tunnel and field measurements of turbulent flow in forests. Part I: uniformly thinned stands. Boundary-Layer Meteorol., 95: 457-495.

Oncley, S.P., Foken, T., Vogt, R., Bernhofer, C., Kohsiek, W., Liu, H., Pitacco, A., Grantz, D., Riberio, L. and Weidinger, T., 2002. The energy balance experiment EBEX-2000, 15th Symposium on Boundary Layers and Turbulence. Am. Meteorol. Soc., Wageningen, The Netherlands, pp. 1-4.

Paw U, K.T., Brunet, Y., Collineau, S., Shaw, R.H., Maitani, T., Qiu, J. and Hipps, L., 1992. Evidence of turbulent coherent structures in and above agricultural plant canopies. Agric. For. Meteorol., 61: 55-68.

Raupach, M.R., 1981. Conditional statistics of Reynolds stress in rough-wall and smooth-wall turbulent boundary layers. J. Fluid. Mech., 108: 363-382.

Raupach, M.R., Finnigan, J.J. and Brunet, Y., 1996. Coherent eddies and turbulence in vegetation canopies: the mixing-layer analogy. Boundary-Layer Meteorol., 78: 351-382.

Raupach, M.R., Finnigan, J.J. and Brunet, Y., 1989. Coherent eddies in vegetation canopies, 4th Australasian Conference on Heat and Mass Transfer, Christchurch, New Zealand, pp. 75-90.

Ruppert, J., Thomas, C. and Foken, T., 2005. Scalar similarity for relaxed eddy accumulation methods. Boundary-Layer Meteorol.: submitted.

Shaw, R.H., 1985. On diffusive and dispersive fluxes in forest canopies. In: B.A. Hutchinson and B.B. Hicks (Eds.), The Forest-Atmosphere Interaction. Reidel Publishing Company, Dordrecht, pp. 407-419.

Shaw, R.H., Tavangar, J. and Ward, D.P., 1983. Structure of the Reynolds stress in a canopy layer. J. Clim. Appl. Meteorol., 22: 1922-1931.

Stull, R.B., 1988. An Introduction to Boundary Layer Meteorology. Kluwer Acad. Publ., Dordrecht, Boston, London, 666 pp.

Thomas, C. and Foken, T., 2005a. Coherent structures in a tall spruce canopy: temporal scales, structure spacing and terrain effects. Boundary-Layer Meteorol.: submitted.

Thomas, C. and Foken, T., 2005b. Detection of Long-term Coherent Exchange over Spruce Forest Using Wavelet Analysis. Theor. Appl. Climatol.: DOI:10.1007/s00704-004-0093-0.

Thomas, C. and Foken, T., 2005c. Flux contribution of coherent structures and its implications for the exchange of energy and matter in a tall spruce canopy. Boundary-Layer Meteorol.: submitted.

Thomas, C., Mayer, J.-C., Meixner, F.X. and Foken, T., 2005. Analysis of low-frequency turbulence above tall vegetation using a Doppler sodar. Boundary-Layer Meteorol.: submitted.

Thomas, C., Ruppert, J., Lueers, J., Schröter, J., Mayer, J.-C. and Bertolini, T., 2004. Documentation of the WALDATEM-2003 Experiment. Arbeitsergebnisse, Universität Bayreuth, Abt. Mikrometeorologie. Print ISSN 1614-8916. No. 24, 59 pp.

Turner, B.J. and Leclerc, M.Y., 1994. Conditional sampling of coherent structures in atmospheric turbulence using the wavelet transform. J. Atmos. Ocean. Technol., 11: 205-209.

Vickers, D. and Mahrt, L., 1997. Quality control and flux sampling problems for tower and aircraft data. J. Atmos. Ocean. Technol., 14: 512-526.

Wallace, J.M., Eckelmann, H. and Brodkey, R.S., 1972. The wall region in turbulent shear flow. J. Fluid. Mech., 54: 39-48.

Wichura, B., Ruppert, J., Delany, A.C., Buchmann, N. and Foken, T., 2004. Structure of carbon dioxide exchange processes above a spruce forest. In: E. Matzner (Ed.), Biogeochemistry of Forested Catchments in a Changing Environment. Ecological Studies, No. 172. Springer, Berlin, Heidelberg, pp. 161-176.

Wilczak, J.M., Oncley, S.P. and Stage, S.A., 2001. Sonic anemometer tilt correction algorithms. Boundary-Layer Meteorol., 99: 127-150.

Zhang, G., Thomas, C., Leclerc, M.Y., Karipot, A., Gholz, H.L. and Foken, T., 2005. On the effect of clearcuts on forest canopy fluxes. Theor. Appl. Climatol.: submitted.

List of appendices

Appendix A: Individual contributions to the joint publications

The publications of which this cumulative thesis consists were composed in close cooperation with other researcher. Hence, many authors contributed to the publications listed in Appendices B to G in many different ways. This section specifies my own contributions to the individual manuscripts.

Appendix B

Thomas, C.* and Foken, T., 2005. Detection of long-term coherent exchange over spruce forest using wavelet analysis. Theor. Appl. Climatol.: DOI: 10.1007/s00704-004-0093-0.

I alone developed, established and verified the method of analysis as presented in the paper. The extensive tests with both artificial signals and real turbulent time series collected under different environmental conditions arose from my ideas. It was me how implemented the described algorithm in a software tool suited for quasi-online application in the field and subsequent application in post-field analysis. I also wrote the entire text of the paper.

T. Foken encouraged the composition of this manuscript as my supervisor and contributed to it through helpful discussions and editorial work.

Appendix C

Thomas, C.*, Mayer, J.-C., Meixner, F.X. and Foken, T., 2005. Analysis of low-frequency turbulence above tall vegetation using a Doppler sodar. Boundary-Layer Meteorol.: submitted.

The application of acoustic remote sensing (Sodar-Rass) to observe coherent structures in the proximity to plant canopies was my own idea. I alone selected the required specific technical settings for the acoustic remote sensing system for this purpose and conducted the measurements during the field campaigns. I developed and improved the applied quality assessment and quality control protocol required for the specific treatment of the collected time series and did the analysis of the data. It was my idea to derive the results in a spatial-temporal context from the correlation coefficients of the wavelet variance spectra. I also wrote the entire text.

J.–C. Mayer assisted in the operation of the acoustic remote sensing system during the field campaigns and extracted the desired time series from the collected raw data. He also contributed to this manuscript through the skilful composition of the contained topographical maps.

F. X. Meixner facilitated the application of the acoustic remote sensing system generally by making it available for the field experiments. He essentially contributed to the manuscript through editing it and sharing his thoughts in many discussions.

Corresponding author

T. Foken introduced me into the field of acoustic remote sensing and shared his large experience in many discussions. He also supervised the course of the experiments and the composition of the manuscript. In particular, he contributed by editorial work and in discussing its contents.

Appendix D

Thomas, C.* and Foken, T., 2005. Coherent structures in a tall spruce canopy: temporal scales, structure spacing and terrain effects. Boundary-Layer Meteorol.: submitted.

I alone performed the analysis of the entire data presented in this manuscript. I also conducted the measurements at the tower during the field campaign. It was my merit to work out the influence of the surrounding terrain and the canopy structure as dominating sources of influence for the dynamical properties of coherent structures. The entire text of the manuscript was written by me.

My supervisor T. Foken guided me through the process of composing the manuscript by sharing his encouraging and critical thoughts. He was mainly involved in the development of the section about internal gravity waves.

Appendix E

Thomas, C.* and Foken, T., 2005. Flux contribution of coherent structures and its implications for the exchange of energy and matter in a tall spruce canopy. Boundary-Layer Meteorol.: submitted.

I alone implemented the automated conditional sampling procedure in the analysis software tool to derive the flux contributions of coherent structures and performed the analysis of the data. The mathematical approach to estimate the impact of coherent structures on the eddy covariance method arose from my own ideas. I also developed the scheme for the classification of the exchange of energy and matter between the forest and the atmosphere into typical exchange regimes. The entire manuscript was composed by me.

The manuscript was improved by many fruitful discussions with the supervisor T. Foken who also contributed through editorial work.

Appendix F

Ruppert, J.*, Thomas, C. and Foken, T., 2005. Scalar similarity for Relaxed Eddy Accumulation methods. Boundary-Layer Meteorol.: submitted.

As the first author, J. Ruppert was responsible for bringing up the idea to investigate the scalar similarity specifically for the indirect flux determination method of the relaxed eddy accumulation. He also performed the simulations for the relaxed eddy accumulation and wrote the major part of the manuscript.

Corresponding author

My contributions to this manuscript were to perform the spectral wavelet analysis of the data and to prepare its results for the presentation, to participate in the overall interpretation of all results, to redesign the structure of the manuscript substantially and to assist in working out the specific goals of the manuscript. I also wrote the part of the text related to the spectral wavelet analysis and performed editorial work for the entire text.

T. Foken essentially contributed to this manuscript through sharing his critical thoughts and helpful comments throughout the course of it's preparation. He also initiated this manuscript as he was the supervisor of both the first and second author.

Appendix G

Zhang, G., Thomas, C., Leclerc, M. Y.*, Karipot, A., Gholz, H. L. and Foken, T., 2005. On the effect of clearcuts on forest canopy fluxes. Theor. Appl. Climatol.: submitted.

This manuscript originates from the close cooperation of my supervisor T. Foken with his colleague M. Y. Leclerc from the University of Georgia. Both were responsible for supervising the analysis of the data and essentially contributed to the general idea presented in this manuscript.

My contribution to this manuscript was supplying the software tool for the spectral analysis, performing the spectral analysis of the raw data, performing additional specific analysis of selected time series and editing the manuscript. I also wrote the part related to the spectral wavelet analysis.

Corresponding author

Appendix B

Theoretical
and Applied
Climatology
Printed in Austria

University of Bayreuth, Department of Micrometeorology, Bayreuth, Germany

Detection of long-term coherent exchange over spruce forest using wavelet analysis

Chr. Thomas and **Th. Foken**

With 4 Figures

Summary

This study presents a discussion of a method for automated and quasi-online analysis of coherent structures using wavelet transform. The method is optimised for rapid processing of vector and scalar variables obtained over tall vegetation. It has been designed to assess long-term statistics of coherent structures, as it is applicable over a wide range of atmospheric conditions. Data of artificial and real turbulent signals are used to perform the analysis and to evaluate the presented method.

Different wavelet functions are used for filtering the original signals, determining characteristic time scales, and detecting individual coherent structures. On this basis, statistics of temporal separation of coherent structures and phase shift between different variables can be calculated.

'Background' turbulence and spikes are found to be efficiently removed without changing the shape, particularly the sharp localised gradients, of coherent structures. The determined peak in the calculated wavelet variance spectrum is observed to correspond very well to characteristic event durations and to satisfy the definition of coherent structures present in vector and scalar variables. The detection algorithm was successful in analysing data covering a wide range of atmospheric conditions. Detected individual coherent structures provide a parallel temporal pattern for scalar variables, but a phase shift between scalar and vector components.

1. Introduction

The turbulent transport above and within tall vegetated canopies is to a large extent dominated by large-scale, intermittent coherent structures and has been subject to many studies within the last decades (Bergström and Högström, 1989; Brunet and Irvine, 2000; Collineau and Brunet, 1993a; Gao et al., 1989; Katul et al., 1997; Paw et al., 1992; Raupach et al., 1989). Coherent structures manifest themselves as an aperiodic pattern of ramp-like events consisting of large-amplitude excursions from the mean in turbulent time series of vector and scalar variables. A single structure is defined by a slow and moderately sloped upward motion (ejection, burst) out of the canopy and a subsequent fast downward motion with a sharp localised gradient (sweep, gust) into the canopy. The exchange of momentum, heat and mass through coherent structures were found to contribute significantly to the overall turbulent exchange between the surface and the atmosphere (Gao et al., 1989; Lu and Fitzjarrald, 1994). This observation underlines their great importance in determining budgets of energy and matter in forested ecosystems.

The crucial step in analysing coherent exchange is to find an objective method to identify and extract the individual coherent events from the high frequent 'background' turbulence. Based on the results of the detection, their characteristic spatial and temporal flow properties

Chr. Thomas and Th. Foken

such as e.g. the streamwise distance Λ_x between adjacent events and their size L_s (Raupach et al., 1996) can be calculated. Various detection methods have been developed. Classical approaches widely used by turbulence researchers such as the Variable Interval Time-Averaging (VITA) method, (e.g. Blackwelder and Kaplan, 1976) or the Windowed Averaged Gradient (WAG) technique (Bisset et al., 1990), are based on the comparison of statistical moments between an entire time series to be analysed and a short-time subsample thereof. These methods are sensitive to sharp jumps of the signal given by the rapid sweep motion. In depending on the adjustment of threshold values (Bogard and Tiederman, 1986) these methods are limited in their application for objective detection. Quadrant analysis has been found successfully to estimate the contribution of coherent structures to momentum and scalar fluxes (e.g. Katul et al., 1997; Shaw, 1985), but provide only poor information about their spatial or temporal characteristics. Collineau and Brunet (1993a, b) discussed and demonstrated the general applicability of the wavelet transform to analyse coherent structures applying it to generated signals and time series obtained in the Roughness Sublayer (RSL) above a pine forest. As the wavelet transform is a time-scale analysis, it can be used to identify processes such as coherent ramps at certain durations in the time domain, being sensitive also to the sharp drops of the sweep phase. Since then, various studies were performed with filter and detection algorithms based on wavelet analysis dealing with time series analysis in the atmospheric boundary layer (Brunet and Irvine, 2000; Chen and Hu, 2003; Gamage and Hagelberg, 1993; Handorf and Foken, 1997; Turner and Leclerc, 1994).

This study presents a detection algorithm for coherent structures based on the wavelet transform advancing previously published works in two significant ways: (i) separating low frequency motion from high frequency turbulence and (ii) using an objective automated detection algorithm that can be applied in the field as the data is collected. The method presented here was developed to assess the long-term behaviour of coherent motion above and within a mid-European spruce forest, requiring a fairly robust and objective detection applicable over a wide range of atmospheric conditions. This task is in contrast to many experimental studies mainly focusing on short-term observations up to several weeks under defined stability conditions. The detection method is implemented in a wavelet analysis tool featuring (i) automated quasi-online processing of the time series directly applicable in the field, (ii) fast and objective detection of individual coherent structures and (iii) subsequent determination of their statistics.

The aim of this study is to perform a methodological discussion of the detection algorithm by applying it to artificial signals and real turbulent time series collected above tall vegetation. At first, a short overview of the wavelet transform and the wavelets used will be given. The subsequent section deals with the experimental and artificial time series followed by a detailed discussion of the implemented detection methodology. The achieved results will be summed up with concluding remarks in the last section.

2. The wavelet transform

This section will give a short review of the wavelet transform (Grossmann and Morlet, 1984; Grossmann et al., 1989; Kronland-Martinet et al., 1987) and the wavelets used in this study, limited to the basics necessary for its application to coherent structure detection. The wavelet transform, that was introduced into turbulence studies by Farge (1992), is a local transform revealing information in both the frequency and time domain. This basic feature of the wavelet transform is used for the detection of single coherent structures taking place at characteristic frequencies at a certain time. A detailed introduction into the wavelet transform and the various wavelets can be found in textbooks such as Daubechies (1992), Holschneider (1995), Kumar and Foufoula-Georgiou (1994).

2.1 Basic mathematical principle

The one-dimensional wavelet transform of a given signal $f(t)$ is defined as

$$T_p(a,b) = \int_{-\infty}^{+\infty} f(t)\overline{\Psi_{p,a,b}(t)}dt, \qquad (1)$$

Detection of long-term coherent exchange over spruce forest

where $T_p(a,b)$ are called the wavelet coefficients and with $\Psi_{p,a,b}(t)$ being the wavelet function given by

$$\Psi_{p,a,b} = \frac{1}{a^p} \Psi\left(\frac{t-b}{a}\right), \qquad (2)$$

where $\Psi((t-b)/a)$ is called 'mother wavelet' with the dilation parameter a and the translation parameter b. With the help of these parameters, the shape and the location of the mother wavelet is altered respectively. The dilation parameter a is also called the 'scale' of the wavelet, as for values $a < 1$ it causes a contraction and for $a > 1$ a broadening of the mother wavelet. The factor $1/a^p$ in Eq. (2) is a normalization factor that keeps the energy of the scaled wavelet to the original mother wavelet with values $p = 1$ or $p = 1/2$ normally being used (Gamage and Hagelberg, 1993). In this study, only wavelets with $p = 1$ will be used. In simple words, the wavelet transform compares a given time series $f(t)$ with a wavelet function $\Psi_{p,a,b}$ on every scale a and time $t - b$.

The wavelet transform Eq. (1) can be inverted and is then defined as

$$f(t) = \frac{1}{C_G} \int_{-\infty}^{+\infty} \int_0^{+\infty} T_p(a,b) \Psi_{p,a,b}(t) \frac{da\,db}{a^{3-2p}} \qquad (3)$$

if the normalizing factor C_G satisfies the admissibility condition. The combination of Eqs. (1) and (3) reveals the opportunity of using the wavelet as a frequency filter when decomposing the signal $f(t)$ with the scales $a_1 \cdots a_n$ and selecting only a certain range of scales $a_{1+y} \cdots a_{n-x}$ for the reconstruction. Thus, the filter acts as a high-pass for small scales $a_{1+y} \cdots a_{n-x}$ and as a low-pass filter when large scales are used for reconstructing the signal. Wavelets have been successfully used as a filter separating the low-frequent coherent structures from high-frequent 'background' turbulence (e.g. Handorf and Foken, 1997; Turner and Leclerc, 1994).

As the use of the angle frequency ω in turbulence studies is more common and convenient than the scale a, Eq. (4) links these two parameters:

$$\omega = \frac{\omega^0_{\Psi_{p,1,0}}}{a \cdot \Delta t}, \qquad (4)$$

introducing the peak frequency $\omega^0_{\Psi_{p,1,0}}$ of the mother wavelet and Δt being the time resolution of the time series, i.e. the temporal separation between adjacent data. The peak frequency only depends on the specific wavelet used and corresponds to the maximum peak in a Fourier spectrum of the given mother wavelet with $a = 1$, $b = 0$ and $p = 1$ (see next section for details).

Analogous to the spectral density of a Fourier transformed signal over a frequency range examined, the energy contained in the time series on a certain scale a can be expressed for the wavelet transform as

$$W_p(a) = \int_{-\infty}^{+\infty} |T_p(a,b)|^2 db, \qquad (5)$$

where $W_p(a)$ is called the wavelet variance. Due to the local character of the wavelet transform, the maximum in a wavelet variance spectrum corresponds to the characteristic duration of the coherent structures contained in the time series (Mahrt and Howell, 1994). In contrast to this, the maximum in a Fourier spectrum corresponds to the periodicity of the coherent structures, i.e. to their arrival frequency. Assuming a local or global maximum peak in the $W_p(a)$ spectrum at scale a_e, where the subscript 'e' stands for '*event*', a characteristic time scale D for events occurring at this frequency can be defined as $D = 1/2f^{-1}$ (Collineau and Brunet, 1993b), with $\omega_0 = f \cdot 2\pi$ and Eq. (4) yielding the relationship

$$D = \frac{1}{2 \cdot f} = \frac{a_e \cdot \Delta t \cdot \pi}{\omega^0_{\Psi_{p,1,0}}}. \qquad (6)$$

The factor $1/2$ was introduced to adapt the size to one elementary event in a $\sin(\omega_0 \cdot t)$ function exhibiting two elementary events per cycle. This time scale D will be used throughout this study to express the results of the wavelet analysis as it embodies the central issue about the characteristic duration of the coherent structures.

2.2 Wavelet functions

After introducing the wavelet transform as a mathematical transformation, we now deal with the wavelet functions $\Psi_{p,a,b}$ used in the detection methodology applied in this study.

The applicability of a certain wavelet function for a certain purpose depends very much on its localisation in frequency and time. Wavelet functions being well-localised in frequency are to be preferred when filtering and determining characteristic scales of coherent structures, while

Chr. Thomas and Th. Foken

wavelets well-localised in time yield more accurate results when detecting the individual events. In this study, a wavelet filter based on the biorthogonal set of wavelets BIOR5.5 is used for separating the low frequencies of coherent motion from high frequent turbulence. The complex Morlet wavelet MORL is used for computing the wavelet variances and the determination of characteristic scales. These wavelets are well-localised in frequency. Succeeding these two, the Mexican hat wavelet MHAT is applied for detection of the individual coherent structures, being rather well localised in both frequency and time. The three named wavelets will be described shortly in the following subsections.

2.2.1 Biorthogonal wavelets

A filter using biorthogonal wavelets uses different wavelets for decomposition and recomposition purposes. Figure 1a, b plot the corresponding $\Psi(t)$ functions of these wavelets. This applied filter introduces the discrete wavelet transform that discretizes the dilation parameter a and translation parameter b for the sake of increased analysing speed. This is necessary in practical applications as it limits the scales and times to be analysed, but leads to a decreased resolution and accuracy at large scales. Normally, a discretisation of dyadic scales $a_i = 2^i$, where i is called the decomposition level, and with $i \geq 1$ is chosen. A detailed discussion of
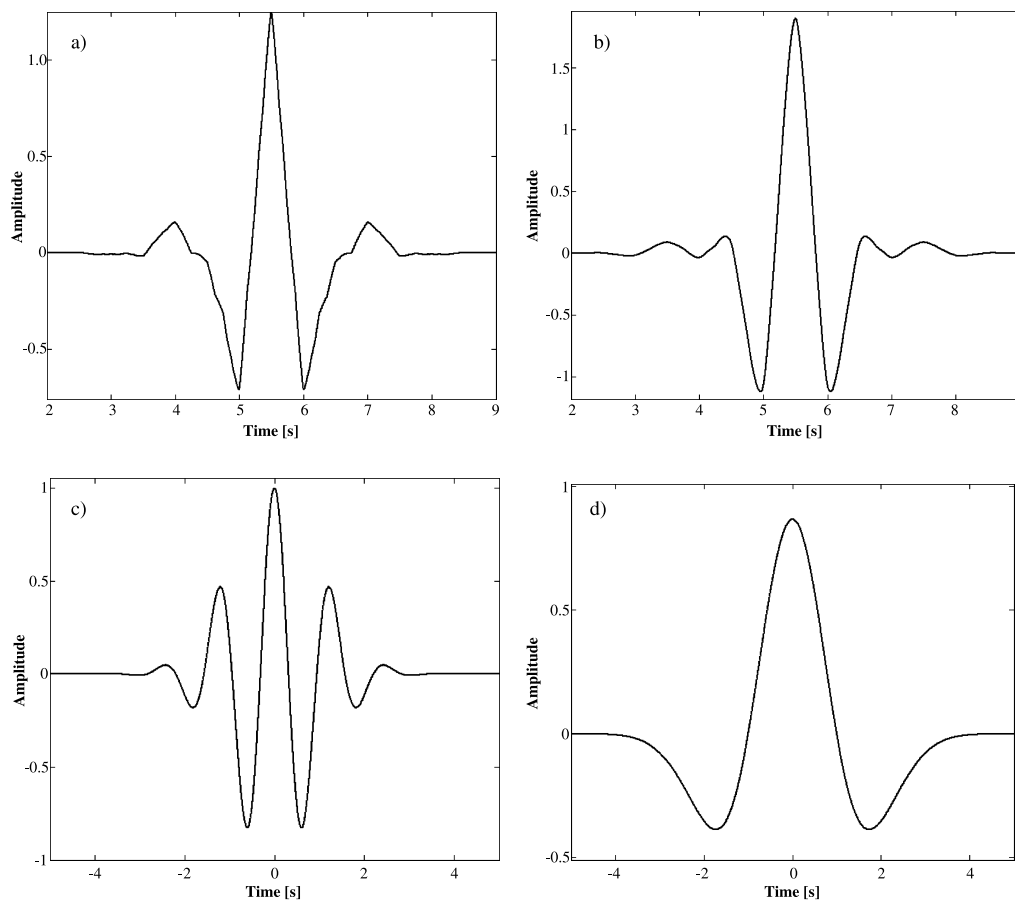
Fig. 1. Wavelet functions Ψ used in the method of analysis for detection of coherent structures: Biorthogonal BIOR5.5 set of wavelets applied for filtering: (**a**) decomposition and (**b**) reconstruction of the signal; (**c**) real part of the complex Morlet wavelet used for determination of the wavelet variance spectrum; (**d**) Mexican hat wavelet used for single event detection

Detection of long-term coherent exchange over spruce forest

biorthogonal wavelets and the discrete wavelet transform can be found in Kumar and Foufoula-Georgiou (1994). In contrast to studies that apply digital filtering using the HAAR wavelet (e.g. Turner and Leclerc, 1994), we use the BIOR5.5 set of wavelets as the localisation in frequency is better (Kumar and Foufoula-Georgiou, 1994).

2.2.2 Morlet wavelet

The complex Morlet MORL wavelet has quite often been used in geophysical studies (e.g. Pike, 1994). Figure 1c plots its real part of the $\Psi(t)$ function. Its localisation in the frequency domain is very good as it exhibits only one distinct peak at $\omega^0_{\Psi_{p,1,0}}$. For this reason, it was chosen to compute the wavelet variance spectrum of the signals with subsequent determination of the characteristic event scale a_e, in contrast to other studies using different wavelet functions for this purpose (e.g. Mahrt, 1991).

2.2.3 Mexican hat wavelet

The Mexican hat wavelet MEXH is defined as the second-order derivative of a Gaussian function $f(t) = e^{-t^2/2}$ with the shape of $\Psi(t)$ given in Fig. 1d. It has found practical application in edge detection (e.g. Mallat and Zhong, 1992) and for coherent structure analysis (Chen and Hu, 2003; Collineau and Brunet, 1993a; Gao and Li, 1993). As Collineau and Brunet (1993b) pointed out, the detection of individual coherent structures is more objective than using other non second-order derivative wavelet functions such as HAAR, RAMP or WAVE, as the wavelet coefficients $T_p(a,b)$ gained by a second-order derivative function exhibit a zero crossing with a defined change in sign at the event time. Given this objectivity criteria, MEXH was therefore chosen to detect the individual events.

2.3 Scales of analysis

As we have already pointed out, the continuous wavelet transform with the Morlet wavelet is used to find characteristic durations for coherent structures. When performing the wavelet transform according to Eq. (1), one must select the scales of analysis ranging from $a_1 \cdots a_n$ covering the entire range of expected event durations D. Despite this fairly subjective expectation crite-

rion, there are objective criteria limiting the possible scales of analysis originating from the wavelet function used. According to Kumar and Foufoula-Georgiou (1994), the minimum frequency $\omega^0_{\Psi_{p,1,0}}/a_{\min}$ should not exceed the Nyquist frequency $2\pi/2\Delta t$, implying

$$a_{\min} \geq \frac{\omega^0_{\Psi_{p,1,0}} \cdot \Delta t}{\pi}. \tag{7}$$

The maximum scale of analysis is given by the support width of the wavelet function with the lower border $\text{supp}_{\min}$ and upper border $\text{supp}_{\max}$, i.e. the range of non-zero values of $\Psi_{p,1,0}(t)$. Satisfying the condition that the wavelet support range should not exceed the data range, the maximum permissible scale $a_{\max}$ is given by

$$a_{\max} \leq \frac{t_{\max} - t_{\min}}{\text{supp}_{\max} - \text{supp}_{\min}}, \tag{8}$$

where $t_{\min}$ and $t_{\max}$ are the starting and end points of time of the signal $f(t)$ respectively. Note that $\text{supp}_{\min} < 0$ and for symmetrical wavelet functions $\text{supp}_{\min} = -\text{supp}_{\max}$ is valid.

3. Data

The exclusive application of a given method of analysis to real turbulent data is not sufficient for a complex discussion of the method itself. Thus, we use generated time series with known properties and statistics in addition to field data for validation purposes.

The first artificial time series is a triple-mode sine function $f(t) = \sum_{n=1}^{3} \sin(2\pi t T_n^{-1})$ with periods $T_n = 10$, 60 and 230 s defined over a time period $t = [0, 1800]$ s. Referring to Eq. (6), the resulting characteristic event durations are $D = 5$, 30 and 115 s. The trigonometric signal was chosen for its well-known properties and their extensive use in signal analysis.

An irregularly spaced pattern of $n = 7$ ramps with a constant duration of $D = 100$ s for each ramp spread over a period of $t = [0, 1800]$ s was selected as the second artificial signal. It was chosen for two reasons: first observed coherent structures are supposed to have a ramp-like shape, and second for reasons of intercomparison to previous studies (e.g. Collineau and Brunet, 1993b).

The real turbulent time series were collected during the WALDATEM-2003 experiment at

Chr. Thomas and Th. Foken

the FLUXNET Waldstein/Weidenbrunnen site, Germany (Gerstberger, 2001). This experiment was designed for intensive investigation of coherent structures and carbon fluxes within and above a tall spruce forest. Its name was chosen from the analysing systems used in the campaign, whereas WALD stands for WaveLet Detection and ATEM for Atmospheric Turbulence Exchange Measurements. Data used in this study were obtained at a sampling height of $z = 33$ m over spruce forest with a mean canopy height $h_c = 19$ m, at a sampling frequency of 20 Hz using a sonic anemometer (type R3-50, Gill Instruments Ltd.) in combination with an open path gas analyser (type LI-7500, Licor Instruments) for fast CO_2- and H_2O-concentration measurements also operated at 20 Hz. During the entire field campaign more than 13000 individual half hour datasets obtained by 5 sonic anemometers and gas analysers were processed by applying the detection algorithm presented in the following section. The achieved results will be presented in a different paper as this study focuses on the method of detection. The half hour intervals presented in this study were collected during WALDATEM-2003 in June, 24th 13:00–13:30, June, 20th 14:30–15:00, June, 27th 15:00–15:30 and June, 25th 01:30–02:00 CET, hereafter referred to as Data A, B, C and D respectively. For each interval, the vertical wind velocity w, the potential sonic temperature θ_s, the carbon dioxide concentration c_{CO_2} and the specific humidity q were selected for analysis. The selected intervals cover a wide range of atmospheric conditions with their characteristics given in Table 1: Data A is characterised by moderate horizontal wind speeds, thermally and dynamically driven turbulence under slightly unstable stratification at daytime; Data B represents strong winds with dominating

wind shear under near neutral stratification at daytime; Data C was collected during negligible wind speeds under strong unstable stratification with dominating thermally driven turbulence at daytime; Data D represents a typical night time situation with moderate wind speeds under stable stratification.

4. Method of analysis

This section will give detailed information about the implemented methodology of analysis for detection of coherent structures in each single half hour time series.

In a first step, the wind vector components are rotated according to Wilczak et al. (2001), i.e. the planar-fit method is applied, using rotation coefficients determined on a monthly base. Afterwards, the sampling frequency is reduced from the original 20 to 2 Hz resolution by applying standard block averaging. In most studies, the analysis method is applied to data at the original sampling frequency that ranges from 4 to 20 Hz. The reduction of the sample frequency seems to be justified considering the following: (i) the wavelet filter applied subsequently (described later in this section) discards all fluctuations occurring at high frequencies focusing on the low frequency physical processes only, (ii) a reduction of data by a factor of 10 significantly shortens the computation time for the subsequent continuous wavelet transform and (iii) the accuracy of the peak at scale a_e in the $W_p(a)$ spectrum that is used for the determination of the characteristic event duration is not dominated by the resolution of the data. The latter is defined by the used wavelet function and the redundancy of information between adjacent scales a_{x-1}, a_x and a_{x+1} (Collineau and Brunet, 1993b). Thus,

Table 1. Characteristic meteorological parameters and atmospheric fluxes of the real turbulent Data A, B, C and D: Mean horizontal wind speed $\bar{U}$, mean wind direction $\bar{\phi}$, friction velocity u^*, atmospheric stability ζ, carbon dioxide flux F_c, buoyancy flux H and latent heat flux λE. Fluxes were calculated using data of the original sample frequency of 20 Hz

Data	Date, Time CET	$\bar{U}$ [ms^{-1}]	$\bar{\phi}$ [°]	u^* [ms^{-1}]	ζ [1]	F_c [µmol m^{-2} s^{-1}]	H [Wm^{-2}]	λE [Wm^{-2}]
A	24/06/03 13:00–13:30	3.3	280	1.00	−0.13	−11.4	495	230
B	20/06/03 14:30–15:00	5.7	290	1.26	−0.04	−14.3	301	300
C	27/06/03 15:00–15:30	0.4	52	0.48	−0.68	−11.7	301	144
D	25/06/03 01:30–02:00	2.0	347	0.34	0.16	3.9	−27	4

Detection of long-term coherent exchange over spruce forest

the computation time is shortened without altering the results significantly. Tests on various sampling frequencies did not yield different results for the peak scales a_e.

The next step is normalising the data by subtracting the mean and dividing by standard deviation except for the vertical wind w that is only normalised by its standard deviation. The prior planar-fit rotation already accounts for adjusting the mean vertical wind $\bar{w}$ to zero on a long-term base, whereas a single half hour signal of w is allowed to have a $\bar{w} \neq 0$.

The signal is then extended using a zero-padding method, i.e. adding zero values at both ends. According to Eq. (8), the maximum permissible scale a_{max} depends on the length of the signal $(t_{max} - t_{min})$. An artificial extension of the signal thus allows to use larger scales $a > a_{max}$, covering larger event durations D. Additionally, border effects are suppressed by signal extension. The period of time of the zero-padded data was chosen according to the 'cone of influence' (see Holschneider, 1995), stating that wavelet coefficients $T(a,b)$ with b beyond $[t_{min}, t_{max}]$ must be taken into account when calculating the $W_p(a)$ spectrum according to Eq. (5). For the symmetric wavelet MORL used for subsequent wavelet transform, a period of $|a_n \cdot \text{supp}_{min}|$ s was added at both ends, where a_n is the maximum scale of analysis.

The low-pass wavelet filter is then applied to the data using the BIOR5.5 set of wavelet functions with discrete wavelet transform retaining all events at scales with $i \geq 4$ (see Section 2.2.1). Combining Eq. (6) with the known peak frequency $\omega^0_{\Psi_{1,1,0}} \approx 4\,\text{Hz}$ for the BIOR5.5, one yields that all fluctuations of the signal with event durations $D_c \leq 6.2\,\text{s}$ are removed, with D_c called the critical event duration. This value is in agreement with other studies that used critical event durations of $D_c \approx 5.7\,\text{s}$ (Chen and Hu, 2003) and $D_c \approx 5\,\text{s}$ (Lykossov and Wamser, 1995) and corresponds to the spectral gap between high frequency turbulence and low frequency flow patterns such as coherent structures.

The next step in analysis procedure is the continuous wavelet transform (Eq. (1)) with MORL using scales $[a_1, a_n]$ corresponding to event durations D ranging from 8 to 140 s with a resolution of 0.5 s. The peak frequency $\omega^0_{\Psi_{1,1,0}}$ of MORL is 5. The lower limit was chosen in respect to the

critical event duration D_c of the wavelet filter applied and Eq. (7) giving the theoretical limit. The upper border corresponds to the limitation given by Eq. (8) with an effective support width of MORL $\text{supp}_{min} = -4\,\text{s}$ under consideration of the extended zero-padded signal.

For the subsequent computation of the wavelet variance $W_p(a)$ according to Eq. (5), translation parameters b satisfying the 'cone of influence' condition (Holschneider, 1995) given by $b \in [t_{min} - a \cdot \text{supp}_{max}, t_{max} - a \cdot \text{supp}_{min}]$ are taken into account. Real turbulent time series collected above tall vegetation were observed to exhibit several peaks in the $W_p(a)$ spectrum sometimes, representing different characteristic event durations. In such a case, we define the peak scale a_e as the first clearly expressed maximum in the spectrum. For a robust determination of a_e, a cubic spline interpolation is applied to the approximate derivatives between adjacent wavelet variances. The corresponding characteristic length D_e of the coherent structures is given through Eq. (6).

As we use the Mexican hat wavelet MEXH for the following detection of the individual coherent structures, the scale a_e determined using MORL must be converted under consideration of the peak frequency $\omega^0_{\Psi_{1,1,0}} = \sqrt{2}$ for MEXH. Referring to Section 2.2.3, the wavelet coefficients $T(a_e, b)$ exhibit a zero crossing with a defined change in sign at the event time of occurrence. As our method aims at the long-term behaviour of coherent structures valid for a wide range of eco-systematical processes and conditions, we must define the change in sign in dependence of the vector and scalar flux considered and its direction. The correlation coefficient r_{xy} was chosen being the chief parameter for defining the direction of the change in sign. Referring to Eq. (9), the sign of r_{xy} indicates the direction of the considered flux when using eddy covariance technique, with the overbar depicting the covariance of two variables and σ standing for the standard deviation.

$$r_{xy} = \frac{\overline{x'y'}}{\sigma_x \cdot \sigma_y} \tag{9}$$

Table 2 lists the defined changes in sign of $T(a_e, b)$ of the zero crossings used for detection. The time series used in this study are linked to their fluxes by the momentum flux $\tau = -\rho \overline{u'w'}$

Chr. Thomas and Th. Foken

Table 2. Definition of changes in sign of $T(a_e, b)$ of the zero crossings used for detection of the individual coherent structures for various variables and typical situation of their occurrence (in brackets)

Variables x, y	$r_{xy} < 0$	$r_{xy} > 0$
w, u	$+ \rightarrow -$	$-$
θ_s, w	$- \rightarrow +$ (night)	$+ \rightarrow -$ (day)
c_{CO_2}, w	$- \rightarrow +$ (day)	$+ \rightarrow -$ (night)
q, w	$- \rightarrow +$ (dew)	$+ \rightarrow -$ (day)

for the vertical wind w, the buoyancy flux $H = \rho c_p \overline{w'\theta_s'}$ for the potential sonic temperature θ_s, the carbon dioxide flux $F_c = \rho \overline{w'c_{CO_2}'}$ for the carbon dioxide concentration c_{CO_2}, and the latent heat flux $\lambda E = \lambda \rho \overline{w'q'}$ for the specific humidity q, where the primes indicate the fluctuations, ρ is air density, c_p the constant heat at constant pressure and λ the specific heat of vaporisation.

The total number of coherent structures N, i.e. the number of zero-crossings with the defined change in sign (see Table 2), is then determined within the range $[t_{min}, t_{max}]$, giving their individual moment of occurrence. Basing on this information, the mean temporal separation of the coherent structures $\overline{T_x}$ and its standard deviation σ_{T_x} are calculated.

5. Results

The results achieved by applying the method previously described will be presented in this section.

At first, the effect of the wavelet filter applied will be discussed. The extended and normalized original and filtered time series for the generated signals and Data A are plotted in Fig. 2. Comparing the unfiltered and filtered generated signal consisting of a triple sine function, we can clearly see that the wavelet filter removes the oscillations with the highest frequency. This is due to the fact that this sine function has an event duration $D = 5$ s and thus smaller than the critical event duration D_c of the wavelet filter equal to 6.2 s. The remaining two sinusoidal functions with $D > D_c$ are still clearly present in the filtered time series. The ramp signal that exhibits three events within the considered period of time was not changed significantly by the filtering procedure despite some noise added around the sharp drops of the signals. This is due to the fact that the time scale for this sudden change is much

less than the critical event duration of the filter. Recalling that the drop of the ramp happens within a time step of 0.5 s (at 2 Hz sample resolution) by its definition, the applied filter removes this 'high frequent event' resulting in a tendency to smooth it. Real turbulent data collected above tall vegetation rarely exhibits such instantaneous drops with a change in amplitude of about 3σ of the signal. Thus, the added noise remains an inherent effect of the generated signal and is regarded as negligible for real observations. However, the overall event duration of the ramps does not seem to be effected by the applied wavelet filter.

The comparison between the unfiltered and filtered time series of w, θ_s, c_{CO_2} and q support the observations found in the artificial signals: high frequent changes due to 'background' turbulence are removed efficiently without changing the contained lower frequency tendencies. Nonetheless, the sharp localised gradients during the sweep phase of a coherent structure seem to be slightly smoothed sometimes. This observation is due to same reason as for the generated ramp signal. However, this effect has a negligible influence on the characteristic event duration D_e at peak scale a_e, as we will see in the next paragraphs. Small effects of the filter on all time series can be observed where the signals were extended by zero-padding. No smoothing function has been applied to prevent these artificially caused sharp changes. However, this border effect was found to have only little effect on the subsequent computation of the wavelet variance and can thus be regarded as negligible.

The next fundamental step in extracting the coherent structures from the filtered signals is to find their characteristic event duration D_e by plotting the wavelet variance spectrum and determining the maximum peak. Figure 3 plots the computed wavelet variances as a function of the event duration for both generated signals (Fig. 3a) and the real field Data A (Fig. 3b), Data B (Fig. 3c) and Data D (Fig. 3d). The variances were normalised by their maximum value within the considered range for enhanced visibility of the peaks. The displayed range of the event duration D was chosen for an optimised determination of the maxima, although the entire range of event durations was considered as given by the method of analysis. Detailed results of the

Detection of long-term coherent exchange over spruce forest
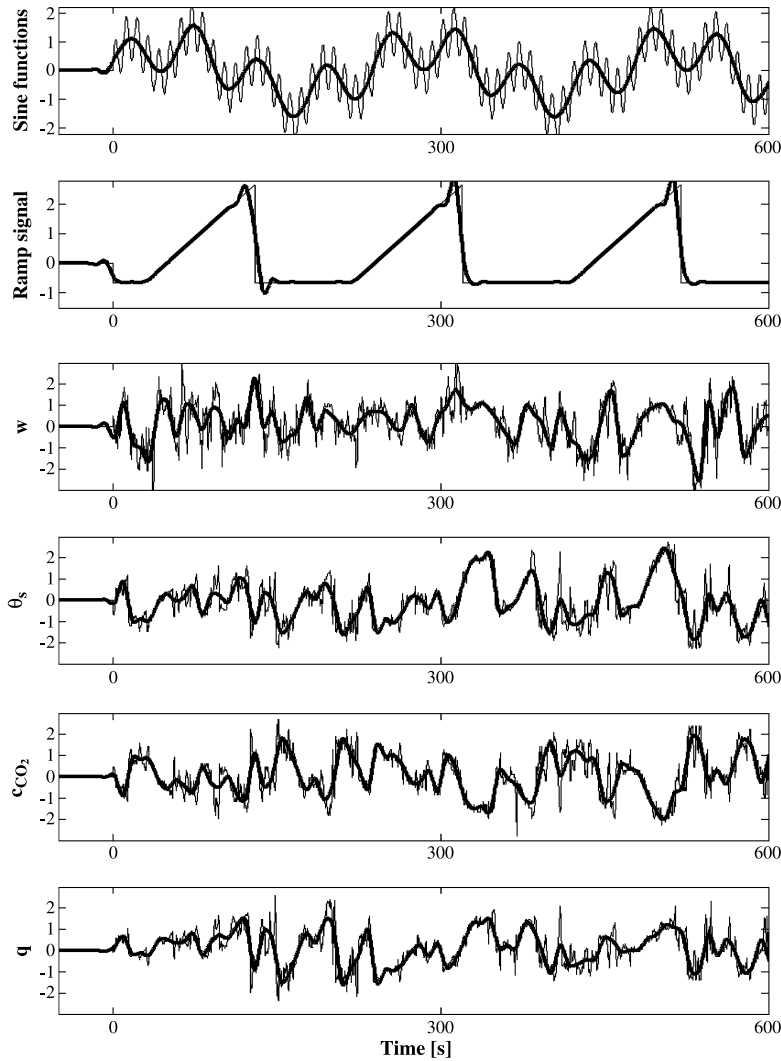
Fig. 2. Extended and normalized original (fine) and filtered (bold) data (2 Hz) of the generated signals and Data A for vertical wind w, potential sonic temperature θ_s, carbon dioxide concentration c_{CO_2} and specific humidity q for $t \in [-50, 600]$ s

detected maxima are given in Table 3 for all considered time series.

The wavelet variance of the sine functions clearly exhibits two maxima located at 30.5 and 118.0 s event duration. This is in good agreement with the expectations of $D = 30$ and 115 s given by the definition of this signal. The maximum of the wavelet variance for the ramp signal was determined to be at $D_e = 99.5$ s, which corresponds very well with the defined ramp duration of 100 s. Therefore we can support our statement that the smoothing effect of the wavelet filter has a negligible effect for practical appli-

cation. One might find that the bands around the peak frequencies are large although the applied MORL is well-localised in the frequency domain. This is an inherent property of the wavelet transform where the redundancy of information between adjacent scales is much larger than e.g. for the Fourier transform. Collineau and Brunet (1993b) determined characteristic event duration of 98–100 s for a ramp signal consisting of an infinite number of irregularly spaced ramps with a duration of 100 s each by applying wavelet transform using various wavelet functions. Thus, the accuracy observed in this study is equal to

Chr. Thomas and Th. Foken
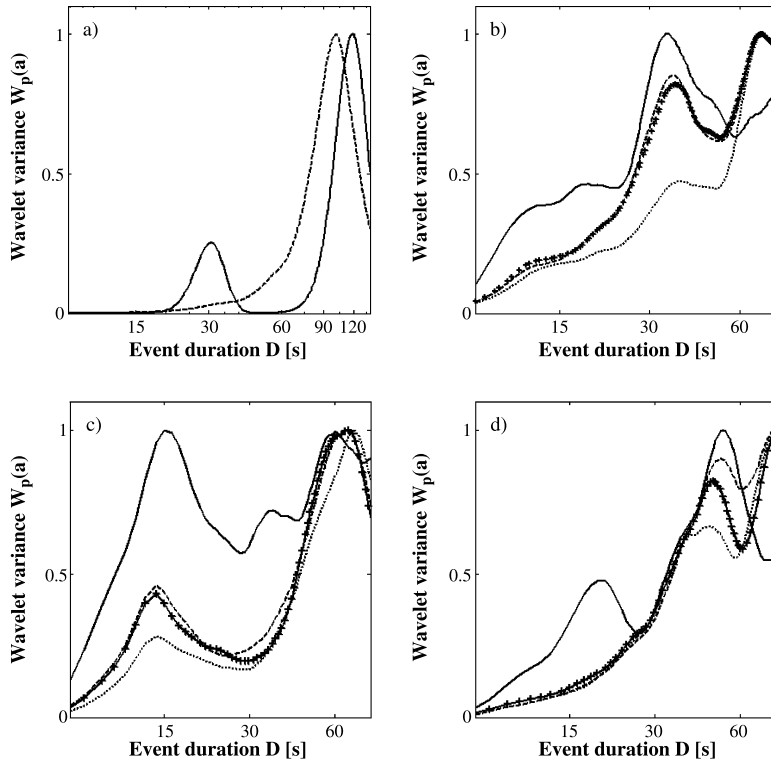
Fig. 3. Normalised wavelet variance versus event duration D of the (**a**) generated signals: sine functions (solid) and ramp signal (dashed) and real turbulent (**b**) Data A, (**c**) Data B, (**d**) Data D: vertical wind (solid), potential sonic temperature (dashed), carbon dioxide (crosses) and specific humidity (dotted)

Table 3. Results of the analysis of the wavelet variance spectra and the detection of individual coherent structures for the considered time series; D_{max}: maxima detected in wavelet variance spectrum with $D \in [8, 140]$ s, D_e: characteristical event duration, N: total number of detected events, $\overline{T_x}$, σ_{T_x}: mean and standard deviation of the temporal separation between the detected individual coherent structures

Variable		D_{max} [s]	D_e [s]	N [1]	$\overline{T_x}$ [s]	σ_{T_x} [s]
Sine functions		30.5, 118.0	30.5	30	59.9	1.7
Ramp signal		99.5	99.5	7	262.0	104.1
Data A	w	18.5, 34.5, 116.0	34.5	26	71.4	19.2
	θ_s	36.0, 69.0, 115.0	36.0	26	68.9	18.5
	c_{CO_2}	36.5, 69.5, 120.5	36.5	26	69.0	18.8
	q	37.5, 70.5, 120.5	37.5	26	68.8	19.6
Data B	w	15.5, 36.0, 60.0, 130.0	15.5	61	29.7	8.7
	θ_s	14.0, 65.5	14.0	64	28.3	9.2
	c_{CO_2}	14.0, 60.0	14.0	64	28.3	9.1
	q	14.5, 70.0, 104.0	14.5	61	29.7	9.1
Data C	w	22.0, 53.5	22.0	41	44.2	14.5
	θ_s	31.5, 60.0, 119.5	31.5	26	67.3	22.2
	c_{CO_2}	31.5, 60.5, 119.0	31.5	28	62.3	17.5
	q	110.0	110.0	8	227.1	68.6
Data D	w	19.0, 52.0, 99.0	19.0	50	35.4	11.3
	θ_s	51.0, 80.4	51.0	19	93.7	21.2
	c_{CO_2}	48.0, 81.0	48.0	20	87.5	24.9
	q	46.5, 81.0	46.5	20	87.1	25.2

Detection of long-term coherent exchange over spruce forest

other methodological studies. Following our definition of the characteristic event duration, $D_e = 30.5\,\text{s}$ and $99.5\,\text{s}$ were chosen for the sine functions and the ramp signal respectively.

The wavelet variance spectra of the real field data are not as smooth and symmetric as those for the generated signals due to the presence of a whole range of event scales. For Data A, the variance spectrum obtained from the time series of vertical wind velocity w exhibits two maxima within the displayed period of $D \in [8, 80]\,\text{s}$. The first maximum is located at $18.5\,\text{s}$, the second more pronounced one is determined to $34.5\,\text{s}$ event duration. The three scalar variables, i.e. potential sonic temperature, carbon dioxide concentration and specific humidity, exhibit their first maximum nearly at the same event duration of about $36\,\text{s}$, with the exact values given in Table 3. This maximum coincides very well with the second well expressed maximum found for the vertical wind velocity. Thus, the maximum at about $36\,\text{s}$ was selected for the definition of D_e for both vector and scalar variables according to the physical definition of coherent structures as a parcel of vortical fluid with a distinct phase relationship between the flow properties, i.e. vector components, and its constituents, i.e. the scalar quantities, given by Blackwelder and Kaplan (1976). However, the first dominant scale of the vertical velocity is often found to be smaller than for scalar variables. This finding can be supported by the observation that spectra of scalar variables tend to be similar to those of the horizontal velocity rather than of the vertical velocity in the lower frequencies. This fact leads to the conclusion that the overall transport by lower frequency processes such as coherent structures is more related to the horizontal transport. The time series of Data B consistently exhibit their first maximum at about $15\,\text{s}$ event duration, showing no difference between vector and scalar variables. This might be due to the large wind shear caused by the strong horizontal wind dominating the transport processes and causing homogeneous coherent exchange patterns. In comparison to the characteristic event durations determined for Data A, the event durations for Data B are significantly shorter yielding a significantly shorter mean temporal separation (see Table 3). The first detected maximum at $22\,\text{s}$ in the vertical velocity of Data C is smaller than for

the simultaneously obtained potential sonic temperature and the carbon dioxide both showing peak scales at $31.5\,\text{s}$. The spectrum of the specific humidity is very different from the other both vector and scalar variables, exhibiting only one maximum at $110\,\text{s}$ event duration. During this part of the experiment, the water vapour concentration of the air was decreasing resulting in an increased dryness. This observation is in consistence with the small magnitude of the observed latent heat flux (Table 1) in opposite to the buoyancy and carbon dioxide fluxes that were not affected. Thus, the humidity can be expected to show a different exchange pattern. The second maximum does not clearly coincide between the vector and scalar variables so that it seems to be justified to detect the coherent structures at the first maximum of the individual time series. The spectra of the nighttime Data D are similar to the daytime Data A despite the fact that the first maximum of the vertical wind velocity at $19\,\text{s}$ is clearly pronounced and the maximum consistently found across all time series was determined to about $49.5\,\text{s}$. It is worth noting that the scatter in the individual time series around this peak is larger compared to the daytime conditions of Data A and B, especially for the specific humidity deviating about $3\,\text{s}$. This finding is due to the fact that the standard deviation of the data is much less, i.e. the fluctuations are less clearly expressed than under daytime conditions leading to a more indistinct separation of adjacent fluctuations and thus a greater uncertainty in the determination of the characteristic event duration. In case of the specific humidity of Data D, the standard deviation was determined to $1.26\,\text{mmol}\,\text{m}^{-3}$ compared to a mean of $11.82\,\text{mmol}\,\text{m}^{-3}$ for Data A, B and C.

The wavelet variance spectrum may also be useful to collect information about scalar similarity. Indirect flux determination methods, as e.g. the Relaxed-Eddy-Accumulation (Businger and Oncley, 1990), assume scalar similarity, as they use proxy scalars, which can be measured very fast, for the flux calculation of the parameter of interest, which normally cannot be determined with a sufficient temporal resolution. In this case, the wavelet variance spectra of different scalar variables determined at a high frequency can be used to verify this assumption and to infer the admissibility of proxy scalars.

Chr. Thomas and Th. Foken
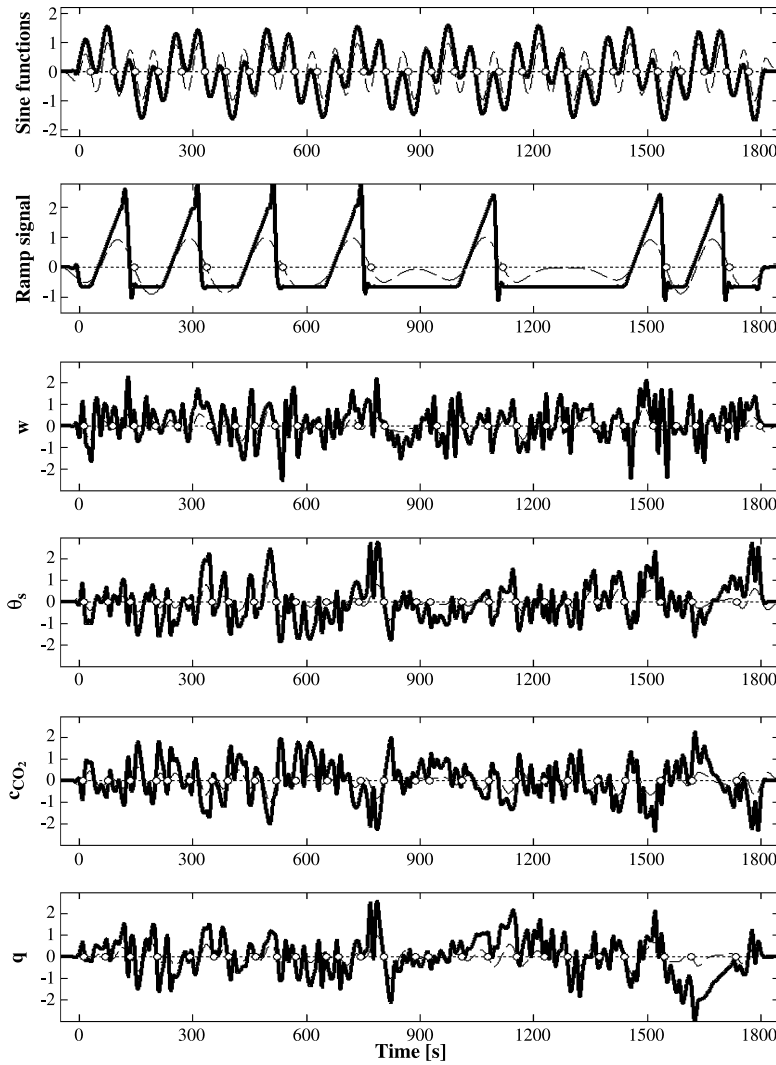
Fig. 4. Normalised and filtered time series (bold line) of the generated signals and Data A with detected individual coherent structures (open circles) at event duration D_e and shown wavelet coefficients $T(a_e, b)$ (dashed line) for $t \in [-50, 1850]$ s

After determining the characteristic event durations D_e we now proceed on detecting the individual coherent structures in the time series. Figure 4 displays the results of the detection using wavelet transform with MHAT at D_e in combination with the zero-crossing method for the generated signals and Data A. Table 3 lists the corresponding statistical results of the detection for both the generated and the field data.

The individual events detected in the sine functions signal show a regularly spaced pattern with a mean temporal separation $\overline{T_x}$ determined to 59.9 s. The total number of detected events yields 30. These results are in agreement with the definition of the sine function with a period T of 60 s and a total number given by $(t_{\min} - t_{\max})/T$. However, the corresponding standard deviation σ_{T_x} was found to be slightly different from zero. This might be due to the determined D_e value that does not exactly match the theoretically expected value causing some scatter between adjacent events. The qualitative results for the ramp signal analysed are not different from those of the sine functions, as the determined values match the expected ones. The high standard deviation found for the temporal separation of the ramps is due to the irregular spacing with a span from 60 to 340 s.

Detection of long-term coherent exchange over spruce forest

Considering the filtered time series and the corresponding detected individual events, we can clearly see that the detection method is sensitive to sharp drops in the signal.

The individual coherent structures detected in the field Data A match the visually evident ramps in the time series, supporting the sensitivity of the method to the steep localised gradients of the sweep phase (Fig. 4). Their temporal distribution in each individual time series follows an irregularly spaced pattern satisfying the values of $\overline{T_x}$ and σ_{T_x} listed in Table 3. It is clearly visible that the time series of the scalar quantities exhibit their coherent structures almost at the same time. However, the coherent structures in the vertical velocity signal are slightly shifted in time compared to the scalars, whereas the sign of this temporal shift is not constant. Referring to the definition of coherent structures according to Blackwelder and Kaplan (1976), there might be a phase shift between vector flow properties and scalar constituents in a coherent structure. The best agreement between signals can be found for the sonic temperature θ_s and the carbon dioxide concentration c_{CO_2}. The number of detected events and the mean and standard deviation of the temporal separation of the coherent structures in Data B are consistent across all time series with a small scatter. This finding underlines the homogeneous exchange processes observed in the characteristic event durations. Data C shows large differences in the statistics of the detected coherent structures between the time series resulting from the different values of D_e. The number of detected coherent structures decreases with increasing values of D_e leading to an increased $\overline{T_x}$ and σ_{T_x}. The differences across the scalar variables reflect the different exchange processes due to the dry environmental conditions. The scalar variables of Data D show a uniform number of detected coherent structures, while the vertical wind exhibits a number of events increased by a factor of 2.5 compared to the scalars due to the differences in D_e.

6. Conclusions

This study presents a methodological discussion of an algorithm for automated and quasi-online analysis of coherent structures in turbulent time series obtained over tall vegetation. The applied method of analysis uses the wavelet transform with various wavelet functions for filtering the original data, determining characteristic time scales and detecting the individual coherent structures. Through application of this method to artificial time series with well-known properties and analysis of selected real field data collected above spruce forest, we arrive at the following conclusions:

- The applied wavelet filter was successful in removing high frequency fluctuations of the 'background' turbulence and spikes without altering the low frequent coherent motion. In particular, the sharp localised gradients during the sweep phase are well conserved.
- The wavelet variance spectrum yields the characteristic time scale for coherent structures contained in the time series by showing a peak at its corresponding event duration. The comparison of wavelet variances between scalar and vector variables can give useful information about ongoing physical processes in the atmosphere and scalar similarity, important for indirect flux determination methods.
- The use of individual detection criteria depending on the examined variable and its corresponding flux qualifies the method of analysis for an observation of the long-term behaviour of coherent structures valid over a wide range of atmospheric conditions.
- The objective detection of individual coherent structures yields their individual time of occurrence. On this basis, statistical parameters such as their total number, mean and deviation of their temporal separation can be calculated. The comparison of their temporal pattern between simultaneously collected time series can help understanding differences in atmospheric fluxes and scalar similarity.

After validating the method of analysis, it can now be applied to the long-term dataset to obtain a statistically well-founded climatology of coherent structures.

14   Chr. Thomas and Th. Foken: Detection of long-term coherent exchange over spruce forest

References

Bergström H, Högström U (1989) Turbulent exchange above a pine forest. II. Organized structures. Bound-Layer Meteor 49: 231–263

Bisset DK, Antonia RA, Browne LWB (1990) Spatial organisation of large structures in the turbulent far wake of a cylinder. J Fluid Mech 162: 389–413

Blackwelder RF, Kaplan RE (1976) On the wall structure of the turbulent boundary layer. J Fluid Mech 76: 89–112

Bogard DG, Tiederman WG (1986) Burst detection with single-point velocity measurements. J Fluid Mech 162: 389–413

Brunet Y, Irvine MR (2000) The control of coherent eddies in vegetation canopies: streamwise structure spacing, canopy shear scale and atmospheric stability. Bound-Layer Meteor 94: 139–163

Businger JA, Oncley SP (1990) Flux measurement with conditional sampling. J Atmos Oceanic Technol 7: 349–352

Chen J, Hu F (2003) Coherent structures detected in atmospheric boundary-layer turbulence using wavelet transforms at Huaihe River Basin, China. Bound-Layer Meteor 107: 429–444

Collineau S, Brunet Y (1993a) Detection of turbulent coherent motions in a forest canopy. Part II: Time-scales and conditional averages. Bound-Layer Meteor 66: 49–73

Collineau S, Brunet Y (1993b) Detection of turbulent coherent motions in a forest canopy. Part I: Wavelet analysis. Bound-Layer Meteor 65: 357–379

Daubechies I (1992) Ten lectures on wavelets. Philadelphia: SIAM Publ., 357 pp

Farge M (1992) Wavelet transforms and their application to turbulence. Ann Rev Fluid Mech 24: 395–347

Gamage N, Hagelberg C (1993) Detection and analysis of microfronts and associated coherent events using localized transforms. J Atmos Sci 50: 750–756

Gao W, Shaw RH, Paw U KT (1989) Observation of organized structure in turbulent flow within and above a forest canopy. Bound-Layer Meteor 47: 349–377

Gao W, Li BL (1993) Wavelet analysis of coherent structures at the atmosphere-forest interface. J Appl Meteor 32: 1717–1725

Gerstberger P (ed) (2001) Die BITÖK-Untersuchungsflächen im Fichtelgebirge und Steigerwald. Bayreuter Forum Ökologie, 90. 193 pp

Grossmann A, Morlet J (1984) Decomposition of hardy functions into square integrable wavelets of constant shape. J Math Anal 15: 723–736

Grossmann A, Kronland-Martinet R, Morlet J (1989) Reading and understanding continous wavelet transforms. In: Combes JM, Grossmann A, Tchamitchian P (eds) Wavelets: time-frequency methods and phase space. New York: Springer, pp 2–20

Handorf D, Foken T (1997) Analysis of turbulent structure over an Antarctic ice shelf by means of wavelet transformation. 12th Symosium on Boundary Layer and Turbulence, Vancouver BC, Canada, 28 July–1 August 1997. Am Meteorol Soc, pp 245–246

Holschneider M (1995) Wavelets, an analysis tool. New York: Oxford

Katul G, Kuhn G, Schieldge J, Hsieh C-I (1997) The ejection-sweep character of scalar fluxes in the unstable surface layer. Bound-Layer Meteor 83: 1–26

Kronland-Martinet R, Morlet J, Grossmann A (1987) Analysis of sound patterns through wavelet transforms. Int J Pattern Recognition and Artificial Intelligence 1: 273–302

Kumar P, Foufoula-Georgiou E (1994) Wavelet analysis in Geophysics: An Introduction. In: Foufoula-Georgiou E, Kumar P (eds) Wavelets in geophysics. Wavelet analysis and its applications. San Diego: Academic Press, pp 1–43

Lu CH, Fitzjarrald DR (1994) Seasonal and diurnal variations of coherent structures over a deciduous forest. Bound-Layer Meteor 69: 43–69

Lykossov VN, Wamser C (1995) Turbulence intermittency in the atmospheric surface layer over snow-covered sites. Bound-Layer Meteor 72: 393–409

Mahrt L (1991) Eddy asymmetry in the sheared heated boundary layer. J Atmos Sci 48: 472–492

Mahrt L, Howell JF (1994) The influence of coherent structures and microfronts on scaling laws using global and local transforms. J Fluid Mech 260: 247–270

Mallat S, Zhong S (1992) Wavelet transform maxima and multiscale edges. In: Ruskai MB et al (eds) Wavelets and their applications. Boston: Jones and Bartlett

Paw U KT, Brunet Y, Collineau S, Shaw RH, Maitani T, Qiu J, Hipps L (1992) Evidence of turbulent coherent structures in and above agricultural plant canopies. Agric Forest Meteorol 61: 55–68

Pike CJ (1994) Analysis of high resolution marine seismic data using wavelet transform. In: Foufoula-Georgiou E, Kumar P (eds) Wavelets in geophysics. Wavelet analysis and its applications. San Diego: Academic Press, pp 183–211

Raupach MR, Finnigan JJ, Brunet Y (1989) Coherent eddies in vegetation canopies. 4th Australian Conference on Heat and Mass Transfer, Christchurch, NZ, 75–90

Raupach MR, Finnigan JJ, Brunet Y (1996) Coherent eddies and turbulence in vegetation canopies: the mixing-layer analogy. Bound-Layer Meteor 78: 351–382

Shaw RH (1985) On diffusive and dispersive fluxes in forest canopies. In: Hutchinson BA, Hicks BB (eds) The forest-atmosphere interaction. Dordrecht: Reidel Publishing Company, pp 407–419

Turner BJ, Leclerc MY (1994) Conditional sampling of coherent structures in atmospheric turbulence using the wavelet transform. J Atmos Oceanic Technol 11, Part 2: 205–209

Wilczak JM, Oncley SP, Stage SA (2001) Sonic anemometer tilt correction algorithms. Bound-Layer Meteor 99: 127–150

Authors' address: Dipl. Geooeckol. Christoph Thomas (e-mail: christoph.thomas@uni-bayreuth.de), Prof. Dr. Thomas Foken (e-mail: thomas.foken@uni-bayreuth.de), Department of Micrometeorology, University of Bayreuth, 95440 Bayreuth, Germany.

Appendix C

Analysis of the low-frequency turbulence above tall vegetation using a Doppler sodar[*]

Christoph Thomas (christoph.thomas@uni-bayreuth.de)
Department of Micrometeorology, University of Bayreuth, Bayreuth, Germany

Jens-Christopher Mayer
Department of Micrometeorology, University of Bayreuth, Bayreuth, Germany

Franz X. Meixner
Biogeochemistry Department, Max-Planck-Institute for Chemistry, Mainz, Germany

Thomas Foken
Department of Micrometeorology, University of Bayreuth, Bayreuth, Germany

Abstract.   This study applies acoustic sounding to observe coherent structures in the proximity of tall vegetated surfaces. Data were collected on 22 days of measurements during two different field experiments in the summer 2003. A quality control scheme was developed to ensure high data quality of the collected time series. The data analysis was done using the wavelet transform. Coherent structures were successfully observed in the vertical wind and the backscatter intensity. They can be subdivided into small-scale events with typical time scales of 20 s - 30 s and large-scale events with typical time scales of 190 s - 210 s. Both were found to coexist close to the canopy, but show different temporal and spatial patterns. The small-scale coherent structures are dominant, constantly present and most likely generated by dynamical instabilities originating from the inflected wind profile. The large-scale coherent structures show an intermittent occurrence, largely vary with incoming solar radiation and are thus assumed to be generated by thermal processes. The maximum height of the roughness sublayer was estimated to 5 times the canopy height.

Keywords: Acoustic sounding, Coherent structures, Turbulence, Vegetation, Wavelet transform

1. Introduction

The turbulent flow statistics above tall vegetation differ from those in the surface layer above homogeneous surfaces and are predominantly controlled by large-scale coherent structures. Coherent structures are an inherent part of the turbulent flow originating from the instabilities of the inflected mean horizontal velocity profile (e.g. Raupach et al., 1996; Finnigan, 2000) and contribute significantly to atmospheric turbulent fluxes. This contribution is crucial for the understanding of

---

[*] submitted to Boundary-Layer Meteorology

2   Thomas et al.

exchange processes of momentum, heat and matter between the surface, the canopy and the atmosphere. Various definitions of coherent structures can be found in literature, depending on the time scale and the height where they were observed. In our study we consider data obtained above tall vegetation. In the proximity to the plant canopy, coherent structures become evident in time series of scalars as aperiodic ramp-like patterns. In vector time series they manifest themselves as more symmetric, triangle-like patterns. The underlying physical process of an individual event can be described as a slow upward motion (ejection, burst) followed by a rapid downward motion (sweep, gust) covering a duration from several seconds to a few minutes.

Coherent structures in and above tall vegetation have been observed by many authors (Gao et al., 1989; Bergström and Högström, 1989; Paw U et al., 1992; Raupach et al., 1989; Lu and Fitzjarrald, 1994; Brunet and Irvine, 2000). Most data used in literature were obtained using sonic anemometers and fast gas analysers providing data with sampling frequencies of several Hertz. Despite the high temporal resolution, the spatial resolution and representativeness of such data is often limited as the devices are deployed on towers. In contrast, acoustic sounding is commonly used to obtain vertically well resolved mean profiles of wind velocities. Therefor single soundings are averaged over a certain period of time commonly not less than several minutes. However, the individual soundings provide time series with a temporal resolution of several seconds with a high spatial resolution given by the individual observations levels. Various authors have been taking advantage of this acoustic sounding technique to observing large coherent plumes in the convective boundary layer (e. g. Hall et al., 1975; Taconet and Weill, 1982; Petenko and Bezverkhnii, 1999; Petenko et al., 2004). They evidenced large convective flow structures with characteristical durations between 1 min and 20 min within a vertical range of 60 m to 550 m above ground using detection methods based on either visual, spectral or wavelet analysis. If one applies acoustic sounding in the proximity of a plant canopy the questions arise (i) if the data quality of the single soundings is sufficient as the acoustic backscatter intensity largely varies with the regime of the atmospheric stability and (ii) whether the temporal resolution of the time series is sufficiently high for the observation of coherent structures characterised by event durations smaller than those of convective plumes. The data quality can be controlled through a thorough selection of (a) the sampling site, (b) the acoustic sounding frequency with a low intensity of background noise and (c) an efficient quality control to exclude inaccurate data due to the random nature of the backscattered acoustic signal (Spizzichino, 1974). The temporal resolution of the time series can be increased by

limiting the number of observed variables and the vertical range of the measurements.

This study presents the results of observation and analysis of coherent structures above tall vegetation in time series consisting of single soundings of a commercially available acoustic sounding system. Data were collected during two individual field experiments in Germany both conducted in the summer of 2003. The objectives of the study are (i) to demonstrate the applicability of acoustic remote sensing for the observation of coherent structures above tall vegetation, and (ii) to get deeper insight into the dynamics of low-frequency turbulent flow in this part of the atmospheric boundary layer. The objectives will be achieved through the analysis of a large quantity of nighttime and daytime observations, overall representing 22 days of measurements.

At first, the experimental sites and setup will be described. The subsequent part will deal with the method of analysis including the applied data quality control scheme, the preparation of the time series to analysis and a brief description of the wavelet analysis. After presentation and discussion of the results the final part will summarise the main conclusions.

2. Experimental description

The datasets were obtained during two different field experiments, namely the WALDATEM-2003 (WAveLet Detection and Atmospheric Turbulent Exchange Measurements) and the ECHO (Emission and CHemical transformation of biogenic volatile Organic compounds) campaigns. The main objective of WALDATEM-2003 was the extensive investigation of coherent structures and exchange processes above a spruce forest through a combination of tower-based measurements and ground-based acoustic remote sensing technique. The experiment was conducted during May - July 2003 at the Fluxnet station Weidenbrunnen Waldstein 775 m a. s. l. in the Fichtelgebirge mountains, Germany (Fig. 1a). The data were collected on 18 consecutive days, yielding an overall number of 632 datasets each representing 25 min of sounding. The ECHO experiment aimed on a better understanding of forest stands as a complex source of reactive trace gases into the troposphere (Koppmann, 2003). The ECHO data were obtained on 4 consecutive days during a field campaign in July - August 2003 conducted at the Research Center Jülich (Fig. 1b), with an overall number of 110 datasets. In this paper, observation levels of the acoustic sounding system and tower measurements are given as heights about ground level (a. g. l.) unless otherwise stated.

4   Thomas et al.

2.1. EXPERIMENTAL SITES

The ambient conditions of a sampling site are crucial for both the successful operation and the interpretation of the data of an acoustic sounding system. They determine the intensity and spectral distribution of background noise and fixed echoes. The measurements during WALDATEM-2003 were conducted above a spruce forest with a mean canopy height h_c of 19 m, during ECHO above a mixed forest with an mean canopy height of 30 m. Detailed descriptions of the experimental sites can be found in Gerstberger et al. (2004) and Aubrun et al. (2004) for the WALDATEM-2003 and ECHO experiments respectively. The acoustic sounding system was located in clearings during both experiments (see Fig. 1a and Fig. 1b): During WALDATEM-2003 the clearing had the dimensions of approx. 100 m x 200 m, during ECHO approx. 500 m x 500 m. During the WALDATEM-2003 experiment, fixed echoes were caused by the large step changes of forest edges and appeared in the data up to an observation level of 30 m. The level of background noise was very low with an evenly distributed amplitude over the analysed range of the acoustic spectra. The site can be classified as remote without any permanent influence of road traffic and other sound sources and thus ideal for acoustic sounding systems. During the ECHO experiment, the acoustic sounding system was located close to the waste water treatment plant of the Research Center Jülich. No fixed echoes could be found in the data records. In contrast to this, the level of background noise was high with intermittent peaks of very high intensity caused by numerous pumps, flushing water and road traffic. The site can thus be classified as non ideal for acoustic sounding systems allowing high data availability and quality only from the late afternoon to the early morning hours.

2.2. ACOUSTIC SOUNDING SYSTEM

The acoustic sounding system was a phased-array Doppler-Sodar (model DSDPA90.64, Metek GmbH) in combination with a 1290-MHz-RASS extension (Metek GmbH). The operating settings were optimised in respect to high time resolution. Thus, only the vertically orientated acoustic antenna and the radioacoustic antenna were selected for operation yielding measurements of vertical velocity, acoustic backscatter intensity and acoustic temperature. When increasing the repetition rate of the sound pulses, one may run into the problem that starting from a certain repetition rate the current sounding is disturbed by the backscatter of the preceding sound pulse, which results in erroneous data. Thus, one must await until the intensity of the backscatter of the preceding sound pulse is indiscernible from the level of background
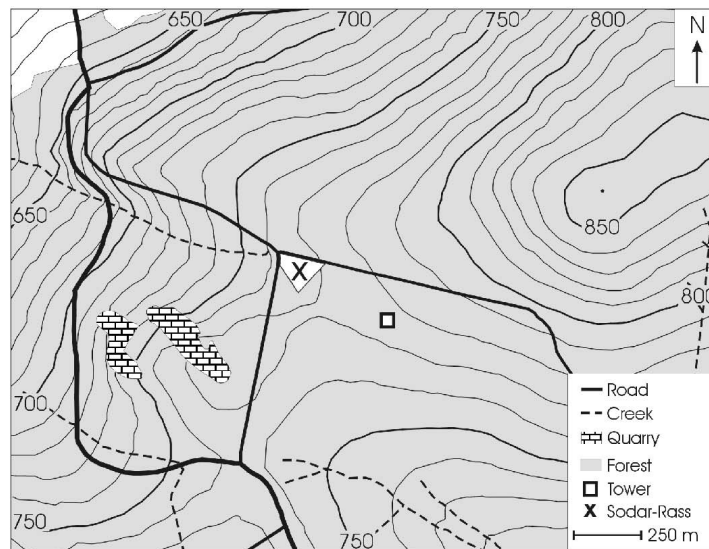
Figure 1a. Map of the experimental site of WALDATEM-2003; numbers on isopleths are heights [m] a. s. l.
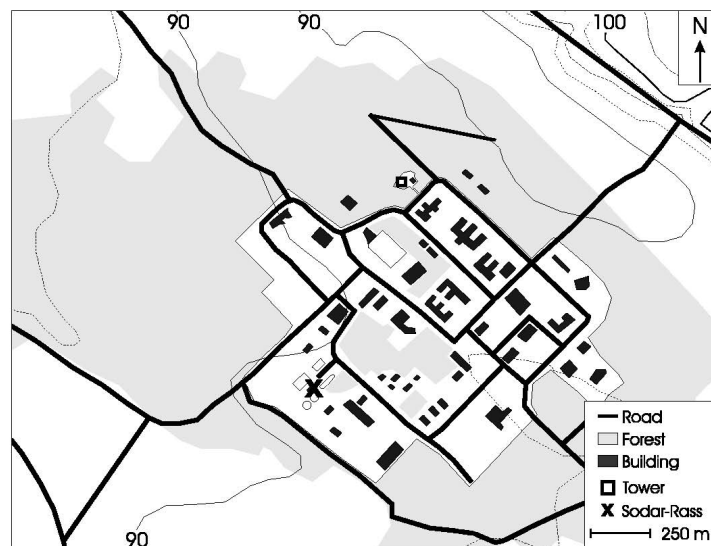
Figure 1b. Map of the experimental site during ECHO; numbers on isopleths are heights [m] a. s. l.

6   Thomas et al.

noise before emitting the next sound puls. The height corresponding to this period of time is called noise height. As the absorption of sound waves in the atmosphere depends on the acoustic frequency (Neff, 1975), an optimal adjustment of sounding frequency, observation levels and noise height is necessary. Corresponding tests resulted in an optimal acoustic sounding frequency of 2000 Hz. The minimum and maximum observation levels z_{min} and z_{max} were selected to 35 m and 145 m respectively during WALDATEM-2003 and to 40 m and 150 m respectively during ECHO. The noise height was chosen to 180 m. The effective sampling frequency was determined to 0.4 Hz, which is equivalent to a repetition rate of 2.5 s. The vertical resolution was set to 10 m. Unfortunately, the vertical resolution turned out to be insufficient to obtain reliable instantaneous profiles of the acoustic temperature, as the radioacoustic system was operated beyond its technical specifications. Therefore, the measurements of the acoustic temperature were excluded from further analysis. Between adjacent 25 min intervals of sounding with the settings described above, mean profiles of horizontal and vertical velocities and sonic temperature were obtained throughout the atmospheric boundary layer up to an observation level of 900 m using an acoustic sounding frequency of 1650 Hz and a vertical resolution of 20 m.

2.3. TOWER-BASED MEASUREMENTS

A profile equipped with 6 sonic anemometers was installed on the tower during the WALDATEM-2003 experiment. The data of the sonic anemometer (sonic type R3-50, Gill Instruments Ltd.) at the uppermost observation level of 33 m operated at 20 Hz sampling frequency was used for the determination of atmospheric fluxes according to Foken et al. (2004). The mean canopy height h_c was 19 m. Radiation measurements were carried out at 30 m using up- and downward facing shortwave (CM-14, Kipp&Zonen) and longwave (CG-2, Kipp&Zonen) radiation sensors. The main tower was located approx. 250 m apart from the acoustic sounding system (Fig. 1a).

3. Method of analysis

Data were postprocessed after the field experiments. This procedure can be subdivided into data preparation and wavelet analysis. Data preparation includes the quality control, i. e. detecting and discarding erroneous data, and filling the resulting gaps in the time series. These steps are very important as the data obtained by the acoustic sounding system are highly affected by occasionally occurring environmental

Low-frequency turbulence above tall vegetation   7

noise (Miller and Rochwarger, 1970; Neff and Coulter, 1986; Crescenti, 1998).

3.1. QUALITY CONTROL AND GAP FILLING

In a first step, data were filtered using the error flag output by the sodar system. The error flags were assigned to each single value of the vertical profile by the spectrum analyser of the acoustic sounding system based on the properties of the received spectrum. It includes an assessment of the shape of the spectrum, i. e. extremly narrow or broad peaks, the signal-to-noise ratio and the presence of multiple peaks. All flagged data were discarded and replaced by an error wildcard. As a next step, a self-developed quality assessment scheme was applied. The quality of each time series consisting of 25 min of measurements was assessed individually for each observation height z regarding the length D_g and the number $n_g(D_g)$ of the contained gaps. The size of a gap is given through $D_g = n \cdot f_s^{-1}$, where n is the number of consecutive error wildcards and f_s the sampling frequency in Hz. A quality flag adopting values of $1, 2, 3, 4$ and 9 was assigned to each time series in dependence of the fraction F_g of small gaps not exceeding the critical gap size D_c (Eq. 1),

$$F_g = \frac{n_g(D_g \le D_c)}{N_g},\tag{1}$$

where N_g is the total number of gaps in a time series. The applied criteria of the quality flag are listed in Tab. I. The critical gap size D_c was chosen to 5 s in respect to the subsequent wavelet analysis. Only time series with assigned quality flags of 1 or 2 were regarded as 'good data' and passed to the subsequent steps of data processing. The detailed statistics on data quality are given in Tab. IIa and Tab. IIb for both experiments. The data quality of the lower observation heights is high for both the WALDATEM-2003 and ECHO data. The data quality decreases with increasing observation height depending on the level of background noise. The WALDATEM-2003 data show a continuously decreasing number of high quality data reaching $\sim 54\%$ of the available data at a height of 115 m. For the ECHO data, the number of good data rapidly decreases as the observation height exceeds 80 m due to the very noisy environment. Defining an arbitrary threshold of 50 % data availability of high quality data, the analysis of the vertical profiles could be performed up to 115 m and 80 m for the WALDATEM-2003 and ECHO experiments respectively. Subsequently, the gaps in the time series were interpolated using a non-linear algorithm (Akima, 1970). The last step in data preparation was the normalisation of the time series by their mean and standard deviation.

8   Thomas et al.

Table I. Quality assessment of the data;
the fraction F_g is given by Eq. 1

Quality flag	$F_g \geq$
1	0.9
2	0.8
3	0.7
4	0.5
9	< 0.5

Table IIa. Data quality during WALDATEM-2003: number (percentage) of 25 min files; the
total number of files is 632.

Quality flag	Height a. g. l.					
	35 m	45 m	55 m	65 m	75 m	85 m
1	474 (75.0)	502 (79.4)	490 (77.5)	417 (66.0)	397 (62.8)	328 (51.9)
2	57 (9.0)	30 (4.7)	39 (6.2)	93 (14.7)	100 (15.8)	136 (21.5)
3	12 (1.9)	8 (1.3)	10 (1.6)	23 (3.6)	32 (5.1)	44 (7.0)
4	4 (0.6)	6 (0.9)	4 (0.6)	12 (1.9)	16 (2.5)	34 (5.4)
9	85 (13.4)	86 (13.6)	89 (14.1)	87 (13.8)	87 (13.8)	90 (14.2)

Quality flag	Height a. g. l.					
	95 m	105 m	115 m	125 m	135 m	145 m
1	316 (50.0)	231 (36.6)	186 (29.4)	141 (22.3)	112 (17.7)	69 (10.9)
2	114 (18.0)	157 (24.8)	155 (24.5)	149 (23.6)	127 (20.1)	134 (21.2)
3	65 (10.3)	80 (12.8)	103 (16.3)	111 (17.6)	118 (18.7)	119 (18.8)
4	37 (5.9)	52 (8.2)	70 (11.1)	99 (15.7)	127 (20.1)	135 (21.4)
9	100 (15.8)	112 (17.7)	118 (18.7)	132 (20.9)	148 (23.4)	175 (27.7)

3.2. WAVELET ANALYSIS

A detailed description and discussion of the method of analysis can be
found in Thomas and Foken (2005). Here, only the main steps will be
outlined.
The analysis starts from the application of a low-pass filter to the
quality checked time series using a biorthogonal wavelet function. This
filter discards fluctuations smaller than the critical event duration D_c
of 5 s. Recalling the preceding subsection, this is the same value used
for the critical gap size when assessing the data quality. The wavelet
variance spectrum is then calculated by continuous wavelet transform

Low-frequency turbulence above tall vegetation 9

Table IIb. Data quality during ECHO: number (percentage) of 25 min files; the total number of files is 110.

Quality flag	Height a. g. l.					
	40 m	50 m	60 m	70 m	80 m	90 m
1	87 (79.1)	73 (66.4)	73 (66.4)	51 (46.4)	38 (34.5)	15 (13.6)
2	15 (13.6)	22 (20.0)	19 (17.3)	32 (29.1)	29 (26.4)	29 (26.4)
3	4 (3.6)	7 (6.4)	12 (10.9)	15 (13.6)	27 (24.5)	32 (29.1)
4	3 (2.7)	7 (6.4)	5 (4.5)	11 (10.0)	14 (12.7)	27 (24.5)
9	1 (0.9)	1 (0.9)	1 (0.9)	1 (0.9)	2 (1.8)	7 (6.4)

Quality flag	Height a. g. l.					
	100 m	110 m	120 m	130 m	140 m	150 m
1	4 (3.6)	13 (11.8)	0 (0.0)	4 (3.6)	2 (1.8)	0 (0.0)
2	23 (20.9)	23 (20.9)	19 (17.3)	11 (10.0)	18 (16.4)	4 (3.6)
3	30 (27.3)	26 (23.6)	25 (22.7)	31 (28.2)	23 (20.9)	16 (14.5)
4	37 (33.6)	36 (32.7)	42 (38.2)	41 (37.3)	46 (41.8)	50 (45.5)
9	16 (14.5)	12 (10.9)	24 (21.8)	23 (20.9)	21 (19.1)	40 (36.4)

performed on scales representing event durations D ranging from 10 s to 240 s. The event duration D is defined as (e. g. Collineau and Brunet, 1993a)

$$D = \frac{1}{2} \cdot f^{-1} = \frac{a \cdot \pi}{f_s \cdot \omega^0_{\Psi_{1,1,0}}}, \qquad (2)$$

where f is the frequency corresponding to the event duration, a the wavelet dilation scale, f_s the sampling frequency of the time series and $\omega^0_{\Psi_{1,1,0}}$ the center frequency of the mother wavelet function. For a sine function, the event duration D represents half the length of a single period. The minimum event duration was chosen to as twice the critical gap size and the critical event duration of the wavelet filter D_c according to the Nyquist frequency (Kumar and Foufoula-Georgiou, 1994), which ensures preventing aliasing effects in the calculated spectra. The characteristic time scales of coherent structures D_e are derived from the maxima in the wavelet variance spectra. The analysis is completed by detecting the individual coherent structures through a wavelet transform at event duration D_e using the Mexican hat wavelet function. The last step reveals the number and the time of occurrence of the individual coherent structures in a time series.

10   Thomas et al.

4. Results and discussion

We shall now discuss the results from the analysis of the time series
of vertical velocity and backscatter intensity derived from the acoustic
sounding system.

4.1. Vertical wind

The vertical wind and its spectrum represent the active turbulence
near the canopy at $z \simeq h_c$ which controls the vertical exchange of
momentum and scalar variables to a major extent (Raupach et al.,
1989). The probability density function (pdf) of the detected char-
acteristic time scales of coherent structures D_e of the vertical wind
during WALDATEM-2003 are plotted in Fig. 2. Almost no variation
with height can be observed. The distributions clearly show a maxi-
mum density peak located between 20 s and 30 s event duration, then
continuously decreasing densities towards a minimum at ~ 150 s. A
second maximum of density becomes evident between 190 s and 220 s
event duration, while the exact location of the peak slightly depends
on the observation level. The global maximum peak at ~ 25 s event
duration is in close agreement with the findings of Collineau and Brunet
(1993b), Chen and Hu (2003), Thomas and Foken (2005), who found
similar characteristic time scales for coherent structures in the time
series of vertical wind ranging between 10 s and 30 s. The second, local
maximum found at ~ 210 s corresponds well to the findings of Petenko
et al. (2004) for convective coherent structures. The little differences of
the pdf between the displayed observation levels is not surprising as the
highest observation level is still close to the canopy with a normalised
height $z \cdot h_c^{-1}$ of 6. The merging of small coherent convective elements
to larger convective plumes has been observed by some authors (e. g.
Hall et al., 1975, Williams and Hacker, 1993, Petenko and Bezverkhnii,
1999), but in greater heights $z \geq 300$ m. The predominant reason for the
similar pdfs in Fig. 2 is that they represent an integral over all analysed
data, i. e. daytime and nighttime data under different thermal stability
and dynamical conditions. From this one may conclude that the inte-
gral pdf of the characteristic time scales reveals only little information
about the dynamics of coherent structures in neighbored observation
levels. Therefore, it is important to know (i) if one or more maxima
exist in the spectrum of a single observation level and (ii) if these
maxima are consistent across different observation levels. An example
will be given using spectra of time series of selected observation levels
(Fig. 3a, Fig. 3b). The data of the lower observation heights in Fig. 3a
consistently exhibit the first maximum at ~ 18 s event duration. This
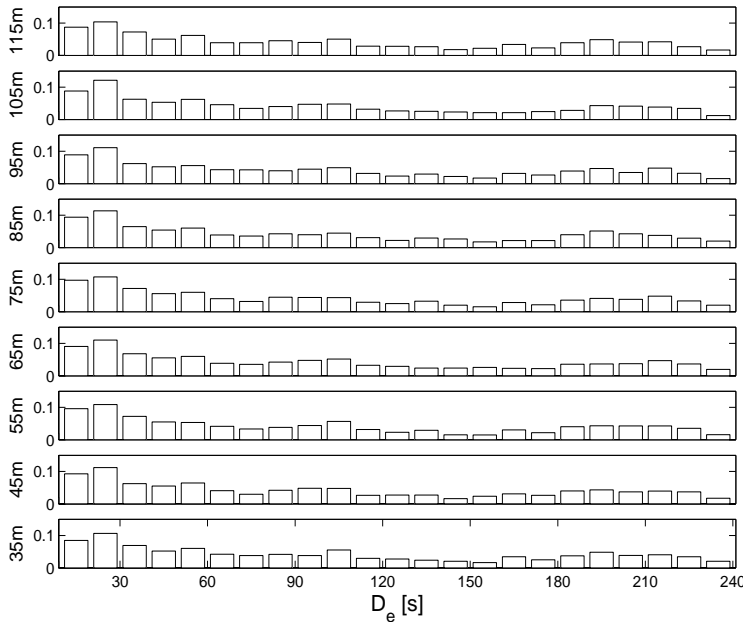
Figure 2. Probability density function (pdf) of the characteristic event durations D_e of coherent structures in the vertical wind for the WALDATEM-2003 data; the resolution ΔD_e is 10 s.

maximum vanishes with increasing height suggesting that the corresponding small coherent structures persist only close to the canopy. In case of Fig. 3b, only the data of the lowest observation level exhibit a maximum at ~ 19 s, while the observation levels above show the first maximum beyond 40 s. The corresponding time-height cross-section of the vertical wind is presented in Fig. 4 for a 13 min period. The large-scale updraft evident in the center of the plot is consistent across all observation levels and persists approx. 130 s in the lower and approx. 250 s in the upper observation levels. These visually estimated event durations are in good agreement with the event durations of the spectral maxima in Fig. 3b. Despite this dominating large-scale updraft other smaller updrafts can be seen around the times 100 s, 500 s and 660 s. These bursts are consistently found in the lower observation levels but barely reach a height of 150 m. The large-scale events show a complex substructure consisting of smaller accelerated or slowed structures with an estimated event duration of approx. 20 s.

In respect to the statistics of these observations, we introduce the correlation coefficient R_s between the wavelet variance spectrum at a reference level z_{ref} and a comparison level z_{comp},

12   Thomas et al.

(a)   (b)
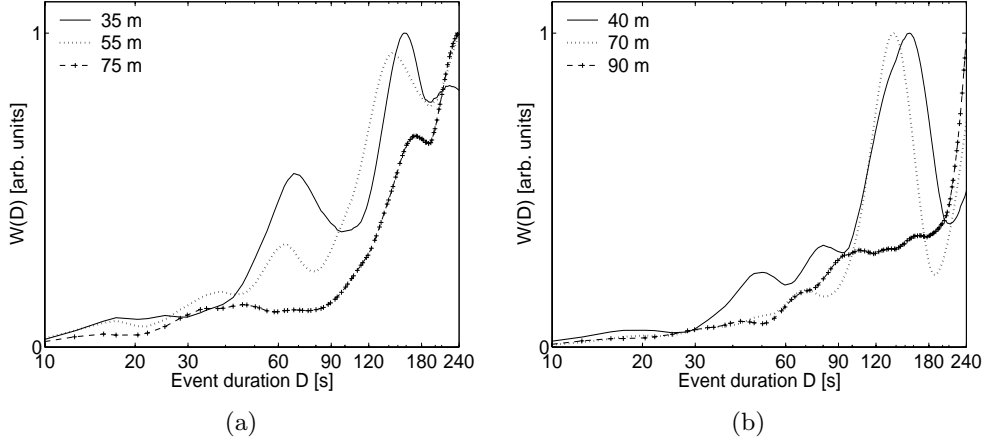
Figure 3. Spectra of the wavelet variance $W(D)$ of selected observation levels for the vertical wind during (a) WALDATEM-2003 June 8, 2003 12:30-12:55 CET and (b) ECHO July 29, 2003 15:45-16:10 CET
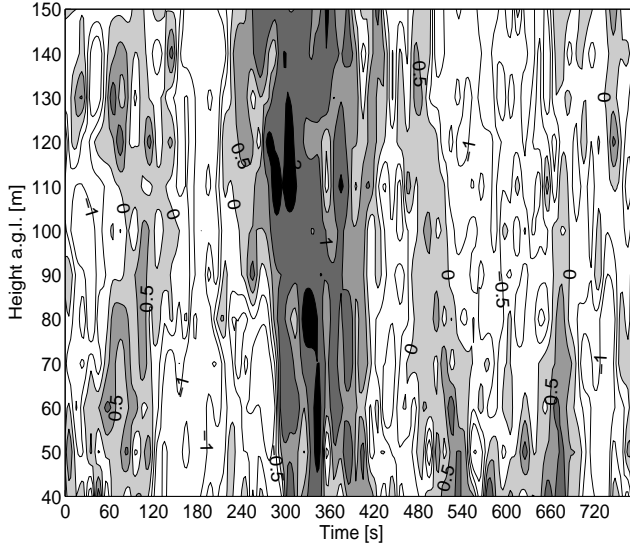
Figure 4. Time-height cross-section of the low-pass filtered and normalised vertical wind during ECHO July 29, 2003 15:54 - 16:07 CET corresponding to the spectra presented in Fig. 3b; updrafts are grey-shaded, downdrafts are filled white

$$R_s(z_{ref}, z_{comp}) = \frac{\overline{W(D)_{z_{ref}} W(D)_{z_{comp}}}}{\sigma_{W(D)_{z_{ref}}} \cdot \sigma_{W(D)_{z_{comp}}}}. \tag{3}$$

$W(D)$ denotes the wavelet variance, i.e. the spectral density at event duration D, σ the standard deviation and the overbar depicts the phase mean over the fluctuations. Thus, we are able to take into account the

entire information contained in the spectra.

For the investigation of the statistics, only the WALDATEM-2003 provides a dataset with a sufficient number of data and will thus be used in the following. The reference height z_{ref} was set to z_{min}, i.e. 35 m, while the comparison height z_{ref} ranged between 45 m and 115 m. The mean diurnal course of R_s was calculated for 15 selected days all characterised by high incoming short-wave radiation, low cloudiness and moderate wind speeds (Fig. 6). The connection between adjacent observation levels reveals complex dynamics of low-frequency turbulence of the vertical wind above the canopy. The assumption of a coupled state between neighboured levels is based on the definition of coherent structures as correlated motions throughout the roughness sublayer (RSL) (Gao et al., 1989). Proceeding from this definition, coherent structures are expected to be represented by the same maximum peak in spectral density between neighboured observation levels and thus to yield higher correlation coefficients R_s.

Under stable conditions, during the second half of the night (from 0 CET to 5 CET), the correlation coefficient R_s is < 0.3 (Fig. 5a). The individual levels are not or only very loosely coupled. Around 6 CET we see a first coupling between the observation levels from 35 m to about 75 m, yielding $R_s \geq 0.4$, which is followed by a short period of smaller correlation.

A second, even stronger coupling enclosing the vertical profile up to 115 m can be observed around 9 CET, yielding $R_s \geq 0.5$ up to 65 m and ≥ 0.4 up to 115 m. And again, after 9 CET the coupling is decreasing before picking up again after 10 CET, reaching a maximum of $R_s \geq 0.6$ at about 13 CET and enclosing layers up to 95 m. Beyond 14 CET the coupling gradually decreases with R_s dropping below 0.4 at about 18 CET. During the first half of the night from 20 CET to 0 CET, the layers are almost decoupled showing only small correlation between neighboured observation levels. An interesting feature is the increase of $R_s \geq 0.5$ in the height range between 95 m and 115 m at around 17 CET. It coincides with the beginning transition from neutral to stable conditions (Fig. 6). As the stabilisation of the layer above the canopy is caused by cooling processes of the canopy and thus the stabilisation starts from below, the stratification in the upper layers is more unstable than below. In this local residual layer coherent structures apparently exist while being somewhat suppressed below. However, as R_s reflects the correlation to the reference level $z_{ref} = 35$ m, the coherent structures observed above 95 m must be present also in the lowest layer. This phenomenon might be explained by a continuing instabilisation of the layer very close to the canopy caused by rising air coming out of the canopy and subcanopy space. This air is warmer

14   Thomas et al.
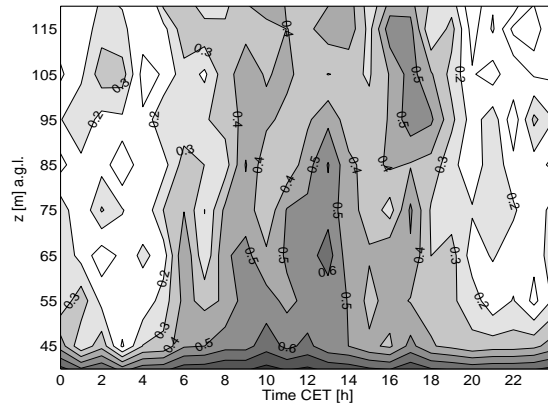
Figure 5a. Time-height cross-section of the ensemble averages of the correlation coefficient R_s (Eq. 3) calculated for the vertical wind spectra with event durations $10\,s \leq D \leq 240\,s$ for 15 selected days during WALDATEM-2003.
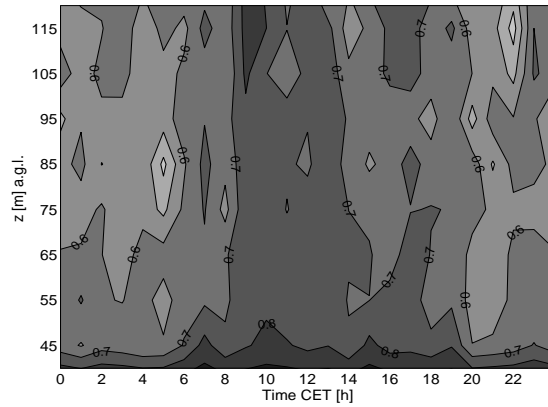
Figure 5b. The same as in Fig. 5a, but with event durations $10\,s \leq D \leq 60\,s$.
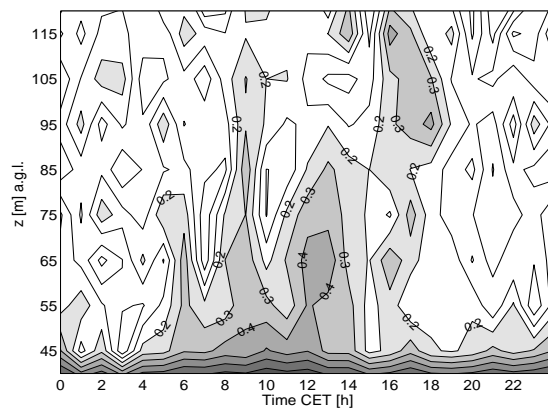
Figure 5c. The same as in Fig. 5a, but with event durations $60\,s \leq D \leq 240\,s$.

Low-frequency turbulence above tall vegetation   15
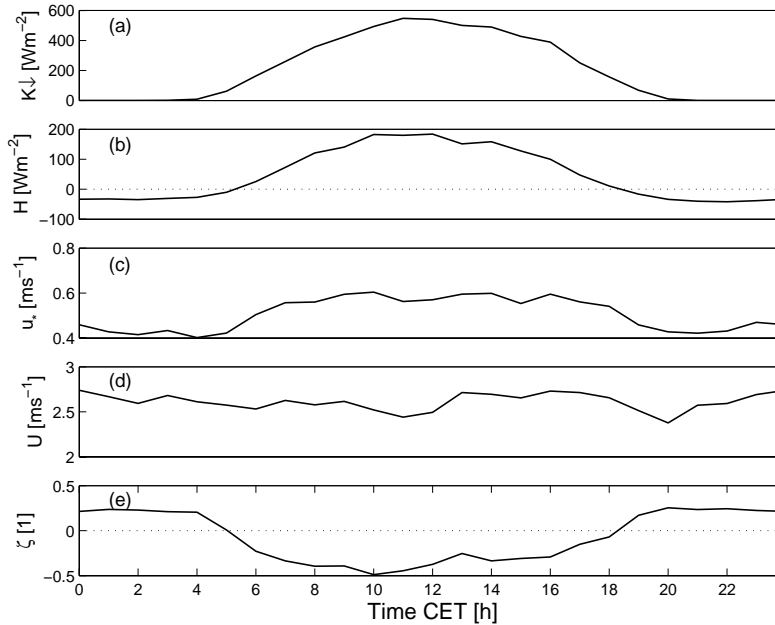
Figure 6. Mean diurnal course of (a) incoming shortwave radiation K↓, (b) sensible heat flux H, (c) friction velocity u_*, (d) mean horizontal wind speed U and (e) atmospheric stability ζ, measured at the tower at a height of 33 m for 15 selected days during WALDATEM-2003.

compared to the cooled air above and thus counteracts the ongoing stabilisation. This effect is limited to the layer very close the canopy reaching up to the lowest observation level at 35 m.

For understanding of the results presented above, we like to consider the underlying mechanisms of coherent structures. In literature dealing with coherent structures above tall vegetation, dynamical instabilities originating from the strong wind shear of the inflected mean horizontal wind profile were identified as the main driving force of coherent structures in the RSL. This finding resulted in the mixing-layer-analogy theory (Raupach et al., 1989, Raupach et al., 1996). According to this theory, the horizontal spacing between adjacent coherent structures is a unique, linear function of a wind shear scale, analogous to the properties of the turbulent mixing layer that evolves between two coflowing streams of different velocities. The theory, basically established for near neutral conditions, was proven to be valid also over a wide range of stabilities (Brunet and Irvine, 2000). However, we cannot neglect the fact that there might be other, thermal processes which might influence the generation of coherent structures. The existence of large-scale coherent motions corresponding to event durations between 190 s and 210 s in

16   Thomas et al.

Fig. 2 supports this assumption. Assuming that coherent structures originating from different processes coexist in the RSL and are characterised by different time scales, we might be able to separate them. This will be achieved by splitting the spectrum into different parts which enclose corresponding characteristic event durations. Therefore, we subdivide the entire spectrum into two parts: (a) the small-scale coherent structures with $10\,s < D < 60\,s$ and (b) the large-scale coherent structures with $60\,s < D < 240\,s$. The separation at $D = 60\,s$ seems justified by visually inspecting the probability density function plotted in Fig. 2. The corresponding results are displayed in Fig. 5b and Fig. 5c. The correlation coefficient R_s is generally high for the small-scale part of the spectrum with values ≥ 0.6 compared to the large-scale part with R_s typically not exceeding 0.4. As demonstrated in Fig. 5b, R_s exceeds 0.6 between $45\,m$ and $115\,m$ during 6 CET and 20 CET, and $R_s \geq 0.7$ between 8 CET and 17 CET. This latter period of high correlation coincides with the period of increased u_* which is constant between 0.55 and $0.60\,ms^{-1}$ (see Fig. 6). Small-scale coherent structures were thus found to be present during the day and the night. This observation leads us to the conclusion that the small-scale coherent structures are generated by dynamical processes which are independent on the stability regime of the air. As far as the large-scale part of the spectrum is concerned, the excursions of $R_s \geq 0.3$ in Fig. 5c coincide with the intermittent coupling processes prior observed for periods with $R_s \geq 0.4$ in Fig. 5a. It is worth noting that the elevated layer of high correlation between $95\,m$ and $115\,m$ observed around 17 CET (Fig. 5c), assumed to be a local residual layer, appears in both the small-scale and large-scale part as an area of increased correlation. From the magnitude of correlation we can conclude that the small-scale coherent structures with $20\,s \leq D_e \leq 40\,s$ are the dominant coherent structures present throughout the observed RSL. In addition, there exist large-scale coherent structures with $90\,s \leq D_e \leq 210\,s$ showing generally lower correlation within the RSL. They carry an intermittent character and are most probably controlled by thermal processes.

The RSL is a concept to separate a layer adjacent to rough surfaces, which is significantly influenced by the surface inhomogeneities, from a layer above, in which the surface roughness ceases to effect the flow. The height of the RSL above vegetated canopies is typically estimated to $3 \cdot h_c$. If we define the RSL as (i) the layer close to the canopy where correlated, coherent motion takes place, and (ii) assume that the coherent motion is mainly generated by the surface roughness effecting the flow, we can now estimate its maximal height to approx. $5 \cdot h_c$ based on the results presented above.

Low-frequency turbulence above tall vegetation 17

4.2. BACKSCATTER INTENSITY

The backscattered acoustic intensity $P(z)$ of an emitted sound pulse is a fundamental parameter in the field of acoustic sounding. $P(z)$ of a monostatic acoustic sounding system can be related to the parameter of the temperature structure function C_T^2 through

$$\sigma(z) = 0.0039 \cdot \lambda^{-1/3} \cdot C_T^2 \cdot \overline{T}^{-2} \tag{4}$$

(Tatarskii, 1971) and the radar equation (Little, 1969)

$$P(z) = S \cdot e^{-2\alpha z} \cdot \sigma(z). \tag{5}$$

Combining Eq. 4 and Eq. 5 one yields

$$C_T^2 = 256 \cdot S^{-1} \cdot \lambda^{1/3} \cdot e^{2\alpha z} \cdot \overline{T^2} \cdot P(z), \tag{6}$$

where $\sigma(z)$ is the scattering cross section, λ the wavelength of the acoustic frequency, $\overline{T}$ the mean air temperature over the range of interest, $e^{2\alpha z}$ power loss due to atmospheric attenuation with α being the attenuation coefficient, z the travel distance to the scattering volume, i. e. height for the vertical antenna and S a system calibration function specific for the acoustic sounding system (see e. g. Haugen and Kaimal, 1978, Coulter and Wesely, 1980). $P(z)$ is a non-Doppler variable directly measured by the acoustic sounding system which reflects the degree of density inhomogeneities present in the air.

The pdf of the detected time scales of coherent structures in the backscatter intensity is presented in Fig. 7. The maximum densities are located between 20 s and 30 s and 190 s and 200 s event duration for the small-scale and large-scale coherent structures respectively. Comparing the results to those obtained for the vertical wind (Fig. 2), the pdf for the backscatter intensity is stronger skewed towards smaller scales. A further difference can be found for the smaller scales centered at 15 s and 25 s event duration. Except for the lowest level, the maximum of the distribution changes from the smaller to the larger D_e with increasing height, suggesting that larger coherent structures dominate with increasing height. Unfortunately, the acceptable maximum observation level of the acoustic sounding system applied in this study was too low in order to follow the trend higher up. Nonetheless, the result points to the findings of Hall et al. (1975), Williams and Hacker (1993), Petenko and Bezverkhnii (1999), who observed the merging of small convective elements into larger ones, but in greater heights.

The correlation coefficient R_s, introduced in Eq. 3, was calculated for the entire range of event durations from 10 s to 240 s, the small-scale part from 10 s to 60 s and the large-scale part from 60 s to 240 s for

18   Thomas et al.
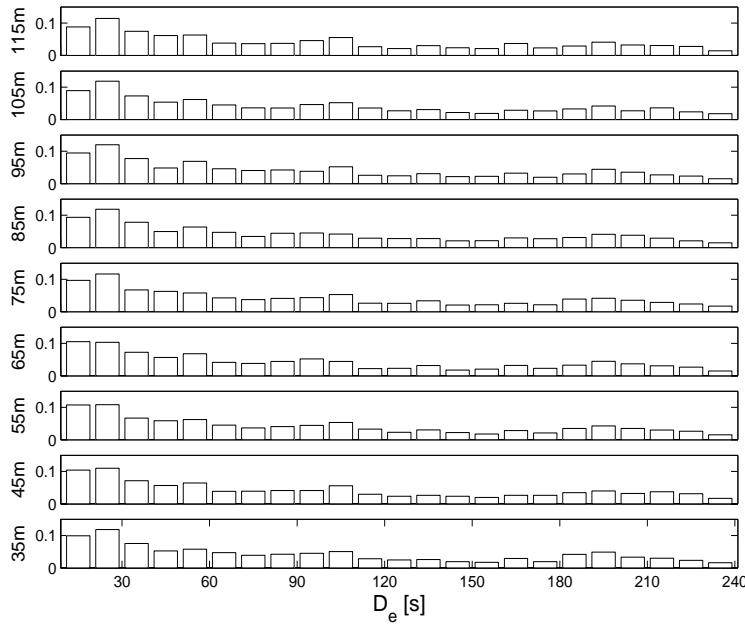
Figure 7. Probability density function (pdf) of the characteristic event durations D_e of coherent structures in the acoustic backscatter intensity for the WALDATEM-2003 data; the resolution ΔD_e is 10 s.

the 15 selected days during WALDATEM-2003. The correlation coefficient determined for the entire range of event durations (Fig. 8a) varies between 0.3 and 0.6. Higher correlations can be found for conditions of unstable stratification (Fig. 6) between 5 CET and 18 CET. Almost no temporal and spatial variation of R_s becomes evident from for the small-scale coherent structures (Fig. 8b), where R_s is only occasionally dropping below 0.7. From this result we can conclude that the small-scale coherent structures detected in the backscatter intensity are omnipresent in the considered layer (35 m - 115 m) and cannot be linked to the merging of small structures under convective conditions as presumed from the pdf in Fig. 7. This conclusion is strengthened by the conception of convection as a large-scale process occupying the entire atmospheric mixing layer and taking place on time scales much larger than 60 s. Furthermore we can conclude that the presence of small-scale coherent structures in the backscatter intensity is not sufficient to derive the state of coupling between the canopy and the overlying atmosphere. Additional information is required from the analysis of the large-scale coherent structures. The correlation coefficient for the large-scale coherent structures (Fig. 8c) is typically small (< 0.3) during stable stratification.

Low-frequency turbulence above tall vegetation   19
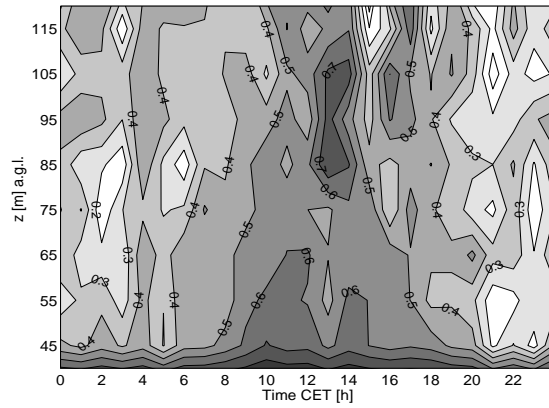
Figure 8a. Time-height cross-section of the ensemble averages of the correlation coefficient R_s (Eq. 3) calculated for the spectra of backscatter intensity with event durations $10\,s \leq D \leq 240\,s$ for 15 selected days during WALDATEM-2003.
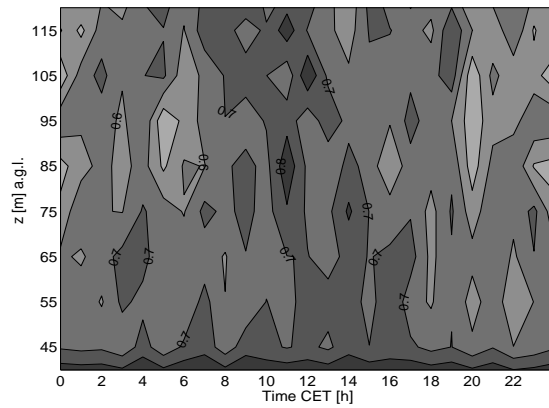
Figure 8b. The same as in Fig. 8a, but with event durations $10\,s \leq D \leq 60\,s$.
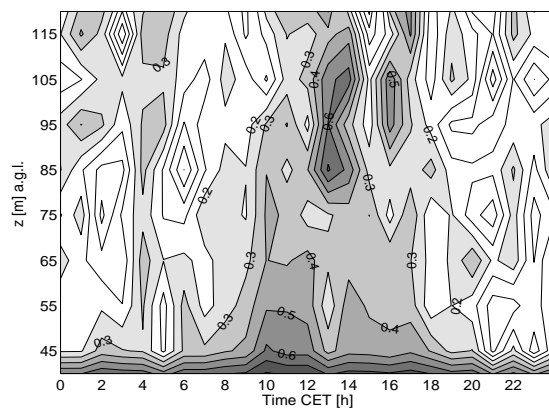
Figure 8c. The same as in Fig. 8a, but with event durations $60\,s \leq D \leq 240\,s$.

It increases during solar insolation and reaches its maximum (≥ 0.5) between 10 CET and 12 CET. Comparing R_s for the entire range of event durations (Fig. 8a) to those for the large-scale ones (Fig. 8c) one can see that the dynamics present in the diurnal course can be addressed to the presence of large-scale coherent structures with event duration beyond 60 s. An interesting phenomenon is the elevated spot of increased correlation of large-scale coherent structures occurring at about 13 CET between 85 m and 105 m. At this height R_s was found to exceed 0.6. In the layer beneath, the correlation is significantly decreased ($R_s \leq 0.4$). Its occurrence coincides with peaks in the mean diurnal courses of the atmospheric stability, sensible heat flux and incoming shortwave radiation (Fig. 6). Based on the simultaneous excursions in time series collected using independent sampling devices we can exclude possible random artifacts. The suggested interpretation is a short-term stabilisation of the stratification regime of the air above the canopy due to the development of convective clouds. We recall that only days with well-developed convection and fairly unstable stratification during the day were selected for calculating the ensemble averages. The same phenomenon has been observed for the vertical wind but for the transition time from unstable to stable stratification around 17 CET (Fig. 5a). Thus, we assume that the occurrence of an elevated area of increased correlation is generally connected to a transition towards stable stratification due to a decrease in incoming solar radiation.

In general we can state that the results obtained by analysing the time series of the backscatter intensity differ from those found for the vertical wind. This observation is especially true for large-scale coherent structures with time scales exceeding 60 s. Large-scale coherent structures in the vertical wind show an intermittent pattern of occurrence, while those in the backscatter intensity follow the diurnal course of the sensible heat flux.

5. Conclusions

The present study is an analysis of time series of vertical wind and acoustic backscatter intensity obtained by an acoustic sounding system in the layer adjacent to a tall vegetated canopy. Based on the results derived from wavelet analysis we can draw the following conclusions:

 — Acoustic sounding was successfully tested for the observation of coherent structures above tall vegetation. It provides time series with a temporal resolution sufficient for the observation of coherent structures during stable and unstable stratification. A thorough

Low-frequency turbulence above tall vegetation 21

quality control is necessary to sort out false data and to minimise effects due to random nature of the signals.

– Spectral correlation between neighboring observation levels was found to yield reasonable information about the degree of coupling between the vegetation and the atmosphere.

– Both small-scale coherent structures with characteristic time scales of $20\,s \leq D_e \leq 30\,s$ and large-scale coherent structures with time scales of $190\,s \leq D_e \leq 210\,s$ were observed in the vertical wind and the backscatter intensity. They coexist in the layer above the canopy, while temporal and spatial dynamics were found to differ.

– The small-scale coherent structures are constantly present and most likely generated by dynamical instabilities originating from the inflected wind profile. The large-scale coherent structures show an intermittent occurrence varying with incoming solar radiation suggesting a generation by thermal processes.

– The maximum height of the roughness sublayer, defined as the layer adjacent to the plant canopy characterised by coherent, correlated motion, could be estimated to as 5 times the canopy height.

This presented method is a powerful tool for those who deal with the exchange of energy and matter of forested ecosystems. It offers the opportunity to derive the state of coupling between the vegetation and the overlying atmosphere and can thus help to identify the physical processes responsible for the exchange.

Acknowledgements

References

Akima, H.: 1970, 'A new method of interpolation and smooth curve fitting based on local procedures'. *J Assc Comp Mach* **17**, 589–602.

Aubrun, S., R. Koppmann, B. Leitl, M. Moellmann-Coers, and A. Schaub: 2004, 'Physical modelling of an inhomogeneous finite forest area in a wind tunnel - Comparison with field data and Lagrangian dispersion calculations'. *Agric.For.Meteorol.* p. in press.

22 Thomas et al.

Bergström, H. and U. Högström: 1989, 'Turbulent exchange above a pine forest. II. Organized structures'. *Boundary-Layer Meteorol.* **49**, 231–263.

Brunet, Y. and M. Irvine: 2000, 'The control of coherent eddies in vegetation canopies: streamwise structure spacing, canopy shear scale and atmospheric stability'. *Boundary-Layer Meteorol.* **94**, 139– 163.

Chen, J. and F. Hu: 2003, 'Coherent structures detected in atmospheric boundary-layer turbulence using wavelet transforms at Huaihe River Basin, China'. *Boundary-Layer Meteorol.* **107**, 429–444.

Collineau, S. and Y. Brunet: 1993a, 'Detection of turbulent coherent motions in a forest canopy. Part I: Wavelet analysis'. *Boundary-Layer Meteorol.* **65**, 357–379.

Collineau, S. and Y. Brunet: 1993b, 'Detection of turbulent coherent motions in a forest canopy. Part II: Time-scales and conditional averages'. *Boundary-Layer Meteorol.* **66**, 49–73.

Coulter, R. and M. Wesely: 1980, 'Estimates of surface heat flux from sodar and laser scintillation measurements in the unstable boundary layer'. *J. Applied Meteorol.* **19**, 1209–1222.

Crescenti, G.: 1998, 'The degradation of Doppler sodar performance due to noise: a review'. *Atmos. Environ.* **32**, 1499–1509.

Finnigan, J.: 2000, 'Turbulence in plant canopies'. *Ann. Rev. Fluid Mech.* **32**, 519– 571.

Foken, T., M. Göckede, M. Mauder, L. Mahrt, B. Amiro, and J. Munger: 2004, 'Post-field data quality control'. In: X. Lee (ed.): *Handbook of Micrometeorology: A Guide for Surface Flux Measurements.* Dordrecht: Kluwer, pp. 181–208.

Gao, W., R. H. Shaw, and K. T. Paw U: 1989, 'Observation of organized structure in turbulent flow within and above a forest canopy'. *Boundary-Layer Meteorol.* **47**, 349–377.

Gerstberger, P., T. Foken, and K. Kalbitz: 2004, 'The Lehstenbach and Steinkreuz chatchments in NE Bavaria, Germany'. In: E. Matzner (ed.): *Biogeochemistry of forested catchments in a changing environment:. Ecological Studies*, Vol. 172. Heidelberg: Springer, pp. 15–41.

Hall, F. J., J. Edinger, and W. Neff: 1975, 'Convective plumes in the planetary boundary layer, investigated with an acoustic echo sounder'. *J. Applied Meteorol.* **14**, 513–523.

Haugen, D. and J. C. Kaimal: 1978, 'Measuring temperature structure parameters profiles with an acoustic sounder'. *J. Applied Meteorol.* **17**, 895–899.

Koppmann, R.: 2003, 'Emission and chemical transformation of biogenic volatile organic compounds (ECHO)'. *AFO2000 Newsletter* **5**, 7–10.

Kumar, P. and E. Foufoula-Georgiou: 1994, 'Wavelet analysis in Geophysics: An Introduction'. In: E. Foufoula-Georgiou and P. Kumar (eds.): *Wavelets in Geophysics*, Vol. 4 of *Wavelet analysis and its applications.* San Diego: Academic Press, pp. 1–43.

Little, C.: 1969, 'Acoustic methods for the remote probing of the lower atmosphere'. In: *IEEE*, Vol. 53. pp. 571–578.

Lu, C. and D. Fitzjarrald: 1994, 'Seasonal and diurnal variations of coherent structures over a deciduous forest'. *Boundary-Layer Meteorol.* **69**, 43–69.

Miller, K. and M. Rochwarger: 1970, 'On estimates of spectral moments in the presence of colored noise'. In: *IEEE Trans. Inf. Theory IT-16.* pp. 303–308.

Neff, W.: 1975, 'Quantitative evaluation of acoustic echoes from the planetary boundary layer'. TR ERL 322-WPL 38, NOAA.

Low-frequency turbulence above tall vegetation 23

Neff, W. and R. Coulter: 1986, 'Acoustic remote sensing'. In: D. Lenschow (ed.): *Probing the atmospheric boundary layer.* Boston: American Meteorological Society, pp. 201–239.

Paw U, K. T., Y. Brunet, S. Collineau, R. H. Shaw, T. Maitani, J. Qiu, and L. Hipps: 1992, 'Evidence of Turbulent Coherent Structures in and above Agricultural Plant Canopies'. *Agric.For.Meteorol.* **61**, 55–68.

Petenko, I., S. Argentini, A. Bolignano, G. Mastrantonio, and A. Viola: 2004, 'Time and horizontal scales of convective plumes at mid-latitudes'. In: P. Anderson, S. Bradley, and S. von Hunerbein (eds.): *12th International Symposium on Acoustic Remote Sensing.* Cambridge, UK, British Antarctic Survey.

Petenko, I. and V. Bezverkhnii: 1999, 'Temporal scales of convective coherent structures derived from sodar data'. *Meteorol. Atmosph. Phys.* **71**, 105–116.

Raupach, M. R., J. J. Finnigan, and Y. Brunet: 1989, 'Coherent Eddies in Vegetation Canopies'. In: *4th Australian Conference on Heat and Mass Transfer.* Christchurch, NZ, pp. 75–90.

Raupach, M. R., J. J. Finnigan, and Y. Brunet: 1996, 'Coherent eddies and turbulence in vegetation canopies: the mixing-layer analogy'. *Boundary-Layer Meteorol.* **78**, 351–382.

Spizzichino, A.: 1974, 'Discussion of the operating conditions of a Doppler sodar'. *J. Geophys. Res.* **79**, 5585–5591.

Taconet, O. and A. Weill: 1982, 'Vertical velocity field in the convective bounadry layer as observed with an acoustic Doppler sodar'. *Boundary-Layer Meteorol.* **23**, 133–151.

Tatarskii, V.: 1971, *The effects of the turbulent atmosphere on wave propagation.* Moscow, 1967, Israel Program for Scientific Translations, U.S. Dept. of Commerce: Nauka.

Thomas, C. and T. Foken: 2005, 'Detection of Long-term Coherent Exchange over Spruce Forest Using Wavelet Analysis'. *Theor. Appl. Climatol.* p. (in print).

Williams, A. and J. Hacker: 1993, 'Interactions between coherent eddies in the lower convective boundary layer'. *Boundary-Layer Meteorol.* **64**, 55–74.

Address for Offprints:
Christoph Thomas
University of Bayreuth
Department of Micrometeorology
95440 Bayreuth, Germany
Tel. (49) 921 55 2320
Fax (49) 921 55 2366
Email christoph.thomas@uni-bayreuth.de

Appendix D

Coherent structures in a tall spruce canopy: temporal scales, structure spacing and terrain effects

Christoph Thomas (`christoph.thomas@uni-bayreuth.de`)
Department of Micrometeorology, University of Bayreuth, Bayreuth, Germany

Thomas Foken
Department of Micrometeorology, University of Bayreuth, Bayreuth, Germany

Abstract. This study investigates statistical properties of coherent structures in the proximity of a tall spruce canopy of moderate density in heterogeneous, complex terrain. Data were obtained by single-point measurements along a vertical profile using sonic anemometers and fast-response gas analysers in 4 observation heights within and above the canopy. The analysed variables include the 3-D wind vector, sonic temperature and concentrations of carbon dioxide and water vapour. The extraction of coherent structures from the time series analysis was performed using a detection algorithm based on the wavelet transform.

Temporal scales of coherent structures in the vertical wind and other vector and scalar variables were found to differ significantly above the canopy, whereas they are similar within the canopy caused by the large horizontal momentum absorption. The canopy mixing-layer analogy was observed to be applicable only for coherent structures in traces of the vertical wind, as it represents the active part of turbulence. Departures from the prediction of $m = \Lambda_w L_s^{-1} = 8..10$ could be addressed to terrain effects of the larger-scale topography. The latter acts through a modification of the mean vertical profile on the canopy shear length scale L_s. Ratios m determined within the canopy point to a disintegration of coherent structures into smaller ones if the vertical wind shear is beyond a certain threshold. Internal gravity waves could be separated from coherent structures through an analysis of their temporal scales in relation to the Brunt-Vaisala-frequency. Temporal scales of wave motion and coherent structures were observed to be of the same magnitude. Most of the identified intervals with dominating wave motion could be connected to the heterogeneous, hilly terrain which facilitates the generation of gravity waves downstream of the obstacle.

Keywords: Coherent structures, Mixing-layer Analogy, Vegetation, Gravity Waves, Wavelet transform

1. Introduction

Coherent structures in atmospheric boundary layer flow have been a focus of research in the field of atmospheric turbulence during the past decades. Coherent structures are an inherent part of the turbulent flow above tall vegetated canopies and predominantly control the exchange of energy and matter between the surface, the canopy and the atmosphere. The identification of the driving mechanisms for the generation of coherent structures and their resulting statistical properties

2   Thomas and Foken

is necessary for an enhanced understanding of the complex structure of coherent exchange in vegetated canopies. This knowledge is crucial to find parameterisations describing coherent exchange in a universal manner.

The definitions of coherent structures, which can be found in literature, vary dependent on spatial and temporal scales of the observations. In the proximity and within the plant canopy, we define coherent structures as aperiodic, organised low-frequent flow patterns which differs much from the well-known high-frequency turbulence. In the time series of vectors they show up as fairly symmetric, triangle-shaped like pattern, whereas in time series of scalars one can describe them as asymmetric ramp-like pattern. The physical process of an individual coherent structure can generally be split into an inertial upward motion (ejection, burst) followed by a rapid downward motion (sweep, gust) and spans several seconds up to a few minutes.

Coherent structures in tall vegetation have been observed by many authors focusing on different aspects. The initial studies dealing with real observations in atmospheric boundary layer flow above tall vegetation reported on the presence of coherent structures and their two-dimensional single and higher-order statistics derived from the analysis of single or mean coherent structures over short periods using visual or half-automated detection algorithms (Gao et al., 1989; Bergström and Högström, 1989; Paw U et al., 1992). Based on the similarity of structural characteristics of coherent structures under varying stability conditions, Gao et al. (1989) identified the vertical wind shear as the main creating force of coherent structures. The results of Paw U et al. (1992) supported this finding by demonstrating a functional relationship between the occurrence frequency of coherent structures and the canopy shear scale $U_{h_c} h_c^{-1}$, where U_{h_c} is the mean horizontal wind speed at canopy height h_c. Later studies introduced objective and automated detection algorithms such as the wavelet transform enabling the researchers to process larger datasets and thus to derive robust statistics of coherent structures (Collineau and Brunet, 1993a; Collineau and Brunet, 1993b; Lu and Fitzjarrald, 1994; Turner and Leclerc, 1994; Brunet and Irvine, 2000; Chen and Hu, 2003; Thomas and Foken, 2005, Thomas et al., 2005). Simultaneously to these developments, Raupach et al. (1989) and Raupach et al. (1996) proposed a theory for near neutral conditions, in which the flow within and above tall vegetation is described analogous to the plane mixing-layer evolving between two coflowing streams of different velocities under laboratory conditions. According to this theory, coherent structures originate from the instabilities of the inflected mean horizontal velocity profile and their streamwise spacing Λ_x is a unique, linear function of the canopy

Coherent structures in a tall spruce canopy 3

shear length scale L_s. Brunet and Irvine (2000) then demonstrated the wide applicability of this mixing-layer analogy through its application over a large range of stability conditions and to datasets obtained over several vegetated canopies.

This study applies the concept of the mixing-layer analogy to turbulence observations within and above a tall vegetated spruce canopy at a heterogeneous forest site. Data were collected using sonic anemometers in combination with fast response gas analysers and a mean vertical wind profile of cup anemometers deployed at a tower during an extensive field campaign of approx. 2.5 months duration in late spring/ summer 2003. Preliminary investigations were done by Wichura et al. (2004) analysing a single day of measurements in summer 2000 at the same site. The present study expands previous studies in the following aspects: (i) a large dataset analysed using consistent, objective treatment based on the wavelet transform, (ii) the analysis includes variables such as horizontal and vertical wind velocities and sonic temperature at 4 observation levels, and concentrations of carbon dioxide and water vapour at 2 observation levels within and above the canopy; (iii) a large range of atmospheric stability, (iv) the upstream surface properties largely depend on the wind direction allowing to study their effects on coherent structures.

2. Experimental description

The data were collected during the WALDATEM-2003 (WAveLet Detection and Atmospheric Turbulent Exchange Measurements) field experiment conducted at the Fluxnet Station Weidenbrunnen Waldstein site ($50^o08'N, 11^o52'E$), 775 m a.s.l. in the Fichtelgebirge mountains in NE Bavaria, Germany. The main objective of WALDATEM-2003 was the extensive investigation of coherent structures and exchange processes above a spruce forest through extensive tower-based measurements in combination with ground-based acoustic remote sensing. The coniferous canopy mainly consist of spruce trees (Picea abies) with a mean canopy height h_c=19 m. The plant area index (PAI) is 5.2, with the main leaf mass concentrated within $0.5 - 0.9zh_c^{-1}$ (Fig. 8b), where z is the geometrical height above ground. The understorey is a mixture of small shrubs and graminae about 0.4 m high and fairly sparse. A detailed description of the site can be found in Gerstberger et al. (2004).

4　　　　　　　　　　　　　　Thomas and Foken

2.1. TURBULENCE MEASUREMENTS

The dataset analysed in this study was obtained during May - July 2003 at the 32 m high meteorological tower. High-frequency turbulence observations were performed using sonic anemometers (Solent R3-50, Solent R2, Gill Instruments Ltd.; 81000, R.M. Young) yielding the three dimensional wind velocity components (u, horizontal component; ϕ, wind direction; w, vertical component) and sonic temperature T_s at 4 observation levels in 1.74, 1.18, 0.93 and $0.72 z h_c^{-1}$. The different types of sonic anemometers were prior tested in intercomparison studies (Mauder, 2002). In addition, fast-response gas analysers (Li7500, Li6262, Li-Cor Inc.) were installed at 2 heights in 1.74 and $1.18 z h_c^{-1}$ for concentration measurements of carbon dioxide c_{CO_2} and water vapour q. The overall number of available 30-min raw data files of turbulence measurements was up to ≈ 3400 dependent on the observation level, as measurements were not carried out simultaneously at all observation levels during the entire experiment. Detailed statistics of collected data and their quality are presented in Section 3.3.

2.2. MEAN PROFILE MEASUREMENTS

Measurements of the mean horizontal wind velocity were done by 7 cup anemometers (Wind sensor 4034, Theodor Friedrichs & Co.) located at 1.68, 1.32, 1.11, 0.95, 0.84, 0.53 and $0.11 z h_c^{-1}$. Mean air temperature and humidity were measured by aspirated psychrometers (Psychrometer after Frankenberger 3010, Theodor Friedrichs & Co.) at 5 levels in 1.63, 1.11, 0.66, 0.29 and $0.11 z h_c^{-1}$.

2.3. SURROUNDING TOPOGRAPHY

The larger-scale topographic conditions of the prevailing wind directions at the experimental site are heterogeneous (Fig. 1) and therefore have the potential to effect the flow differently. The wind rose can be divided into 3 prevailing wind sectors with approaching flow from North ($310^o - 60^o$), Southeast ($60^o - 190^o$) and West ($190^o - 310^o$). In the N sector, the flow approaches from down a valley up the mountain ridge, on which the experimental site is located. The vertical separation between the valley and the experimental site is approx. 220 m at an average slope of 5.1^o. Within this sector, the site is shielded by a shallow elevated part of the ridge, which is overflown by the approaching wind before it reaches the site. Winds blowing from the SE sector are channelled between two shallow mountains, the heights of which are ≈ 80 m above the site. The slope of the terrain within this sector is homogeneous, about 2.4^o and thus smaller than in the other sectors.
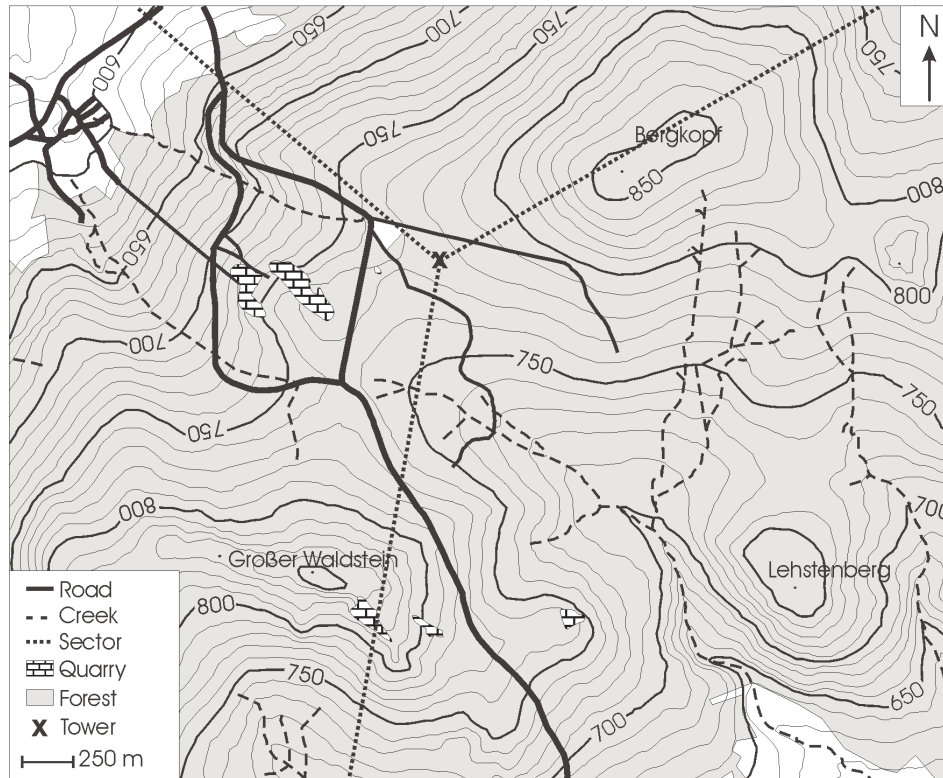
Figure 1. Map of the sampling site during WALDATEM-2003 in the Fichtelgebirge mountains, NE Bavaria with indicated borders of the 3 prevalent sectors of the wind direction. Numbers on isopleths are heights [m] a.s.l. (map adapted from Thomas et al., 2005).

The W sector is characterised by winds coming from down a valley up the mountain ridge at an average slope of 5.0^o reaching a slightly tilted terrain of about 1.3^o slope in the last $400\,$m upstream of the site. No aerodynamical obstacles are located in the flow path within the W sector except for a small quarry in about $600\,$m horizontal distance.

3. Method of analysis

All turbulence data were treated consistently in postprocessing after the field experiments. The method of analysis consists of data preparation, wavelet analysis and quality assessment/ quality control (QA/QC). Several steps during data preparation and application of the QA/QC protocol were adapted from Foken et al. (2004). In the following subsections, a brief description of the steps is presented. A detailed discussion

6   Thomas and Foken

of data preparation and wavelet analysis can be found in Thomas and Foken (2005).

3.1. DATA PREPARATION

In a first step, a despiking test (Vickers and Mahrt, 1997) is applied to each time series eliminating outliers caused by electrical or physical reasons. A window length of $300\,s$ in combination with an initial criteria of $6.5\,\sigma$ (standard deviation) has been found useful to reliably remove spikes while preserving the large and sharply localised gradients of coherent structures. Time series of the wind vector were then rotated according to its mean stream lines using the planar fit rotation method (Wilczak et al., 2001). The rotation coefficients $b_0..b_2$ were determined on a monthly base separately for each sonic anemometer. As a next step, time lags Δt between vertical wind w and scalars s are then determined by finding the maximum of $\overline{w\prime(t)s\prime(t + \Delta t)}$, where the prime denotes the fluctuating part of the signal and the overbar the covariance. The time series of the scalars are subsequently shifted according to the determined Δt to account for delay-times in data acquisition and recording and sensor separation. All time series are then block averaged to $2\,Hz$ significantly reducing computation time for the wavelet analysis and normalised by $(x - X)/\sigma_x$ except for w, which was normalised by w/σ_w, where X stands for the mean part of the signal. In a last step, time series were low-pass filtered by a wavelet filter decomposing and recomposing the time series using the biorthogonal set of wavelets BIOR5.5. The use of this set of wavelet functions is preferred as their localisation in frequency is better than e.g. that of the HAAR wavelet (Kumar and Foufoula-Georgiou, 1994). This filter discards all fluctuations with event durations $D < D_c$, where D_c is the critical event duration chosen according to the spectral gap between high-frequency turbulence and low-frequency coherent structures. A default value of $D_c = 6.2\,s$ was chosen for the entire dataset, which is in close agreement to other authors using similar values, e.g. $D_c = 5\,s$ (Lykossov and Wamser, 1995), $D_c = 7\,s$ (Brunet and Collineau, 1994) or $D_c = 5.7\,s$ (Chen and Hu, 2003).

3.2. WAVELET ANALYSIS

At first, a continuous wavelet transform (Grossmann and Morlet, 1984; Grossmann et al., 1989; Kronland-Martinet et al., 1987) of the prepared and zero-padded time series f(t) was performed using the complex Morlet wavelet as analysing wavelet function $\Psi(t)$,

$$T_p(a,b) = \frac{1}{a^p} \int_{-\infty}^{+\infty} f(t)\Psi\left(\frac{t - b}{a}\right) dt \qquad (1)$$

Coherent structures in a tall spruce canopy 7

where $T_p(a, b)$ are the wavelet coefficients, a the dilation scale, b the translation parameter and the normalisation factor $p = 1$ in our case. The complex Morlet wavelet function is located best in frequency domain and thus found appropriate to extract the intended information about coherent structures (Thomas and Foken, 2005). The dilation scales a used to calculate the continuous wavelet transform represent event durations D ranging from $6\,\mathrm{s}$ to $240\,\mathrm{s}$. The event duration D can be linked to the dilation scale a of the wavelet transform by (e. g. Collineau and Brunet, 1993a)

$$D = \frac{1}{2} \cdot f^{-1} = \frac{a \cdot \pi}{f_s \cdot \omega_{\Psi_{1,1,0}}^0}, \qquad (2)$$

where f is the frequency corresponding to the event duration, f_s the sampling frequency of the time series and $\omega_{\Psi_{1,1,0}}^0$ the center frequency of the mother wavelet function. For a sine function, the event duration D is half the length of a period. The minimum of analysed event durations was chosen according to the critical event duration D_c of the low-pass filter prior applied. The wavelet variance spectrum was then determined by

$$W_p(a) = \int_{-\infty}^{+\infty} |T_p(a, b)|^2 db. \qquad (3)$$

The characteristic event duration of coherent structures D_e in the given time series was derived from the event duration corresponding to the first maximum in the wavelet variance spectrum when plotting $W_p(a)$ against D. The subscript 'e' stands for 'event'. Due to the local character of the wavelet transform, D_e corresponds to the characteristic event duration of coherent structures (Mahrt and Howell, 1994) and not to the periodicity of coherent structures in the given time series. This parameter is derived by the subsequent detection of the individual coherent structures. For this purpose, a wavelet transform at D_e using the Mexican-hat wavelet function was chosen as it (i) is well located in both frequency and time domain and (ii) the wavelet coefficients $T_p(a_e, b)$ exhibit a zero-crossing with defined change in sign at the moment of occurrence of the coherent structure. The scale a_e is the corresponding dilation scale to the characteristic event duration D_e given by Eq. 2. The use of the zero-crossing enables the method to be objective and reliable for the detection of individual coherent structures as it does not require the definition of thresholds like other methods (Collineau and Brunet, 1993a). Based on the individual moments of occurrence t_x of coherent structures, the total number of coherent structures in a time series N and the mean and standard deviation of their temporal separation $\overline{T_x}$ and $\sigma_{\overline{T_x}}$ were determined according to Eqs. 4a and 4b

8   Thomas and Foken

respectively. The inverse temporal separation $\overline{T_x}^{-1}$ is equivalent to the periodicity, which is the arrival frequency of coherent structures.

$$\overline{T_x} = \frac{1}{N-1} \sum_{i=1}^{N-1} |t_{x,i} - t_{x,i+1}| \tag{4a}$$

$$\sigma_{\overline{T_x}} = \sqrt{\frac{1}{N-2} \sum_{i=1}^{N-1} \left(|t_{x,i} - t_{x,i+1}| - \overline{T_x} \right)^2} \tag{4b}$$

The mean streamwise spacing of adjacent coherent structures Λ_x of the variable x was then determined applying a pseudo Taylor's hypothesis according to Raupach et al. (1996) by

$$\Lambda_x = \overline{T_x} U_c, \tag{5}$$

where U_c is the convective velocity of the mixing layer given as $1.8 U_{h_c}$ proposed by Finnigan (1979) and confirmed by Shaw et al. (1995). U_{h_c} is the mean horizontal velocity at canopy top derived from the mean cup anemometer profile. Brunet and Irvine (2000) discussed the use of this rather simple prediction of U_c as it may reflect the influence of stability on $U_c U_{h_c}^{-1}$. In conclusion they found only a little dependence on atmospheric stability which becomes important under stable conditions when $U_c U_{h_c}^{-1}$ exceeds 1.8. This point is addressed further in Section 4.2. In Eq. 5, the term $\overline{T_x}$ (Eq. 4a) replaces the term TN^{-1} used by Raupach et al. (1996), whereas T is the total length of the time series. Although the results for the determination of Λ_x using both the terms were found to differ insignificantly, the method we used is more accurate as it reflects the real temporal separation of coherent structures rather than distributing them homogeneously among the entire time series. In addition, it provides the opportunity to derive their standard deviation $\sigma_{\overline{T_x}}$ as a measure of regularity for the occurrence of coherent structures. The latter may help to indicate the stationarity of processes in time series.

3.3. QUALITY ASSESSMENT AND QUALITY CONTROL

The calculated results were filtered according to their quality. A strict QA/QC protocol was applied to the results of the turbulence data employing the following criteria:

— Data collected during fog or precipitation events were discarded because of the possible effects of water droplets on transducer heads of sonic anemometers and on windows of open-path gas-analysers significantly influencing the shape of the time series.

- Data collected during calm or stormy conditions were discarded, leaving a range $0.3 \leq U_{h_c} \leq 2.5 \, ms^{-1}$ of acceptable values at this site.

- Intervals were rejected characterised by disturbed vertical profiles of mean horizontal velocity, i. e. if the gradient of mean horizontal velocity at canopy top $(dU/dz)_{z=h_c} \leq 0$.

- Results of an interval k were approved if its total number of detected events N_k in comparison to the preceding interval $k-1$ was within $1/2 \cdot N_{k-1} < N_k < 2 \cdot N_{k-1}$. This criteria efficiently removes erroneous and unrealistic results of D_e determination in wavelet variance spectra, i. e. if its first maximum did not correspond to the characteristic event duration of coherent structures. This happens predominantly during the late morning and early evening hours when the atmosphere was in transition to a different stability regime.

- The stability range was limited to $|h_c L^{-1}| \leq 1$ to exclude conditions of free convection and very stable stratification, where L is the Obukhov-length.

The applied QA/QC protocol rejected up to $40\,\%$ of the available data (Tab. I). The few data were rejected for the time series of vertical wind ($\approx 23\,\%$), whereas most data were discarded for the scalar concentrations of water vapour q ($\approx 40\,\%$) and carbon dioxide c_{CO_2} ($\approx 37\,\%$). The fraction of approved data p was found to be dependent on the measured variable rather than on height $z h_c^{-1}$ of the observation level or instrumentation.

4. Results and discussion

We now proceed to present the results gained by the analysis of coherent structures detected in the WALDATEM-2003 data. The following subsections will deal with both statistics and discrete analysis of coherent structures. The results will be presented as a function of height and direction of the approaching flow selected for the three main sectors as one major aspect of this paper is dedicated to the influence of the different surface conditions on coherent structures.

4.1. Temporal scales

Characteristic temporal scales of coherent structures in the individual 30-min intervals were derived from the characteristic event duration

10   Thomas and Foken

Table I. Data quality of 30-min turbulence data intervals during WAL-
DATEM-2003 for vertical wind w, horizontal wind u, wind direction ϕ, sonic
temperature T_s and concentrations of carbon dioxide c_{CO_2} and water vapour q in
different heights zh_c^{-1}: total number of collected intervals n_{tot}; number of rejected
intervals n_{reject}; number of approved intervals within the prevailing wind sectors
N $(310^o - 60^o)$ n_N, SE $(60^o - 190^o)$ n_{SE} and W $(190^o - 310^o)$ n_W; fraction of
approved data $p = (n_N + n_{SE} + n_W)/n_{tot}$.

Variable	zh_c^{-1}	n_{tot}	n_{reject}	n_N	n_W	n_{SE}	p
w	1.74	3391	858	709	857	967	0.75
	1.18	3363	820	707	852	984	0.76
	0.93	2596	574	619	661	742	0.78
	0.72	2521	525	635	619	742	0.79
u	1.74	3391	1209	616	720	847	0.64
	1.18	3363	1129	630	742	862	0.66
	0.93	2596	754	561	598	683	0.71
	0.72	2521	716	582	542	683	0.72
ϕ	1.74	3391	1080	652	755	904	0.68
	1.18	3363	1070	628	754	911	0.68
	0.93	2596	671	585	616	726	0.74
	0.72	2521	660	570	587	704	0.74
T_s	1.74	3391	1157	602	730	902	0.66
	1.18	3363	1049	659	730	925	0.68
	0.93	2596	745	565	583	703	0.71
	0.72	2521	682	588	564	687	0.73
c_{CO_2}	1.74	3391	1241	582	655	913	0.63
	1.18	2128	769	386	493	480	0.64
q	1.74	3391	1317	574	628	872	0.61
	1.18	2128	852	371	450	455	0.60

D_e given by the first spectral peak in the wavelet variance spectrum.
For a statistical analysis, probability density functions (pdf) of the
experientially derived results were calculated with a bin resolution of
4 s. To avoid a subjective interpretation of the derived pdfs due to visual
inspection, normal Gaussian distribution functions were fitted to the
pdfs with their statistical parameters listed in Tab. II and their means
μ plotted in Fig. 2 for all analysed variables and heights.
The probability density functions of the vertical wind show a consistent
pattern in variation with height for all three wind direction sectors
(Fig. 3): Temporal scales of coherent structures above the forest are
smaller than those in the forest. Coherent structures in the vertical wind
at $0.72zh_c^{-1}$ are approx. 3 - 4 s longer compared to those at $1.74zh_c^{-1}$,
which corresponds to a relative extension of approx. 18 %. However, the
absolute numbers were found to very only little with the wind direction.

In contrast to this, the coherent structures in the horizontal wind show a reverse behaviour: The temporal scales in the canopy are decreased compared to those above the canopy. The shortening of the coherent structures is dependent on the wind direction sector, and yields approx. 8 s in the W sector (23 %), 10 s in the N sector (30 %) and 4 s in the SE sector (14 %). Temporal scales of coherent structures in horizontal wind were also observed to vary with wind direction. The SE sector is characterised by shorter coherent eddies (≈ 30 s) than in the W and N sectors (≈ 35 s). For coherent structures in vector variables, the canopy acts as frequency shifter: the small vertical duration is shifted towards larger values, whereas the large horizontal duration is diminished. Thus, the symmetry of coherent structures regarding their horizontal and vertical temporal scales increases in the canopy. The ratio $\mu_u \mu_w^{-1}$ was determined to 1.5 at $1.74 z h_c^{-1}$ and found to equal one at $0.72 z h_c^{-1}$ (Tab. II). Contrary to the results obtained for the vertical and horizontal wind, the analysis of temporal scales of coherent structures in wind direction ϕ reveals only little variations in height. For this variable, the pdfs were found to peak at approx. 24 s to 26 s showing no systematic height-dependent pattern. The somewhat smaller values μ_ϕ of 21.8 and 19.8 s for the N and SE sector respectively at $0.93 z h_c^{-1}$ are most likely the effect of a branch close to the sonic anemometer, waving at higher wind speeds and thus disturbing the instantaneous measurements of wind direction.

Temporal scales of coherent structures in scalar variables were not found to show clearly pronounced variations with height, but with wind direction. For the sonic temperature T_s, the pdfs of the N sector show coherent structures typically 2.5 s and 3 s longer than those in the W or SE sectors respectively (Tab. II). In the W and N sectors, coherent structures tend to be slightly extended above the canopy at the top level in $1.74 z h_c^{-1}$ and exhibit their minimum close to the canopy height at $0.93 z h_c^{-1}$. However, this pattern is not well pronounced. For carbon dioxide concentration c_{CO_2}, the shortest coherent structures were also observed for the SE sector. Here, the temporal scale is approx. 3 s smaller at $1.74 z h_c^{-1}$ than for the other sectors. For the lower level at $1.18 z h_c^{-1}$, where closed-path gas analyser measurements were performed, no clear picture could be derived. In case of winds from W, the temporal scale is approx. 2.5 s diminished compared to the top level, but slightly increases by approx. 2 s for winds coming from N . Observations in the water vapour q were analogous to those in carbon dioxide at least for the top level at $1.74 z h_c^{-1}$. The lower level at $1.18 z h_c^{-1}$ clearly shows large deviations from the temporal scales found for other variables and observation heights. As these concentration measurements were carried out using a closed-path gas analyser in connection with a sampling tube

12   Thomas and Foken

Table II. Characteristic temporal scales of coherent structures for the observed turbulent variables during WALDATEM-2003 as a function of normalised height zh_c^{-1} and wind direction sector: mean μ and standard deviation σ of the normal Gaussian distribution function fitted to the experientially derived probability density functions (Fig. 3 for w).

Variable	zh_c^{-1}	Sector W		Sector N		Sector SE	
		μ [s]	σ [s]	μ [s]	σ [s]	μ [s]	σ [s]
w	1.74	22.1	7.5	21.9	7.7	21.4	6.6
	1.18	20.9	7.0	21.1	7.3	20.1	6.3
	0.93	22.4	7.3	24.6	8.4	22.5	6.7
	0.72	25.3	8.7	26.3	9.1	25.3	8.0
u	1.74	35.8	16.3	35.5	14.2	29.5	12.7
	1.18	33.1	13.0	33.8	12.9	29.9	11.6
	0.93	28.6	11.2	29.9	11.7	26.6	9.1
	0.72	27.5	10.1	25.1	8.7	25.5	8.9
ϕ	1.74	26.5	10.6	23.7	9.6	24.4	8.7
	1.18	24.7	9.6	23.4	9.3	24.0	9.1
	0.93	26.2	9.2	21.8	8.1	19.8	7.0
	0.72	26.1	9.2	25.0	9.1	23.5	7.8
T_s	1.74	29.7	12.5	31.5	13.2	27.7	10.7
	1.18	27.6	12.1	29.6	11.9	26.4	9.5
	0.93	26.8	10.4	29.5	11.6	27.3	9.1
	0.72	27.8	11.02	30.6	12.3	28.0	9.9
c_{CO_2}	1.74	31.0	18.1	30.3	11.8	27.4	9.7
	1.18	27.3	12.7	32.0	14.9	27.0	8.9
q	1.74	32.4	19.5	30.8	12.7	27.0	10.3
	1.18	45.1	34.4	42.3	25.3	30.5	13.9

of approx. 3 m length, a smearing of individual coherent structures in the traces of water vapour is possible (and probable).The adsorption and desorption processes of gaseous water molecules at the inner wall of the tubing apparently attenuate the sharp gradients in the signals of coherent structures, which leads to a smearing of smaller structures towards larger ones and an attenuation of the fluctuations (Lenschow and Raupach, 1991,Massman, 1991). This results in a systematic overestimation of the characteristic temporal scales of coherent structures. The temporal scales observed for water vapour at $1.18zh_c^{-1}$ are assumed to be dominated by effects of the sampling technique and regarded as false values. Therefore we cannot recommend the use of closed-path gas analysers for time series analysis of water vapour. The question arises, if there is a cross-sensitivity of water vapour to instantaneous carbon dioxide measurements as both variables are measured in the same air volume by the same device (Leuning and Moncrieff, 1990).

Coherent structures in a tall spruce canopy   13
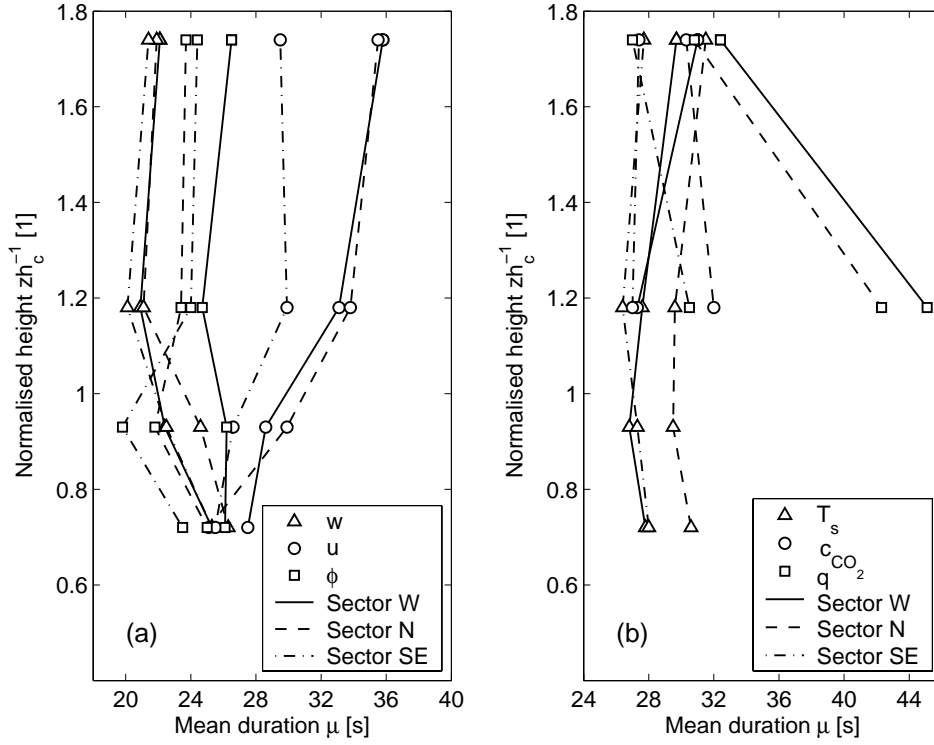
Figure 2. Vertical profile of characteristic temporal scales of coherent structures μ according to Tab. II as a function of wind direction sector for (a) vertical velocity w, horizontal velocity u, wind direction ϕ and (b) sonic temperature T_s, carbon dioxide c_{CO_2} and water vapour q.

As the results for c_{CO_2} are plausible compared to those obtained by the open-path device at $1.74zh_c^{-1}$, we assume the effect as negligible. However, the unclear picture obtained for c_{CO_2} at $1.18zh_c^{-1}$ may be due to some residual effect of this cross-sensitivity. The characteristic temporal scales of scalar variables are related rather to those of u than of w at least for heights above the canopy. The ratios $\mu_u\mu_{T_s}^{-1}$, $\mu_u\mu_{CO_2}^{-1}$ and $\mu_u\mu_q^{-1}$ are close to unity independent on height, whereas those for μ_w instead of μ_u are about 0.75 above the canopy and increase to 0.9 in the canopy due to the increasing symmetry in $\mu_u\mu_w^{-1}$ mentioned before. The statistical results about the characteristic temporal scales of coherent structures revealed a dependency on wind direction for u, T_s, c_{CO_2} and q, but no variation could be observed for w in the different wind direction sectors. This finding points to the fact that the properties of coherent structures in the vertical wind are dominated by local processes rather than by large-scale ones. We recall that the large-scale surface conditions within the different wind sectors vary largely

14   Thomas and Foken

at scales of several hundred meters, whereas the canopy in the proximity to the tower is quite homogeneous. The vertical wind is therefore assumed to represents the active, locally generated part of the low-frequency turbulence, which is in agreement with observations of many authors (e. g. Raupach et al., 1996, Katul et al., 1998, Finnigan, 2000). The pattern of dependence on wind direction, which was consistently extracted for the horizontal velocity and the scalars, can be connected to the large-scale variations of surface conditions. This point will be addressed further in the following subsections.

Only little information can be found in literature about temporal scales of vector and scalar variables above and within tall vegetated canopies. Most studies are limited to the analysis of temperature traces or vertical wind above the canopy, sometimes providing only poor statistics due to small datasets. However, similar profile observations were done by Collineau and Brunet (1993b) although for single 30-min intervals. They obtained temporal scales of $20\,s$, $5.5\,s$ and $13\,s$ above and $13\,s$, $7\,s$ and $13\,s$ within the canopy for the streamwise velocity, vertical wind and temperature respectively when analysing a single 30-min period. They also observed a decrease of temporal scales for horizontal velocity, an increase for those of vertical velocity and no variation for the scalar variable. However, the asymmetry in horizontal to vertical scales is 3.6 above and 1.9 within the canopy, and thus far away from our results approaching unity within the canopy. A possible explanation for the large deviations are the different surface conditions, as they collected data above a $13.5\,m$ tall regularly planted pine forest with large spacings between adjacent trees. Gao et al. (1989) also found that the mean duration of coherent structures in vertical wind traces was greater within the $18\,m$ high mixed forest than above. They observed temporal scales for w of $63.9\,s$ at $0.58 z h_c^{-1}$ and $41.9\,s$ at $1.9 z h_c^{-1}$. Despite the fact that absolute numbers for temporal scales of coherent structures obviously differ from those in our forest, analogies in variation with height could be found.

4.2. Canopy shear scales

It was demonstrated by many researchers that the flow above tall canopies is dominated by shear processes. This shear is caused by the drag of the canopy elements efficiently absorbing horizontal momentum, which results in the characteristic inflected profile of horizontal velocity found in tall canopies. Here, statistical moments of the flow scale with single length or time scales rather than with height or atmospheric stability. Diabatic effects primarily are quantitative than qualitative (Finnigan, 2000), causing some scatter in observed veloc-
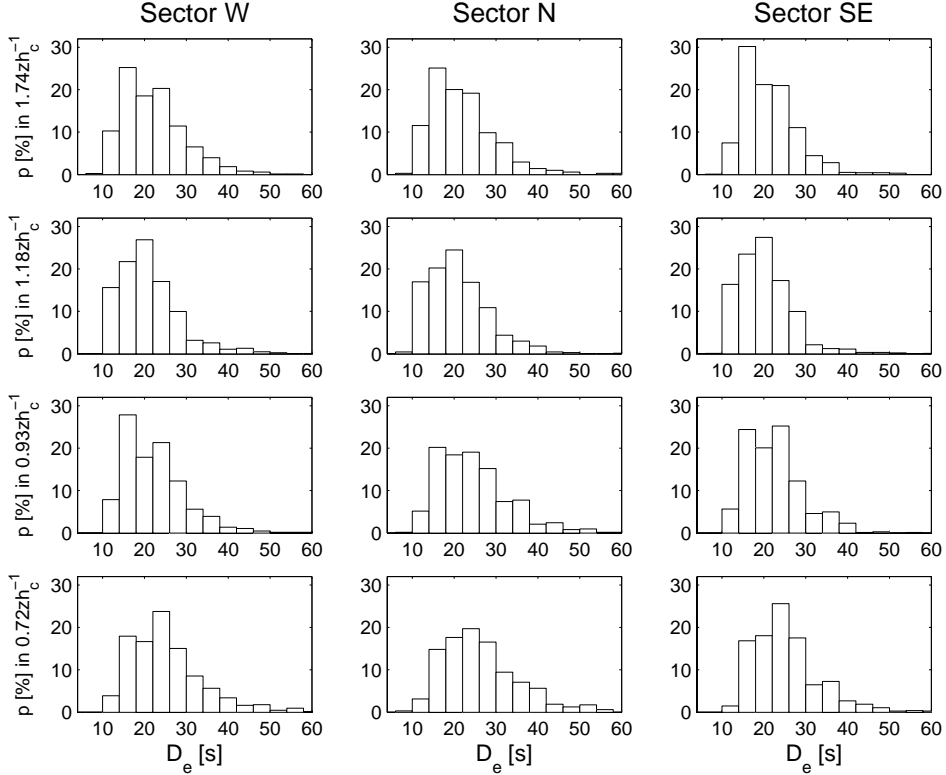
Figure 3. Density function of the probability p of characteristic temporal scales for coherent structures D_e in the vertical wind as a function of normalised height zh_c^{-1} and wind direction sector during the WALDATEM-2003 experiment. The bin resolution is 4 s.

ity moments. Various scales for such shear processes within or close to canopies can be found in literature: Most of them link the mean horizontal velocity at canopy top U_{h_c} to characteristic length scales of the canopy, e.g. the canopy height, or to statistical moments of the inflected wind profile. As mentioned in the introduction, Paw U et al. (1992) proposed a canopy shear scale

$$F_s = \frac{U_{h_c}}{h_c},$$

which has the physical units of a frequency. Raupach et al. (1989) and later Raupach et al. (1996) identified the canopy shear scale

$$L_s = \frac{U_{h_c}}{(dU/dz)_{z=h_c}}$$ (7)

16   Thomas and Foken
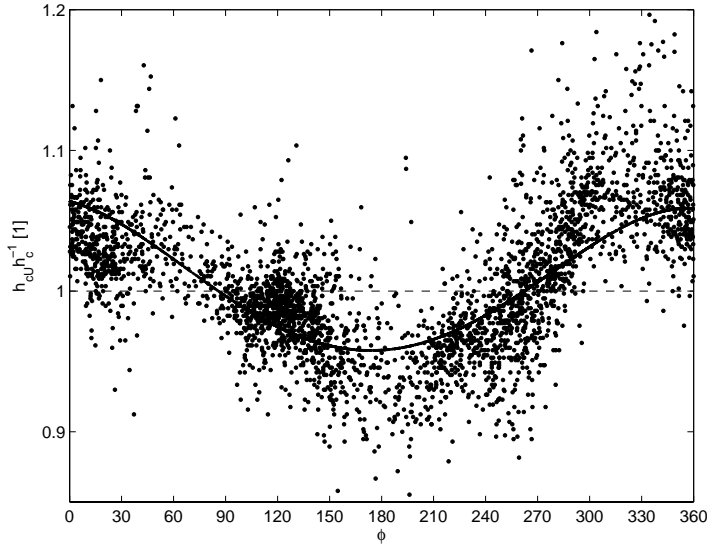
Figure 4. Aerodynamic canopy height h_{cU} normalised by estimated canopy height h_c=19 m as a function of wind direction ϕ for the WALDATEM-2003 data; the thick line represents the fitted mean aerodynamic canopy height $\overline{h_{cU}}(\phi)$.

as an appropriate scale for shear induced processes in vegetated canopies, which has the physical units of a length. The denominator in Eq. 7 is the gradient of the mean horizontal wind velocity at canopy top. In the following, we will limit our discussion of canopy shear scales to those given in Eqs. 6 and 7. A crucial parameter for the determination of input variables for both canopy shear scales is the height of the canopy top h_c. The measuring of tree heights is (i) subject to statistical errors due to an insufficient number of included trees characterised by a large natural scatter and (ii) connected to great practical complications in a dense, irregularly spaced tall forest. Therefore we use the aerodynamic definition of canopy height, i. e. the height z of the inflection point in the vertical profile of mean horizontal velocity. For this purpose, a polynomial function was fitted to the vertical velocity profile obtained by the cup anemometers consisting of 7 discrete measurement points (see Section 2.2) using a least square fit. The aerodynamic canopy height h_{cU} was then assigned to the height of the zero-crossing of its second derivative. This procedure was repeated for each single 30-min interval, whereas the data were filtered for calm and stormy conditions and unrealistic gradients according to the second and third quality criteria given in Section 3.3.

The aerodynamic canopy height clearly depends on wind direction (Fig. 4). The different surface conditions of the wind direction sectors

Coherent structures in a tall spruce canopy   17
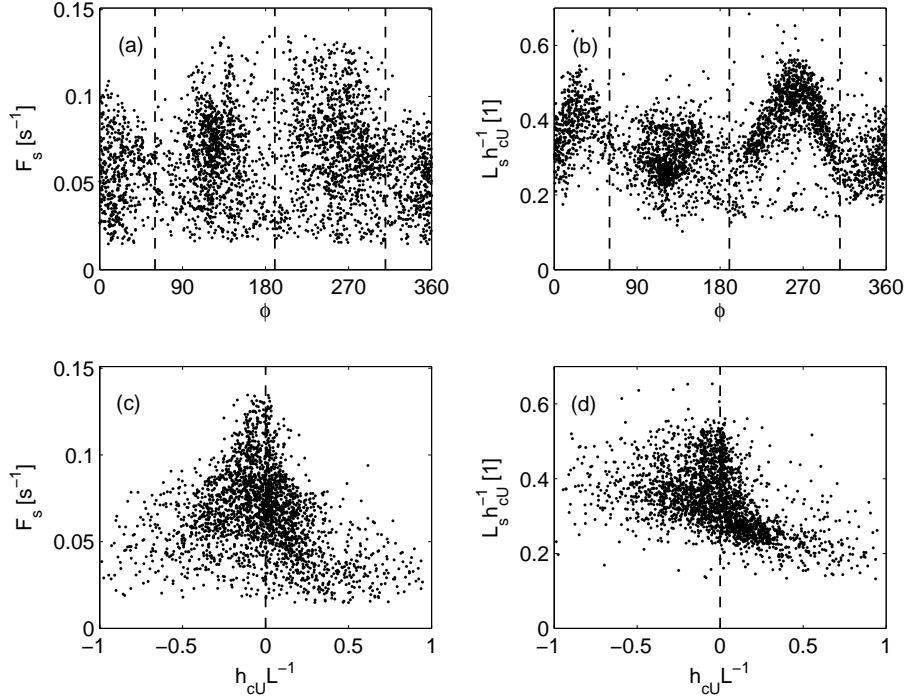
Figure 5. Canopy shear scales F_s (Eq. 6) and normalised $L_s h_{cU}^{-1}$ (Eq. 7) as function of (a) - (b) wind direction ϕ with marked borders of wind direction sectors (dashed lines) and (c) - (d) atmospheric stability $h_{cU} L^{-1}$. The Obukhov-length L was evaluated at $1.74 z h_c^{-1}$.

are most likely the reason for this observation, as they effect the shape of the velocity profiles. This assumption will be addressed further. Individual values for h_{cU} were found to scatter up to 20 % around h_c, which was our visual estimate for the canopy height. However, the estimate h_c=19 m turned out to be a robust prediction of the mean aerodynamic canopy height $\overline{h_{cU}}$, which basically is a function of ϕ. The scatter around $\overline{h_{cU}}$ is created by (i) naturally occurring variability of the wind profile due to the heterogeneity of the canopy, (ii) some numerical effect of the polynomial fitting procedure and (iii) influence of atmospheric stability on the wind profile. The latter was found to be responsible for the scatter in the SE and N sectors, whereas no discernable effect was observed for the W sector. In the following, we replaced the canopy height h_c by its aerodynamic value h_{cU} in the calculations of Eqs. 5, 6 and 7 to account for canopy heterogeneity and for stability effects. The mean horizontal velocity at canopy top and the gradient of the mean horizontal wind velocity at canopy top were determined correspondingly as $U_{h_{cU}}$ and $(dU/dz)_{z=h_{cU}}$ respectively.

18   Thomas and Foken

The results from both evaluated canopy shear scales are presented in
Fig. 5. F_s shows a small effect on wind direction only. Mean values
of $0.05 \, s^{-1}$ for the N sector and approx. $0.08 \, s^{-1}$ for the SE and W
sectors become evident. A dependence on stability could be observed
only for the near neutral range, where F_s tends to greater values. Be-
yond $|h_{cU} L^{-1}| \geq 0.2$ no particular trend is visible. The overall range
of observed values for our canopy spans 0.02-$0.14 \, s^{-1}$, which is in
agreement with the range of values observed by Paw U et al. (1992)
for a deciduous forest, who found values up to 0.2. The shear scale
L_s, which was normalised by the aerodynamic canopy height, shows a
specific behaviour in each wind direction sector. Within the N sector,
mean $L_s h_{cU}^{-1}$ increases linearly from 0.25 to 0.45 corresponding to a turn
in wind direction from 320° to 50°. Individual data scatter approx. ± 0.1
around the increasing mean. The SE sector does not show any signif-
icant trend within its borders and has a constant value of 0.3 ± 0.15.
The W sector is characterised by the highest values of $L_s h_{cU}^{-1}$, which
strongly depend on wind direction. The mean increases from 0.3 to 0.5
with winds turning from 190° to 260°, but decreases at the same slope
when ϕ turns further to 300°. The individual data seem to scatter less
and are closely located around their mean. The strong dependence of
the canopy shear scale on ϕ points to a dominating effect of canopy
and surface heterogeneity on the wind profile within the W sector. We
recall that no diabatic effect on the aerodynamic canopy height was
found. Referring to Eq. 7, the increase of $L_s h_{cU}^{-1}$ in the W sector is due
to a decrease in wind shear, while $U_{h_{cU}}$ is not typically larger for winds
coming from W than from other wind directions (not shown here). The
wind shear $(dU/dz)_{z=h_{cU}}$ typically ranges within 0.1-$0.25 \, ms^{-1} m^{-1}$ in
the W and N sectors and is nearly constant at $0.3 \, ms^{-1} m^{-1}$ in the SE
sector. The wind shear is thus a function of ϕ and was not found to
decrease with increasing stability, which gives strong support to our
assumption that surface conditions predominantly control the canopy
flow. For increasing stability $h_{cU} L^{-1} \geq 0.1$, $L_s h_{cU}^{-1}$ collapses towards
smaller values (Fig. 5d). However, this trend is less pronounced than ob-
served by Brunet and Irvine (2000), who did not find any $L_s h_c^{-1} \geq 0.35$
on the stable side. Compared to their results, the maximum $L_s h_{cU}^{-1}$ in
our neutral data is much greater reaching values of 0.55. Comparing
Figs. 5b and 5d one can see, that these high values are associated with
winds coming from W, where shear effects were identified to dominate
rather than stability. For unstable data, a slight increase of $L_s h_{cU}^{-1}$ with
decreasing stability may be present, which agrees with the findings
of Brunet and Irvine (2000). The overall range of $L_s h_{cU}^{-1}$ is 0.15-0.6
with a mean value of 0.35. The latter agrees with the range of values
for moderate canopies found by Raupach et al. (1996), who observed

Coherent structures in a tall spruce canopy   19

$L_s h_c^{-1}$ in the order of 0.1, 0.5 and 1 for dense, moderate and sparse canopies respectively, and in perfect agreement to the data presented by Brunet and Irvine (2000), who found a mean $L_s h_c^{-1}$ of 0.35 from data of multiple canopies.

4.3. CANOPY MIXING-LAYER ANALOGY

The concept of the canopy mixing-layer analogy was first proposed by Raupach et al. (1989), and later published by Raupach et al. (1996) in its full extent. This theory links the turbulence and coherent structures in the air layer near the top of the canopy to a plane mixing layer evolving between two coflowing streams with different velocities under laboratory conditions. It is based on the many analogies between these different types of mixing layers, such as the inflected mean velocity profile $U(z)$, integral length scales and statistical flow properties, e.g. the integral turbulence characteristics of velocity components and the correlation coefficient for momentum. Initially proposed for thermally neutral conditions only, its applicability was demonstrated for a broad range of stabilities by Brunet and Irvine (2000). Up to now, the canopy mixing layer analogy is the only useful concept satisfyingly predicting the properties of coherent structures observed under real turbulent conditions in tall canopies. Thus we will apply this concept to our data.

According to the theory, the basic length scale for canopy flows is L_s (Eq. 7), which corresponds to

$$L_s = \frac{1}{2}\delta = \frac{U_{h_c}}{(dU/dz)_{z=h_c}}, \qquad (8)$$

where δ is the typical thickness of vortices in a plane mixing layer. This canopy shear scale was discussed in Section 4.2 for our data. The relationship between the streamwise spacing of coherent structures Λ_x (Eq. 5), which represents a typical length scale for coherent motion, and L_s is then given by

$$\frac{\Lambda_x}{h_{cU}} = m\frac{L_s}{h_{cU}}. \qquad (9)$$

The ratio m was found to be constant within $7 \leq m \leq 10$ (Raupach et al., 1996) for the active, canopy-scale coherent structures, which vertical scales are of the order of L_s. These values are typically obtained from vertical velocity statistics, as it represents the active part of turbulence.

In Fig. 6, the mean streamwise spacing of coherent structures in vertical wind Λ_w is plotted versus L_s both normalised by the aerodynamic canopy height h_{cU} for two levels at 1.74 and $0.72 z h_c^{-1}$. The differences
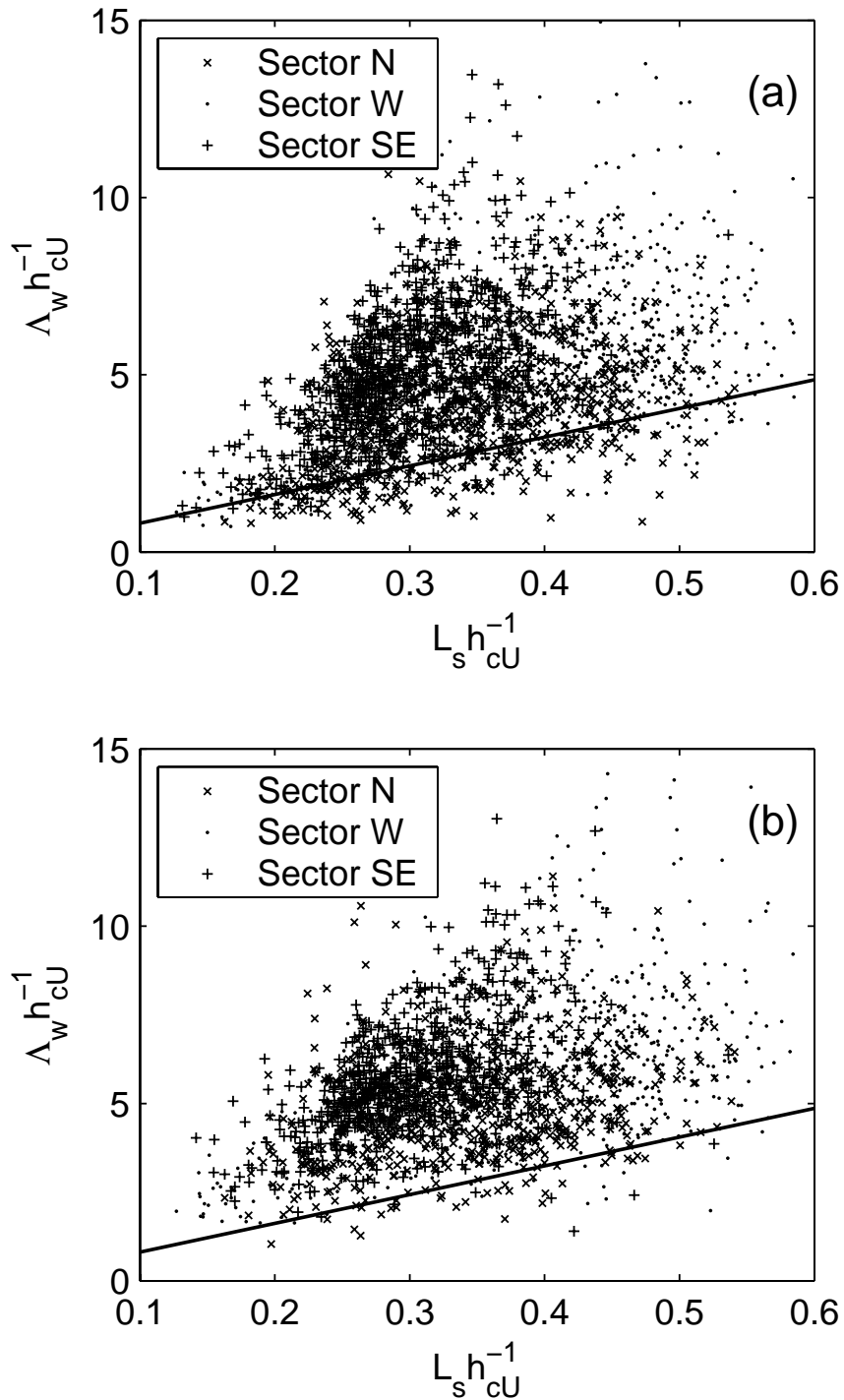
Figure 6. Normalised mean streamwise spacing of adjacent coherent structures in vertical wind Λ_w plotted versus normalised canopy shear length L_s as a function of wind direction sector for the WALDATEM-2003 dataset at (a) $1.74zh_c^{-1}$ and (b) $0.72zh_c^{-1}$. The linear function is the neutral prediction $\Lambda_w h_c^{-1} = 8.1L_s h_c^{-1}$ by Raupach et al. (1996).

Coherent structures in a tall spruce canopy 21

Table III. Determined ratios m (Eq. 9) according to the canopy mixing layer analogy for the observed turbulent variables during WALDATEM-2003 as a function of normalised height zh_c^{-1} and wind direction sector. R^2 is the coefficient of determination of the linear regression model in Eq. 9.

Variable	zh_c^{-1}	Sector N		Sector W		Sector SE	
		m	R^2	m	R^2	m	R^2
w	1.74	7.5	0.33	10.1	0.43	17.2	0.51
	1.18	8.2	0.40	10.0	0.48	15.4	0.53
	0.93	5.5	0.25	11.0	0.53	14.3	0.45
	0.72	5.1	0.25	11.4	0.50	14.4	0.48
u	1.74	11.7	0.27	15.0	0.29	34.4	0.54
	1.18	12.8	0.34	15.1	0.38	30.7	0.54
	0.93	5.9	0.19	14.4	0.45	23.7	0.52
	0.72	8.1	0.29	13.6	0.44	17.0	0.39
ϕ	1.74	10.1	0.33	13.6	0.38	29.0	0.50
	1.18	9.5	0.32	12.3	0.39	26.4	0.56
	0.93	3.6	0.15	13.3	0.46	21.8	0.55
	0.72	3.6	0.14	12.3	0.44	16.5	0.48
T_s	1.74	9.3	0.27	11.5	0.30	24.5	0.48
	1.18	7.6	0.26	11.1	0.31	20.4	0.50
	0.93	7.7	0.25	14.7	0.45	15.8	0.38
	0.72	7.9	0.26	12.4	0.43	12.1	0.32
c_{CO_2}	1.74	7.8	0.24	15.0	0.24	22.7	0.47
	1.18	4.5	0.12	10.7	0.29	23.4	0.35
q	1.74	7.5	0.23	13.4	0.25	19.8	0.39
	1.18	2.8	0.05	14.4	0.12	25.7	0.35

between the wind direction sectors become evident specifically for the data located at the outer regions of the scatterplot. The greatest values Λ_w can be found in the SE and W sectors, whereas the smallest values are typically observed for the N sector. The differences in $L_s h_{cU}^{-1}$ between the SE and W sectors (Section 4.2) causes them occupying different spatial regions of the plot. At a first look, the prediction $\Lambda_w h_c^{-1} = 8.1 L_s h_c^{-1}$ by Raupach et al. (1996) underestimates the data particularly at $0.72 z h_{cU}^{-1}$, but the slopes between the prediction and the presented are similar. The mean ratio m was determined according to Eq. 9 for all measured variables and as a function of wind direction sector through a linear regression using a least-square fit, whereas the linear function was not forced through zero. The results of the regression are listed in Tab. III and the mean m_x are plotted in Fig. 7.

The vertical profiles $m_x(z)$ show specific patterns, which are consistently found for all variables x within a wind direction sector (Fig. 7). For the SE sector, m_w, m_u, m_ϕ and m_{T_s} show a distinct decrease in m

22   Thomas and Foken
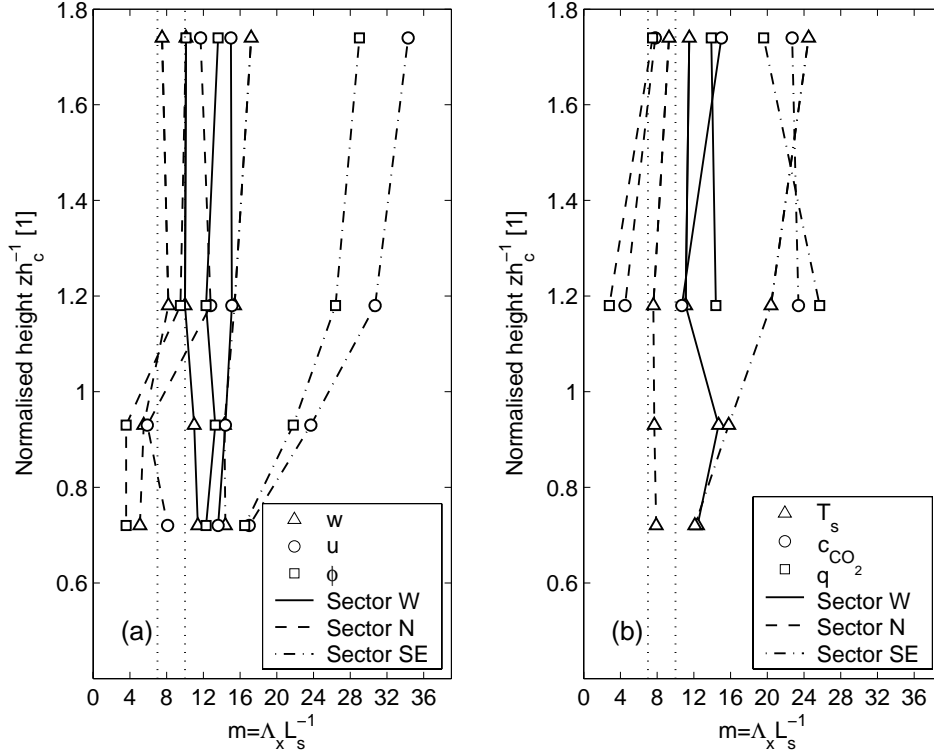
Figure 7. Vertical profile of ratio m (Eq. 9) according to the canopy mixing layer analogy as a function of wind direction sector for (a) vertical velocity w, horizontal velocity u, wind direction ϕ and (b) sonic temperature T_s, carbon dioxide c_{CO_2} and water vapour q. The prediction of $7 \leq m \leq 10$ by Raupach et al. (1996) is marked with dotted lines. The exact values are given in Tab. III.

with decreasing z. This trend is continued even for the data within the canopy. Absolute values lie within $12 \leq m \leq 35$ and are larger than is the other sectors. The only exceptions to this pattern are m_{CO_2} and m_q, which even tend to increase with decreasing height. We recall that the data at $1.18 z h_c^{-1}$ were obtained using a closed-path gas analyser, which has been identified to alter the temporal scales of q in Section 4.1. The smearing of smaller coherent structures to larger ones would lead to an increase in Λ for carbon dioxide and water vapour, which becomes evident from Tab. III. We thus assume this effect to be present also for calculated streamwise structure spacings and exclude these data from further discussions. Unfortunately, no data of gas concentrations were available within the canopy to exclude possible outliers more safely. Almost no trend with decreasing height can be found for the data of the W sector, as the determined m_x is height-constant between 10 and

15 depending on the observed variable only. In contrast to this, the N sector is characterised by a specific height-dependent pattern separating the data collected above and within the canopy into groups of nearly constant, but different ratios m. The variable inter-relationships $\Lambda_x \Lambda_w^{-1}$ follow the same pattern, i. e. almost no variation with height for the W sector, a continuous decreasing trend with decreasing height for the SE sector and a change of the inter-relationship as it enters the canopy for the N sector. Absolute values do not exceed 2.0 and are mostly within $0.7 \leq \Lambda_x \Lambda_w^{-1} \leq 1.6$.

Our results differ from those obtained in other studies and need to be discussed. It is surprising, that the prediction of the canopy mixing layer analogy for the streamwise structure spacing of active turbulence is satisfied only by the coherent structures in w for two sectors (N, W) above the canopy. A mean $m_w = 7.9$ for the upper two heights above the canopy in the N sector is very close to the predicted 8.1 and corresponds to the lower border of observed values. The mean m_w above the canopy yields 10.1 in the W sector, which corresponds to the upper border of the neutral prediction. The streamwise spacing of active coherent eddies in the SE sector largely deviates from the results of Raupach et al. (1996). As one can assume that vertical exchange of energy and matter between the canopy and the atmosphere takes place also for flow coming from SE and is dominated by coherent eddies to a large extent, the following explanations should be taken into consideration: (i) the wavelet detection of coherent structures failed by systematically overestimating the characteristic event duration D_e, leading to an increase in the mean temporal separation $\overline{T_w}$ and an increased streamwise structure spacing Λ_w, (ii) the canopy mixing layer analogy does not apply in this sector, as basic assumptions are not fulfilled or (iii) there are processes modifying the active eddy motion causing the actual ratio m to differ from prediction. The first, rather technical explanation can be excluded based on the results of Thomas and Foken (2005), who discussed the method of analysis using artificial and real turbulent time series and did not find a systematic over- or underestimation of event scales. A failure of the wavelet detection scheme normally leads to unrealistic event scales largely differing from those observed under similar meteorological conditions. These false results were discarded by the applied QA/QC protocol. The canopy mixing layer analogy is mainly based on the strong inflection in the $U(z)$ profile, which was observed also for winds coming from SE. The theory holds for a large variety of different canopies under differing stability , as was demonstrated by many researchers (Raupach et al., 1989; Raupach et al., 1996; Katul et al., 1998; Brunet and Irvine, 2000). The effect of processes modifying the predicted m is the most possible explanation
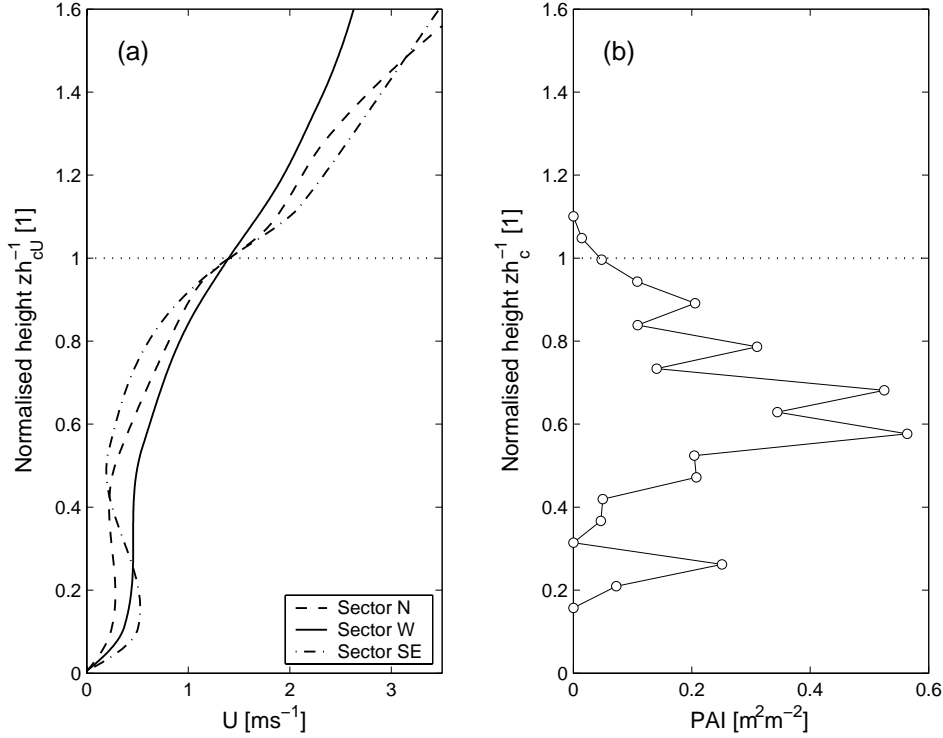
Figure 8. (a) Selected mean (30 min) profiles of horizontal velocity $U(zh_{cU}^{-1})$ within the three wind direction sectors under neutral conditions $|h_c L^{-1}| \leq 0.0625$. Profiles were interpolated using the algorithm by Akima (1970). Statistical properties are listed in Tab. IV. (b) Mean profile of plant area index (PAI) for the sampling site Weidenbrunnen Waldstein. The cumulative ΣPAI is 5.2.

for the results we obtained. We recall that we already identified surface properties to effect the canopy shear length scale. Referring to Eq. 9, m can be increased through either increasing the numerator, i.e. Λ_w, or through a decrease in the denominator, i. e. L_s. To answer this question, we selected three typical mean profiles of $U(z)$ one for each wind direction sector satisfying $U_{h_{cU}} = 1.4 \, ms^{-1}$, which is an arbitrarily selected moderate value, under neutral stability $|h_c L^{-1}| \leq 0.0625$ (Fig. 8). The profiles were prior interpolated using the algorithm by Akima (1970). The statistics of the selected wind profiles are presented in Tab. IV.

The vertical wind shear at canopy top is greatest for the SE sector while the wind speed at canopy top was the same for all sectors (which was one of the selection criteria), resulting in the smallest L_s. The derived instantaneous $m= 23$ for the SE sector is larger than in the other sectors. Thus one can clearly identify the increased vertical shear being responsible for the deviations of m from the prediction of Raupach et al.

Coherent structures in a tall spruce canopy   25

Table IV. Statistical moments of the three mean wind profiles plotted in Fig. 8 and corresponding results from wavelet analysis of the sonic data: wind direction ϕ, horizontal velocity an canopy top $U_{h_{cU}}$, atmospheric stability $h_c L^{-1}$, vertical shear gradient at canopy top $(dU/dz)_{z=h_cU}$, aerodynamic canopy height h_{cU}, canopy shear scale L_s, streamwise structure spacing in the vertical wind Λ_w evaluated at $1.18zh_{cU}^{-1}$ and ratio $m_w = \Lambda_w L_s^{-1}$.

Sector	ϕ $[^o]$	$U_{h_{cU}}$ $[ms^{-1}]$	$h_c L^{-1}$ $[1]$	$(dU/dz)_{z=h_{cU}}$ $[ms^{-1}m^{-1}]$	h_{cU} $[m]$	L_s $[m]$	Λ_w $[m]$	m_w $[1]$
N	8	1.4	0.049	0.20	19.4	7.0	99	14.1
W	263	1.4	0.002	0.15	18.2	9.3	98	10.6
SE	120	1.4	0.009	0.29	18.6	4.8	111	23.2

(1996), while the streamwise structure spacing is similar for all wind direction sectors. A probable explanation for the large vertical wind shear in the SE sector is the channelling of the flow by the shallow mountains (Fig. 1), which compress the mean streamlines of the flow leading $U(z)$ to increase beyond its typical values observed for the W and N sectors. The obstacles seem to be too close to the site ($\approx 500\,m$) to allow the flow fully adapting the new surface conditions. Hence, the surface conditions may have a modifying effect on the proportionality between the streamwise structure spacing of the active turbulence and the canopy shear length scale through modifying the mean velocity profile. It is interesting to note that the secondary wind velocity maximum in the canopy subspace is typically pronounced for winds blowing from SE (Fig. 8a).

The determined m for heights $z < h_{cU}$ tend to be smaller than those observed for $z > h_{cU}$ in the SE and N sectors, corresponding to a larger number of detected coherent structures within the canopy than above. This finding may be explained by the large drag of the canopy elements absorbing the momentum of coherent structures as they enter the canopy, which leads to a splitting of larger coherent structures to smaller ones. Comparing the profiles plotted in Fig. 8a, the drag seems to be larger for SE and N wind directions causing a great decrease in $U(z)$ for $z < h_{cU}$. In case of winds from W, m was observed to be almost constant for all variables. This finding points to the fact that coherent structures that approach the sampling site within the W sector are not altered by the canopy, as the momentum absorption is much smaller. Unfortunately, no studies have been published yet providing results for observed streamwise structure spacing within the canopy to our knowledge.

Departures from the relationship $\Lambda_w = 8.1 L_s^{-1}$ have been reported also by Novak et al. (2000) from wind tunnel studies. The ratio m was

26   Thomas and Foken

observed to fall below the prediction by Raupach et al. (1996) with decreasing tree density. The tree density was thus identified to have an altering effect on streamwise structure spacing of coherent eddies.

The variable inter-relationships $\Lambda_x \Lambda_w^{-1}$ reported by other authors are similar to those we found in the present study. Brunet and Irvine (2000) found $\Lambda_x \Lambda_w^{-1}$ to be 3.1, 2.2 and 1.7 for the streamwise and cross-wind components and temperature respectively. These values compare well to our results yielding 2.0, 1.7 and 1.3 for the horizontal velocity, the wind direction and sonic temperature respectively at $zh_c^{-1} > 1$. Inter-relationships tend to approach unity for $zh_c^{-1} < 1$. However, our results underestimate their observations by the factor of about 1.5. It was reported by Katul et al. (1998) that the canopy mixing layer analogy is not applicable for the horizontal velocity and scalar fluctuations, as they are largely contaminated by inactive eddy motion, which is caused by large-scale atmospheric boundary layer processes.

4.4. INTERNAL GRAVITY WAVES

In the previous section, the theoretical concept of the canopy mixing layer analogy was found to reliably predict the streamwise spacing of active coherent eddies despite some exceptions. The identification and detection of coherent structures in time series was based on the spectral peak in the wavelet variance spectrum yielding their typical event duration D_e. One may reasonably claim that under stable conditions the spectral peak may also be due to internal gravity waves, as they also cause well-organised, regularly spaced patterns in time series. Gravity waves have already been observed by researchers under similar conditions or using similar techniques (e. g. Paw U et al., 1990, Handorf and Foken, 1997, Gedzelman, 1983). We will dedicate this section to compare typical temporal scales of coherent structures and gravity waves to assess whether some of the data presented in the previous section can be linked to wave motion.

Linear gravity waves result from Kelvin-Helmholtz instabilities and can be predicted by linear stability analysis of the dynamical flow equations (De Baas and Driedonks, 1985; Einaudi and Finnigan, 1981). Internal (buoyancy) waves occur under statically stable stratification through the restoring forces of buoyancy on fluid particles, which were displaced from their equilibrium position (e. g. Kantha and Clayson, 2000). The analysis of the dynamical flow equations reveals a characteristic frequency of the wave, called the Brunt-Vaisala frequency N_{BV}, as a

Coherent structures in a tall spruce canopy   27
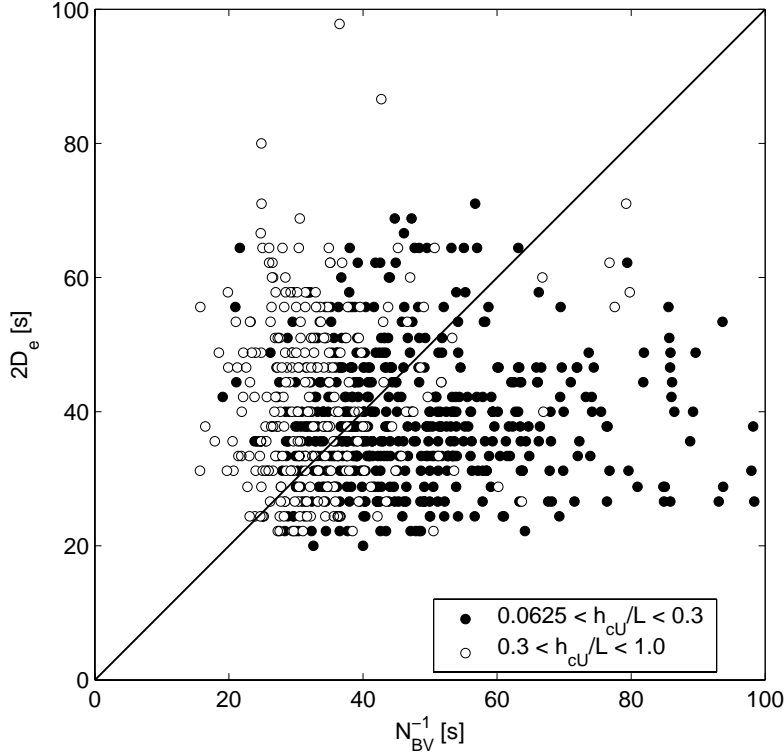
Figure 9. Characteristic temporal scales of detected events D_e in the vertical wind at $1.74zh_c^{-1}$ plotted versus the inverse Brunt-Vaisala frequency N_{BV}^{-1} for stable stratification during WALDATEM-2003. The solid line marks unity $(2D_e = N_{BV}^{-1})$. The total number of data with $2D_e > N_{BV}^{-1}$ is 864.

function of the mean vertical temperature gradient and is given by

$$N_{BV} = \left(\frac{g}{\overline{T}} \frac{\partial \overline{T}}{\partial z} \right)^{\frac{1}{2}}, \tag{10}$$

where g is the acceleration due to gravity. The Brunt-Vaisala frequency represents the upper border for frequencies of internal gravity waves (e. g. Gill, 1982). Internal gravity waves thus exhibit wave frequencies f ranging between zero and N_{BV}. Referring to Eq. 2, the event duration D used throughout this study corresponds to half the length of period for a wave. Hence, we consider internal gravity waves to dominate the recorded signals if the characteristic temporal scale of detected events is greater than half the inverse Brunt-Vaisala frequency, i. e. $2D_e \geq N_{BV}^{-1}$ or $f = 1/2D_e^{-1} \leq N_{BV}$.

N_{BV} was calculated for each 30-min period using the mean temperature gradient $\partial \overline{T}/\partial z$ of the mean temperature profile between 1.63

28   Thomas and Foken

and $1.11 z h_c^{-1}$. Two main groups of points can be found when plotting the determined characteristic temporal scales of detected events in the vertical wind versus the inverse Brunt-Vaisala frequency (Fig. 9). For moderately stable stratification $0.0625 \leq h_{cU} L^{-1} \leq 0.3$, the temporal scales of detected events predominantly fall below N_{BV}^{-1}. With stability increasing beyond $h_{cU} L^{-1} > 0.3$, the temporal scales of detected events tend to exceed N_{BV}^{-1} and therefore indicate the presence of internal gravity waves. As our condition is necessary, but not sufficient in terms of reliably separating wave motion from coherent structures, we applied the same criteria for the sonic temperature data. Now, only data satisfying $2 D_e \geq N_{BV}^{-1}$ for both vertical wind and temperature were selected, leaving 384 out of 424 data. Fig. 10a,b plot the data matching this condition as a function of wind direction. Most data (62 %) lie within the SE sector connected with moderate stability and moderate horizontal velocities at $U_{h_{cU}} \leq 1.5 \, ms^{-1}$. The close grouping of the data at $\phi \approx 130^o$ suggests that these waves may be induced initially by the flow over the shallow mountain 'Lehstenberg' (Fig. 1) and thus correspond to mountain-type gravity waves (e. g. Stull, 1988). The looser, but evident grouping of data at $\phi \approx 0^o$ and $\phi \approx 190^o$ point to the northern shallow ridge crest and the mountain 'Waldstein' respectively (Fig. 1), which also serve as flow obstacles inducing wave motion. These events are typically observed at low wind speeds $U_{h_{cU}} \approx 0.5 \, ms^{-1}$. Nappo (2002) extensively discusses the generation of gravity waves through terrain and provides software codes for the calculation of two-dimensional terrain-generated wave fields for both surface corrugations and ridges.

For the sake of interest, we introduced another criteria assessing the coherence of internal gravity waves in vector and scalar time series. In addition to the selection criteria mentioned prior, data were discarded if the temporal scale of events in the vertical wind $D_e(w)$ departs more than 10 % from those in the sonic temperature $D_e(T_s)$, leaving 123 out of the 384 data shown in Fig. 10a,b. The results confirm the above observations (Fig. 10c,d): Almost all data (75 %) are located in the SE sector closely grouping at $\phi \approx 130^o$ and can be classified as mountain-type gravity waves. This finding is a agreement with the observations of Gedzelman (1983), who observed enhanced spatial coherence of gravity waves generated by impulses, such as explosions, thunderstorms and flow over mountains.

In case of uniform wave motion without periods of quiescence between adjacent events, from Eqs. 2 and 4a follows, that the mean temporal separation of events, which is the streamwise spacing or inverse periodicity, is expected to equal the full period length of events, i. e. $\overline{T_x} \approx 2 D_e$. From the definition of Eq. 4b it follows, that the standard deviation of

Coherent structures in a tall spruce canopy   29
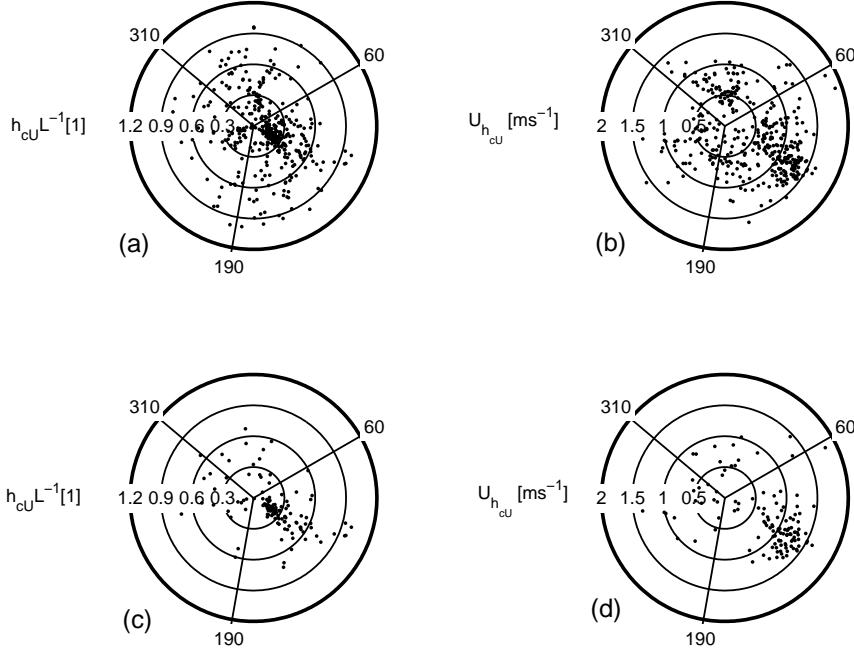
Figure 10. Data fulfilling the condition $2D_e > N_{BV}^{-1}$ for both the vertical wind w and sonic temperature T_s ($n = 384$) as a function of wind direction and (a) atmospheric stability $h_{cU}L^{-1}$ and (b) mean horizontal velocity at canopy top $U_{h_{cU}}$. Data in subplots (c) and (d) additionally satisfy the coherence criterion between w and T_s given by $D_e(w) = D_e(T_s) \pm 10\%$ ($n = 123$). The straight lines mark the borders of the wind direction sectors.

temporal separation $\sigma_{\overline{T_x}}$ should be close to zero then. Evaluating the results for the vertical wind data at $1.74zh_c^{-1}$ satisfying the coherence criterion, one yields $\overline{T_w} = 0.93 \cdot 2D_e + 0.5$ ($R^2 = 0.97$) and $\sigma_{\overline{T_w}} = 12.6\,s$. As the empirical results very well compare to our theoretical expectations, these findings give strong support to the presence of internal gravity waves during the selected intervals.

5. Conclusions

Based on the results gained by the analysis of coherent structures in and above a tall vegetated spruce canopy we arrive at the following conclusions:

Coherent structures are largely asymmetric above the canopy as their mean temporal scales detected in the vertical component were found to be smaller than those in other vector or scalar variables. Within the canopy, this asymmetry is balanced through the large drag by the

30   Thomas and Foken

canopy elements acting as an efficient sink of horizontal momentum forcing the ratio of horizontal and vertical scales to approach unity. Based on the agreement between our results and those by other authors concerning the general variations with height and the differences found in absolute numbers for temporal scales of coherent structures, we conclude that durations of coherent structures are highly variable and follow local properties of the canopy and the surrounding terrain rather than non-local scaling laws.

The use of the aerodynamic canopy height h_{cU}, defined by the height of the inflection point in the mean profile of horizontal velocity, is a reasonable concept for assessing canopy heterogeneity and effects of surface properties on the mean flow. The application of its variable heights instead of a fixed, estimated value is particularly useful for scaling purposes of vertical profiles under varying stability and flow conditions.

The theoretical concept of the canopy mixing-layer analogy, proposed by Raupach et al. (1996), was found to successfully predict the streamwise spacing of active coherent structures Λ_w embodied in the vertical velocity. Departures from the prediction of $m = \Lambda_w L_s^{-1} = 8..10$ by Raupach et al. (1996) could be addressed to decreased values of L_s which are due to an influence of the larger-scale topography on the mean profile of horizontal velocity $U(z)$. In contrast to the vertical wind, the canopy mixing-layer analogy is not applicable for coherent structures of the inactive turbulent motion such as the horizontal velocity. For the first time, typical mean values for m were determined within the canopy. These results point to a disintegration of coherent structures into smaller ones if the canopy drag exceeds a certain threshold. This effect could not be observed for flows characterised by small vertical wind shear dU/dz at canopy top. Analysing scales for shear processes in the proximity of the canopy top, the canopy shear scale L_s (Eq. 7) was identified to be appropriate rather than other scales as it is more sensitive to canopy and surface heterogeneity.

Internal gravity waves can be separated from coherent structures through an analysis of their temporal scales in relation to the Brunt-Vaisala frequency N_{BV}. It was demonstrated that the occurrence of wave motion increases with increasing stability. Hence, one must carefully select periods with dominating wave motion when studying coherent structures under increased stable atmospheric stratification. This point becomes particularly important as temporal scales of coherent structures and those of internal gravity waves are similar.

Acknowledgements

References

Akima, H.: 1970, 'A new method of interpolation and smooth curve fitting based on local procedures'. *J Assc Comp Mach* **17**, 589–602.

Bergström, H. and U. Högström: 1989, 'Turbulent exchange above a pine forest. II. Organized structures'. *Boundary-Layer Meteorol.* **49**, 231–263.

Brunet, Y. and S. Collineau: 1994, 'Wavelet analysis of diurnal and nocturnal turbulence above a maize canopy'. In: E. Foufoula-Georgiou and P. Kumar (eds.): *Wavelets in Geophysics*, Vol. 4 of *Wavelet analysis and its applications*. San Diego: Academic Press, pp. 129–150.

Brunet, Y. and M. Irvine: 2000, 'The control of coherent eddies in vegetation canopies: streamwise structure spacing, canopy shear scale and atmospheric stability'. *Boundary-Layer Meteorol.* **94**, 139– 163.

Chen, J. and F. Hu: 2003, 'Coherent structures detected in atmospheric boundary-layer turbulence using wavelet transforms at Huaihe River Basin, China'. *Boundary-Layer Meteorol.* **107**, 429–444.

Collineau, S. and Y. Brunet: 1993a, 'Detection of turbulent coherent motions in a forest canopy. Part I: Wavelet analysis'. *Boundary-Layer Meteorol.* **65**, 357–379.

Collineau, S. and Y. Brunet: 1993b, 'Detection of turbulent coherent motions in a forest canopy. Part II: Time-scales and conditional averages'. *Boundary-Layer Meteorol.* **66**, 49–73.

De Baas, A. F. and A. G. M. Driedonks: 1985, 'Internal gravity waves in a stably stratified boundary layer'. *Boundary-Layer Meteorol.* **31**, 303–323.

Einaudi, F. and J. J. Finnigan: 1981, 'The interaction between an internal gravity wave and the planetary boundary layer'. *Quart.J.Roy.Meteor.Soc.* **107**, 793–806.

Finnigan, J.: 2000, 'Turbulence in plant canopies'. *Ann. Rev. Fluid Mech.* **32**, 519–571.

Finnigan, J. J.: 1979, 'Turbulence in waving wheat. II. Structure of momentum transfer'. *Boundary-Layer Meteorol.* **16**, 213–236.

Foken, T., M. Göckede, M. Mauder, L. Mahrt, B. Amiro, and J. Munger: 2004, 'Post-field data quality control'. In: X. Lee (ed.): *Handbook of Micrometeorology: A Guide for Surface Flux Measurements*. Dordrecht: Kluwer, pp. 181–208.

Gao, W., R. H. Shaw, and K. T. Paw U: 1989, 'Observation of organized structure in turbulent flow within and above a forest canopy'. *Boundary-Layer Meteorol.* **47**, 349–377.

Gedzelman, S. D.: 1983, 'Short-period atmospheric gravity waves: A study of their statistical properties and source mechanisms'. *Mon.Wea.Rev.* **111**, 1293–1299.

Gerstberger, P., T. Foken, and K. Kalbitz: 2004, 'The Lehstenbach and Steinkreuz chatchments in NE Bavaria, Germany'. In: E. Matzner (ed.): *Biogeochemistry*

32   Thomas and Foken

of forested catchments in a changing environment:. *Ecological Studies*, Vol. 172. Heidelberg: Springer, pp. 15–41.

Gill, A. E.: 1982, *Atmosphere-ocean dynamics*, Vol. 30 of *International Geophysics Series*. Orlando, FL: Academic Press.

Grossmann, A., R. Kronland-Martinet, and J. Morlet: 1989, 'Reading and Understanding Continous Wavelet Transforms'. In: J. Combes, A. Grossmann, and P. Tchamitchian (eds.): *Wavelets: Time-Frequency Methods and Phase Space*. New York: Springer-Verlag, pp. 2–20.

Grossmann, A. and J. Morlet: 1984, 'Decomposition of Hardy Functions into Square Integrable Wavelets of Constant Shape'. *J. Math. Anal* **15**, 723–736.

Handorf, D. and T. Foken: 1997, 'Analysis of turbulent structure over an Antarctic ice shelf by means of wavelet transformation'. In: *12th Symosium on Boundary Layer and Turbulence*. Vancouver BC, Canada: Am. Meteorol. Soc., pp. 245–246.

Kantha, L. H. and C. A. Clayson: 2000, *Small Scale Processes in Geophysical Fluid Flows*, Vol. 67 of *International Geophysics Series*. San Diego, CA: Academic Press.

Katul, G., C. Geron, C. I. Hsieh, B. Vidakovic, and A. Guenther: 1998, 'Active Turbulence and Scalar Transport near the Forest-Atmosphere Interface'. *J. Applied Meteorol.* **37**, 1533– 1546.

Kronland-Martinet, R., J. Morlet, and A. Grossmann: 1987, 'Analysis of Sound Patterns Through Wavelet Transforms'. *Int. J. Pattern Recognition and Artificial Intelligence* **1**, 273–302.

Kumar, P. and E. Foufoula-Georgiou: 1994, 'Wavelet analysis in Geophysics: An Introduction'. In: E. Foufoula-Georgiou and P. Kumar (eds.): *Wavelets in Geophysics*, Vol. 4 of *Wavelet analysis and its applications*. San Diego: Academic Press, pp. 1–43.

Lenschow, D. and M. R. Raupach: 1991, 'The attenuation of fluctuations in scalar concentrations through sampling tubes'. *J. Geophys. Res.* **96**, 15,259–15,268.

Leuning, R. and J. Moncrieff: 1990, 'Eddy-covariance CO_2 flux measurements using open- and closed-path CO_2 analysers: Corrections for analyser water vapor sensitivity and damping of fluctuations in air sampling tubes'. *Boundary-Layer Meteorol.* **53**, 63–76.

Lu, C. and D. Fitzjarrald: 1994, 'Seasonal and diurnal variations of coherent structures over a deciduous forest'. *Boundary-Layer Meteorol.* **69**, 43–69.

Lykossov, V. and C. Wamser: 1995, 'Turbulence Intermittency in the Atmospheric Surface Layer over Snow-Covered Sites'. *Boundary-Layer Meteorol.* **72**, 393–409.

Mahrt, L. and J. Howell: 1994, 'The influence of coherent structures and microfronts on scaling laws using global and local transforms'. *J. Fluid. Mech.* **260**, 247–270.

Massman, W. J.: 1991, 'The attenuation of concentration fluctuations in turbulent flow through a tube'. *J. Geophys. Res.* **96**, 15,269–15,273.

Mauder, M.: 2002, 'Auswertung von Turbulenzmessgerätevergleichen unter besonderer Berücksichtigung von EBEX-2000'. Diploma-thesis, Univ. of Bayreuth.

Nappo, C. J.: 2002, *An introduction to atmospheric gravity waves*, Vol. 85 of *International Geophysics Series*. San Diego: Academic Press.

Novak, M., J. Warland, A. Orchansky, R. Kettler, and S. Green: 2000, 'Wind tunnel and field measurements of turbulent flow in forests. Part I: uniformly thinned stands'. *Boundary-Layer Meteorol.* **95**, 457–495.

Paw U, K. T., Y. Brunet, S. Collineau, R. H. Shaw, T. Maitani, J. Qiu, and L. Hipps: 1992, 'Evidence of Turbulent Coherent Structures in and above Agricultural Plant Canopies'. *Agric.For.Meteorol.* **61**, 55–68.

Coherent structures in a tall spruce canopy   33

Paw U, K. T., R. H. Shaw, and T. Maitani: 1990, 'Gravity waves, coherent structures and plant canopies'. In: *Reprints of the 9th Symposium on turbulence and difussion.* Boston: Am. Meteorol. Soc., pp. 244–246.

Raupach, M. R., J. J. Finnigan, and Y. Brunet: 1989, 'Coherent Eddies in Vegetation Canopies'. In: *4th Australasian Conference on Heat and Mass Transfer.* Christchurch, NZ, pp. 75–90.

Raupach, M. R., J. J. Finnigan, and Y. Brunet: 1996, 'Coherent eddies and turbulence in vegetation canopies: the mixing-layer analogy'. *Boundary-Layer Meteorol.* **78**, 351–382.

Shaw, R. H., Y. Brunet, J. J. Finnigan, and M. R. Raupach: 1995, 'A wind tunnel study of air flow in waving wheat: Two-point velocity statistics'. *Boundary-Layer Meteorol.* **76**, 349–376.

Stull, R. B.: 1988, *An Introduction to Boundary Layer Meteorology.* Dordrecht, Boston, London: Kluwer Acad. Publ.

Thomas, C. and T. Foken: 2005, 'Detection of Long-term Coherent Exchange over Spruce Forest Using Wavelet Analysis'. *Theor. Appl. Climatol.* pp. DOI: 10.1007/s00704–004–0093–0.

Thomas, C., J.-C. Mayer, F. Meixner, and T. Foken: 2005, 'Analysis of low-frequency turbulence above tall vegetation using a Doppler sodar'. *Boundary-Layer Meteorol.* p. (submitted).

Turner, B. J. and M. Y. Leclerc: 1994, 'Conditional sampling of coherent structures in atmospheric turbulence using the wavelet transform'. *J Atmosph. & Oceanic Techn.* **11, Part 2**, 205–209.

Vickers, D. and L. Mahrt: 1997, 'Quality control and flux sampling problems for tower and aircraft data'. *J. Atmosph. & Oceanic Techn.* **14**, 512–526.

Wichura, B., J. Ruppert, A. C. Delany, N. Buchmann, and T. Foken: 2004, 'Structure of carbon dioxide exchange processes above a spruce forest'. In: E. Matzner (ed.): *Biogeochemistry of forested catchments in a changing environment:. Ecological Studies*, Vol. 172 of *Ecological Studies.* Berlin, Heidelberg: Springer, pp. 161–176.

Wilczak, J. M., S. P. Oncley, and S. A. Stage: 2001, 'Sonic anemometer tilt correction algorithms'. *Boundary-Layer Meteorology* **99**, 127–150.

Address for Offprints:
Christoph Thomas
University of Bayreuth
Department of Micrometeorology
95440 Bayreuth, Germany
Tel. (49) 921 55 2320
Fax (49) 921 55 2366
Email christoph.thomas@uni-bayreuth.de

Appendix E

Flux contribution of coherent structures and its implications for the exchange of energy and matter in a tall spruce canopy

Christoph Thomas (`christoph.thomas@uni-bayreuth.de`)
Department of Micrometeorology, University of Bayreuth, Bayreuth, Germany

Thomas Foken
Department of Micrometeorology, University of Bayreuth, Bayreuth, Germany

Abstract. The flux contribution of coherent structures to the total exchange of energy and matter is investigated in a spruce canopy of moderate density in heterogeneous, complex terrain. A wavelet detection method is applied to extract the coherent structures from the turbulent time series. Their flux contribution is determined using conditional averages. The data were obtained by high-frequency single-point measurements using sonic anemometers and gas analysers at several observation levels above and within the canopy and represent a period of about 2.5 months. The analysis is performed for the transfer of momentum, buoyancy, carbon dioxide and water vapour.

Coherent structures contribute approx. 16 % to the total Reynolds stress and approx. 26 % to the exchange of buoyancy, carbon dioxide and water vapour on average. The flux contribution of coherent structures increases with increasing vertical wind shear. The sweep phase of coherent structures is the dominant process close to and within the canopy, whereas the ejection phase gains importance with increasing distance to the canopy. The efficiency of the coherent exchange in transporting scalars exceeds that for momentum by a factor of two. The presence of coherent structures results in a flux error less than 4 % for the eddy covariance method. Based on the physical processes derived from the analysis of the ejection and sweep phases along the vertical profile, a classification scheme for typical exchange regimes is developed. This scheme estimates the spatial volume of the canopy which is in exchange with the overlying atmosphere during varying environmental conditions.

Keywords: Coherent structures, Eddy Covariance Method, Forest, Conditional Sampling, Wavelet Transform

1. Introduction

Coherent structures have been receiving close attention by the turbulence community investigating flow dynamics in laboratory flows and the atmospheric boundary layer over the past decades. Particularly over rough surfaces, these low-frequent large-scale events contribute large fractions to the overall budgets of momentum, heat and matter (e. g. Raupach, 1981, Bergström and Högström, 1989). Coherent structures are an inherent phenomenon of atmospheric turbulence and represent

2   Thomas and Foken

the deterministic part rather than the stochastic high-frequency part
of a turbulent signal. The occurrence of coherent structures makes
turbulent flow above rough surfaces intermittent, as large fractions of
the flux are transported within a small fraction of time. In this paper
another aspect of coherent structures becomes important as we are
concerned with the turbulent exchange of energy and matter between
a forested ecosystem and the atmosphere. The strong vertical motion
typically associated with coherent structures enables them to penetrate
deep into the canopy forcing an exchange of air between different layers
of the canopy and subcanopy spaces. Therefore the residence time of
air is predominantly controlled by the arrival frequency of coherent
structures limiting the time for physical, chemical and photochemical
ongoing processes. The spatial volume which underlies this control is
a function of how deep coherent structures penetrate into the canopy.
Particularly the strong downward motion of the sweep phase of coherent
structures, which is subsequent to the moderate upward motion of the
ejection phase, is responsible for the renewal of air within this volume.
It is necessary to note that some studies refer to the terms of *ejection*
and *sweep* for the momentum flux only (e. g. Bergström and Högström,
1989). In our study, we will refer to as *ejections* and *sweeps* for the
upward and downward phases of coherent structures for momentum
and scalar fluxes respectively.

The mechanisms of flux contributions of coherent structures in turbu-
lent shear flows close to rough surfaces have been studied in laboratory
experiments (e. g. Wallace et al., 1972, Lu and Willmarth, 1973, Rau-
pach, 1981) and in vegetated canopies (e. g. Finnigan, 1979, Shaw et al.,
1983, Bergström and Högström, 1989, Maitani and Shaw, 1990, Katul
et al., 1997). Most studies focused on the relative importance of the
sweep and ejection phases in Reynolds stress or heat flux as a function of
proximity to the rough surface. An overview can be found in Katul et al.
(1997). In summary, these studies evidenced increasing flux contribu-
tions of sweeps F_{sw} in relation to those of ejections F_{ej} with decreasing
distance to the surface. Very close and within the roughness elements,
ratios $F_{sw}F_{ej}^{-1}$ were observed to exceed unity in some cases. For the
momentum transfer, the tendency for sweeps to dominate rather than
ejections scales with the degree of roughness (Raupach, 1981). The flux
contribution of ejections increases with growing distance to the surface
exceeding F_{sw} by far. All studies applied the hole or quadrant analysis
(Wallace et al., 1972, Lu and Willmarth, 1973, Shaw et al., 1983) to
determine the contribution of coherent structures and specifically those
of sweep and ejection phases to the flux of interest. This technique sorts
an instantaneous value into one of the quadrants of a 2-D plane which
is spanned by the fluctuations of the two variables corresponding to

Flux contribution of coherent structures 3

the flux. The membership of a value to one of the quadrants then determines how it contributes to the observed net flux. The particular contribution of coherent structures is extracted by either (i) introducing a hyperbolic threshold criteria for the hole size which passes only the more violent events to analysis or (ii) by conditionally sampling the time series for the periods where coherent structures are dominant. A review of both the methods can be found in Antonia (1981). However, traditional quadrant analysis has some shortcomings as it (i) depends on the definition of threshold values for the hyperbolic threshold criteria which introduces subjectivity at least to a certain degree and (ii) systematically underestimates the flux contribution of ejections (Gao et al., 1989). The latter results from the naturally occurring asymmetry between the sweep and ejection phases, as the sweep motion consists of fewer strong events in contrast to the ejection motion which is characterised by more frequent moderate events. This leads to a systematic exclusion of values corresponding to the ejection phase using a fixed hyperbolic threshold criteria for both the sweep and ejection quadrants. In addition, the use of a fixed threshold criteria represents the increasing contribution of stronger low-frequent events in general rather than the contribution of coherent structures in particular, as amplitudes of coherent structures may change during day.

Besides the aspect of flow dynamics in the proximity to rough surfaces, only little information is available about the implication of coherent structures to the intermittent exchange processes in vegetated canopies. Wichura et al. (2004) proposed a scheme for the classification of typical exchange situations in a tall spruce forest. The authors addressed the question which spatial volume of the canopy is coupled with the atmosphere during the diurnal cycle. Therefore, they analysed the streamwise spacing of adjacent coherent structures according to the canopy mixing-layer analogy (Raupach et al., 1996) in the traces of the vertical wind velocity and the concentration of carbon dioxide at a single observation level above the forest. Based on this analysis and its comparison to measured fluxes of the stable carbon isotope ^{13}C in the atmospheric carbon dioxide, they distinguished between four typical exchange situations between the atmosphere and the canopy: a well-coupled state, a coupling due to strong vertical winds only, a decoupled state, and decoupled state with present long wave motion. However, no satisfying answers have been given to the questions how deep and under which conditions coherent structures penetrate into the canopy and the subcanopy spaces in particular. These problems are crucial when studying the turbulent exchange of energy and matter in natural ecosystems.

The present study is dedicated to get deeper insight into the coherent

4   Thomas and Foken

flux contribution and its implication for exchange processes in a tall
vegetated spruce canopy. It applies the method of conditional sampling
to extract the coherent structures in turbulent time series, whereas the
moments of occurrence of coherent structures are given by an objective
method of detection (Thomas and Foken, 2005b) based on the wavelet
transform. The use of conditional averages to extract quantitative in-
formation about the flux contribution outclasses traditional quadrant
analysis as part of the temporal information about the flow dynam-
ics in coherent structures is preserved (Collineau and Brunet, 1993b).
In addition, flux contributions are calculated reliably and objectively
without requiring the definition of threshold values. In the present
study, the analysis of the flux contribution of coherent structures is
expanded to the transfer of momentum, buoyancy, carbon dioxide and
water vapour within and above the forest. In addition, the impact of
coherent structures on conventional flux determination methods such as
the eddy covariance method will be discussed. The data were obtained
during the WALDATEM-2003 experiment in summer 2003 yielding
continuous turbulence measurements over a period of several months.
The analysis of the dynamical properties of coherent structures in the
layer well above the canopy using acoustic remote sensing was presented
in Thomas et al. (2005). Thomas and Foken (2005a) presented the
analysis of the dynamical properties of coherent structures using the
tower-based observations in the proximity to the canopy. These data
will be used also in the present study for the determination of the flux
contributions of coherent structures. A specific emphasis will be placed
on the spatial region, i. e. the volume of the canopy which is controlled
by coherent structures under varying dynamic conditions and stability
regimes.

2. Experimental setup

Data were obtained during the field experiment WALDATEM-2003
(WAveLet Detection and Atmospheric Turbulent Exchange Measure-
ments) conducted at the FLUXNET site Weidenbrunnen Waldstein
($50^o08'N$, $11^o52'E$), 775 m a. s. l. in the Fichtelgebirge mountains in NE
Bavaria, Germany, in the period May - July 2003. A detailed description
of the surrounding terrain of the experimental site was given by Gerst-
berger et al. (2004), an overview over the objectives of the experiment
can be found in Thomas and Foken (2005a). The spruce canopy is of
moderate density with a plant area index (PAI) of 5.2 (Thomas and
Foken, 2005a). The main leaf mass is concentrated within $0.5 - 0.9zh_c^{-1}$,
where z is the geometrical height above ground and h_c=19 m the mean

canopy height. The topography of the experimental site is different for the three prevailing wind direction sectors N ($310^o - 60^o$), SE ($60^o - 190^o$) and W ($190^o - 310^o$). In the N sector, the flow approaches the site from a valley coming up the mountain ridge, on which the experimental site is located. As the site is located beyond the uppermost part of the ridge, it is overflown directly upstream to the site resulting in a downward tilted flow. The average slope of the terrain where the flow ascends the ridge is 5.1^o within this sector. The flow within the SE sector is channelled between two shallow mountains. The elevation of the terrain within this sector increases homogeneously towards the site at a mean slope of 2.4^o. In the W sector the winds approach the site from the bottom of a valley coming up the mountain ridge at an average slope of 5.0^o. Upstream close to the site, the slope of the terrain reduces to approx. 1.3^o.

Turbulence measurements were performed using sonic anemometers in 4 observation heights in 1.74, 1.18, 0.93 and $0.72h_c$ and fast-response gas analysers in 2 observation heights in 1.74 and $1.18h_c$. Time series with a minimum sample frequency of 10 Hz were obtained for the horizontal wind velocity u, vertical wind velocity w, sonic temperature T_s, carbon dioxide density c_{CO_2} and water vapour density q. The number of recorded 30-min raw data files was approx. 3400 dependent on the observation level. In addition to the high-frequency turbulence data, measurements of mean wind speed and temperature were performed along a vertical profile of cup anemometers and aspirated psychrometers. Details about the instrumentation and the number of raw and quality filtered data can be found in Thomas and Foken (2005a).

3. Flux determination

The method of analysis which was applied to the collected turbulence data consists of two steps: The extraction of coherent structures from the time series and subsequent flux determination of the extracted coherent structures. The first step can be subdivided into data preparation, wavelet analysis and quality control which were discussed in detail by Thomas and Foken (2005b) and Thomas and Foken (2005a). Hence we will limit the descriptions given in the first subsection to the basics necessary for the understanding of the present paper. The method of flux determination of coherent structures using conditional averages is presented subsequently.

6   Thomas and Foken

3.1. COHERENT STRUCTURE DETECTION

The characteristic event duration (temporal scale) of coherent structures D_e was determined by the location of the first spectral peak in the wavelet variance spectrum for each 30-min interval. The wavelet variance was derived from a continuous wavelet transform using the complex Morlet wavelet function. The event duration of coherent structures is defined by $D = \frac{1}{2}f^{-1}$ (e.g. Collineau and Brunet, 1993a), i.e. it corresponds to half the period length of the frequency f. A subsequent wavelet transform at the determined event duration D_e was then calculated using the real Mexican-hat wavelet function. The latter step yields the individual moments of occurrence of coherent structures t_i, whereas $t \in [1, 1800]s$, the index $i \in [1, N]$ and N is the total number of detected coherent structures.

3.2. CONDITIONAL AVERAGES

The conditional sampling and averaging technique enables one to derive quantitative information about interesting regions in turbulent flows (Antonia, 1981). In the present study it was applied for determining the flux contribution of coherent structures. According to the classical Reynolds' decomposition scheme, any instantaneous fluid variable x can be divided into a mean part $\overline{x}$ and a fluctuating part $x\prime$, whereas the mean fluctuating part $\overline{x\prime}$ is assumed to equal zero. Based on the assumption that the fluctuating part is excited by small-scale and large-scale turbulent eddies, it is convenient to divide the fluctuating part into

$$x' = x_l + x_t, \tag{1}$$

where x_l is the contribution of the large-scale and x_t the contribution of the small-scale eddies. Hence, we arrive at a triple decomposition of an instantaneous turbulent variable x (Antonia et al., 1987, Bergström and Högström, 1989) given by

$$x = \overline{x} + x_l + x_t. \tag{2}$$

If we now sample the time series $x(t)$ using the detected moments of coherent structures t_i as the sampling condition and subsequently apply the averaging operator $\langle \ \rangle$ over all subsamples to Eq. 1, we obtain

$$\langle x' \rangle = \langle x_l \rangle, \tag{3}$$

where the right-hand term is the mean contribution of coherent structures to the fluctuation. Eq. 3 is valid under the assumption that the large-scale and small-scale motions are uncorrelated which results in

Flux contribution of coherent structures   7

$\langle x_t \rangle = 0$. For the product of two instantaneous variables x and y one may derive (Collineau and Brunet, 1993b)

$$\langle x'y' \rangle = \langle x' \rangle \langle y' \rangle + \langle x_t y_t \rangle. \tag{4}$$

To obtain the corresponding flux contributions to the total flux, an averaging operator $\widetilde{\langle \ \rangle}$ is defined over the conditional average in Eq. 3 at the characteristical temporal scale D_e given by

$$\widetilde{\langle x \rangle} = \frac{1}{2D_e} \int_{-D_e}^{+D_e} \langle x'(t) \rangle \ \delta t. \tag{5}$$

The window of the conditional averages is centered at the moment of detection t_i and spans $2D_e$. From Eq. 4 we now derive

$$\widetilde{\langle x'y' \rangle} = \widetilde{\langle x' \rangle \langle y' \rangle} + \widetilde{\langle x_t y_t \rangle}, \tag{6}$$

whereas the left-hand term $\widetilde{\langle x'y' \rangle}$ represents the total flux of the conditionally sampled region of the turbulent flow. If the window of the conditional average is representative for the mean flow of the entire time series, it follows that $\widetilde{\langle x'y' \rangle} \approx \overline{x'y'}$, where $\overline{x'y'}$ is the conventional Reynolds averaged flux. The flux contribution of coherent structures is represented by $\widetilde{\langle x' \rangle \langle y' \rangle}$, and $\widetilde{\langle x_t y_t \rangle}$ is the flux contribution of the high-frequency stochastic turbulence. For convenience, we will hereafter refer to as

$$F(x,y)_{tot} = F(x,y)_{cs} + F(x,y)_t \tag{7}$$

for the terms given in Eq. 6. The fluxes are then given by $\tau = F(u,w)$ for momentum, by $H = F(w,T_s)$ for buoyancy, by $C = F(w,c_{CO_2})$ for carbon dioxide and by $\lambda E = F(w,q)$ for latent heat. The flux contribution of the ejection phase F_{ej} and the flux contribution of the sweep phase F_{sw} are determined by applying the averaging operator in Eq. 5 within the borders of $[-D_e, 0[$ and $]0, +D_e]$ respectively, whereas $F_{cs} = F_{ej} + F_{sw}$.

4. Results and discussion

The following three subsections presents the results of the analysis. In the first subsection, some conditional average patterns of coherent structures will be presented exemplarily to demonstrate the physical process of transfer in coherent structures. The next subsection deals with the mean flux contribution of coherent structures along the vertical profile for the momentum and the scalar exchange. In the last

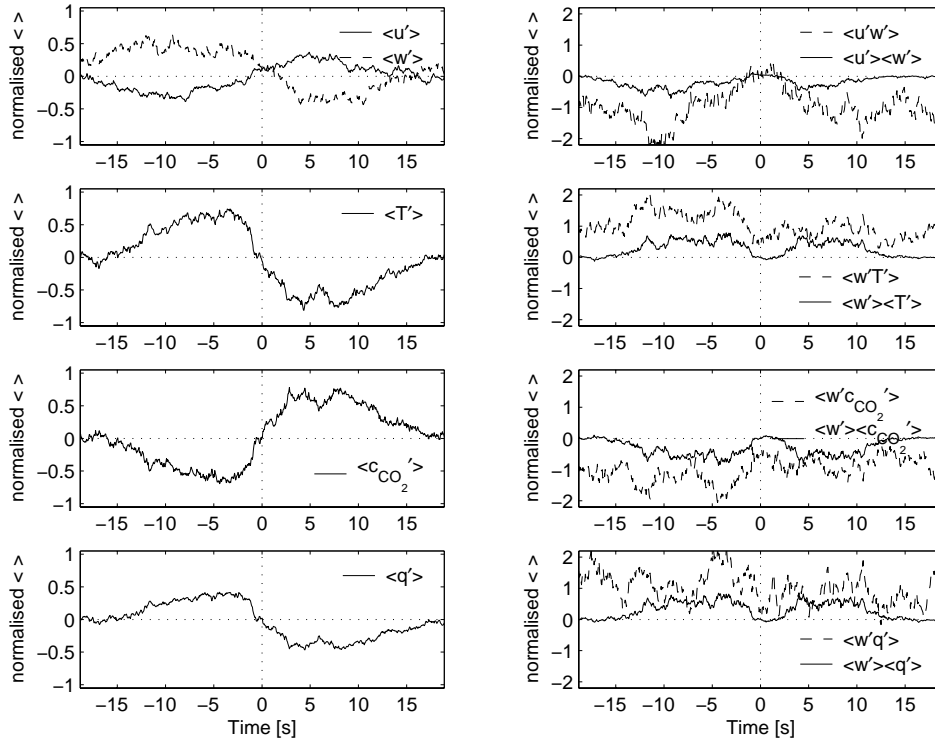8   Thomas and Foken

Figure 1. Normalised conditional averages $\langle\ \rangle$ of (a) - (d) u, w, T_s, c_{CO_2}, q according to Eq. 3 and (e) - (h) corresponding cross-products according to Eq. 4 determined above the canopy at $1.74 h_c$ on June 25, 2003, 13:00 - 13:30 CET, $N = 46, D_e = 19s$, time resolution is 20 Hz. $\langle x'y'\rangle$ corresponds to the total flux F_{tot} and $\langle x'\rangle\langle y'\rangle$ to the flux contribution of coherent structures F_{cs} (see Section 3.2 for details). Data in subplots (a) - (d) were normalised by the corresponding standard deviation σ of the time series and (e) - (h) by the conventional Reynolds averaged flux $|\overline{x'y'}|$.

subsection, an attempt is made to sketch typical exchange regimes in forested ecosystems.

4.1. CONDITIONAL AVERAGE PATTERNS

The time series of vector and scalar variables were sampled at moments t_i and at event durations D_e detected in the sonic temperature data T_s. This choice seems justified as (i) coherent structures were found to be well ramp-shaped in time series of T_s during daytime and nighttime, (ii) measurements were available at all four observation heights and (iii) the use of T_s facilitates the comparison of the results to those available in literature, as T_s has been used most frequently.

The averaged conditionally sampled patterns of coherent structures are shown exemplarily for a single 30-min interval collected above the

Flux contribution of coherent structures 9

canopy during daytime (Fig. 1). The difference between the asymmetric ramp-like shape of coherent structures in the scalar traces of T_s, c_{CO_2} and q and the more symmetric triangle-like shape in the vectors u and w becomes obvious. The orientation of the ramps in the scalar traces indicates the direction of the scalar fluxes which is upward in case of H and λE and downward in case of the carbon dioxide flux C. The conditional averages of the scalars consistently cross zero at the origin (0,0) of the presented window, which supports the choice of sampling coherent structures after t_i and D_e detected in T_s. However, u and w were observed to cross zero at approx. -2 s and +2 s respectively, resulting in an upward directed momentum transfer near the origin. This finding is compatible with previous results from traditional quadrant analysis of Reynolds stress (e. g. Wallace et al., 1972, Raupach, 1981, Shaw et al., 1983, Bergström and Högström, 1989), who observed the flux contribution of outward and inward interactions to be opposite in sign. The temporal offset we found between the conditional averages of vector and scalar variables is in agreement with Collineau and Brunet (1993b), who also observed a small temporal offset between conditional averages of u, w and T_s above the canopy. Comparing the magnitudes of the normalised conditional averages in Figs. 1b-d, one sees that the coherent structures in T_s and c_{CO_2} reach 0.8, whereas those in q do not exceed 0.5. From Eq. 6 one should expect that the relative flux contribution of coherent structures to the buoyancy flux $H_{cs}H_{tot}^{-1}$ and to the carbon dioxide flux $C_{cs}C_{tot}^{-1}$ are greater than that to the latent heat flux $\lambda E_{cs}\lambda E_{tot}^{-1}$. However, the relative flux contribution for the data in Fig. 1 were determined to 0.27, 0.29 and 0.29 for H, C and λE respectively. Although the magnitude of the conditional averaged q falls below T_s and c_{CO_2}, the relative flux contribution is about the same. From Fig. 1h one can see that this can be addressed to frequent breakdowns of the flux contributed by the high-frequency turbulence $F_t = F_{tot} - F_{cs}$ (Eq. 7). During the presence of coherent structures, the latent heat flux λE_{tot} is thus characterised by a quite constant contribution of coherent structures λE_{cs}, and an intermittent contribution of high-frequency turbulence λE_t. This observation is in contrast to that for the buoyancy and the carbon dioxide flux, where H_t and C_t are also quite constant during the presence of coherent structures. The ratio of flux fractions from sweeps to ejections $F_{sw}F_{ej}^{-1}$ was determined to 0.49, 0.66, 0.71 and 0.72 for τ, H, C and λE respectively. Hence, the ejection motion is dominant for the transfer of momentum and scalar fluxes above the canopy. This finding is in agreement with the results of many authors (e. g. Raupach, 1981, Shaw et al., 1983, Bergström and Högström, 1989, Gao et al., 1989), who demonstrated that F_{ej} exceeds F_{sw} with increasing distance from the rough surface.

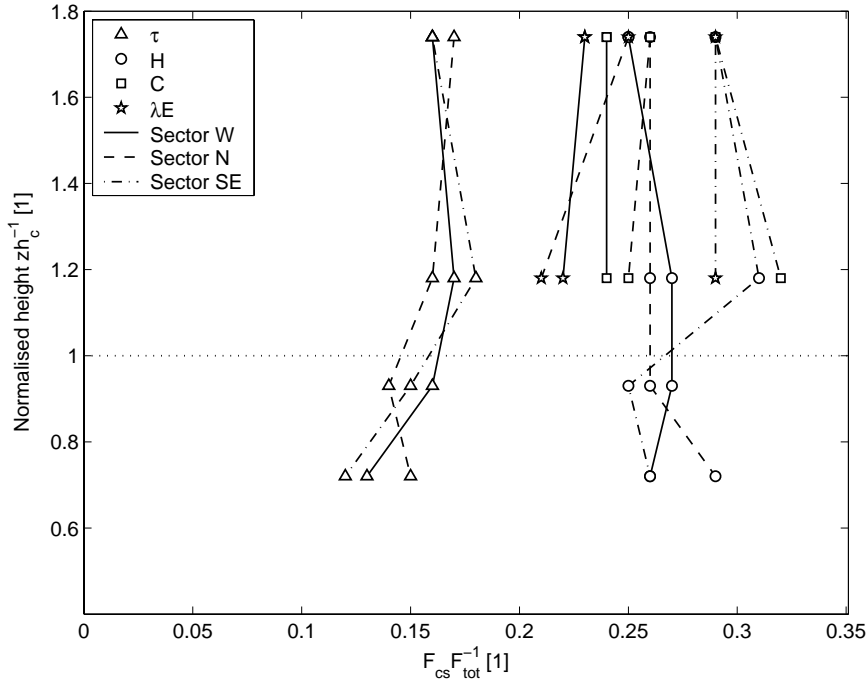10   Thomas and Foken

Figure 2. Mean relative flux contribution of coherent structures to the total flux $F_{cs}F_{tot}^{-1}$ as a function of height h_c and wind direction sectors N ($310^o - 60^o$), SE ($60^o - 190^o$) and W ($190^o - 310^o$) for momentum τ, buoyancy H, carbon dioxide C and latent heat λE. The exact values are given in Tab. I.

4.2. MEAN FLUX CONTRIBUTION

After discussing the results for a single interval in the preceding sub-section, the statistics are now presented to derive a general picture. The results were also obtained using the moments of occurrence t_i and the event durations D_e of coherent structures in the sonic temperature data. The applied QA/QC protocol discarded data (i) collected during inappropriate weather conditions such as rain, fog, calm and storm, (ii) characterised by disturbed mean wind profiles or (iii) unrealistic event durations D_e and (iv) if the flow of the conditional average was not representative for the flow of the entire time series. The latter discarded fluxes not satisfying the condition $0.8 \leq F_{tot}\overline{x\prime y\prime}^{-1} \leq 1.2$. The fraction of rejected data by the criteria (i)‑(iv) was approx. 30 %. For details on the criteria (i)‑(iii) and on statistics about rejected and approved data see Thomas and Foken (2005a).

The mean relative flux contribution of coherent structures $F_{cs}F_{tot}^{-1}$ was derived by fitting a normal Gaussian distribution function to the results. The results are plotted in Fig. 2 while the exact values are given

Flux contribution of coherent structures 11

Table I. Relative flux contribution of coherent structures to the total flux $F_{cs}F_{tot}^{-1}$ observed during WALDATEM-2003 for momentum τ, buoyancy H, carbon dioxide C and latent heat λE: mean μ and standard deviation σ of the normal Gaussian distribution function fitted to the experientially derived data.

$F_{cs}F_{tot}^{-1}$	h_c [1]	Sector W		Sector N		Sector SE		Mean
		μ [1]	σ [1]	μ [1]	σ [1]	μ [1]	σ [1]	$\overline{\mu}[1]$
τ	1.74	0.16	0.08	0.17	0.08	0.16	0.08	0.16
	1.18	0.17	0.09	0.16	0.09	0.18	0.08	0.17
	0.93	0.16	0.08	0.14	0.09	0.15	0.07	0.15
	0.72	0.13	0.09	0.15	0.10	0.12	0.09	0.13
H	1.74	0.25	0.08	0.26	0.10	0.29	0.12	0.27
	1.18	0.27	0.10	0.26	0.11	0.31	0.13	0.28
	0.93	0.27	0.10	0.26	0.12	0.25	0.10	0.26
	0.72	0.26	0.13	0.29	0.13	0.26	0.18	0.27
C	1.74	0.24	0.11	0.26	0.11	0.29	0.14	0.26
	1.18	0.24	0.15	0.25	0.14	0.32	0.15	0.27
λE	1.74	0.23	0.11	0.25	0.13	0.29	0.14	0.26
	1.18	0.22	0.15	0.21	0.15	0.29	0.15	0.24

in Tab. I. For the momentum transfer, $\tau_{cs}\tau_{tot}^{-1}$ was found to be independent on wind direction. Above the canopy, the mean contribution is approx. 0.17 with a slight tendency to increase close to the canopy top. Entering the canopy, $\tau_{cs}\tau_{tot}^{-1}$ reduces reaching 0.13 near the bottom of the canopy space. In contrast to the momentum transfer, the scalar fluxes show a dependence on the wind direction. Above the canopy, $F_{cs}F_{tot}^{-1}$ was observed to exhibits its maximum for winds coming from SE, where the streamwise spacing of coherent structures was found to indicate significant departures from theoretical concepts (Thomas and Foken, 2005a). Within this sector $H_{cs}H_{tot}^{-1}$, $C_{cs}C_{tot}^{-1}$ and $\lambda E_{cs}\lambda E_{tot}^{-1}$ were determined to 0.30, 0.31 and 0.29 respectively. For the N and W sectors, the relative flux contribution ranges between 0.21 and 0.27. Comparing $F_{cs}F_{tot}^{-1}$ for all considered scalar fluxes, it becomes obvious that the ratios for H and C are typically greater or equal λE. Within the canopy, no sector dependent pattern can be found for the scalar fluxes. The relative flux contributions $H_{cs}H_{tot}^{-1}$ collapse around 0.26 with the exception of the N sector at the bottom of the canopy (0.29). One may question the significance of the mean flux contributions presented in Fig. 2 as the results are characterised by large standard deviations (Tab. I). Hence, the flux contribution of individual 30-min intervals may vary significantly from its mean which results in a broadening of the probability density function. One must notice that the mean relative flux contribution represents the integral over the entire

12   Thomas and Foken

WALDATEM-2003 experiment over a period of about 2.5 months. The large standard deviation of the probability density functions are due to the diurnal variation, to different physical processes, and to the stochastic nature of the turbulence. However, the relative flux contribution of coherent structures in the order of 0.16 to the momentum flux and of about 0.26 to the transfer of buoyancy, carbon dioxide and latent heat gives reliable numbers for the importance of coherent structures to the total exchange of energy and matter between the atmosphere and the forest. The analysis of individual physical processes of interest must be done using the flux contribution for the individual 30-min intervals. An example for such an analysis is given in Section 4.3.2.

Our results partially disagree with findings reported by other authors and need to be discussed. Gao et al. (1989) reported about a relative flux contribution of coherent structures of 0.5 - 0.6 at about twice the canopy height and of 0.7 - 0.8 within the canopy for both momentum and buoyancy flux at a deciduous forest site. These results exceed our results by a factor of 4 and 3 for τ and H respectively. However, the detection and flux calculation technique applied by the authors largely differs from ours, as their calculations were based on 18 visually extracted ramps in a temperature trace which have been filtered prior using a 10 s running average 'to reduce the influence of background turbulence'. One may suspect that the visual detection prefers the larger coherent structures showing a pronounced ramp-like pattern rather than smaller events. The smoothing filter applied to the temperature traces may also effect the results in two ways: first, it removes the sharp gradients of smaller events which leads to prefer larger ones and, secondly, the chosen length of the 10 s window may keep some residual flux of high-frequency random turbulence in the derived fluxes for coherent structures. Hence, the objectivity of a visual detection procedure for coherent structures remains unknown in general. In addition, the results by Gao et al. (1989) carry a more exemplary character as they represent a single 30-min interval only. Bergström and Högström (1989) reported about relative flux contribution of organised coherent structures to the transfers of momentum, buoyancy and latent heat which are in the same order of magnitude (0.93, 0.88 and 0.91 respectively) as reported by Gao et al. (1989). However, these results were derived for periods when coherent structures were detected only excluding periods of dominating high-frequency random turbulence systematically. Therefore, nothing can be said about the representativeness of the conditionally sampled periods in relation to the entire time series which represented two 100 min intervals of temporally and spatially separated turbulence measurements above a pine forest.

Results similar to ours were reported by Antonia et al. (1987) in the

far wake of a cylinder and by Collineau and Brunet (1993b) above a
pine forest. They derived relative flux contributions of coherent struc-
tures of 0.28 and 0.33 for momentum and 0.44 and 0.35 for buoyancy,
respectively, using the same triple decomposition technique. Although
the mean relative flux contributions derived in this study are somewhat
smaller, they are in good agreement with the findings of Antonia et al.
(1987) and Collineau and Brunet (1993b). It is important to note that
our and their findings point to a greater efficiency of coherent structures
in transporting scalars than momentum.

It is surprising that $\tau_{cs}\tau_{tot}^{-1}$ was observed to decrease within the canopy
which is in contradiction to the results of Gao et al. (1989) and Collineau
and Brunet (1993b). It must be noted that the spruce canopy acts as
a very efficient sink for momentum in the region where the main leaf
mass is concentrated. This absorption reduces τ to $58\,\%$ and $21\,\%$ at
0.93 and $0.72h_c$ respectively compared to its value above the canopy at
$1.13h_c$. The observed effect that $\tau_{cs}\tau_{tot}^{-1}$ diminishes within the canopy
may thus be addressed to the structure of the canopy at the experi-
mental site. However, no satisfying answer can be given to the observed
discrepancies.

4.2.1. *Mean efficiency of coherent exchange*

Assessing the efficiency α of the turbulent exchange contributed by the
well-organised coherent structures and by the random high-frequency
turbulence, one must take into account their corresponding time frac-
tions of occurrence, i. e. their occupancy times. The efficiency of the
turbulent exchange α is then given by the ratio of the flux fraction to
the time fraction $\alpha = F(F_{tot}\gamma)^{-1}$. For this purpose, we define the time
fraction of coherent structures γ_{cs} given by

$$\gamma_{cs} = \frac{ND_e}{t_{max} - t_{min}}, \tag{8}$$

where $t_{max} - t_{min}$ is the length of the entire series equal to $1800\,\mathrm{s}$
in our case. For the calculation of γ_{cs} according to Eq. 8 we use the
determined values of D_e of the sonic temperature for all vector and
scalar fluxes, as the conditionally calculated fluxes were derived using
the same indicator. For the time fraction of the random high-frequency
turbulence γ_t it seems justified to assume $\gamma_t = 1$ for well-developed
turbulent flow conditions. However, γ_t may differ from unity during
decaying turbulence under nighttime conditions. The time fraction γ_{cs}
was found to range from 0.39 to 0.62, with a mean value of approx. 0.5
independent on height. This is compatible with the results reported
by Gao et al. (1989), who found values between 0.42 and 0.60. The
calculated efficiencies α are listed in Tab. II for the mean relative flux

14   Thomas and Foken

Table II. Mean efficiency of turbulent exchange $\alpha_x = F_x(F_{tot}\gamma_x)^{-1}$ for the flux contribution F of organised coherent structures (index 'x=cs') and the random high-frequency turbulence (index 'x=t') averaged over all observation heights. The time fraction γ_{cs} was calculated according to Eq. 8 and γ_t set to 1.

$Flux$	$\alpha_t[1]$	$\alpha_{cs}[1]$	$\alpha_{cs}\alpha_t^{-1}[1]$
τ	0.85	0.30	0.35
H	0.73	0.54	0.74
C	0.73	0.54	0.74
λE	0.75	0.50	0.67

contribution in Tab. I averaged over all heights. The efficiency of the turbulent exchange contributed by coherent structures for scalar fluxes exceeds this for momentum at a factor of approx. 2.

4.2.2. *Representation of coherent exchange by eddy covariance*
The question arises if the total flux of turbulent exchange F_{tot} calculated using the conditional averages according to Eqs. 6 and 7 systematically differs from the conventional Reynolds averaged flux $\overline{x\prime y\prime}$. The idea behind this assumption is that the presence of intermittent coherent structures which represent non-stationaritites in terms of the flow dynamics effects the conventional Reynolds averaged fluxes and lead to a systematical over- or underestimation of the 'true' flux. In other words, one may question if the flux contribution of coherent structures is entirely covered by the conventional eddy covariance method as coherent structures violate its basic assumption of stationarity. The covariance function is defined by

$$\overline{x\prime y\prime} = \frac{1}{n-1}\sum_{i=1}^{n-1} x\prime y\prime = \frac{1}{n-1}\sum_{i=1}^{n-1}(x - \overline{x}_R)(y - \overline{y}_R), \qquad (9)$$

where $\overline{x}_R$ is the mean of the entire time series using the conventional Reynolds decomposition. During the presence of coherent structures, we hypothesize that the triple decomposition (Eq. 2) becomes valid and the flux is given by

$$\overline{x\prime y\prime} = \frac{1}{n-1}\sum_{i=1}^{n-1}(x_l + x_t)(y_l + y_t) = \frac{1}{n-1}\sum_{i=1}^{n-1}(x - \overline{x})(y - \overline{y}), \quad (10)$$

with $\overline{x} \neq \overline{x}_R$. We further assume that in a time series with both coherent structures and high-frequency turbulence present (i) the 'true' mean can be expressed as $(\overline{x}_R + \Delta\overline{x})$, where $\Delta\overline{x}$ is the assumed error in

calculating $\overline{x}_R$ due to the presence of coherent structures, and (ii) the fluctuations in a time series are similar $(x\prime) \approx (x_l + x_t)$. Substituting the corresponding terms in Eq. 9, one arrives at

$$\overline{x\prime y\prime}_{corr} = \frac{1}{n-1} \sum_{i=1}^{n-1} [x - (\overline{x}_R + \Delta\overline{x})][y - (\overline{y}_R + \Delta\overline{y})] \qquad (11\text{a})$$

$$= \overline{x\prime y\prime} - \frac{1}{n-1} \sum_{i=1}^{n-1} [x\prime\Delta\overline{y} + y\prime\Delta\overline{x} - \Delta\overline{y}\Delta\overline{x}] \qquad (11\text{b})$$

$$= \overline{x\prime y\prime} - \Delta\overline{x\prime y\prime}. \qquad (11\text{c})$$

for the corrected flux. $\Delta\overline{x\prime y\prime}$ is the flux error of the eddy covariance method resulting from the influence of coherent structures. Under the assumptions that

$$\Delta\overline{x} \approx \overline{x}_R - \widetilde{\langle x\prime \rangle} \qquad (12)$$

and that the window of the conditional averages is representative of the mean flow ($0.8 \leq F_{tot}\overline{x\prime y\prime}^{-1} \leq 1.2$), we can determine $\Delta\overline{x\prime y\prime}$ to assess whether the conventional eddy covariance method truly covers the entire flux. In a strict sense, the substitution we applied to derive Eq. 11c and Eq. 12 is valid only for the periods during the presence of coherent structures. However, the assumption seems justified on the background that the mean time fraction of coherent structures $\gamma_{cs} \approx$ 0.5 and that the flux contribution of coherent structures F_{cs} and the conditional averages $\widetilde{\langle x\prime \rangle}$ were calculated over the window with a length of $2D_e$.

The relative flux error $(\Delta\overline{x\prime y\prime})\,\overline{x\prime y\prime}^{-1}$ was determined according to Eq. 11b for the fluxes of momentum, buoyancy, carbon dioxide and latent heat (Fig. 3). One can see that the relative flux error does not exceed 4 % in the majority of cases for the considered fluxes. The largest values are found for fluxes around zero, where absolute fluxes are negligible leading to an increase of the relative flux errors. All calculated flux errors tend to decrease with in increasing magnitude of the absolute fluxes. No evidence was provided that the relative flux errors scales with the relative flux contribution of coherent structures $F_{cs}F_{tot}^{-1}$. It is important to note that no systematic over- or underestimation of the 'true' flux was determined with the method described above as the average over all determined relative flux errors is close to zero. The flux derived by the conventional eddy covariance method is thus not affected by the occurrence of coherent structures
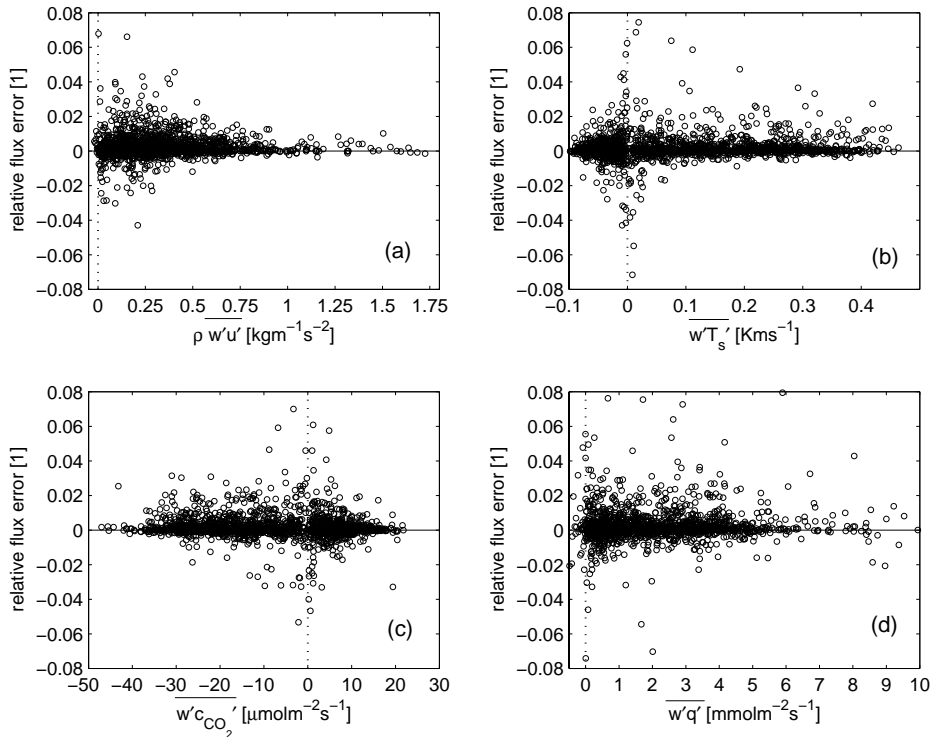
Figure 3. Relative flux error of the conventional eddy covariance method $\Delta \overline{x'y'}\ \overline{x'y'}^{-1}$ through the presence of coherent structures according to Eq. 11c for the exchange of (a) momentum $-\rho\overline{w'u'}$ with ρ being air density, (b) kinematic buoyancy flux $\overline{w'T_s'}$, (c) carbon dioxide flux $\overline{w'c'_{CO_2}}$ and (d) latent heat flux $\overline{w'q'}$ for the WALDATEM-2003 dataset. Negative (positive) values indicate an underestimation (overestimation) of the flux using the conventional eddy covariance method.

4.3. EXCHANGE REGIMES

In this subsection, the spatial region of the canopy which is controlled by the exchange through coherent structures is investigated under varying dynamic and diabatic conditions. An attempt is made to identify typical exchange regimes within and above a forest using the results of the analysis of coherent structures.

For the investigation of the volume controlled by coherent structures, we base our hypothesis on the assumption that the flux transported by the coherent structures is expected to be in the same order of magnitude throughout this volume. A coherent structure is thus expected to contribute about equally at all observation levels within and above the canopy if they are located within this volume. From this follows, that spaces which are decoupled from this volume are expected to a

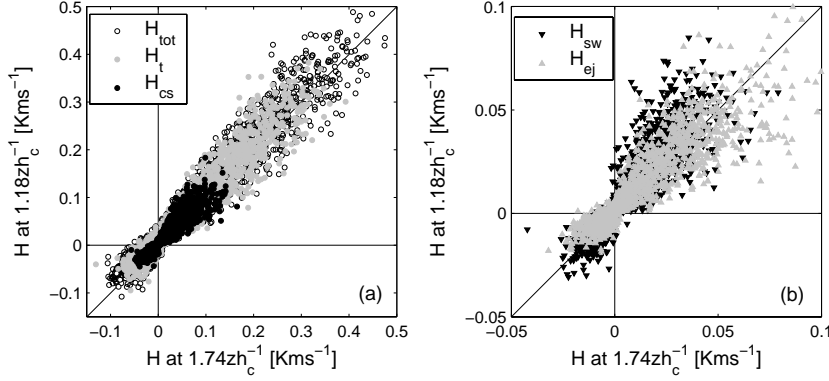Flux contribution of coherent structures   17

Figure 4. Kinematic buoyancy flux H calculated using conditional averages according to Eq. 6 at $1.18h_c$ versus $1.74h_c$ during WALDATEM-2003: (a) total flux H_{tot}, high-frequency stochastic exchange H_t and coherent exchange H_{cs}; (b) coherent exchange of the sweep phase H_{sw} and of the ejection phase H_{ej}.
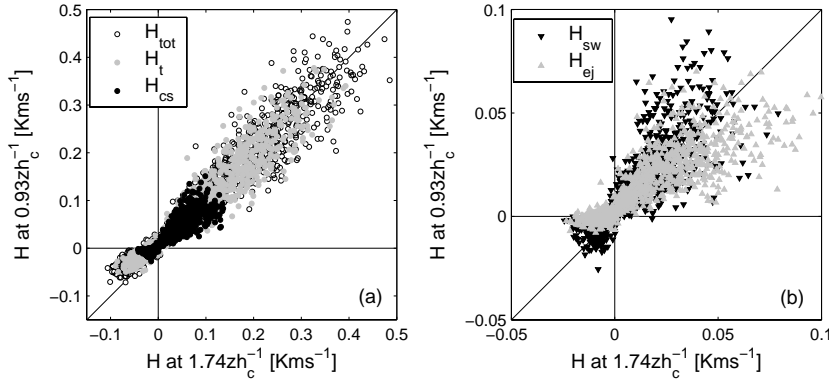

Figure 5. See Fig. 4, but for H at $0.93h_c$ versus $1.74h_c$.

show significantly different flux contribution of coherent structures. We chose the uppermost observation level located at $1.74h_c$ as the reference level for our considerations, as coherent structures are assumed to be generated by instabilities resulting from the large vertical wind shear near the canopy/ atmosphere interface in the roughness sublayer above the canopy (e. g. Raupach et al., 1996, Finnigan, 2000).

In Figs. 4a, 5a and 6a, the buoyancy flux calculated using the conditional averages at the observation levels in 1.13, 0.93 and $0.72h_c$ respectively are presented in relation to the reference level. The observation levels represent different spaces within the considered volume: The layer above but close to the canopy ($1.13h_c$), the canopy top ($0.93h_c$) and the lower part of the canopy space near the interface to the
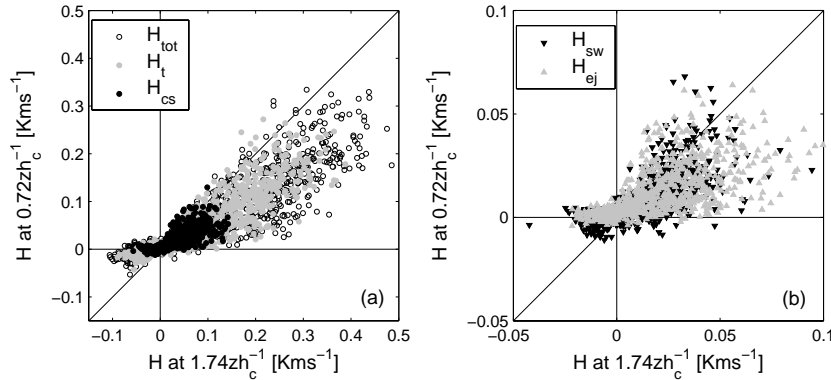
18   Thomas and Foken

Figure 6. See Fig. 4, but for H at $0.72h_c$ versus $1.74h_c$.

subcanopy space ($0.72h_c$). In terms of the flow, the lowest level depicts the 'bottleneck' of the canopy, as most of the leaf mass is concentrated here. Above and at the canopy top, all data closely scatter around the one-to-one line showing no systematic departures for fluxes $H \geq 0$. For $H < 0$, the fluxes observed at the canopy top tend to be smaller than above. A linear regression model ($f(x) = ax + b$) fitted to the data $H_{tot} < 0$ yields a slope $a = 0.59$ ($b \approx 0\,Kms^{-1}$). At the lowest level near the lower border of the canopy space, the fluxes significantly departure from the one-to-one line, yielding $a = 0.56$ ($b \approx 0\,Kms^{-1}$) for fluxes $H_{tot} \geq 0$. For negative fluxes, the slope of the regression line reduces to $a = 0.30$ ($b = 0.01\,Kms^{-1}$). The flux contribution of the high-frequency stochastic turbulence H_t and the organised coherent structures H_{cs} follow the trend of the total flux showing no systematic deviations. From these results one can see that the mean buoyancy flux decreases with decreasing height in the canopy. The magnitude of decrease for data observed during radiative cooling during nighttime is larger than for an upward directed buoyancy flux during daytime. This finding already points to a change in the exchange regimes during the diurnal course involving different volumes, but no particular influence of the high-frequency turbulence, the coherent structures and the spatial extent of the controlled volume can be extracted so far.

A detailed picture about the physical processes of the exchange in the volume coupled by coherent structures can be derived by plotting H_{cs} separated into the flow contributions of ejections H_{ej} and sweeps H_{sw} (Figs. 4b, 5b and 6b). Above the canopy, both H_{ej} and H_{sw} closely scatter around the one-to-one ratio. Sweeps tend to dominate the exchange close to the canopy ($a = 1.1, b \approx 0\,Kms^{-1}$), whereas ejections are stronger at the reference level ($a = 0.8, b \approx 0\,Kms^{-1}$). The in-

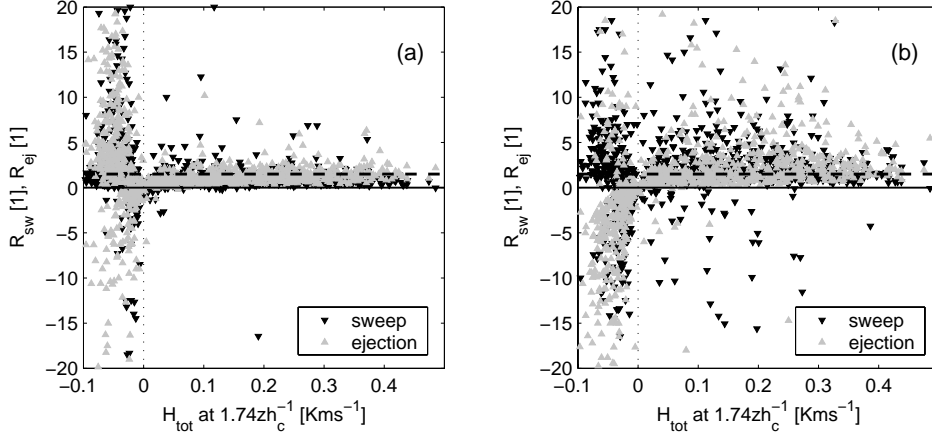Flux contribution of coherent structures   19

Figure 7. Ratio of the flux contribution of sweep phases $R_{sw} = (H_{sw})_{z_1} (H_{sw})_{z_2}^{-1}$ and ejection phases $R_{ej} = (H_{ej})_{z_1} (H_{ej})_{z_2}^{-1}$ for the exchange between the atmosphere ($z_1 = 1.74 z h_c^{-1}$) and (a) the canopy top ($z_2 = 0.93 z h_c^{-1}$) and (b) the lower border of the canopy space ($z_2 = 0.72 z h_c^{-1}$) as a function of the kinematic buoyancy flux H_{tot} at ($z1 = 1.74 z h_c^{-1}$). The dashed lines represent the threshold ratios for the definition of the exchange regimes. Negative ratios indicate an opposite flux direction between the heights z_1 and z_2.

creasing importance of the ejection motion with increasing distance to the rough surface compares well to the findings of other authors (e. g. Wallace et al., 1972, Raupach, 1981, Shaw et al., 1983, Bergström and Högström, 1989). The differences between the sweep and ejection phases intensify with decreasing height: At the canopy top during day-time conditions, H_{sw} is typically greater than H_{ej} for the exchange with the overlying atmosphere. During nighttime, only the strong sweeps contribute to the exchange of buoyancy between the two levels, while the contribution of the ejections to the exchange is negligible. At the lower border of the canopy space, the exchange caused by the sweep phases also exceeds those of the ejection phases for $H \geq 0$. During nighttime conditions, the exchange with the overlying atmosphere is forced by sweeps only. However, comparing H_{sw} in Figs. 5b and 6b one can see that number of sweeps significantly contributing to the exchange between the subcanopy and the atmosphere is much less than between the canopy top and the atmosphere.

More insight into the influence of sweep and ejection phases to the exchange between the atmosphere and the forest can be gained by plotting the ratio of sweeps $R_{sw} = (H_{sw})_{z_1} (H_{sw})_{z_2}^{-1}$ and the ratio of ejections $R_{ej} = (H_{ej})_{z_1} (H_{ej})_{z_2}^{-1}$ between the reference level ($z_1 = 1.74 h_c$) and the canopy ($z_2 = 0.93 h_c$) (Fig. 7a) and the reference level ($z_1 = 1.74 h_c$)

20   Thomas and Foken

and the lower border of the canopy ($z_2 = 0.72 h_c$) (Fig. 7b). For the
interpretation of the data, it is crucial to note that negative ratios
indicate an opposite flux direction of the coherent sweep or ejection
phase at the two considered levels. Hence, they indicate a decoupling
between the levels limiting the volume in which the exchange of en-
ergy and matter takes place. Ratios close to unity indicate a coupled
state. For positive fluxes between the atmosphere and the canopy top
(Fig. 7a), R_{sw} and R_{ej} typically fall below 2 which means that the flux
contribution in the atmosphere is maximally twice the flux contribution
at the canopy top. The ratios of the ejections are typically beyond those
of the sweeps indicating a dominant effect of the stronger sweep phase.
Almost no negative ratios can be observed. The situation changes dra-
matically for fluxes $H_{tot} < 0$: the ratios of the ejections split into groups
of negative and positive values. Almost all values of R_{sw} are greater
than zero, which indicates that predominantly the sweeps contribute
to the exchange throughout the coupled volume. A different picture
was derived for the exchange between the atmosphere and the lower
border of the canopy (Fig. 7b): For $H_{tot} \geq 0$ during daytime conditions,
both R_{sw} and R_{ej} show larger scatter and typically fall below 5. The
number of negative sweep ratios is much greater than in Fig. 7a. During
the night for $H_{tot} < 0$, almost all R_{ej} values are negative, i.e. no
exchange is forced by the ejection phase of coherent structures. The
dominant process contributing to the exchange is the sweep phase. Its
is important to note that the magnitude of the ratios during nighttime
exceeds the daytime values by far. This observation indicates that only
small fractions of the flux above the canopy is transported down to
the lower levels within the canopy. Given this case, a coupling between
the levels seems questionable although $R_{sw} \geq 0$. Hence, we need to
define a reasonable threshold value to arrive at a reliable decision on
the extent of the coupled volume. For an objective definition of this
threshold value, a linear regression model was fitted to the data rep-
resenting fluxes $H_{tot} \geq 0.2 \, K m s^{-1}$ in Fig. 6a yielding a slope $a = 0.65$
($b \approx 0 \, K m s^{-1}$). For these fluxes, we assume a coupling between the
atmosphere and the lower border of the canopy. Therefore the required
threshold value for R_{sw} and R_{ej} indicating a coupled state between the
two levels z_1 and z_2 is given by the inverse slope, i.e. $0.65^{-1} \approx 1.5$.
Based on the results of the analysis of the coherent exchange one may
now extract characteristic exchange regimes in a tall vegetated canopy.

4.3.1. *Definition of exchanges regimes*
In the following, a brief description is given for the 5 different exchange
regimes which were proposed basing on the results presented in the
preceding sections and from the detection of internal gravity waves by

Flux contribution of coherent structures 21

Thomas and Foken (2005a). Details about the applied indicators are presented in Tab. III.

Wave motion (Wa)
The flow above the canopy is dominated by wave motion rather than by turbulence. Thomas and Foken (2005a) reported that periods characterised by internal gravity waves can be separated from those with coherent exchange through comparing the temporal scale of coherent structures to the Brunt-Vaisala frequency. For this exchange regime, no ultimate statement about the transfer processes can be made, as waves may produce turbulence under stable stratification in several ways (e. g. Nappo, 2002). However, we assume the atmosphere to be decoupled basically from the canopy and subcanopy spaces and thus the exchange of energy and matter to be negligible.

Decoupled canopy (Dc)
The atmospheric layer above the canopy is decoupled from the canopy and subcanopy layers. The direction of the fluxes by the sweep and ejection phases of coherent structures are opposite to those in the overlying atmosphere. In general, there is no transfer of energy and matter into or from the canopy.

Decoupled subcanopy (Ds)
The atmosphere is coupled with the canopy, but decoupled from the subcanopy space. The volume in which coherent structures penetrate is limited to the canopy layer, as the flux contribution of sweeps and ejections at the 'bottleneck' (lower border) of the canopy either indicate fluxes opposite in sign or negligible fractions of the fluxes in relation to the canopy top and the overlying atmosphere.

Coupled subcanopy by sweeps (Cs)
The exchange between the atmosphere and the subcanopy space is forced by the strong sweep motion of the coherent structures only. The ejection phases either do not contribute significantly to the transfer of energy and matter exchange or are opposite in sign in relation to the canopy top and the overlying atmosphere. This exchange regime is a typical transition regime between Ds and C.

22   Thomas and Foken

Table III. Characteristics of the indicators applied for the separation of the 5 different exchange regimes in tall vegetated canopies: The ratio of flux contribution of sweep phases and ejection phases are defined as $R_{sw} = (H_{sw})_{z_1} (H_{sw})_{z_2}^{-1}$ and $R_{ej} = (H_{ej})_{z_1} (H_{ej})_{z_2}^{-1}$ respectively. H_{sw} and H_{ej} are the flux contributions of the sweep and ejection phases of coherent structures to the buoyancy flux respectively. $D_e(w)$ and $D_e(T_s)$ are the characteristic event duration of coherent structures in the vertical wind and sonic temperature respectively, N_{BV} is the Brunt-Vaisala frequency. See text for details.

Code	$D_e(w)$, $D_e(T_s)$	Atmosphere - canopy $z_1 = 1.74h_c, z_2 = 0.93h_c$		Atmosphere - subcanopy $z_1 = 1.74h_c, z_2 = 0.72h_c$	
		R_{sw}	R_{ej}	R_{sw}	R_{ej}
Wa	$\geq N_{BV}^{-1}$	-	-	-	-
Dc	-	$R_{sw} \leq 0$ or $R_{sw} > 1.5$	$R_{ej} \leq 0$ or $R_{ej} > 1.5$	-	-
Ds	-	$0 \leq R_{sw} \leq 1.5$	$R_{ej} > 0$	$R_{sw} \leq 0$ or $R_{sw} > 1.5$	$R_{ej} \leq 0$ or $R_{ej} > 1.5$
Cs	-	$0 \leq R_{sw} \leq 1.5$	$R_{ej} > 0$	$0 \leq R_{sw} \leq 1.5$	$R_{ej} \leq 0$ or $R_{ej} > 1.5$
C	-	$0 \leq R_{sw} \leq 1.5$	$R_{ej} > 0$	$R_{sw} \geq 0$	$0 \leq R_{ej} \leq 1.5$

Fully coupled canopy (C)
The atmosphere, the canopy and the subcanopy spaces are in a fully coupled state. Both ejection and sweep phases of coherent structures significantly contribute to the exchange of energy and matter throughout the entire volume of the roughness sublayer.

4.3.2. *Application of the exchange regimes to observations*
For a verification of the proposed classification scheme, it will be applied to real observations. In Figs. 8 and 9, two periods of measurements of 4 days each during WALDATEM-2003 are presented. The displayed turbulent fluxes were calculated using the conditional averages according to Section 3.2. In Figs. 8d and 9d, the exchange between the atmosphere and the canopy was classified using the scheme presented in the preceding section based on the ratios R_{sw} and R_{ej} (Tab. III).
The most characteristic feature in Fig. 8 is the presence of persisting internal gravity waves during the nights (Wa). Their generation was facilitated through the strong radiative cooling indicated by large negative buoyancy fluxes and leading to a very stable stratification ($h_c L^{-1} \approx 0.9$). The classification of the exchange regimes indicates a persistent decoupling of the entire canopy from the atmosphere (Wa, Dc). The relative flux contribution of the scalar fluxes in Fig. 8a seem
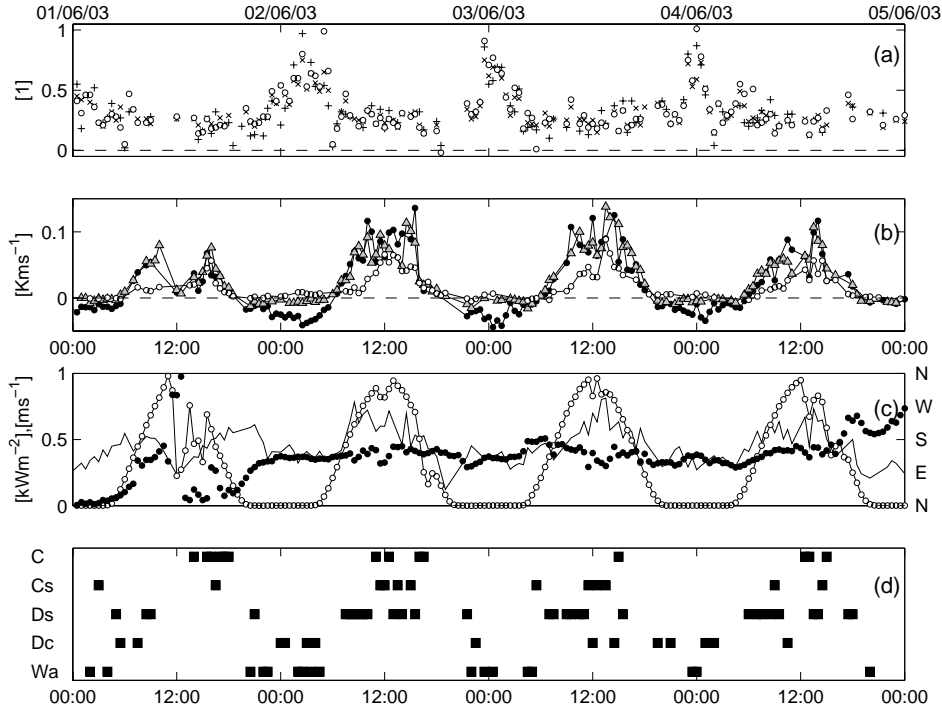
Figure 8. Measurements and characterisation of the turbulent exchange for the period June 1 to June 4, 2003 during WALDATEM-2003: (a) Relative flux contribution of coherent structures $F_{cs}F_{tot}^{-1}$ for carbon dioxide (open circles), buoyancy (crosses) and latent heat (pluses) at $1.74h_c$; (b) Kinematic buoyancy flux of coherent structures H_{cs} at $1.74h_c$ (filled circles), $0.93h_c$ (grey triangles) and $0.72h_c$ (open circles); (c) Friction velocity u_* (solid line), incoming shortwave radiation $K \downarrow$ (open circles) and wind direction (filled circles) at $1.74h_c$; (d) Exchange regimes according to Section 4.3.1.

to increase up to unity during the periods of detected wave motion in all nights. For these periods, the relative flux contribution of coherent structures to the momentum exchange remains at a constant level observed also during other exchange regimes (not shown here). The increasing flux contribution of coherent structures in the scalar fluxes are 'pseudo' fluxes caused by the uniform wave motion present in vector and scalar variables, but does not force any exchange between the forest and the atmosphere. During daytime, the intense solar radiation, which was significantly damped only on June 1 and June 4 due to developing convective clouds, and the low horizontal wind speeds ($< 3.5\,ms^{-1}$ at $1.74h_c$) resulted in a fairly unstable stratification ($h_cL^{-1} \approx -0.8$) close to the transition to free convection. However, during the first half of the presented days, the buoyancy flux at the lower border of the canopy

24   Thomas and Foken

was clearly reduced compared to the levels above. This resulted in a decoupling of the subcanopy space from the exchange between the forest and the atmosphere (Ds) during this time of the day, whereas intermittent exchange was forced by the strong sweep motions of coherent structures (Cs). A complete mixing of the entire air layer within and above the forest was reached generally in the second half of the day. June 3 is characterised by limited exchange conditions throughout the entire diurnal cycle. An interesting feature not mentioned yet is the systematic increase of $C_{cs}C_{tot}^{-1}$ up to 0.5 (Fig. 8a) in the early morning hours between 6 and 9 CET present during all days. The time of these events compare well to a transition from Dc to Ds and can thus be addressed to an intense transport of carbon dioxide by coherent structures from above into the canopy. In all cases, these events are preceded with very low $C_{cs}C_{tot}^{-1}$ values pointing to a small contribution of coherent structures only. However, these periods are mostly characterised by negative sweep / ejection ratios $C_{sw}C_{ej}^{-1}$ indicating an opposite flux direction of both terms. Hence, the small flux fraction $C_{cs}C_{tot}^{-1}$ is a mathematical artifact not representing the exchange conditions as the flux contribution C_{cs} is given by $C_{cs} = C_{sw} + C_{ej}$, as C_{sw} and C_{ej} are opposite in sign. During these periods, coherent structures transport carbon dioxide enriched air, which results from the nocturnal respiration, from the subcanopy into the atmosphere. Note, that during 3 days (June 2, 3, 4) $H_{cs}H_{tot}^{-1}$ is also increased during these times.

During the second period displayed in Fig. 9, internal gravity waves were detected during 2 nights only (while neglecting the single interval in the night from June 15 to June 16). When gravity waves were absent in the nights of June 15 and June 16, the winds were coming from N. In contrast, all intervals with detected gravity waves were characterised by winds coming from the SE sector. In this sector, internal gravity waves were found to be induced by the flow over a shallow mountain (Thomas and Foken, 2005a) and are thus classified as terrain-generated gravity waves. It is surprising that for the detected Wa intervals in Fig. 9 no increase of $F_{cs}F_{tot}^{-1}$ could be found although the wind direction was SE as observed in Fig. 8. The reason for this difference remains unclear and a more detailed investigation is desirable. During nighttime on June 15 and June 16, a persistent decoupling of the canopy from the atmosphere was found. However, a sudden change in the exchange regime was observed on June 15 at approx. 5 CET: The exchange regime changes from Dc to C, indicating a fully coupled state between the atmosphere and the forest. During this night, the friction velocity was found to very high pointing to a intense dynamic forcing of the exchange. During daytime, a fully coupled state was reached in the second half of the day with the exception of June 14, when the first

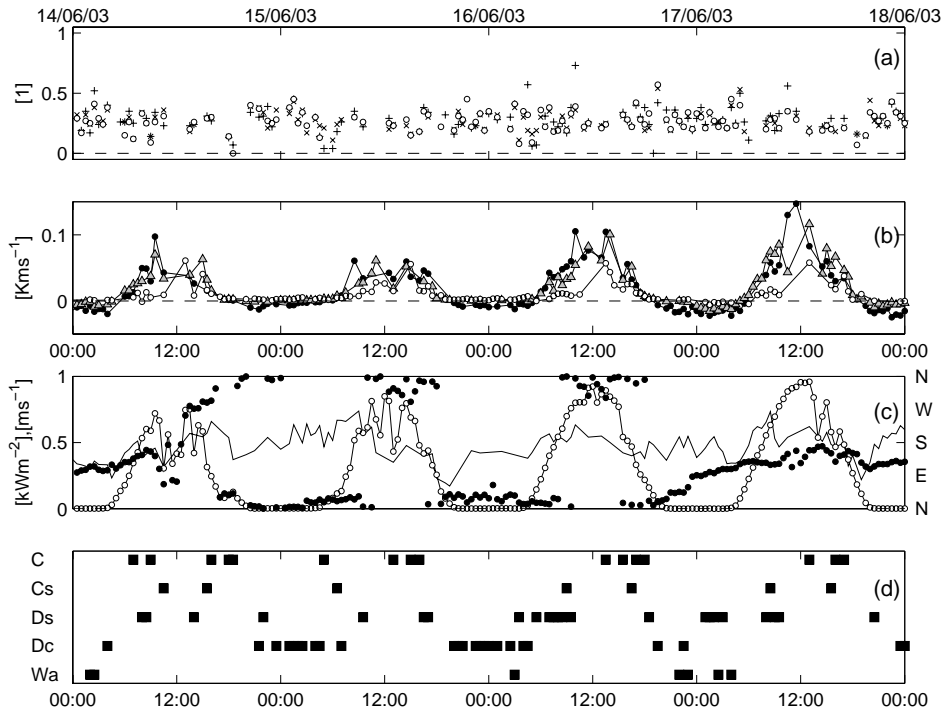Flux contribution of coherent structures   25

Figure 9. See Fig. 8, but for the period June 14 to June 18, 2003 during WAL-DATEM-2003.

intervals classified by C were found in the early morning hours with a subsequent limitation of the exchange indicated by intervals with Cs and Ds. This pattern can possibly be addressed to the changing cloud cover, which results in frequent peaks in the incoming solar radiation. Although the incoming shortwave radiation and thus the buoyancy flux are significantly reduced during June 14 and June 15, the diurnal course of the exchange regimes does not differ in general from the pattern observed during days of intensive solar radiation. This observation points to the fact that the dynamical forcing plays an important role in the exchange regime between the atmosphere and the forest. Summarising, the proposed classification scheme of exchange regimes represents the exchange of energy and matter in a reasonable manner under varying meteorological conditions.

26   Thomas and Foken

5. Conclusions

In the present study we investigated the flux contribution of coherent structures to the exchange of energy and matter between a forested ecosystem and the atmosphere. A particular emphasis was placed on the influence of coherent structures on the exchange processes between the subcanopy, the canopy and the atmosphere.

Coherent structures significantly contribute to the transfer of energy and matter and are thus essential for the understanding of any exchange process in vegetated canopies. A scale-specific investigation of coherent structures through conditional averages allows to derive a physical picture of the exchange process. In particular, the separation between the contributions of up- and downward motion throughout the canopy is crucial for a deeper insight into the physical process. This information is not provided by conventional analysis using flux data determined by the eddy-covariance method only.

The analysis of the flux contribution as a function of the wind direction points to a link between the flow dynamics and the contribution to the transport by coherent structures. Together with results from Thomas and Foken (2005a) we found that the largest contributions of coherent structures were observed for flows characterised by largest vertical wind shears and smallest event durations of coherent structures. From this we can draw the conclusion that short coherent structures are more efficient in transporting energy and matter. In addition, the importance of coherent structures increases in strongly sheared flows. The efficiency of the exchange by coherent structures, which is defined by the ratio of the relative flux contribution to the time fraction, for scalar fluxes is twice as high as for momentum. The observed decreasing contribution of coherent structures to the momentum transfer within the canopy may be attributed to the large momentum sink of the canopy elements. They efficiently damp the large-scale coherent structures leading to a dominating importance of the high-frequency turbulence. Hence, the physical structure of the canopy such as density and vertical distribution of roughness elements is expected to play a significant role for the magnitude of the coherent exchange.

In the present study we further made the attempt to assess the problem if the conventional eddy covariance represents the entire flux and the flux contribution of coherent structures in particular. From the results we learn that the eddy covariance method gives reliable estimates for budgets of energy and matter above tall vegetation as flux errors average out over longer periods. However, flux errors of individual intervals are generally small, but may significantly departure from zero and need to be accounted for when studying short-term balances.

Flux contribution of coherent structures 27

The proposed scheme for classifying the exchange of energy and matter into different exchange regimes was observed to give reasonable results during day- and nighttime conditions as well as changing flow dynamics. It allows a more reliable classification of the exchange between the atmosphere and the forest than schemes basing on the canopy-mixing layer analogy only. Therefore it is a helpful, objective tool for the identification of exchange processes in tall vegetated canopies as it bases upon a few physical assumptions only. However, the required definition of the threshold ratio may introduce subjectivity to a certain degree. This threshold value is expected to be a function of the local properties of the canopy and the terrain and must be adjusted for each site individually. A comparison of our results to the findings derived from different observation techniques such as isotope or reactive scalar flux measurements are highly desirable and need to be done in future. In conclusion, neither the exclusive analysis of the dynamical properties of coherent structures nor the detailed analysis of their flux contribution alone is sufficient to assess the important role of coherent structures for the exchange in tall vegetated canopies entirely. Together they reveal insight into the complex exchange of energy and matter in natural ecosystems.

Acknowledgements

References

Antonia, R., L. Browne, D. Bisset, and L. Fulachier: 1987, 'A description of the organized motion in the turbulent far wake of a cylinder at low Reynolds numbers'. *J. Fluid. Mech.* **184**, 423–444.

Antonia, R. A.: 1981, 'Conditional sampling in turbulence measurements'. *Ann. Rev. Fluid Mech.* **13**, 131–156.

Bergström, H. and U. Högström: 1989, 'Turbulent exchange above a pine forest. II. Organized structures'. *Boundary-Layer Meteorol.* **49**, 231–263.

Collineau, S. and Y. Brunet: 1993a, 'Detection of turbulent coherent motions in a forest canopy. Part I: Wavelet analysis'. *Boundary-Layer Meteorol.* **65**, 357–379.

Collineau, S. and Y. Brunet: 1993b, 'Detection of turbulent coherent motions in a forest canopy. Part II: Time-scales and conditional averages'. *Boundary-Layer Meteorol.* **66**, 49–73.

28   Thomas and Foken

Finnigan, J.: 2000, 'Turbulence in plant canopies'. *Ann. Rev. Fluid Mech.* **32**, 519–571.

Finnigan, J. J.: 1979, 'Turbulence in waving wheat. II. Structure of momentum transfer'. *Boundary-Layer Meteorol.* **16**, 213–236.

Gao, W., R. H. Shaw, and K. T. Paw U: 1989, 'Observation of organized structure in turbulent flow within and above a forest canopy'. *Boundary-Layer Meteorol.* **47**, 349–377.

Gerstberger, P., T. Foken, and K. Kalbitz: 2004, 'The Lehstenbach and Steinkreuz chatchments in NE Bavaria, Germany'. In: E. Matzner (ed.): *Biogeochemistry of forested catchments in a changing environment:. Ecological Studies*, Vol. 172. Heidelberg: Springer, pp. 15–41.

Katul, G., G. Kuhn, J. Schieldge, and C.-I. Hsieh: 1997, 'The ejection-sweep character of scalar fluxes in the unstable surface layer'. *Boundary-Layer Meteorol.* **83**, 1–26.

Lu, S. S. and W. W. Willmarth: 1973, 'Measurements of the structure of Reynolds stress in a turbulent boundary layer'. *J. Fluid. Mech.* **60**, 481–512.

Maitani, T. and R. H. Shaw: 1990, 'Joint probability analysis of momentum and heat fluxes at a deciduous forest'. *Boundary-Layer Meteorol.* **52**, 283–300.

Nappo, C. J.: 2002, *An introduction to atmospheric gravity waves*, Vol. 85 of *International Geophysics Series*. San Diego: Academic Press.

Raupach, M. R.: 1981, 'Conditional statistics of Reynolds stress in rough-wall and smooth-wall turbulent boundary layers'. *J. Fluid. Mech.* **108**, 363–382.

Raupach, M. R., J. J. Finnigan, and Y. Brunet: 1996, 'Coherent eddies and turbulence in vegetation canopies: the mixing-layer analogy'. *Boundary-Layer Meteorol.* **78**, 351–382.

Shaw, R. H., J. Tavangar, and D. P. Ward: 1983, 'Structure of the Reynolds stress in a canopy layer'. *J. Clim. Appl. Meteorol.* **22**, 1922–1931.

Thomas, C. and T. Foken: 2005a, 'Coherent structures in a tall spruce canopy: temporal scales, structure spacing and terrain effects'. *Boundary-Layer Meteorol.* p. (submitted).

Thomas, C. and T. Foken: 2005b, 'Detection of Long-term Coherent Exchange over Spruce Forest Using Wavelet Analysis'. *Theor. Appl. Climatol.* pp. DOI: 10.1007/s00704–004–0093–0.

Thomas, C., J.-C. Mayer, F. Meixner, and T. Foken: 2005, 'Analysis of low-frequency turbulence above tall vegetation using a Doppler sodar'. *Boundary-Layer Meteorol.* p. (submitted).

Wallace, J. M., H. Eckelmann, and R. S. Brodkey: 1972, 'The wall region in turbulent shear flow'. *J. Fluid. Mech.* **54**, 39–48.

Wichura, B., J. Ruppert, A. C. Delany, N. Buchmann, and T. Foken: 2004, 'Structure of carbon dioxide exchange processes above a spruce forest'. In: E. Matzner (ed.): *Biogeochemistry of forested catchments in a changing environment:. Ecological Studies*, Vol. 172 of *Ecological Studies*. Berlin, Heidelberg: Springer, pp. 161–176.

Address for Offprints:
Christoph Thomas
University of Bayreuth
Department of Micrometeorology
95440 Bayreuth, Germany
Tel. (49) 921 55 2320
Fax (49) 921 55 2366
Email christoph.thomas@uni-bayreuth.de

Appendix F

Scalar Similarity for Relaxed Eddy Accumulation Methods

Johannes Ruppert (`johannes.ruppert@uni-bayreuth.de`)
Department of Micrometeorology, University of Bayreuth, Bayreuth, Germany

Christoph Thomas
Department of Micrometeorology, University of Bayreuth, Bayreuth, Germany

Thomas Foken
Department of Micrometeorology, University of Bayreuth, Bayreuth, Germany

Abstract. The relaxed eddy accumulation (REA) method allows the measurement of trace gas fluxes when no fast sensors are available for eddy covariance measurements. The flux parameterisation used in REA is based on the assumption of scalar similarity, i.e. similarity of the turbulent exchange of two scalar quantities. In this study changes in scalar similarity between carbon dioxide, sonic temperature and water vapour were assessed using scalar correlation coefficients and spectral analysis. The influence on REA measurements was assessed by simulation. The evaluation is based on data recorded during experiments over grassland, an irrigated cotton plantation and spruce forest.

Scalar similarity between carbon dioxide, sonic temperature and water vapour showed a distinct diurnal pattern and change within the day. Poor scalar similarity was found to be linked to dissimilarities in the energy contained in the low frequency part of the turbulent spectra ($< 0.01\,\mathrm{Hz}$).

The simulations of REA showed significant change in b-factors throughout the diurnal course. The diurnal course of b-factors for carbon dioxide, sonic temperature and water vapour matched well. Relative flux errors induced in REA by varying scalar similarity were generally below $\pm 10\,\%$. For the use of REA applying a hyperbolic deadband (HREA) systematic underestimation of the flux up to -40 % were addressed to poor scalar similarity between the scalar of interest and the scalar used as proxy for the deadband definition.

Keywords: Scalar Similarity, Relaxed Eddy Accumulation, Trace Gas Flux, Spectral Analysis, Conditional Sampling

1. Introduction

In recent years growing interest was developed to measure the turbulent exchange of various trace gases in the surface layer in order to investigate biogeochemical processes. The relaxed eddy accumulation method (REA, Businger and Oncley, 1990) allows flux measurements for many scalar quantities with air analysis in a laboratory when no fast sensors are available for eddy covariance (EC) measurements. In REA the trace gas flux is calculated using a parametrization applying flux-variance similarity (Obukhov, 1960; Wyngaard et al., 1971) and scalar similarity, i.e. similarity in the characteristics of the turbulent

2   Ruppert et al.

exchange. Scalar similarity is defined as similarity in the scalar time series throughout the scalar spectra (Kaimal et al., 1972; Pearson et al., 1998). Scalar similarity requires that scalar quantities are transported with similar efficiency in eddies of different size and shape.

Differences in the turbulent exchange of scalar quantities and therefore in scalar similarity must be expected when sources and sinks are distributed differently within the ecosystem, e. g. within tall vegetation, or show significant changes in their source/sink strength (Katul et al., 1995; Andreas et al., 1998a; Simpson et al., 1998; Katul et al., 1999). Scalar quantities such as carbon dioxide, temperature and water vapour have different sources and sinks within a plant canopy and a different turbulent structure. While canopy top surfaces are the main source for heating of air during the day, carbon dioxide and water vapour are consumed and respectively released mainly within the canopy. Temperature and to some degree also water vapour actively influence turbulent exchange and are therefore called active scalars. Whereas carbon dioxide does not effect buoyancy and is regarded as passive scalar quantity (Katul et al., 1996; Pearson et al., 1998).

In particular for the REA method scalar similarity is needed for the derivation of b-factors (Oncley et al., 1993 and Section 2). This parameterisation requires similarity in the shape of the joint frequency distribution (JFD) of the scalar of interest and a scalar quantity for which the flux can be determined independently, e. g. with EC (Wyngaard and Moeng, 1992; Katul et al., 1996). Information on the vertical wind velocity in the JFDs for two scalar quantities is identical. The only difference in the shape of the JFDs results from differences in the scalar time series. Scalar similarity needed for REA and HREA therefore can be analyzed by directly comparing the scalar time series and the shape of their frequency distribution or spectra (Kaimal et al., 1972; Pearson et al., 1998).

In this paper we investigate the degree of scalar similarity between three different scalar quantities (carbon dioxide, sonic temperature and water vapour) throughout the diurnal cycle. The analysis is done on the basis of high-frequency time series recorded during field experiments over grassland, an irrigated cotton plantation and a spruce forest. The study (i) characterizes typical changes of scalar similarity during the diurnal cycle for the three surface types. (ii) Wavelet variance spectra are used to test the influence of coherent structures on the turbulent transport and to identify the time scales on which the lack of scalar similarity in the transport of scalars appears. (iii) Finally we evaluate the error that is introduced in flux measurements with REA methods due to lack in scalar similarity. Effects from scalar similarity on flux measurements using REA methods are investigated by simulation. In

the analysis we compare classical REA with those modifications of the REA method, that are able to significantly increase concentration differences of the scalar quantities in updraft and downdraft samples by introducing hyperbolic deadbands (hyperbolic relaxed eddy accumulation, HREA, Bowling et al., 1999b, see Section 2). HREA can increase the concentration difference above critical limits of sensor resolution, e.g. for isotope flux measurements. At the same time the restriction on few samples for flux determination representing strong updrafts and downdrafts increases their vulnerability to the lack of scalar similarity.

2. Theory

The eddy covariance method relies on Reynolds decomposition of the turbulent signals of vertical wind velocity w and the scalar of interest c ($w = \overline{w} + w'$, $c = \overline{c} + c'$). The overbar denotes temporal averaging for a typical measurement period of 30 min. Primes denote the fluctuation of a quantity around its average value. A zero mean vertical wind velocity is assumed ($\overline{w} = 0$). The turbulent flux is determined by $\overline{w'c'}$. This method of direct flux measurement is the basis and reference for the relaxed eddy accumulation method.

2.1. Relaxed Eddy Accumulation (REA)

REA measurements rely on conditional sampling (Desjardins, 1972; Hicks and McMillen, 1984) of the scalar of interest into reservoirs for updraft and downdraft air samples. The temporal averaging of scalar samples occurs physically within the two reservoirs. The 'relaxation' means that samples are taken with a constant flow rate and are not weighted according to the vertical wind velocity (Foken et al., 1995). The sample consequently lacks information on the vertical wind velocity. This lack is compensated by relying on flux-variance similarity and the parametrisation of the proportionality factor b, resulting in the basic Equation (1) for the flux determination in REA (Businger and Oncley, 1990).

$$\overline{w'c'} = b\,\sigma_w(\overline{c_\uparrow} - \overline{c_\downarrow}) \tag{1}$$

σ_w is the standard deviation of the vertical wind velocity. $\overline{c_\uparrow}$ and $\overline{c_\downarrow}$ are the average scalar values for updrafts and downdrafts. The b-factor is well defined with a value of 0.627 for an ideal Gaussian joint frequency distribution (JFD) of w and c (Baker et al., 1992; Wyngaard and Moeng, 1992). However, turbulent transport especially over rough

4   Ruppert et al.

surfaces often violates the underlying assumption of a linear relation-
ship between w and c (Katul et al., 1996). Excursions from the linear
relation occur due to skewness in the JFD and result in smaller b-
factors from parameterisation (Milne et al., 2001). Gao (1995) found
this effect to be most pronounced close to the canopy top and suggested
a scaling of the b-factors with measurement height. b exhibits a relative
independence from stability due to the characteristics of σ_w and σ_c
(Foken et al., 1995). For many experimental data b was found to range
from 0.54 to 0.60 on average. However, Andreas et al. (1998b) and Am-
mann and Meixner (2002) found an increase of average b-factors under
stable conditions in the surface layer. The b-factors can vary also signifi-
cantly for individual 30 min integration intervals (Businger and Oncley,
1990; Baker et al., 1992; Oncley et al., 1993; Pattey et al., 1993; Bev-
erland et al., 1996; Katul et al., 1996; Bowling et al., 1999a; Ammann
and Meixner, 2002), which restricts the use of a fixed b-factor.

2.2. WIND-DEADBAND

The above mentioned values for b were determined for REA without
the use of a deadband in which all updraft and downdraft samples are
collected. However, normally a wind-deadband in which no samples
are collected is applied during REA sampling for technical reasons
(Oncley et al., 1993; Foken et al., 1995). The wind-deadband H_w around
zero vertical wind velocity (w_0) is normally scaled with the standard
deviation of the vertical wind velocity σ_w, Equation (2).

$$\left| \frac{w'}{\sigma_w} \right| \leq H_w \tag{2}$$

The use of a deadband changes the definition of what is regarded as
updraft ($\uparrow$: $w'/\sigma_w > H_w$) and downdraft ($\downarrow$: $w'/\sigma_w < -H_w$) during
REA sampling. The advantage for technical realization of REA is, that
the use of a deadband firstly reduces the frequency of valve switching
for sample segregation significantly. Secondly, the use of a deadband
increases the scalar difference $(\overline{c_\uparrow} - \overline{c_\downarrow})$ and thereby reduces errors in the
chemical analysis. Increased scalar differences decrease corresponding
b-factors according to Equation (1). A functional dependency of average
b-factors on wind-deadband size was determined for the necessary ad-
justment ($b_{(H_w)}$, Businger and Oncley, 1990, Pattey et al., 1993, Katul
et al., 1996, Ammann and Meixner, 2002). Nevertheless, the potential
for variation of individual b-factors around adjusted average values for
b persists. The use of b-factors individually determined from a proxy
scalar may be able to better reflect the correct b-factor for a certain
measurement period and thereby minimize REA flux errors. This deter-

Scalar Similarity for Relaxed Eddy Accumulation Methods   5

mination of individual b-factors requires good scalar similarity between the scalar of interest and the proxy scalar.

2.3. Hyperbolic Relaxed Eddy Accumulation (HREA)

Application of a deadband with hyperbolas as thresholds does not only exclude samples with small fluctuations of the vertical wind velocity w', but also samples with small fluctuations of the scalar quantity c' (Bowling et al., 1999b; Wichura et al., 2000; Bowling et al., 2001; Bowling et al., 2003). Thereby HREA increases scalar differences in the reservoirs even more. The hyperbolic criteria (Wallace et al., 1972; Lu and Willmarth, 1973; Shaw et al., 1983; Shaw, 1985) means rating individual samples by their contribution to the EC flux $\overline{w'c'}$. All samples below a certain threshold of 'importance' (H_h) are not collected into the reservoirs. The hyperbolic deadband is defined as

$$\left| \frac{w'c'}{\sigma_w \sigma_c} \right| \leq H_h \tag{3}$$

The additional increase of the scalar differences in HREA is important when measurement precision for the scalar of interest is limited. Then HREA can significantly increase the signal to noise ratio for the flux measurement of a scalar (Bowling et al., 1999b).

Poor scalar similarity has the potential to induce error in the estimate of b-factors for the scalar of interest from the b-factors determined using data of a proxy scalar. From Equation (1) it is obvious, that any error present in the b-factors will transfer linearly into errors in the fluxes determined by REA or HREA. The use of a deadband in REA or HREA concentrates sampling towards strong updrafts and downdrafts, which increases the effect of non-linearity in the JFD on b-factors (Katul et al., 1996). Deadbands thereby have the potential to increase dissimilarity of b-factors due to poor scalar similarity. HREA uses the assumption of scalar similarity not only when inferring the b-factor from a proxy scalar. In addition scalar similarity is assumed when defining the hyperbolic deadbands during the measurement process from fast measurements of the proxy scalar (Bowling et al., 1999b). Therefore, the validity of scalar similarity is even more essential for HREA methods than for classical REA.

3. Experimental data

Turbulence data with high time resolution from three field experiments over different surfaces were selected for this analysis.

6   Ruppert et al.

Measurements of the experiment GRASATEM-2003 (Grassland Atmospheric Turbulent Exchange Measurements) were performed over short cut grassland (canopy height $h_c = 0.12$ m) during the LITFASS-2003 experiment (Beyrich et al., 2004) at the Falkenberg experimental site of the German Meteorological Service (Meteorological Observatory Lindenberg), Germany ($52^o10'$ N, $14^o07'$ E, 71 m a.s.l.). A Sonic Anemometer (USA-1, METEK, Meteorologische Messtechnik GmbH, Elsmhorn, Germany) and an open path sensor (LI-7500, LI-COR Inc., Lincoln, NE, USA) measured the wind vector and water vapour and carbon dioxide density at 2.25 m above ground. The flux source areas (footprints) of the data used in this analysis showed good homogeneity regarding the grass canopy height with some variability in soil humidity.

The EBEX-2000 (Energy Balance Experiment, Oncley et al., 2002) data set was acquired in the San Joaquin Valley, CA, USA ($36^o06'$ N, $119^o56'$ W, 67 m a.s.l.). The experimental site was located in the middle of an extended irrigated cotton plantation on flat terrain. Canopy height was about 0.9 m. A sonic anemometer (CSAT-3, Campbell Scientific Ltd., Logan, UT, USA) measured 3 dimensional wind vectors and sonic temperature T_s. An open path analyzer (LI-7500) was used to measure water vapour and carbon dioxide density. The sampling rate was 20 Hz. Instruments were installed on a tower at a height of 4.7 m above ground.

During the WALDATEM-2003 (Wavelet Detection and Atmospheric Turbulent Exchange Measurements) experiment a set of micrometeorological measurements was performed on a 33 m high tower over a spruce forest (*picea abies*). This study uses data from a sonic anemometer (R3-50, Gill Instruments Ltd., Lymington, UK) and an open path analyzer (LI-7500) installed at 33 m. The forest has a mean canopy height of 19 m with a plant area index (PAI) of 5.2 (Thomas and Foken, 2005a). Understory vegetation is sparse and consists of small shrubs and grasses. The site Waldstein/Weidenbrunnen (GE1-Wei) is part of the FLUXNET network and is located in the Fichtelgebirge mountains in Germany ($50^o08'$ N, $11^o52'$ E, 775 m a.s.l.) on a slope of 2° (Rebmann et al., 2005; Thomas and Foken, 2005b). A detailed description of the site can be found in Gerstberger et al. (2004). One of the objectives of the GRASATEM-2003 and WALDATEM-2003 experiments was the determination of ^{13}C and ^{18}O isotope fluxes using the HREA method.

4. Method of Analysis

For our study we selected carbon dioxide to be the scalar of interest, for which a flux measurement with REA or HREA shall be per-

Scalar Similarity for Relaxed Eddy Accumulation Methods 7

formed. Sonic temperature T_s and water vapour density ρ_{H2O} serve as proxy scalars which are tested for sufficient similarity in their turbulent exchange compared to carbon dioxide density ρ_{CO2}.

4.1. DATA SELECTION AND PREPARATION

Daytime periods of the three experiment days (GRASATEM-2003: May 24, 2003, EBEX-2000: August 20, 2000, WALDATEM-2003: July 8, 2003) representing different surface types (shortcut grassland, irrigated cotton, spruce forest) were selected for the analysis in this paper after assessing the quality of the flux measurements. This assessment was based on a quality check of the turbulent time series according to Foken et al. (2004) with a test on stationarity and developed turbulent conditions. The three days represent typical diurnal cycles of exchange patterns found during the experiments and provide a continuous high quality data record throughout the diurnal cycle. During the selected days only few data from the early morning (EBEX-2000) and late afternoon (GRASATEM-2003 and EBEX-2000) did not meet the quality criteria. Data from these periods were therefore not included in the analysis. The wind vectors derived from the sonic anemometer measurements were rotated using the planar fit method (Wilczak et al., 2001). Outliers in the scalar data were removed by applying a 5σ criteria ($\mu \pm 5\sigma$). In order to correct time lags between the different sensors each time series was shifted according to the maximum cross-correlation with the vertical wind velocity. All subsequent analysis were performed on 30 min subsets of the data.

4.2. SCALAR SIMILARITY

As a simple measure of scalar similarity we use the scalar correlation coefficient $r_{c,c_{proxy}}$ calculated from the fluctuations in the time series of the scalar of interest c and the proxy scalar c_{proxy}.

$$r_{c,c_{proxy}} = \frac{\overline{c'c'_{proxy}}}{\sigma_c \sigma_{c_{proxy}}} \qquad (4)$$

The scalar correlation coefficient integrates similarity and dissimilarity over the whole frequency range of the time series. In studies by Gao (1995) and Katul and Hsieh (1999) scalar correlation coefficients were already used to discuss similarity between the turbulent exchange of temperature and water vapour.

8   Ruppert et al.

4.3. Spectral analysis

Here, the method for spectral analysis using wavelet functions will be outlined briefly. More details can be found in Thomas et al. (2005). First, any missing data and outliers detected were filled using an interpolation (Akima, 1970). All time series were block averaged to 2 Hz significantly reducing computation time for the wavelet analysis. Scalar time series were normalized to c'/σ_c. Vertical wind velocity w was normalised to w/σ_w. In a second step, time series were low-pass filtered by a wavelet filter decomposing and recomposing the time series using the biorthogonal set of wavelets BIOR5.5. The use of this set of wavelet functions is preferred as their localisation in frequency is better than e. g. that of the HAAR wavelet (Kumar and Foufoula-Georgiou, 1994). This filter discards all fluctuations with event durations $D < D_c$, where D_c is the critical event duration chosen according to the spectral gap between high-frequency turbulence and low-frequency coherent structures. A default value of $D_c = 6.2\,s$ was chosen for all datasets, which is in close agreement to other authors using similar values, e. g. $D_c = 5\,s$ (Lykossov and Wamser, 1995), $D_c = 7\,s$ (Brunet and Collineau, 1994) or $D_c = 5.7\,s$ (Chen and Hu, 2003).

A continuous wavelet transform (Grossmann and Morlet, 1984; Grossmann et al., 1989; Kronland-Martinet et al., 1987) of the prepared and zero-padded time series f(t) was performed using the complex Morlet wavelet as analysing wavelet function $\Psi(t)$,

$$T_p(a,b) = \frac{1}{a^p} \int_{-\infty}^{+\infty} f(t)\Psi\left(\frac{t - b_t}{a}\right) dt \qquad (5)$$

where $T_p(a,b)$ are the wavelet coefficients, a the dilation scale, b_t the translation parameter and the normalisation factor $p = 1$ in our case. The complex Morlet wavelet function is located best in frequency domain and thus found appropriate to extract the intended information about long scale flux contributions e. g. from coherent structures (Thomas and Foken, 2005b). The dilation scales a used to calculate the continuous wavelet transform represent event durations D ranging from 6 s to 240 s. The event duration D can be linked to the dilation scale a of the wavelet transform by (e. g. Collineau and Brunet, 1993)

$$D = \frac{1}{2} \cdot f^{-1} = \frac{a \cdot \pi}{f_s \cdot \omega^0_{\Psi_{1,1,0}}}, \qquad (6)$$

where f is the frequency corresponding to the event duration, f_s the sampling frequency of the time series and $\omega^0_{\Psi_{1,1,0}}$ the center frequency of the mother wavelet function. For a sine function, the event duration D is half the length of a period. The minimum of analysed event durations

Scalar Similarity for Relaxed Eddy Accumulation Methods 9

was chosen according to the critical event duration D_c of the low-pass filter. The wavelet variance spectrum was then determined by

$$W_p(a) = \int_{-\infty}^{+\infty} |T_p(a,b)|^2 db. \qquad (7)$$

Wavelet variance spectra $W_p(a)$ were multiplied by the angle frequency ω. The correlation coefficient of the wavelet variance spectra for the different scalar quantities $r_s(\rho_{CO2}, c_{proxy})$ was calculated as objective measure of similarity in the distribution of energy in the frequency range.

$$r_s(\rho_{CO2}, c_{proxy}) = \frac{\overline{W(D)_{\rho_{CO2}} W(D)_{c_{proxy}}}}{\sigma_{W(D)_{\rho_{CO2}}} \cdot \sigma_{W(D)_{c_{proxy}}}}. \qquad (8)$$

$W(D)$ denotes the wavelet variance, i.e. the spectral density at event duration, σ the standard deviation and the overbar depicts the phase mean over the fluctuations. The spectral correlation in the scalar time series is evaluated for two ranges of event durations, short event durations of 6 s to 60 s and long event durations of 60 s to 240 s.

4.4. REA AND HREA SIMULATION

REA and HREA sampling was simulated using the high resolution time series data for the vertical wind velocity fluctuation w' and the scalar quantities (T_s, ρ_{H2O}, ρ_{CO2}). Time series were sampled and segregated into updrafts, deadband and downdrafts according to the deadband definition (wind-deadband H_w, Equation 2, or hyperbolic deadband H_h, Equation 3) and the sign of the vertical wind velocity fluctuation w'. Updrafts and downdrafts were averaged to yield the scalar difference ($\overline{c_\uparrow} - \overline{c_\downarrow}$). The b-factors were calculated by rearranging Equation (1).

$$b = \frac{\overline{w'c'}}{\sigma_w(\overline{c_\uparrow} - \overline{c_\downarrow})} \qquad (9)$$

Comparison of b-factors calculated for the scalar of interest (b) and a proxy scalar (b_{proxy}) directly yields the relative flux errors ε due to the linear relationship in Equation (1).

$$\varepsilon = \frac{b_{proxy} - b}{b} \qquad (10)$$

In the simulation any error resulting from the instrumentation used for REA or HREA sampling in the field is avoided. For the deadband definitions the simulation is based on statistics of turbulent time series from the complete 30 min sampling interval. This means $\overline{w}$, σ_w and

10   Ruppert et al.

for HREA also $\bar{c}$ and σ_c of the proxy scalar are well known. These parameters must be estimated online during field sampling with REA or HREA, when only previously recorded data is available. Therefor the analysis of these simulations focuses on the methodological error of REA and HREA.

5. Results and discussion

5.1. Scalar correlation coefficients

Absolute values of scalar correlation coefficients $r_{CO2,Ts}$ and $r_{CO2,H2O}$ for three days are presented in Figure 1 as a measure for scalar similarity.

For most cases the maximal absolute correlation coefficients are in the order of 0.9. Smaller values and significant changes in the scalar correlation within the diurnal cycle are found for all three surface types (grassland, irrigated cotton and spruce forest) for many days. The varying scalar similarity is pronounced best on the exemplary days presented in Figure 1, which were selected for this study. Within the diurnal pattern three different cases could be distinguished, which will be used for the discussion of changes in scalar correlation as well as spectral correlation (Section 5.2).

- Case 1: During the morning hours up to about 9-10 h local time on all three days high scalar correlation of $r_{CO2,Ts}$ indicates better scalar similarity compared to $r_{CO2,H2O}$. In the WALDATEM-2003 data this situation persists for most of the day. Early morning data in EBEX-2000 did not meet the quality criteria (see Section 3) and was therefore not included in the analysis.

- Case 2 describes a situation in which both $r_{CO2,Ts}$ and $r_{CO2,H2O}$ show high scalar correlation. This situation can be found in the afternoon in EBEX-2000 data, taking into account that $r_{CO2,Ts} = 0.9$ is already indicating high scalar correlation, and in some of the midday periods in the WALDATEM-2003 data.

- Case 3 denotes situations in which $r_{CO2,Ts}$ shows low scalar correlation compared to $r_{CO2,H2O}$. Such situations are visible in the late afternoon hours ($\sim$16 h local time) in the GRASATEM-2003, EBEX-2000 and WALDATEM-2003 datasets. These afternoon periods were characterized by diminishing buoyancy fluxes, near neutral or even slightly stable stratification and persistent latent heat fluxes.
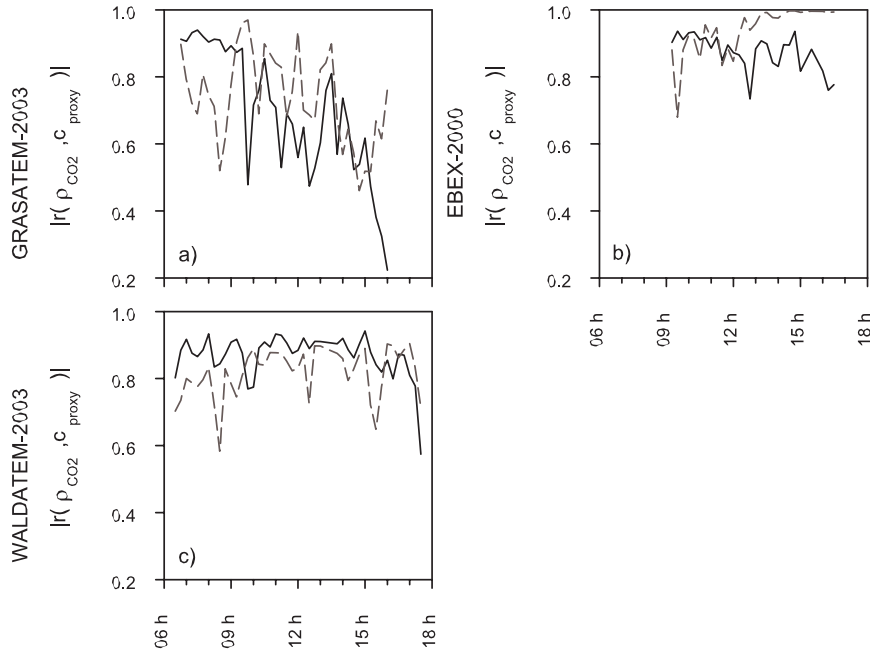
Scalar Similarity for Relaxed Eddy Accumulation Methods   11

Figure 1. Diurnal course of scalar correlation coefficients (absolute values) calculated from carbon dioxide density ρ_{CO2} and sonic temperature T_s (solid lines) or water vapour density ρ_{H2O} (dashed lines) for the three datasets from GRASATEM-2003 (a), EBEX-2000 (b) and WALDATEM-2003 (c). Time is indicated as local time.

The loss of scalar correlation in $r_{CO2,Ts}$ between 10 to 13 h local time in the GRASATEM-2003 data corresponds to a period with significantly reduced global radiation due to cirrus clouds. The scalar correlation during the three days approximately follows the change from case 1 in the morning, case 2 for some periods around noon or during the early afternoon and case 3 in the late afternoon or early evening. This pattern is exhibited very clearly in the EBEX-2000 data, which represent an ideal diurnal cycle of global radiation.

Results presented in Figure 1 show that significant temporal changes in scalar similarity linked to source and sink strength have to be expected even over short vegetation, where sources and sinks are located close together in the vertical profile.

12   Ruppert et al.

5.2. Spectral analysis

In order to identify possible reasons for the lack of scalar similarity we analyzed wavelet variance spectra computed from the scalar time series. The comparison of these spectra allows to identify on which temporal scales the characteristics of turbulent transport correspond or differ. The frequency range was selected to cover typical frequencies of coherent structures commonly found in turbulent time series from the roughness sublayer (Thomas et al., 2005) in order to assess their contribution to changes in scalar similarity.

Figure 2 shows three exemplary wavelet variance spectra $W_p(a) \cdot \omega$ for the cases distinguished in the previous section based on the scalar correlation coefficients (Figure 1). All three spectra show very good similarity for the three scalars T_s, ρ_{H2O} and ρ_{CO2} in short temporal scales. Major deviations are only found for ρ_{H2O} in Figure 2a (case 1) and for T_s in Figure 2c (case 3) in the longer time scales ($D > 60\,s$ and $D > 40\,s$). The spectra in Figure 2b reveals a very good match of all three scalars (case 2) over the complete range of event durations (6 s to 240 s). The visual assessment of the match in the spectra throughout the complete diurnal course for the EBEX-2000 data corresponded to the findings for scalar similarity based on the scalar correlation coefficients i.e. poor similarity between ρ_{H2O} and ρ_{CO2} in the morning (Figure 2a) and poor similarity between T_s and ρ_{CO2} in the late afternoon (Figure 2c). Differences in the spectra occurred solely in the longer time scales with the exemption of spectra after 16:00 h in which differences were present also in shorter event durations due to the diminishing buoyancy flux.

As objective measure for the correlation in the spectra the spectral correlation coefficient, Equation (8), is presented in Figure 3. In order to validate the finding from the visual assessment of wavelet variance spectra, spectral correlation was calculated separately for shorter (6 s to 60 s) and longer (60 s to 240 s) event durations. High values for the spectral correlation in Figure 3a, Figure 3c and Figure 3e confirm that scalar similarity is good for the range of short event durations over all three surface types. However, the spectral correlation for long event durations (Figure 3b, Figure 3d and Figure 3f) shows significant fluctuations. Poor scalar similarity measured with the scalar correlation coefficients must therefor be attributed primarily to processes on larger temporal scales (event durations $> 60\,s$ or frequencies $< 0.01\,Hz$). Dissimilarity on these scales can arise from temporal changes of source/sink strength or due to convective or advective processes. A high degree of scatter is present in the spectral correlation calculated for individual 30 min periods. After smoothing the time series of spectral correlation with a
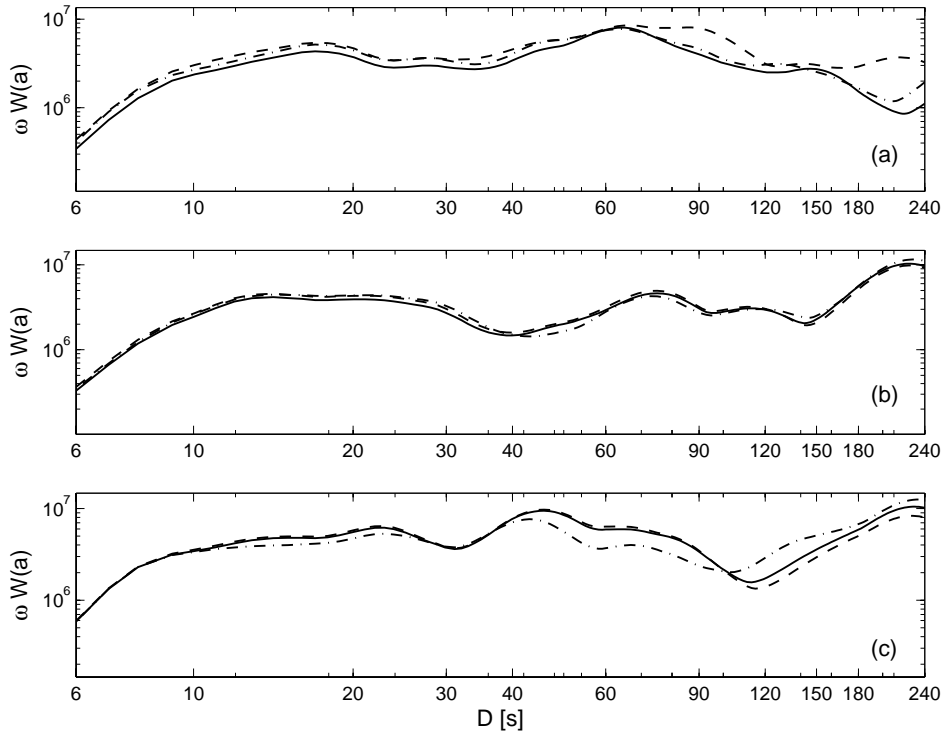
Scalar Similarity for Relaxed Eddy Accumulation Methods 13

Figure 2. Spectra of the normalised wavelet variance ωW versus event duration D of the carbon dioxide ρ_{CO2} (solid line), sonic temperature T_s (dashed line) and water vapour ρ_{H2O} (dash-dotted line) based on data from the EBEX-2000 experiment on August 20, 9:15 to 9:45 h (a), 14:30 to 15:00 h (b) and 15:45 to 16:15 h (c) local time.

running average (lines), the diurnal changes in similarity in the longer timescales correspond approximately to the scalar correlation (Figure 1) and the results for spectral correlation can be compared to the findings in Section 5.1 on the basis of the 3 cases distinguished there:

Case 1 is found correspondingly to the results on scalar correlation for all three surface types in the morning hours and for the entire afternoon in the WALDATEM-2003 data. Case 2 is found between 13 h and 15 h in the EBEX-2000 data and around noon in the WALDATEM-2003 data. The GRASATEM-2003 data shows poor spectral correlation for the rest of the day after a cloud cover appeared at 10 h. Case 3 is only visible clearly in the spectral correlation calculated from the EBEX-2000 data of the late afternoon. The general features of scalar similarity between the three scalar quantities distinguished with the cases 1 and 2 are well reflected in the spectral correlation for the long timescales. Dissimilarity in periods with diminishing buoyancy fluxes
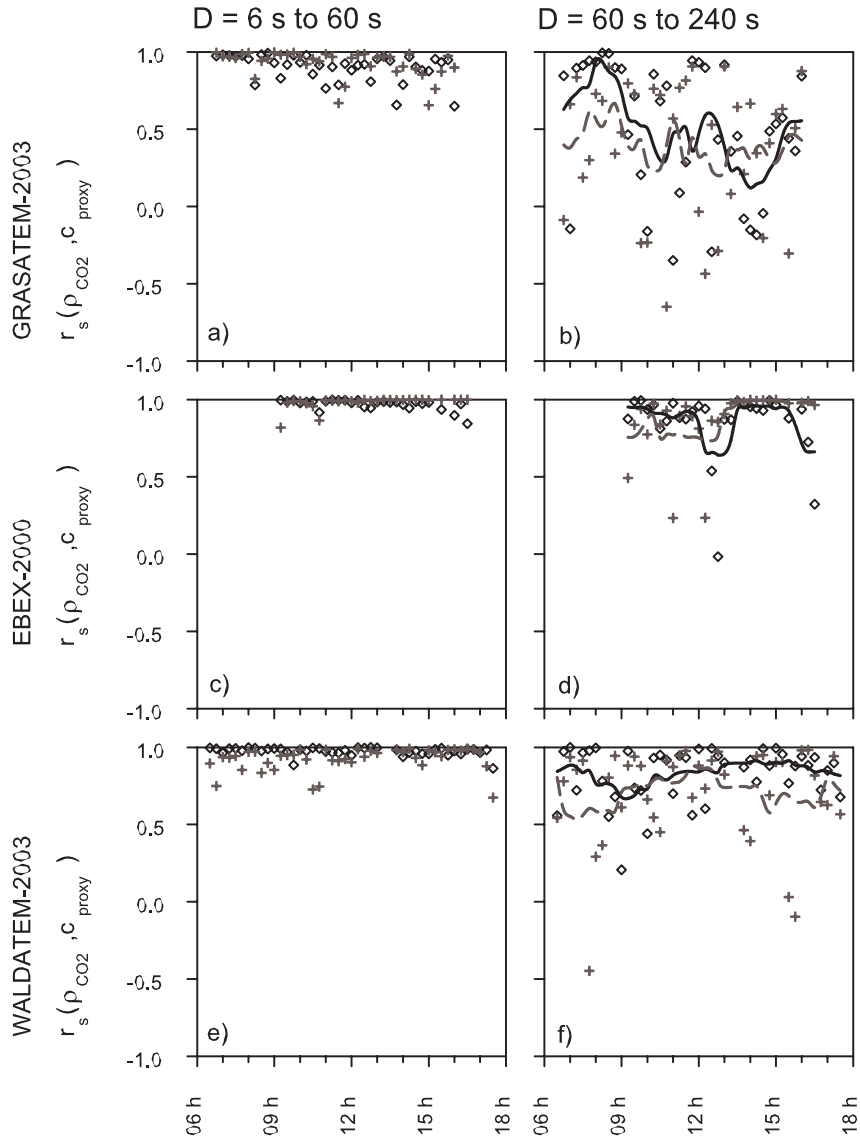
14   Ruppert et al.

Figure 3. Spectral correlation between ρ_{CO2} and T_s (diamonds, solid line) and ρ_{CO2} and ρ_{H2O} (crosses, dashed line). Lines represent the running average of the time series of spectral correlation for individual 30 min periods (symbols). a), c) and e) show the correlation coefficients for short event durations D from 6 to 60 s. b), d) and f) show the correlation coefficients for long event durations D from 60 to 240 s.

Scalar Similarity for Relaxed Eddy Accumulation Methods 15

seems to be reflected less adequately by the spectral correlation for long event durations.

Pearson et al. (1998) studied scalar similarity by comparing non-dimensional power spectra and found good agreement in frequency ranges above $0.01\,\text{Hz}$ for temperature, water vapour and ozon. Results presented in Figure 2 and Figure 3 affirm that scalar similarity is relatively good for short event durations. However, we find that longer event durations ($D > 60\,\text{s}$ corresponding to frequencies $< 0.01\,\text{Hz}$) have to be included in the assessment of scalar similarity. McNaughton and Laubach (1998) showed that unsteadiness in the mean wind and internal boundary layers induced dissimilarity between eddy diffusivities for temperature and water vapour. Gao (1995), Katul et al. (1996) and Andreas et al. (1998b) relate differences in the shape of organized (coherent) structures in the turbulent exchange of scalar quantities to differences in b-factors used in REA. From our spectral analysis most of the variability in scalar similarity has to be attributed to event durations that are even larger ($D > 60\,\text{s}$) than typical event durations of mechanically induced coherent structures in the roughness sublayer.

Combined with the notion, that spectral correlation was predominantly high for the short event durations, we have confidence, that observations of scalar fluctuations on long timescales with slow instruments can already deliver most of the information needed for the assessment of scalar similarity. This is of importance for REA or HREA measurements, when no fast sensor is available for the scalar of interest. In such a situation no data can be generated for the determination of scalar correlation, Equation (4), or the spectral correlation, Equation (8) for short event durations. The use of slow sensors would allow to assess scalar similarity for long event durations for many different trace gases. Similarity in event durations of longer than $60\,\text{s}$ could also be investigated by air sampling in flasks and subsequent laboratory analysis.

For an application of this method of assessment of scalar similarity, additional care has to be taken, when fluxes of the proxy scalar become very small, because poor similarity may not be reflected adequately in the spectral correlation, e. g. diminishing buoyancy fluxes in the late afternoon (case 3). An analysis of scalar similarity by spectral analysis on more extended temporal scales was reported by Watanabe et al. (2000) for the assessment of the 'Bandpass Eddy Covariance method' (e. g. Hicks and McMillen, 1988, Horst and Oncley, 1995). While achieving relatively good latent heat flux results using fast temperature measurements for the spectral correction of a slow humidity sensor, flux errors became large during times with small sensible heat fluxes, which confirms our finding for case 3.

16   Ruppert et al.

5.3. b-FACTORS FROM REA AND HREA SIMULATION

b-factors from simulations of REA with a wind-deadband of $H_w = 0.6$ (classical REA, abbreviated with REA 0.6 here after) on average met the values predicted from models (e.g. Pattey et al., 1993: $b_{(H_w=0.6)} = 0.394$) during all three days. However, results for the EBEX-2000 data (Figure 4a) show a diurnal variation of b-factors in the range of 0.36 to 0.41 with maximum values shortly after noon. This means that the use of the fixed average b-factor would result in flux errors with a systematic diurnal course. The diurnal course does not originate from a change in σ_w, which remains relatively constant for the EBEX-2000 data (0.31 ± 0.02). At the same time there is good agreement in the diurnal course of b-factors calculated for carbon dioxide, sonic temperature and water vapour. The use of a variable b-factors determined from a proxy scalar can therefore reduce REA flux errors.

Figure 4b and 4c display a similar diurnal trend of b-factors for HREA with a hyperbolic deadband size of $H_h = 1.0$ (abbreviated with HREA 1.0 here after). Values in the range of 0.15 to 0.27 correspond to the range of 0.22 ± 0.05 found by Bowling et al. (1999b). The ratio of b-factors for REA 0.6 and HREA 1.0 is proportional to the increase in scalar difference ($\overline{c_\uparrow} - \overline{c_\downarrow}$, Equation 1) that can be achieve by changing to HREA 1.0 when σ_w is more or less constant. For the EBEX-2000 data the increase in scalar difference for HREA 1.0 compared to REA 0.6 averages to 1.65 ± 0.13. b-factors for the proxy scalars T_s and ρ_{H2O} (Figure 4b and 4c, unfilled symbols) are the result of segregating c_{proxy} time series into updrafts and downdrafts with a hyperbolic deadband definition based on the same c_{proxy} data. If we would apply hyperbolic deadbands defined on the carbon dioxide record for the simulation of HREA 1.0 for carbon dioxide (our scalar of interest) the match between b-factors would be similar to the match found for REA 0.6 (Figure 4a). However, we have to rely on a deadband definition from fast measurements of the proxy scalar during HREA sampling of the scalar of interest in the field. In order to give realistic results of the methodological error in HREA we used either T_s (Figure 4b) or ρ_{H2O} (Figure 4c) as proxy scalar for the deadband definition in the simulation of HREA 1.0 for carbon dioxide (filled triangles).

Besides the diurnal trend we see an offset in the b-factors for most sampling periods with higher b-factors for the scalar of interest ρ_{CO2} than for the proxy scalars. The increased b-factors are a result of decreased scalar differences ($\overline{c_\uparrow} - \overline{c_\downarrow}$) according to Equation (1) because Flux $\overline{w'c'}$ and σ_w stay the same for one sampling period of 30 min. The reduction in scalar difference can be explained by small dissimilarities between scalar of interest and proxy scalar. A hyperbolic deadband
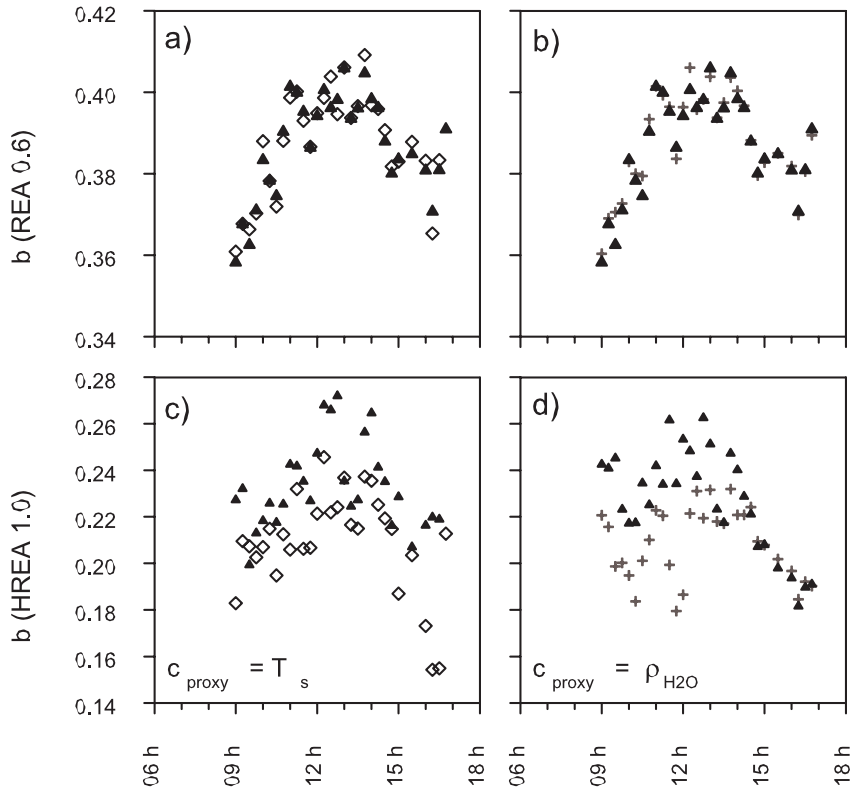
Scalar Similarity for Relaxed Eddy Accumulation Methods   17

Figure 4. b-factors from simulation of REA 0.6 (a, b) and HREA 1.0 (c, d) sampling. The results are based on high resolution time series from the EBEX-2000 dataset. Filled triangles represent *b*-factors for carbon dioxide density ρ_{CO2}, dimonds for sonic temperature T_s and crosses for water vapour density ρ_{H2O}. The difference between *b*-factors for HREA of carbon dioxide (filled triangles in c and d) originates from the use of T_s (c) or ρ_{H2O} (d) as proxy scalar for the definition of the hyperbolic deadband.

definition with a mismatch of the JFDs leads to some inefficiency in the selection of large positive and negative scalar fluctuations. The small inefficiency in correctly sampling the extreme scalar fluctuations causes decreased scalar difference and results in the observed offset of *b*-factors.

5.4. RELATIVE FLUX ERRORS IN REA AND HREA

The difference in *b*-factors is the basis for the determination of relative flux errors ε, Equation (10). Our results show small relative flux errors

for REA 0.6 when using a proxy scalar for the determination of b-factors instead of using a fixed b-factor. Scatter in ε, i. e. the risk of error in the flux, increases slightly with decreasing scalar correlation, but generally stays below $\pm 10\,\%$ (no Figure). ε does not show signs of systematic underestimation or overestimation of fluxes, so that classical REA 0.6 can be regarded as relatively robust against the changes in scalar similarity. This is in agreement with studies finding a relative stability for the b-factor and small errors in REA when using a wind-deadband size H_w of 0.6 to 0.8 (Oncley et al., 1993; Foken et al., 1995; Ammann and Meixner, 2002). Nevertheless, the scaling of the scatter in ε indicates, that the scalar correlation coefficient is an appropriate measure for the description of scalar similarity required for REA methods.

A significant influence of scalar similarity on ε in HREA is visible in Figure 5. The systematic underestimation of the flux correlates with scalar correlation and linear regressions lead to similar coefficients of determination (r^2) for the use of either of the two proxy scalars. A larger degree of scatter in the relative flux errors found for the GRASATEM-2003 data (Figure 5a and Figure 5b) and consequently a reduced coefficient of determination in Figure 5b are the result of small absolute fluxes during and after the period with cloud cover (Section 5.1). Errors remain in the order of $\pm 10\,\%$ for high scalar correlations for all three surface types. Simulation results indicate systematic underestimation of the flux of about -40 % for periods with poor scalar similarity. Only for the WALDATEM-2003 data systematic underestimation was smaller on average when using T_s as proxy scalar compared to using ρ_{H2O} as proxy scalar, which is in agreement with higher scalar correlation (Figure 5e) and spectral correlation (Figure 3f).

The results presented in Figure 5 clearly show that good scalar similarity between the scalar of interest and the proxy scalar is essential to avoid systematic underestimation of fluxes determined with the HREA method. Therefore, great care has to be taken in the selection of an appropriate proxy scalar. Diurnal changes in scalar similarity may require a change of the proxy scalar in order to avoid large errors in the flux measurements using HREA.

The scaling of scatter in ε for REA 0.6 and the scaling of systematic underestimation of fluxes in HREA 1.0 show that the scalar correlation coefficient is an efficient measure for the description of scalar similarity needed in REA or HREA methods. Further investigations of the behavior of the scalar correlation may lead to better understanding of the diurnal changes (case 1, 2, 3) and processes controlling scalar similarity. However, the assessment of suitable proxy scalars especially for flux measurements applying the HREA method can normally only be based on measurements using slow sensors. The spectral analysis
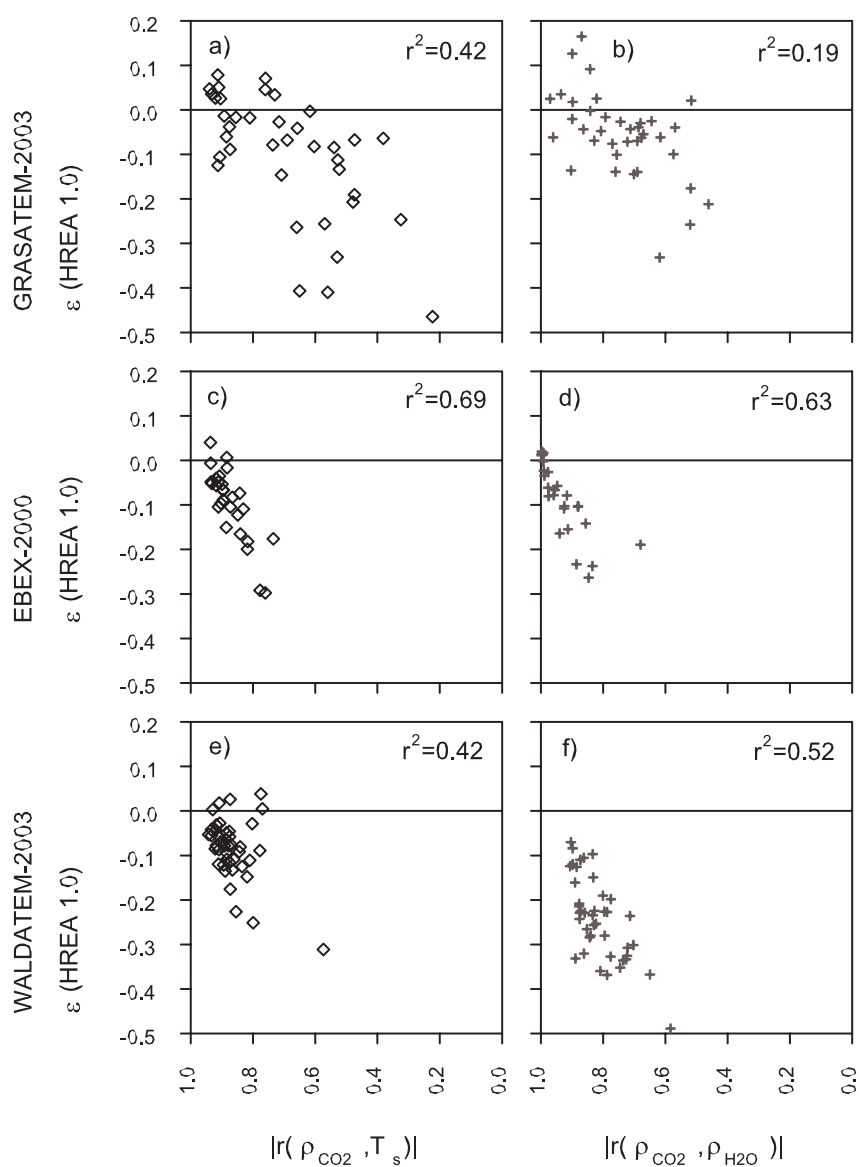
Scalar Similarity for Relaxed Eddy Accumulation Methods   19

Figure 5. Relative flux error ε for carbon dioxide flux from HREA 1.0 simulations in relation to the scalar correlation coefficient r (absolute values). In a), c) and e)(diamonds) sonic temperature T_s was used as proxy scalar, whereas in b), d) and f)(crosses) water vapour density ρ_{H2O} was used as proxy scalar. The coefficient of determination r^2 of a linear regression indicates to which degree scalar correlation can explain the variation in the relative flux error.

20   Ruppert et al.

presented in this study as well as investigations on the 'Bandwidth
Eddy Covariance' method (Watanabe et al., 2000) give confidence, that
enough information on scalar similarity is contained in such slow sensor
measurements.

6. Conclusions

Changes in scalar similarity between carbon dioxide, sonic temperature
and water vapour were analysed with the scalar correlation coefficient.
This evaluation used high quality flux data from experiments over
grassland, an irrigated cotton plantation and spruce forest.

Significant changes of scalar similarity were observed over all three
surface types within the diurnal cycle. We therefore conclude that dif-
ferences in scalar similarity have to be expected even if sources and
sinks are located close together within the vertical profile (short cut
grassland).

Spectral analysis showed constantly good scalar correlation in the
higher frequency range (event durations of $6\,s$ to $60\,s$), which is in
agreement with findings by Pearson et al. (1998). Scalar similarity is
predominantly controlled by events on longer timescales (event dura-
tions $> 60\,s$), which most likely represent changes in the source/sink
strength, convective or advective processes. This finding suggests that
sampling with slow sensors may be sufficient as alternative strategy for
the assessment of scalar similarity required for REA methods when the
scalar of interest can not be measured with a fast sensors.

The scaling of scatter in REA flux errors and scaling of systematic
underestimation of fluxes in HREA confirm that the scalar correlation
coefficient is an efficient measure for the assessment of scalar similarity
needed for REA and HREA methods. The effects of changing scalar
similarity on REA flux measurement errors were relatively small ($\varepsilon <
\pm 10\,\%$). A diurnal course of the b-factors was found for the EBEX-2000
dataset, so that the use of a b-factor determined from a proxy scalar is
recommended compared to the use of a fixed b-factor in order to reduce
relative flux errors in classical REA.

Poor similarity between the scalar of interest and the proxy scalar
leads to systematic underestimation of fluxes determined with HREA
(up to -40 %). Therefore great care has to be taken for the selection of
a suitable proxy scalar. In the absence of fast recorded timeseries for
the scalar of interest, slow sensor could generate appropriate data for
subsequent assessment of HREA measurements or more detailed inves-
tigations on the general behavior of scalar similarity. Diurnal changes in
the scalar similarity may require to change the proxy scalar within the

Scalar Similarity for Relaxed Eddy Accumulation Methods 21

diurnal cycle accordingly in order to correctly measure trace gas fluxes. From the results presented in this study, the use of sonic temperature as proxy for carbon dioxide seems favorable during the morning. However, scalar similarity was poor during situations with diminishing buoyancy fluxes in the late afternoon or during a period with cloud shading during the day.

A preliminary interpretation can be given for the diurnal pattern of scalar correlation. The good scalar similarity between carbon dioxide and sonic temperature found before 9-10 h local time for all three surface types (case 1) could be due to processes of carbon dioxide consumption (assimilation) and heat production that start rapidly and simultaneously with increasing global radiation in the morning. Whereas the atmospheric sink for water vapour, i. e. water vapour deficit, gains strength more slowly throughout the day with the warming of the surface layer. More experimental results on scalar correlation from other sites and flux profile measurements like outlined in Pearson et al. (1998) would be needed to check this hypothesis further. The link to source/sink strength suggests that also plant physiological processes, like e. g. afternoon stomata closure, can have a major effect on the diurnal pattern of scalar similarity.

Acknowledgements

References

Akima, H.: 1970, 'A new method of interpolation and smooth curve fitting based on local procedures'. *J. Assc. Comp. Mach.* **17**, 589–602.

Ammann, C. and F. X. Meixner: 2002, 'Stability dependence of the relaxed eddy accumulation coefficient for various scalar quantities'. *J. Geophys. Res.* **107(D8)**, 4071.

Andreas, E. L., R. Hill, J. R. Gosz, D. Moore, W. Otto, and A. Sarma: 1998a, 'Statistics of Surface Layer Turbulence over Terrain with Meter-Scale Heterogeneity'. *Boundary-Layer Meteorol.* **86**, 379–409.

22   Ruppert et al.

Andreas, E. L., R. J. Hill, J. R. Gosz, D. I. Moore, W. D. Otto, and A. D. Sarma: 1998b, 'Stability dependence of the eddy-accumulation coefficients for momentum and scalars'. *Boundary-Layer Meteorol.* **86**, 409–420.

Baker, J. M., J. M. Norman, and W. L. Bland: 1992, 'Field-scale application of flux measurement by conditional sampling'. *Agric. For. Meteorol.* **62**, 31–52.

Beverland, I. J., R. Milne, C. Boissard, D. H. O'Neill, J. B. Moncrieff, and C. N. Hewitt: 1996, 'Measurements of carbon dioxide and hydrocarbon fluxes from a sitka spruce using micrometeorological techniques'. *J. Geophys. Res.* **101(D17)**, 22807–22815.

Beyrich, F., W. Adam, J. Bange, K. Behrens, F. H. Berger, C. Bernhofer, J. Bösenberg, H. Dier, T. Foken, M. Göckede, U. Görsdorf, J. Güldner, B. Hennemuth, C. Heret, S. Huneke, W. Kohsiek, A. Lammert, V. Lehmann, U. Leiterer, J.-P. Leps, C. Liebethal, H. Lohse, A. Lüdi, M. Mauder, W. Meijinger, H.-T. Mengelkamp, R. Queck, S. Richter, T. Spiess, B. Stiller, A. Tittebrand, U. Weisensee, and P. Zittel: 2004, 'Verdunstung über einer heterogenen Landoberfläche - Das LITFASS-2003 Experiment, Ein Bericht.'. Technical Report Arbeitsergebnisse Nr. 79, German Meteorological Service, Offenbach, Germany. ISSN 1430-0281.

Bowling, D. R., D. D. Baldocchi, and R. K. Monson: 1999a, 'Dynamics of isotopic exchange of carbon dioxide in a Tennessee deciduous forest'. *Global Biogeochemical Cycles* **13**, 903–922.

Bowling, D. R., A. C. Delany, A. A. Turnipseed, D. D. Baldocchi, and R. K. Monson: 1999b, 'Modification of the relaxed eddy accumulation technique to maximize measured scalar mixing ratio differences in updrafts and downdrafts'. *J. Geophys. Res.* **104(D8)**, 9121–9133.

Bowling, D. R., D. E. Pataki, and J. R. Ehleringer: 2003, 'Critical evaluation of micrometeorological methods for measuring ecosystem-atmosphere isotopic exchange of CO2'. *Agric. For. Meteorol.* **116**, 159–179.

Bowling, D. R., P. P. Tans, and R. K. Monson: 2001, 'Partitioning net ecosystem carbon exchange with isotopic fluxes of CO2'. *Global Change Biol.* **7**, 127–145.

Brunet, Y. and S. Collineau: 1994, 'Wavelet analysis of diurnal and nocturnal turbulence above a maize canopy'. In: E. Foufoula-Georgiou and P. Kumar (eds.): *Wavelets in Geophysics*, Vol. 4 of *Wavelet analysis and its applications*. San Diego: Academic Press, pp. 129–150.

Businger, J. A. and S. P. Oncley: 1990, 'Flux Measurement with Conditional Sampling'. *J. Atmos. Ocean. Tech.* **7**, 349–352.

Chen, J. and F. Hu: 2003, 'Coherent structures detected in atmospheric boundary-layer turbulence using wavelet transforms at Huaihe River Basin, China'. *Boundary-Layer Meteorol.* **107**, 429–444.

Collineau, S. and Y. Brunet: 1993, 'Detection of turbulent coherent motions in a forest canopy. Part I: Wavelet analysis'. *Boundary-Layer Meteorol.* **65**, 357–379.

Desjardins, R. L.: 1972, 'A Study of Carbon Dioxide and Sensible Heat Fluxes using the Eddy Correlation Techinique'. Ph.d., Cornell University.

Foken, T., R. Dlugi, and G. Kramm: 1995, 'On the determination of dry deposition and emission of gaseous compounds at the biosphere-atmosphere interface'. *Meteorol. Z.* **4**, 91–118.

Foken, T., M. Göckede, M. Mauder, L. Mahrt, B. Amiro, and W. Munger: 2004, 'Post-Field data Qualtiy Control'. In: X. e. a. Lee (ed.): *Handbook of Micrometeorology*. NL: Kluwer, pp. 181–208.

Scalar Similarity for Relaxed Eddy Accumulation Methods 23

Gao, W.: 1995, 'The vertical change of coefficient b , used in the relaxed eddy accumulation method for flux measurement above and within a forest canopy'. *Atmos. Environ.* **29**, 2339–2347.

Gerstberger, P., T. Foken, and K. Kalbitz: 2004, 'The Lehstenbach and Steinkreuz 'Catchments in NE Bavaria, Germany'. In: E. Matzner (ed.): *Biogeochemistry of Forested Catchments in a Changing Environment: A german case study*, Vol. 172 of *Ecological Studies*. Heidelberg: Springer, pp. 15–41.

Grossmann, A., R. Kronland-Martinet, and J. Morlet: 1989, 'Reading and Understanding Continous Wavelet Transforms'. In: J. Combes, A. Grossmann, and P. Tchamitchian (eds.): *Wavelets: Time-Frequency Methods and Phase Space*. New York: Springer, pp. 2–20.

Grossmann, A. and J. Morlet: 1984, 'Decomposition of Hardy Functions into Square Integrable Wavelets of Constant Shape'. *J. Math. Anal* **15**, 723–736.

Hicks, B. B. and R. T. McMillen: 1984, 'A simulation of the eddy accumulation method for measuring pollutant fluxes'. *J. Climate Appl. Meteor.* **23**, 637–643.

Hicks, B. B. and R. T. McMillen: 1988, 'On the measurement of Dry Deposition Using Imperfect Sensors and in Non-Ideal Terrain'. *Boundary-Layer Meteorol.* **42**, 79–94.

Horst, T. W. and S. P. Oncley: 1995, 'Flux-PAM Measurement of Scalar Fluxes Using Cospectral Similarity'. In: *Proc. 9th Symp. on Meteorological Observations and Instumentation*, Vol. Conference Preprint. Charlotte, North Carolina, American Meteorological Society, Boston. pp. 495-500.

Kaimal, J. C., J. C. Wyngaard, Y. Izumi, and O. R. Cot: 1972, 'Spectral characteristics of surface-layer turbulence'. *Quart. J. Roy. Meteor. Soc.* **98**, 563–589.

Katul, G., C. I. Hsieh, D. Bowling, K. Clark, N. Shurpali, A. Turnipseed, J. Albertson, K. Tu, D. Hollinger, B. Evans, B. Offerle, D. Anderson, D. Ellsworth, C. Vogel, and R. Oren: 1999, 'Spatial variability of turbulent fluxes in the roughness sublayer of an even-aged pine forest'. *Boundary-Layer Meteorol.* **93**, 1–28.

Katul, G. G., P. L. Finkelstein, J. F. Clarke, and T. G. Ellestad: 1996, 'An investigation of the conditional sampling method used to estimate fluxes of active, reactive, and passive scalars'. *J. Appl. Meteor.* **35**, 1835–1845.

Katul, G. G., S. M. Goltz, C. I. Hsieh, Y. Cheng, F. Mowry, and J. Sigmon: 1995, 'Estimation of Surface Heat and Momentum Fluxes Using the Flux-Variance Method above Univorm and Non-Uniform Terrain'. *Boundary-Layer Meteorol.* **80**, 249–282.

Katul, G. G. and C. I. Hsieh: 1999, 'A note on the flux-variance similarity relationships for heat and water vapour in the unstable atmospheric surface layer'. *Boundary-Layer Meteorol.* **90**, 327–338.

Kronland-Martinet, R., J. Morlet, and A. Grossmann: 1987, 'Analysis of Sound Patterns Through Wavelet Transforms'. *Int. J. Pattern Recognition and Artificial Intelligence* **1**, 273–302.

Kumar, P. and E. Foufoula-Georgiou: 1994, 'Wavelet analysis in Geophysics: An Introduction'. In: E. Foufoula-Georgiou and P. Kumar (eds.): *Wavelets in Geophysics*, Vol. 4 of *Wavelet analysis and its applications*. San Diego: Academic Press, pp. 1–43.

Lu, S. S. and W. W. Willmarth: 1973, 'Measurements of the structure of Reynolds stress in a turbulent boundary layer'. *J. Fluid. Mech.* **60**, 481–512.

Lykossov, V. and C. Wamser: 1995, 'Turbulence Intermittency in the Atmospheric Surface Layer over Snow-Covered Sites'. *Boundary-Layer Meteorol.* **72**, 393–409.

24   Ruppert et al.

McNaughton, K. G. and J. Laubach: 1998, 'Unsteadiness as a cause of non-equality of eddy diffusivities for heat and vapour at the base of an advective inversion'. *Boundary-Layer Meteorol.* **88**, 479–504.

Milne, R., A. Mennim, and K. Hargreaves: 2001, 'The value of the beta coefficient in the relaxed eddy accumulation method in terms of fourth-order moments'. *Boundary-Layer Meteorol.* **101**, 359–373.

Obukhov, A. M.: 1960, 'O strukture temperaturnogo polja i polja skorostej v uslovijach konvekcii'. *Izvestia AN SSSR, seria Geofizika* pp. 1392–1396.

Oncley, S., T. Foken, R. Vogt, C. Bernhofer, W. Kohsiek, H. P. Liu, A. Pitacco, D. Grantz, and L. Riberio: 2002, 'The Energy Balance Experiment EBEX-2000'. In: *15th Conference on Boundary Layer and Turbulence.* Wageningen University, Wageningen, Netherlands, AMS Boston. pp. 1-4.

Oncley, S. P., A. C. Delany, T. W. Horst, and P. P. Tans: 1993, 'Verification of flux measurement using relaxed eddy accumulation'. *Atmos. Environ.* **27A**, 2417–2426.

Pattey, E., R. L. Desjardins, and P. Rochette: 1993, 'Accuracy of the relaxed eddy-accumulation technique, evaluated using CO2 flux measurements'. *Boundary-Layer Meteorol.* **66**, 341–355.

Pearson, R. J., S. P. Oncley, and A. C. Delany: 1998, 'A scalar similarity study based on surface layer ozone measurements over cotton during the California Ozone Deposition Experiment'. *J. Geophys. Res.* **103(D15)**, 18919–18926.

Rebmann, C., M. Göckede, T. Foken, M. Aubinet, M. Aurela, P. Berbigier, C. Bernhofer, N. Buchmann, A. Carrara, A. Cescatti, R. Ceulemans, R. Clement, J. Elbers, A. Granier, T. Grünwald, D. Guyon, K. Havrankova, B. Heinesch, A. Knohl, T. Laurila, B. Longdoz, B. Marcolla, T. Markkanen, F. Miglietta, H. Moncrieff, L. Montagnani, E. Moors, M. Nardino, J.-M. Ourcvial, S. Rambal, U. Rannik, E. Rotenberg, P. Sedlak, G. Unterhuber, T. Vesala, and D. Yakir: 2005, 'Quality analysis applied on eddy covariance measurements at complex forest sites using footprint modelling'. *Theor. App. Climatol.* pp. DOI: 10.1007/s00704–004–0095–y.

Shaw, R. H.: 1985, 'On diffusive and dispersive fluxes in forest canopies'. In: B. A. Hutchinson and B. B. Hicks (eds.): *The Forest-Atmosphere Interaction.* Norwell, Mass.: D. Reidel, pp. 407–419.

Shaw, R. H., J. Tavangar, and D. P. Ward: 1983, 'Structure of the Reynolds stress in a canopy layer'. *J. Climate Appl. Meteor.* **22**, 1922–1931.

Simpson, I. J., G. W. Thurtell, H. H. Neumann, G. Den Hartog, and G. C. Edwards: 1998, 'The validity of similarity theory in the roughness sublayer above forests'. *Boundary-Layer Meteorol.* **87**, 69–99.

Thomas, C. and T. Foken: 2005a, 'Coherent structures in a tall spruce canopy: temporal scales, structure spacing and terrain effects'. *Boundary-Layer Meteorol.* p. submitted.

Thomas, C. and T. Foken: 2005b, 'Detection of Long-term Coherent Exchange over Spruce Forest Using Wavelet Analysis'. *Theor. App. Climatol.* pp. DOI: 10.1007/s00704–004–0093–0.

Thomas, C., J.-C. Mayer, F. Meixner, and T. Foken: 2005, 'Analysis of low-frequency turbulence above tall vegetation using a Doppler sodar'. *Boundary-Layer Meteorol.* p. submitted.

Wallace, J. M., H. Eckelmann, and R. S. Brodkey: 1972, 'The wall region in turbulent shear flow'. *J. Fluid. Mech.* **54**, 39–48.

Scalar Similarity for Relaxed Eddy Accumulation Methods 25

Watanabe, T., K. Yamanoi, and Y. Yasuda: 2000, 'Testing of the bandpass eddy covariance method for a long-term measurement of water vapour flux over a forest'. *Boundary-Layer Meteorol.* **96**, 473–491.

Wichura, B., N. Buchmann, and T. Foken: 2000, 'Fluxes of the stable carbon isotope 13C above a spruce forest measured by hyperbolic relaxed eddy accumulation method'. In: *14th Symposium on Boundary Layers and Turbulence*, Vol. Conference Preprint. Aspen, Colorado, American Meteorological Society, Boston. pp. 559-562.

Wilczak, J. M., S. P. Oncley, and S. A. Stage: 2001, 'Sonic anemometer tilt correction algorithms'. *Boundary-Layer Meteorol.* **99**, 127–150.

Wyngaard, J. C., O. R. Cot, and Y. Izumi: 1971, 'Local free convection, similarity and the budgets of shear stress and heat flux'. *J. Atmos. Sci.* **28**, 1171–1182.

Wyngaard, J. C. and C.-H. Moeng: 1992, 'Parameterizing turbulent diffusion through the joint probability density'. *Boundary-Layer Meteorol.* **60**, 1–13.

Address for Offprints:
Johannes Ruppert
University of Bayreuth
Department of Micrometeorology
95440 Bayreuth, Germany
Tel. (49) 921 55 2319
Fax (49) 921 55 2366
Email johannes.ruppert@uni-bayreuth.de

Appendix G

[1] Laboratory for Environmental Physics, The University of Georgia, Griffin, GA, USA

[2] Department of Micrometeorology, University of Bayreuth, Bayreuth, Germany

[3] National Science Foundation, Washington, DC, USA

Research Note

On the effect of clearcuts on turbulence structure above a forest canopy

G. Zhang[1], Chr. Thomas[2], M.Y. Leclerc[1], A. Karipot[1], H. L. Gholz[3], and Th. Foken[2]

With 2 Figures

Summary

Drastic changes in flow modifications are generated following the clearcutting of large patches of trees in a managed forest plantation covering several hundreds of square kilometers near Gainesville, Florida. The present paper illustrates the changes of flow using sonic anemometer measurements above the forest canopy. Using wavelet analysis, this study shows that forest disturbances brought on by clearcutting activities covering several kilometers contribute to enhanced fluxes at the tower eddy-covariance flux measurement system. This result sheds additional insight on our knowledge of carbon uptake and the ideal conditions under which increased uptake occurs.

1. Introduction

The body of experimental evidence suggesting that the atmosphere near the forest-atmosphere interface is characterized by multi-scale eddies is impressive (Shaw, 1985, Raupach et al. 1996, Thomas and Foken 2005b). The eddy-covariance method has made the measurement of fluxes of energy, heat, and mass between vegetation and the atmosphere possible over short and long-term periods, such as measurements of net ecosystem exchange (NEE) in FLUXNET (Baldocchi et al. 2001). But the eddy-covariance method requires both steady-state conditions and infinite fetch upwind. These requirements are difficult to meet since most real-life terrain (including those in the above networks) present departures from the ideal conditions at least for some periods. These departures result in large systematic errors (Foken and Wichura, 1996, Goulden et al. 1996, Mahrt, 1998, Yi et al., 2000) and dramatically modify fluxes and flux footprint characteristics (Leclerc et al. 2003).

During the past two decades, many studies have documented well-organized turbulent structures above and within tall vegetated canopies (Finnigan, 2000, Raupach et al. 1996; Gao et al. 1989; Leclerc et al. 1990, 1991). Klaassen et al. (2002) found an increase of turbulent fluxes on the lee-side of the edge of the forest. Leclerc et al. (2003) indicated that clearcut

induced large-scale heterogeneities in forest could dramatically affect scalar fluxes and flux footprints.

The introduction of objective detection algorithms such as the wavelet transform has facilitated the processing of larger datasets allowing the derivation of robust statistics of coherent structures (Collineau and Brunet 1993, Turner and Leclerc 1994; Turner et al. 1994, Brunet and Irvine 2000; Thomas and Foken 2005b).

The present study examines the influence of contrasting upwind surface properties on the flow field in a managed pine plantation by documenting the introduction of extraneous flow features attributed to the presence of the clearcuts and their impact on turbulent fluxes.

This work is of significance to micrometeorology since it raises questions about the representativeness of a tower in a landscape characterizing surface-atmosphere exchange in a managed forest canopy. Secondly, this work also raises questions about the nature of the required signal processing and data collection and about the necessity of properly evaluating flow variables and fluxes to upwind disturbances.

2. Materials and methods

2.1. Experiment site

The experiment was performed in an 11-year old managed slash pine canopy (*Pinus elliottii* L.) on the Donaldson tract adjoining the Austin Cary Memorial Forest of the University of Florida, Gainesville, FL (29º45´N, 82º10´W) on the premises of the Florida AmeriFlux site. The plantation covers about seven thousand acres. The forest is about 10 m high, with a leaf area index (LAI) of about 2.8. The reader is referred to Gholz and Clark (2002) for further details on the site. An arc-formed area, from the North to the West and Southwest at least 500 m away from the flux measurement tower, was logged in fall of 1999 (Leclerc et al. 2003), transforming an otherwise nearly perfect homogeneous forest canopy into a heterogeneous site for this experiment (Fig. 1). While the logged area is located hundreds of meters outside the footprint area of the flux tower during daytime, the influence of the upwind clearcut has shown up changes of the order of hundreds of percents in fluxes between fluxes from the homogeneous area/non-homogeneous area and between modeled and measured tracer flux footprints (Leclerc et al. 2003).

2.2. Instrumentation, data collection and processing

A three-dimensional sonic anemometer (Campbell Scientific Inc., Logan, UT, Model CSAT3) placed at 17 m height on a tower in the forest was used to measure the time series of three components of wind and virtual temperature with 10 Hz sampling in November 2000 to early January 2001. A detailed overview over the entire measuring program can be found in Zhang et al. (2005).

The analysis of the turbulence structure is based on the wavelet transform. A detailed description and discussion of the method of analysis can be found in Thomas and Foken (2005a). For brevity, the main steps are presented here only. The data was despiked in a manner analogous to that of Vickers and Mahrt (1997), and the planar fit algorithm used to rotate the data in its natural coordinate system (Wilczak et al. 2001). A reduction of the original sampling resolution to 2 Hz was done by block averaging to reduce computation

time. A low-pass filter was then applied to the resulting time series using a biorthogonal set of wavelet functions (BIOR5.5). This filter discards fluctuations less than the critical event duration of 5 s. Subsequently, the spectrum of the wavelet variance is determined by a continuous wavelet transform using the Morlet wavelet function. The transform was performed on scales representing event durations D ranging from 10 s to 280 s, whereas the event duration D is defined as (Collineau and Brunet 1993)

$$D = \frac{1}{2}f^{-1} = \frac{a \cdot \pi}{f_s \cdot \omega^0_{\psi_{1,1,0}}}$$ (1)

where f is the frequency corresponding to the event duration, a the wavelet dilation scale, f_s the sampling frequency of the time series and $\omega^0_{\psi_{1,1,0}}$ the center frequency of the mother wavelet function. For a sine function, the event duration D represents half the length of a single period. The characteristic temporal scales of coherent structures are derived from the event durations corresponding to the maxima in the wavelet variance spectrum.

The present analysis uses daytime (0900 to 1700 hr) 1-h runs classified according to mean wind direction. While winds from the sector ranging from 75-235° are considered to come from a sector in which the forest is homogeneous, the 245-265° wind sector was selected to represent the clear cut (see Fig. 1).

The wavelet analysis was done for the temperature and vertical wind velocity signals using 1-h records to detect the duration of turbulent events above the canopy.

3. Results and Discussion

The clearcut represents a large heterogeneity in the forest. The temperature difference between clearcut and forested areas surrounding the measurement site can exceed more than 5°C in wintertime (Fig. 1) and even more than 10 °C in summer. In addition to the clearcut of interest located at a distance of at least 500 m from the flux tower, similar clearcuts were present at larger distances imparting patchiness in landscape surface properties. This size of the patches of interest in this study range between 200 to 1000 m and, depending on wind direction, were located approximately 500 m from the flux tower. Assuming mean horizontal velocities of 2-5 m s^{-1}, the approximate duration of advected heated air parcels is expected to be in the range of 100 to 300 s. Therefore, the dataset was selected for cases with winds coming from either the nearby clearcut or from directions representing more homogeneous surface conditions where clearcuts are more distant.

For high wind velocities corresponding to near neutral stratification, a visual analysis shows that only turbulence structures of durations larger than 300 s were found. These flow features are unrelated to the structures pertaining to the clearings and are possibly mesoscale contributions to fluxes. Therefore under high wind velocities, it must be assumed that the flow moving over the clearcut is decoupled from the heated air near the ground. When the stratification becomes slightly unstable in the presence of moderate winds, events with durations of approx. 110 - 250 s were found. These scales correspond to the size of the clearcut and the general patchy structure of the area. For further analysis, all available one hour time series for wind directions from the clearcut (3 1–h time series) and from the more homogeneous areas (7 1-h time series) were selected and the wavelet spectra calculated.
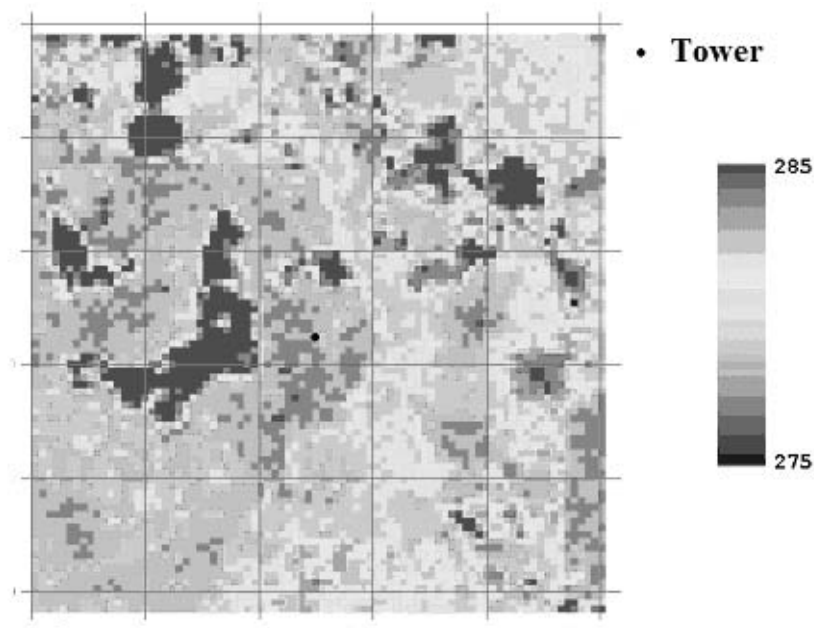
Fig. 1: Temperature [K] at experiment site, clearcut and nearby, remote sensed on January 4, 2001 (Landsat ETM+), which also shows the position and shape of the clearcut. The colder areas are covered with forest. Each grid point corresponds to a 1 km distances, the tower position is 29º45´N, 82º10´W.

In the range of event durations of 120-250 s, significant peaks were found with event durations indicated by the individual maxima slightly differing as a result of different wind speeds and wind directions (fetch). To compare all wavelet spectra, the timescale of the events was detected and all peaks in the wavelet spectra were shifted with up to 40 s to reach an exact superposition of the peaks. Fig. 2a shows the case of wind directions from the more homogeneous areas. A significant event was found with an event duration of 144 s in the average of all spectra in the temperature signal and the vertical wind component. The duration of the temperature events is about 9 s longer than that of the vertical wind. The graphs are given in lin-lin representation to highlight the period of interest and to suppress the microturbulence and coherent structures (characteristic temporal scales of 10-50 s). A shortcoming of the lin-lin representation is that longer structures seem to be dominant, but multiplying the wavelet variance with the angle frequency ω (which is accepted for presentation of spectral densities) leads to vanishing peaks.

A different picture was found for wind directions from the clearcut. Fig. 2b shows two significant peaks at 128 s and at 226 s in the mean spectra. The maximum which corresponds with the peak in Fig. 2a is also significant in the wind and temperature wavelet spectra. It must be assumed that two processes took place. For all wind directions, turbulent eddies originating from the patchy structure are assumed to contribute to turbulent fluxes. To verify whether both events contribute to the turbulent flux, the time series of the temperature and vertical wind velocity of 1-h measurements were band-pass filtered in the range of both maxima. The correlation coefficient between both time series was found to be for both peaks in the order of 0.6 to 0.9, while for events with timescales lower than 80 s, the flow is characterized by microturbulence and coherent structures. In that case, the correlation coefficient ranges from approximately 0.4 to 0.6.
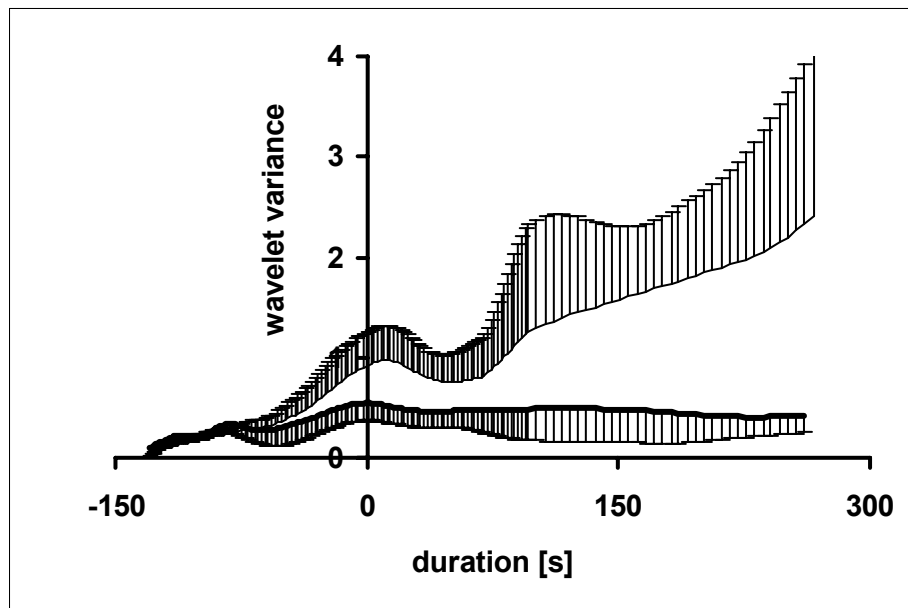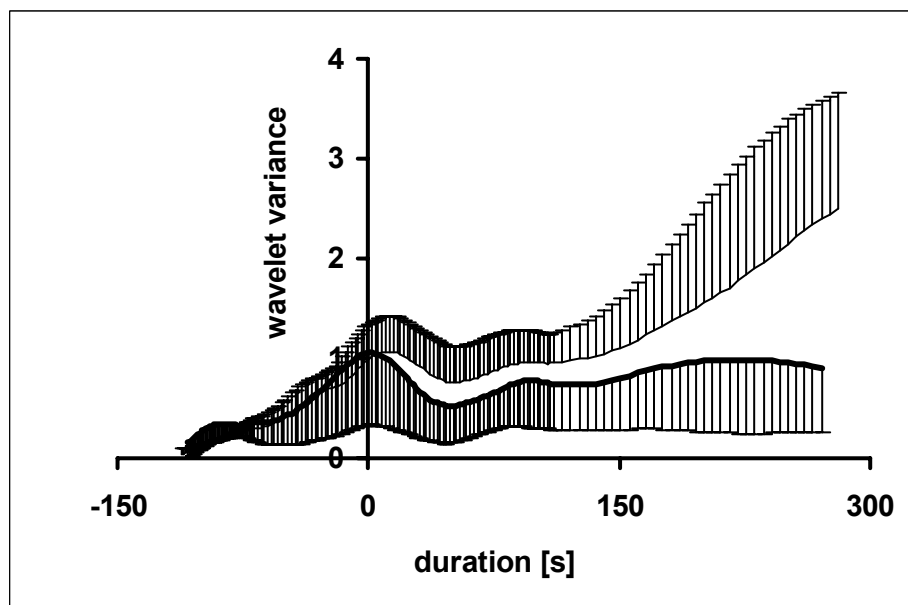
Fig. 2a: Wavelet variance spectrum for the vertical wind velocity and the temperature signal at 17 m height for 7 cases with directions from the homogeneous areas. The average timescale of the turbulent structures (zero on the x-axis in the graph) is 144 s ± 15 s for the vertical wind velocity (lower graph) and 153 s ± 22 s for the temperature (upper graph). The dimension of the wavelet variance is $m^2 s^{-2} \cdot 10^9$ and $K^2 \cdot 10^9$, respectively.

Fig. 2b: Wavelet variance spectrum for the vertical wind velocity and the temperature signal at 17 m height for 3 cases with directions from the clearcut. The average timescale of the first turbulent structures (zero on the x-axis in the graph) is 128 s ± 32 s for the vertical wind velocity (lower graph) and 140 s ± 28 s for the temperature (upper graph). The average timescale of the second turbulent structures is 226 s for the vertical wind velocity and for the temperature. The dimension of the wavelet variance is $m^2 s^{-2} \cdot 10^9$ and $K^2 \cdot 10^9$, respectively.

The flow coming from the clearcut generates additional temperature events which are in phase with respect to events in the vertical wind velocity. This result is in agreement with the numerical study of Friedrichs et al. (2000) who found increased fluxes for a chessboard-type surface.This data suggests that vertical wind velocities show more structures than the temperature, especially those of shorter durations which associated with typical coherent structures above the forest (Thomas and Foken 2005b).

4. Conclusions

The structure of the turbulent flow was observed over a pine forest in North Florida after a clearcut was made several hundreds meters upwind from a flux tower. The influence of the clearcut on the flow structure was examined and compared against turbulence data when the flow came from a homogeneous region upwind from the tower. In daytime unstable conditions, the clearcut causes temperatures to be higher than the surrounding forest with surface temperature differences as high as or higher than 5 °C. This gives rise to several flow modifications arising locally and carried from the freshly logged area over to the adjacent forest canopy. The case presented here is representative of conditions encountered in a managed forest plantation. A more comprehensive picture of the physical mechanisms at play, including details pertaining to the modification of the flow structure inside the canopy, has been investigated in Zhang et al. (2005).

Logged area-related disturbances were found to significantly alter the flow regime at the measurement site when the flow comes from the clearcut or from the more homogeneous forest. The typical mosaic pattern of forest sites, clearcuts, and regrowing clearcuts can generate turbulence structures which contribute to the turbulent flux. The size and duration of these turbulent structures are of a scale such that these flux contributions should be captured by the eddy-covariance method and lie outside the range of contributions from mesoscale fluxes. Nevertheless, tests such as ogives are necessary to secure that eddy-covariance measurements encompass all relevant flux-containing eddies. Otherwise, this omission might introduce large errors in measurements when such measurements are summed over an annual basis (Foken et al. 2004). For strong wind velocities and neutral stratification, our data suggest that the clearcut's characteristic signature is not imparted to the leeside of the clearcut.

Our findings suggest that additional turbulent fluxes are generated by a patchy type surface as well as by clearcuts close to the flux tower. Both increase the flux of energy, heat and mass, suggesting an enhancement in carbon fluxes. Therefore, carbon ecologists must take into account surface heterogeneities of the surrounding terrain even located outside the footprint for their flux analysis.

References

Baldocchi, D, Falge, E, H, G L, Olson, R, Hollinger, D, Running, S, Anthoni, P, Bernhofer, C, Davis, K, Evans, R, Fuentes, J, Goldstein, A, Katul, G, Law, B, Lee, X H, Malhi, Y, Meyers, T, Munger, W, Oechel, W, PawU, K T, Pilegaard, K, Schmid, H P, Valentini, R, Verma, S, Vesala, T (2001) FLUXNET: A new tool to study the temporal and spatial variability of ecosystem-scale carbon dioxide, water vapor, and energy flux densities. Bull Am Meteorol Soc 82: 2415-2434.

Brunet, Y, Irvine, MR (2000) The control of coherent eddies in vegetation canopies: Streamwise structure spacing, canopy shear scale and atmospheric stability. Boundary-Layer Meteorol 94: 139-163.

Collineau, S, Brunet, Y. (1993) Detection of turbulent coherent motions in a forest canopy. Part I: Wavelet analysis. Boundary-Layer Meteorol. 65: 357-379.

Finnigan, J. (2000) Turbulence in plant canopies. Annual Rev Fluid Mech 32: 519–571.

Foken, T, Wichura, B (1996) Tools for quality assessment of surface-based flux measurements. Agricult For Meteorol 78: 83-105.

Foken, T, Göckede, M, Mauder, M, Mahrt, L, Amiro, BD, Munger, JW (2004) Post-field data quality control, in X Lee, WJ Massman and B Law (eds), Handbook of Micrometeorology: A Guide for Surface Flux Measurement and Analysis. Kluwer, Dordrecht, pp 181-208.

Friedrichs, K, Mölders, N, Tetzlaff, G (2000) On the influence of surface heterogeneity on the Bowen-ratio: A theoretical case study. Theor Appl Climatol 65: 181-196.

Gao, W, Shaw, RH, Paw U, KT (1989) Observation of organized structure in turbulent flow within and above a forest canopy. Boundary-Layer Meteorol 47: 349-377

Gholz, HL, Clark, KL (2002) Energy exchange across a chronosequence of slash pine forests in Florida. Agricul Forest Meteorol, 112: 87-102.

Goulden, ML, Munger, JW, Fan, SM, Daube, BC, Wofsy, SC (1996) Exchange of carbon dioxide by a deciduous forest: response to interannual climate variability. Science 271: 1576-1578.

Klaassen, W, van Breugel, PB, Moors, EJ, and Nieveen, JP (2002) Increased heat fluxes near a forest edge. Theor Appl Climatol 72: 231-243.

Leclerc, MY, Beissner, KC, Shaw, RH, den Hartog, G, Neumann HH (1990) The influence of atmospheric stability on the budgets of the Reynolds stress and turbulent kinetic energy within and above a deciduous forest. J Appl Meteorol 29: 916-933.

Leclerc, MY, Beissner, KC, Shaw, RH, den Hartog, G, Neumann, HH (1991) The influence of buoyancy on third-order turbulent velocity statistics within a deciduous forest. Boundary-Layer Meteorol 55:109-123.

Leclerc, M Y, Karipot, A, Prabha, T, Allwine, G, Lamb, B, Gholz, HL (2003) Impact of non-local advection on flux footprints over a tall forest canopy: a tracer flux experiment. Agricul Forest Meteorol 115: 19-30.

Mahrt, L (1998) Flux sampling errors for aircraft and towers. J Atmosph Oceanic Techn 15: 416-429.

Raupach, MR, Finnigan, JJ, Brunet, Y (1996) Coherent eddies and turbulence in vegetation canopies: The mixing-layer analogy. Boundary-Layer Meteorol 78: 351-382.

Shaw, RH (1985) On diffusive and dispersive fluxes in forest canopies. In: BA Hutchinson, BB Hicks (Editors), The Forest-Atmosphere interaction. Reidel Publishing Company, pp. 407-419.

Turner, BJ, Leclerc, MY, Gauthier, M, Moore, K, Fitzjarrald, D 1994. Identification of turbulence structures above a forest canopy using the wavelet transform. J Geophys Res 99(D1):1919-1926; special issue devoted to the NASA ABLE 3-B experiment.

Turner, BJ, Leclerc, MY (1994) Conditional sampling of coherent structures in atmospheric turbulence using the wavelet transform. J Ocean. and Atmos Techn 11(1):205-209.

Thomas, C, Foken, T (2005a) Detection of long-term coherent exchange over spruce forest. Theor Appl Climatol, DOI 101007/s00704-004-0093-0

Thomas, C, Foken, T (2005b) Coherent structures in a tall spruce canopy: temporal scales, structure spacing and terrain effects. Boundary-Layer Meteorol, submitted

Vickers, D, Mahrt, L (1997) Quality control and flux sampling problems for tower and aircraft data. J Atmosph Oceanic Techol 14: 512-526.

Wilczak, JM, Oncley, SP, Stage, SA (2001) Sonic anemometer tilt correction algorithms. Boundary-Layer Meteorol 99: 127-150.

Yi, C, Davis, KJ, Bakwin, PS, Berger, BW, Marr, LC (2000) Influence of advection on measurements of the net ecosystem-atmosphere exchange of CO_2 from a very tall tower. J Geophys Res 105: 9991-9999.

Zhang, G, Leclerc, MY, Karipot, A, Binford, M, Gholz, HL, Thomas, C, Foken, T (2005) The role of clearcuts and spatial disturbances on the downwind canopy layer flow. Agric Forest Meteorol (in progress).

Authors' addresses

G. Zhang, M. Y. Leclerc, and A. Karipot Laboratory for Environmental Physics, The University of Georgia, Griffin, GA 30223, USA

Chr. Thomas and Th. Foken, University of Bayreuth, Dept. of Micrometeorology, D-95440 Bayreuth, Germany
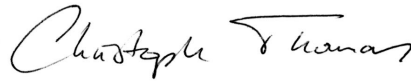
H. L. Gholz, Long Term Ecological Research Program, National Science Foundation, Arlington, VA 22230, USA

Erklärung

Hiermit erkläre ich, dass ich die Arbeit selbstständig verfasst und keine anderen als die angegebenen Hilfsmittel verwendet habe.

Weiterhin erkläre ich, dass ich nicht anderweitig mit oder ohne Erfolg versucht habe, eine Dissertation einzureichen oder mich einer Doktorprüfung zu unterziehen.

Bayreuth, den   24.06.2005

Christoph Thomas